DIRECT CURRENT ELECTRICAL RESISTANCE MEASUREMENT TECHNIQUES FOR ASSESSMENT OF COLORECTAL CANCER DURING LAPAROSCOPIC SURGERY

James Henry Chandler

Submitted in accordance with the requirements for the degree of

Doctor of Philosophy

The University of Leeds

School of Mechanical Engineering

Leeds, UK

September 2015

Declarations

The candidate confirms that the work submitted is his own, except where work which has formed part of jointly-authored publications has been included. The contribution of the candidate and the other authors to this work has been explicitly indicated below. The candidate confirms that the appropriate credit has been given where reference has been made to the work of others.

In all papers listed below, the primary author completed all experimental studies, evaluation of data and preparation of publications. All authors contributed to proof reading of the articles prior to publication.

Papers contributing to this thesis:

- Chandler, J.H., A. Hood, P.R. Culmer, D.G. Jayne, A. Neville. **A bio-galvanic approach to tissue characterisation: technological considerations**. *Hamlyn Symposium on Medical Robotics*, London, UK, 2013. p. 103-104.

- Chandler, J.H., A. Hood, P.R. Culmer, D.G. Jayne, A. Neville. **Technological assessment of the biogalvanic method for tissue characterization**. *Physiological Measurement*. 2014. 35(2): p. 297.

- Chandler, J.H., P.R. Culmer, D.G. Jayne, A. Neville. **Assessment of electrochemical properties of a biogalvanic system for tissue characterisation**. *Bioelectrochemistry*. 2015. 101(0): p. 138-145.

- Chandler, J.H., P.R. Culmer, D.G. Jayne, A. Neville. **A time-dependent model for improved biogalvanic tissue characterisation**. *Medical Engineering & Physics*. 2015. 37(10): p.956-960.

- Chandler, J.H., D.G. Jayne, A. Neville, P.R. Culmer. **A novel multiple electrode direct current technique for characterisation of tissue resistance during surgery**. *Engineering in Medicine and Biology Society (EMBC), 2015 37th Annual International Conference of the IEE,* Milan, Italy, 2015. In Press.

Work was also disseminated through conference presentation (oral and poster). The following presentations contributed to the thesis:

- Chandler, J.H., P.R. Culmer, D.G. Jayne, A. Neville. **Assessment and differentiation of tissue using bio-galvanic measurements**. *8th National Cancer Research Institute Conference*, Liverpool, UK, 2012. [Poster].

- Chandler, J.H., P.R. Culmer, D.G. Jayne, A. Neville. **Incorporation of time-dependent interface effects in biogalvanic tissue resistance characterisation**. *NACE - International Corrosion Conference Series*, San Antonio TX, 2014. [Poster].

- Chandler, J.H., P.R. Culmer, D.G. Jayne, A. Neville. **Adaptation of the biogalvanic characterisation model for improved measurement of biological tissue resistance**. *NACE - International Corrosion Conference Series*, San Antonio TX, 2014. [Oral Presentation].

- Chandler, J.H., P.R. Culmer, D.G. Jayne, A. Neville. **A novel multiple electrode galvanostatic polarisation technique for tissue discrimination and assessment: proof of concept**. 4th *International Conference on Bio-sensing Technology*, Lisbon Portugal, 2015. [Oral Presentation].

This copy has been supplied on the understanding that it is copyright material and that no quotation from the thesis may be published without proper acknowledgement.

©2015 The University of Leeds and James Henry Chandler

The right of James Henry Chandler to be identified as Author of this work has been asserted by him in accordance with the Copyright, Designs and Patents Act 1988.

Acknowledgements

I would first like to acknowledge the support and guidance provided by my supervisors: Pete, Anne and David. Between them they cover an extremely wide range of research areas and their unlikely collaboration has made projects like mine possible. They have supported me throughout all of the challenges of my PhD with technical guidance, patience and unwavering enthusiasm. I would also like to express my appreciation to Cancer Research UK for financially supporting the project.

Being part of the Surgical Technologies group has been an excellent experience. Special thanks go to Zahra, Jen and Adrian for assisting with setting up and conducting tissue testing experiment, and to Earle, William and Evan for their technical advice.

Many academics, technical staff and students across the University have helped me to complete the presented work. I would like to thank David and Mathew from the School of Computing at the University of Leeds who expanded the research greatly through their collaboration and model development. I am also very grateful to Nick West and the histopathology team at St James's University Hospital for giving me access to the histology images of my tested samples. Thanks go to all of the technical staff in the School of Mechanical Engineering, specifically Dave, Andrew, Ron, Graham and Steve. Thanks also to Dominic for working diligently as a summer intern to help develop the indentation testing system.

Lastly, a well overdue thank you is owed to my family and friends. You are now too many to mention but thank you for your emotional, moral and financial support over the years.

I would like to dedicate this to my parents and grandparents who never lost faith in my abilities, even at times when I did. Now I can shave this beard off….maybe!

Abstract

The next generation of surgical tools will employ intraoperative sensing technologies to provide real-time information to the surgeon. Sensing in this way may facilitate personalised tissue resections during cancer surgery, thereby reducing radicality and improving outcomes for the patient.

This thesis details the development and testing of electrochemical based sensing techniques aimed at integration into the next generation of laparoscopic surgical tools. Literature reviewed as part of the work highlights the broad nature of surgically appropriate sensing technologies. Based on the features of simplicity and scalability, the biogalvanic tissue characterisation technique was explored as the most practically suitable candidate.

Development and systematic testing of a biogalvanic measurement system with porcine tissues showed variation that is not explained using the current system model. Correlation with electrochemical measurements verified this unaccounted system complexity. Electrode polarisation and diffusion controlled reduction at the cathode limit the tissue specificity of the output metrics. An improved analytic model fitting technique was developed to reduce the influence of the electrodes. Through collaborative development of a numerical model of the system, the practical limitations of the biogalvanic techniques as a surgical sensor were realised.

To mitigate these limitations, a novel galvanostatic technique for improved resistance characterisation was developed. Testing was conducted on *ex vivo* tissues, showing stability for relevant parametric variation. Surgical applicability was found from a practical perspective, with results showing low sensitivity to switching rate, current range and tissue contact conditions. Testing was also conducted on a number of freshly excised cancerous human colon samples. Measurements were centralised on each tumour and compared to a corresponding healthy region. Every case showed a highly significant difference between tissue types with cancerous tissues having a consistently lower resistance. These findings suggest that the proposed technique of multi-reference galvanostatic resistance characterisation may be a suitable candidate for integration into surgical tools for colorectal cancer surgery.

Table of Contents

List of Figures

List of Tables

Abbreviations

Acronym	Definition
5-ALA	5-aminolevulinic acid
AC	Alternating current
ADC	Analogue to digital
CE	Counter electrode
CIN	Cervical intraepithelial neoplasia
CT	Computed tomography
DAQ	Data acquisition
DC	Direct current
DLL	Dynamic link library
DNA	Deoxyribonucleic acid
EC	Electrochemical
FDA	Food and drug administration
GAIR	Galvanic apparent internal resistance
H&E	Hematoxylin and eosin
ICG	Indocyanine green
LOD	Limit of detection
MIS	Minimally invasive surgery
MRI	Magnetic resonance imaging
NOTES	Natural orifice transluminal endoscopic surgery
OCP	Open circuit potential
OCV	Open circuit voltage
PCB	Printed circuit board
PET	Positron emission tomography
RALS	Robotically assisted laparoscopic surgery
RAS	Robotically assisted surgery
RE	Reference electrode
ROI	Region of interest
SILS	Single incision laparoscopic surgery
US	Ultrasound
WE	Working electrode
WHO	World Health Organisation
ZRA	Zero resistance ammeter

Chapter 1
Introduction to research

There are more than 200 types of cancer and in combination they account for the second largest cause of premature death in the UK [1]. For men and women combined, colorectal cancer (cancer of the colon or rectum) is the third most prevalent form of cancer, with higher incidence rates being found only in lung and prostate cancer [2]. Surgery is typically the primary treatment option for colorectal cancers, which involves removal of the cancer along with a large section of healthy tissue surrounding the tumour. The size and location of the tumour dictate the type and radicality of the resection, a number of typical procedures have been presented in Figure 1.1. Joining the remaining sections (anastomosis) leaves a shortened bowel with a potentially reduced lymphatic and mesenteric network. In many cases a return of normal bowel function is not achievable and a temporary or permanent joining of the bowel to an opening in the abdomen is required. For connection of the large bowel to the abdomen wall, this is called a stoma, while the use of small bowel is termed an ileostomy. Surgical treatment of colorectal cancer can therefore lead to complications and cause a significant impact on a patient's quality of life.

It has been suggested that surgical resection of cancer, and in particular colorectal cancer, may benefit from being personalised [3, 4]. Integration of such a treatment model requires more detailed data regarding tissue health than is currently available through standard preoperative imaging techniques. Therefore, the development of improved intraoperative assessment methods is crucial. Intraoperative sensing has seen much focused research, through imaging using passive and active agents [5, 6] and through direct measurement of mechanical [7] and electrical properties [8]. The challenges associated with sensor development are amplified by the demands associated with laparoscopic and robotically assisted laparoscopic surgery, which are becoming standard practice for many cancer surgeries.

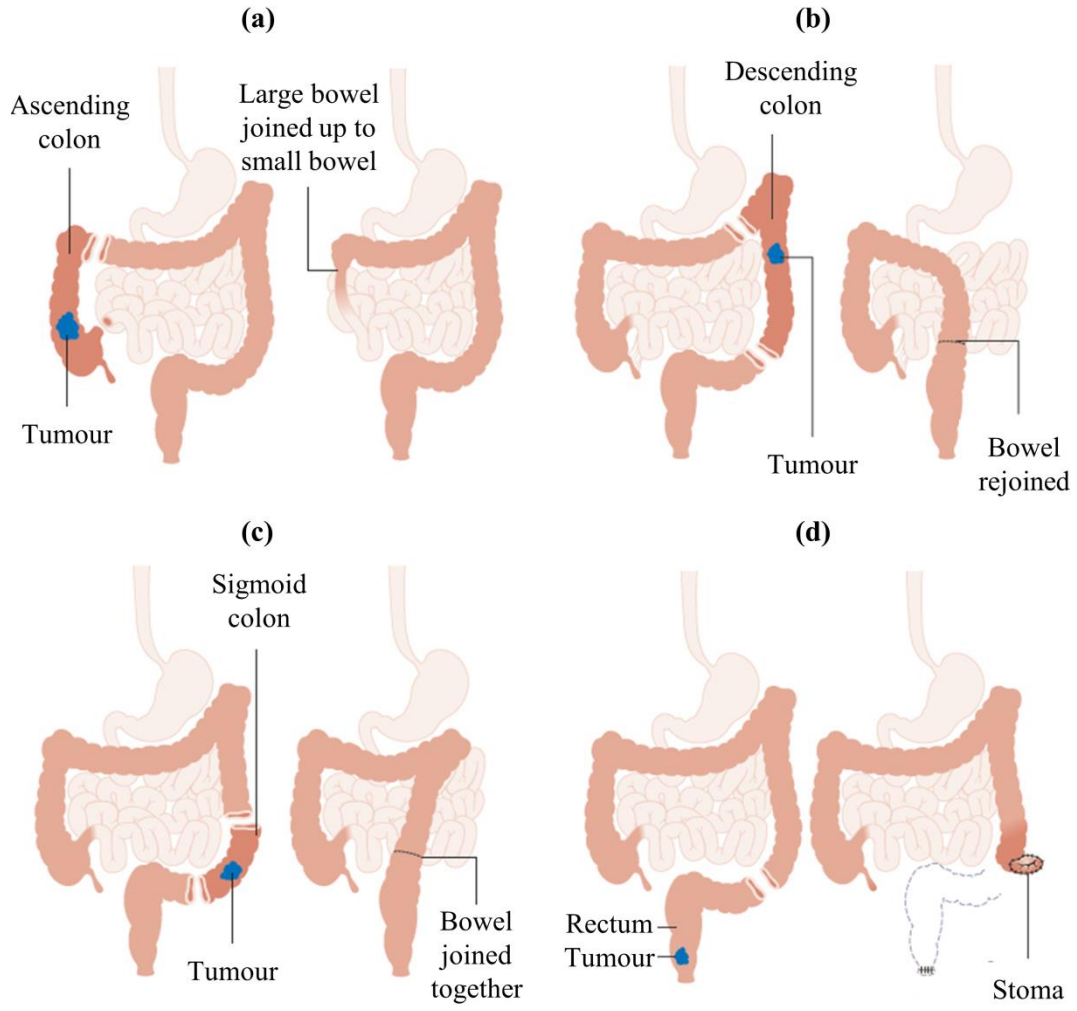

Figure 1.1: Examples of surgical resections for treatment of colorectal cancer in different location, showing (a) right hemi colectomy, (b) left hemi colectomy, (c) sigmoid colectomy and (d) total mesorectal excision for rectal cancer; (images adapted from [9]).

The issue of detecting and delineating cancerous tissue during surgery offers some very specific challenges. Many considerations must be made to develop a suitable technology and to implement it into a suitable sensing system. These include: cancer specificity, contacting conditions, time-variation, reusability, biocompatibility, cost, robustness, scalability, spatial resolution and range,

Many existing technologies have not been fully proven across all of these areas, and new techniques must have their performance assessed across these factors to allow potential efficacy to be established. Due to the large number of possible research areas on this topic, it is essential that the current techniques and sensors be reviewed and research effort focused primarily on those most suitable.

1.1 Project Aim

The aim of the work is to explore and develop sensing technology that may allow for discrimination of tissue health within the setting of laparoscopic colorectal surgery. The sensing techniques developed should be suitable for integration into a surgical device and deliver real-time information to the surgeon regarding the health state of tissue.

Testing and validation of the proposed techniques should be facilitated through development of suitable equipment. Experimentation should be performed on tissue samples and on suitable tissue analogues.

To improve understanding of the technique and to allow meaningful suggestions for device development to be made, computational system modelling should be investigated.

It will be necessary to test suitable sensing technology under settings relevant to surgery, investigating the potential ill-effects of environmental conditions. Testing of the influence of tissue health (colorectal cancer) will be required to demonstrate system efficacy.

1.1.1 Objectives

The objectives defined for the presented work are:

1. To explore the state of the art of relevant sensing technologies that may be appropriate to laparoscopic colorectal surgery.
2. To define and justify a sensing technology suitable for use as a tissue health assessment tool within laparoscopic colorectal surgery.
3. To develop a suitable testing platform for validation and parametric investigation of the selected sensing technology.
4. To investigate the suitability of the technique to surgery through testing with biological tissues.
5. To investigate the underlying properties of the technology through suitable experimentation and modelling.
6. To evaluate the system in the context of colorectal cancer and assess its discrimination performance.

1.2 Thesis Overview

The remainder of the thesis has been divided into eight chapters. The following sections summaries the contents and main findings of each.

Chapter 2: Literature review

Colorectal cancer, its prevalence and treatment is described with a focus on surgical intervention. The technological state of surgical treatment is reviewed detailing the state of the art in laparoscopic and robotically assisted laparoscopic surgery. The remainder of the review covers a broad range of measurement techniques that are suitable for integration into surgical tools. Specific focus is made to mechanical, electrochemical and electrical property measurements. In addition, details of new surgical imaging techniques using contrast agents are also presented. Conclusions from the review are made with consideration given to the practical and technological limitations of the competing techniques.

Chapter 3: A biogalvanic characterisation system

Based on the review findings in Chapter 2, research was focused on biogalvanic tissue characterisation. This chapter describes the development and validation of a biogalvanic measurement system for conducting tissue assessment. The necessary hardware design and developed control and data acquisition software are detailed. In addition, new characterisation models are proposed and tested against the published standard over a range of tests with electronic analogues. Results show that the system produces a high level of characterisation accuracy and the proposed models deliver reduced error and sensitivity to input conditions.

Chapter 4: Biogalvanic tissue testing

This chapter details a selection of tissue tests performed using the biogalvanic technique as developed in Chapter 3. Parametric investigation is made into many of the potential influencing variables, such as: exposure time, tissue thickness, tissue area, mechanical strain, external load switching direction, external load switching rate and tissue health. The findings suggest that although biogalvanic characterisation is possible on tissues, there are numerous influencing factors that are not accounted for within the system model.

Chapter 5: Electrochemical investigation of the biogalvanic system

To improve understanding of the biogalvanic cell, a study into the electrochemical aspects of the system is presented in Chapter 5. The galvanic system is tested using an NaCl salt solution analogue with varied concentrations. Results from standard electrochemical tests are reported

and compared to those of the biogalvanic characterisation and those from tissue tests. Findings indicate that cell potentials are influenced by the concentration of oxygen and that cell current limitation is controlled by the oxygen diffusion rate to the copper cathode. These phenomena and the electrode resistance are not considered in the current biogalvanic characterisation model.

Chapter 6: Biogalvanic system modelling

This chapter focuses on development of two alternative modelling approaches to improve the tissue specificity of biogalvanic characterisation. The first is an adjustment of the electrical components of the current model to include resistive and capacitive aspects of the electrode-tissue interface. The second, a numerical model developed in collaboration with the School of Computing (University of Leeds), explores geometric influence and how characterisation is affected by the relative resistance of the electrodes and tissue medium. The findings of this chapter indicate that improvement is possible through simple characterisation model changes. However, the two electrode configuration makes extraction of tissue specific resistance values challenging for the practical constraints of a surgical sensing system.

Chapter 7: Multi-reference galvanostatic resistance characterisation

An improved measurement technique is proposed, developed and tested in this chapter. A review of relevant methods used to determine (and remove) solution resistance from electrochemical measurements is given. Theory from these techniques and findings from previous investigations into the biogalvanic characterisation are combined in presentation of the new technique. Test system development is described along with parametric investigation into potentially influencing factors. The technique is shown to be capable of characterising a repeatable tissue resistance over a range of measurement rates and current ranges. A concluding study looking at surgical relevance of the technique, with regard to expected contact conditions, is given.

Chapter 8: Testing for tissue health (colorectal cancer)

This final results chapter outlines tests conducted on healthy and cancerous human colon tissues, using the measurement technique developed in Chapter 7. All test cases are shown to give a statistically lower resistance for cancerous tissues. Qualitative relation of the measured resistance to histological analysis is also presented. The chapter is concluded with a discussion of the relevant findings from this measurement technique.

Chapter 9: General discussion

The concluding chapter of the thesis gives a general discussion of the findings from the presented research. Specific attention is independently given to the findings related to the biogalvanic and multi-electrode resistance techniques. The research objectives of the thesis are reviewed in the context of the presented work and the main conclusions described. A range of pertinent research tasks are also suggested in the context of future work.

Chapter 2
Literature review

Many sensing modalities have been developed and investigated for assessing tissue properties. The task of detecting and delineating cancerous tissue during surgery offers some very specific challenges, making direct application of many of these modalities unsuitable. The presented review in this chapter highlights a number of potentially suitable techniques. An overview of colorectal cancer is initially given, making reference to the underlying tissue biology. As the desired application is with laparoscopic surgery, the state of the art of this field is also discussed. The main body of the review focuses on the range of sensing methods utilised for tissue characterisation. This includes methods of mechanical, electrochemical and electrical property assessment along with recent developments in operative imaging techniques. Based on the findings from the literature, the research work presented in this thesis was focused toward electrochemical and electrical tissue characterisation.

2.1 Cancer

In 2008 cancer was listed by the World Health Organization (WHO) as being the second largest cause of premature death in the UK, with 27% of deaths being caused by the disease [1]. There are more than 200 types of cancer, each having distinct causes, symptoms and treatments [10]. At a fundamental level, cancer is a genetic disease resulting from mutations in the genetic material within cells (DNA). This often leads to notable changes in tissue structure and function. Left untreated, cancer will occlude the function of the tissue in which it was primarily evident and in many cases spread (metastasis) to other areas of the body. This inevitably leads to reduced organ function and death.

Treatment options are numerous; some of the most common cancer treatment options offered to patients are [11]:

Surgery:	*The physical removal of cancerous tissue from the body.*
Radiation:	*Application of high dose targeted ionising radiation to shrink, cure or prevent recurrence of cancer.*
Chemotherapy:	*Application of drug based therapy to kill cancer cells.*
Immunotherapy:	*Augmentation of a patient's immune system to help it fight cancer.*
Targeted therapy:	*Treatment with drugs that specially target to cancer cell and block their growth.*
Hormone therapy:	*Exogenous administration of hormones specifically to slow or stop the growth of cancer cells.*
Stem Cell Transplant:	*Treatment to restore blood-forming stem cells destroyed during other cancer treatments.*

The selection of a suitable primary treatment is made based on a wide range of factors, including the type and stage of the cancer and the patient's profile. Each intervention type contains distinct treatment options to improve alignment with variable types and stages of cancer. It is typical for patients to be treated using a combined modality approach, to exploit the benefits of different therapies [11]. However, the primary therapeutic modality with the highest rate of cure remains surgery.

2.1.1 Colorectal cancer

The colon forms the terminal section of the digestive system in humans. It is primarily responsible for the extraction of water and salts from solid waste and the storage and removal of the remaining faeces [12]. Figure 2.1 shows the main features of the human colon. The tube-like structure of the colon is anatomically complex, with several concentric functional layers making up the complete tissue. With reference to Figure 2.2, these are generally classified as (from innermost to outermost): the mucosa, consisting of a simple columnar epithelium; the submucosa made up of a thin layer of loose connective tissue with blood and lymphatic vessels; a circular muscle layer; a longitudinal muscle layer; and the outer most serosa [13].

Normal cell function within colon and rectum can become altered, leading to rapid cell division, invasion of nearby tissues and spread to distinct organs. This is known as colorectal cancer. Statistically, colorectal cancer is the third most prevalent cancer for men and women combined, accounting for a mortality rate in the UK of over 16,000 in 2008 alone. More than 90% of colorectal carcinomas are adenocarcinomas which originate from the epithelial cells of the mucosa [14].

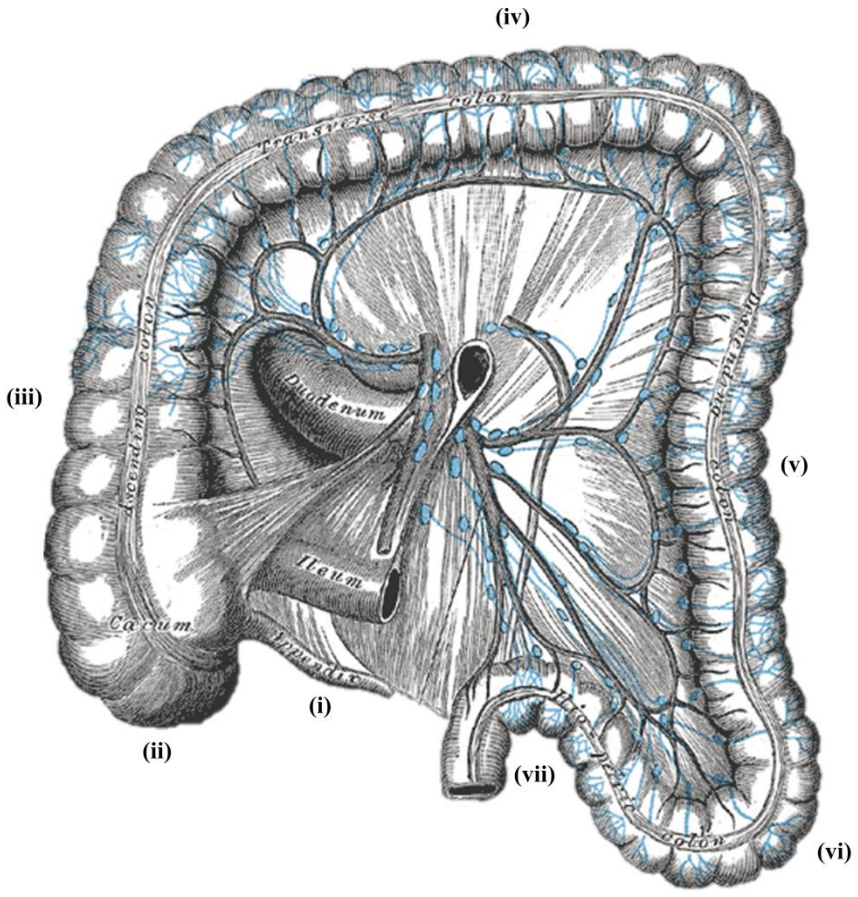

Figure 2.1: Anatomy of the colon showing (i) appendix, (ii) caecum, (iii) ascending colon, (iv) transverse colon, (v) descending colon, (vi) sigmoid colon, (vii) rectosigmoid junction, (image adapted from [15]).

2.1.1.1 Diagnosis

Diagnosis of colorectal cancer is made on the basis on the results of colonoscopy or sigmoidoscopy with tumour biopsy [16]. Following identification through biopsy, physical examination and a CT of the chest, abdomen and pelvis is routine for definition of metastatic disease. Additional assessment may involve CT colonography, PET, MRI and ultrasound among others in order to define the best treatment option [16]. Following assessment, staging of the malignant tumour is made in accordance with the TNM (tumour, node, metastases) system [17]. The system defines the extent of the primary tumour (T0-T4) (shown in Figure 2.2), the level of lymph node involvement (N0-N3), and absence or presence of distant metastasis (M0 or M1) [17].

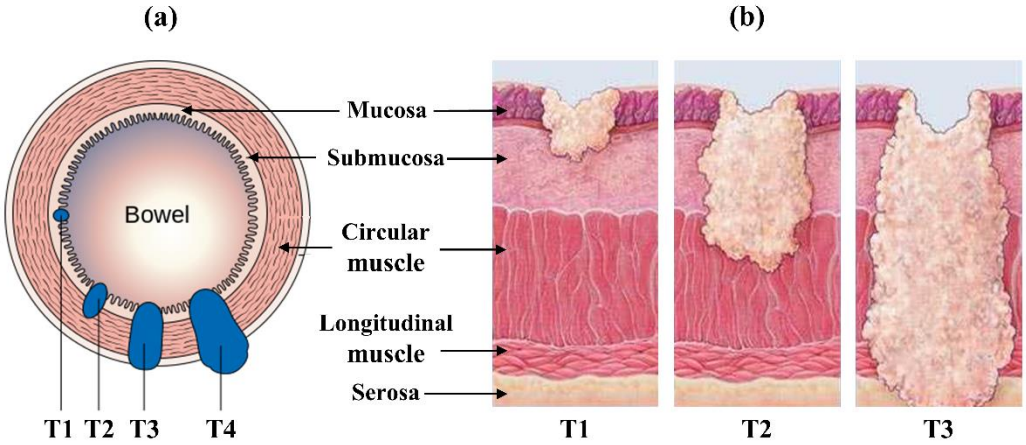

Figure 2.2: Primary tumour staging for colorectal cancer, showing (a) full bowel section view with examples of T1-T4, and (b) section view of wall with layer penetration shown for T1-T3; (image (a) adapted from [18], image (b) adapted from [19])

2.1.1.2 Treatment

Management of this disease in modern medicine has most commonly been through surgical intervention [20]. This is due to surgery offering the highest cure rate for colorectal cancer [21, 22]. Surgical treatment involves the total resection of the tumour including adequate margins (5 cm or more is recommended), as shown in Figure 2.3, along with removal of surrounding lymph nodes (lymphadenectomy) to allow nodal staging [16]. Surgery may be combined with pre or post-operative radiotherapy, chemotherapy or chemoradiation in order to improve the efficacy of the surgical procedure and overall treatment outcome. Unfortunately, surgical resection does not always offer a cure. Cancer recurrence can take place at the site of the primary tumour or within distant organs (typically the liver or lungs in colorectal cancer patients) long after the initial treatment [16].

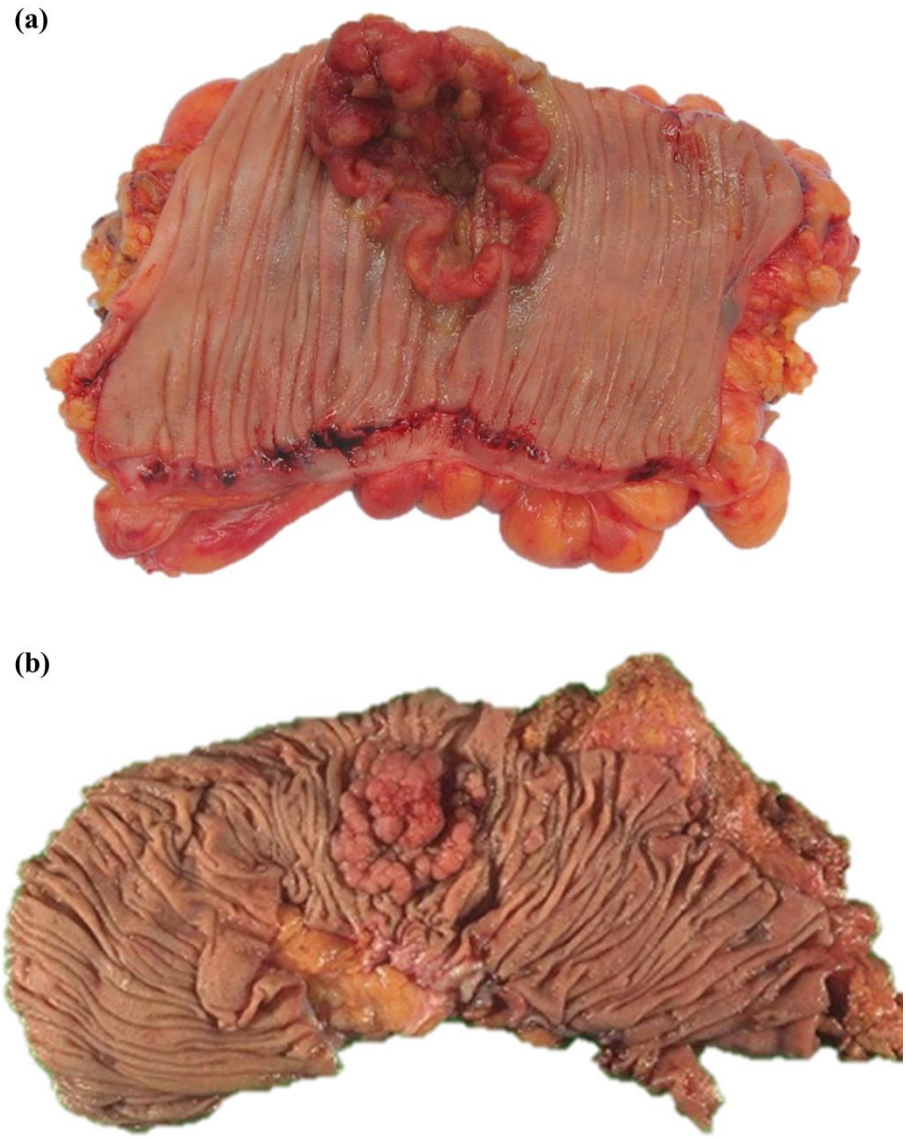

Figure 2.3: Examples of resected colorectal cancerous tumours within the colon, showing (a) invasive colorectal carcinoma (reddish, crater-like and irregularly shaped), and (b) adenocarcinoma arising from a villous adenoma (polyp), located within the sigmoid colon; (image (a) adapted from [23], image (b) adapted from [24])

2.1.1.3 Histopathology

The resected tumour and lymph node tissue will routinely undergo histopathological assessment. That is to study the tissue structure on a cellular level through the use of a light microscope. For the large volume of tissue removed during colorectal cancer surgery, it is necessary to prepare and thinly section the tumour in order to allow light transmission for suitable viewing. To allow sectioning, the tissue specimen will be fixed in order to avoid enzymatic or bacterial digestion. Chemical fixation is typically achieved using a buffered isotonic solution of 4% formaldehyde [25]. Fixed samples are embedded in paraffin or plastic

resin to deliver a supporting structure for thin sectioning (1-10 μm). Sections are floated on water and mounted onto glass slides. Staining is typically applied to allow improved viewing of colourless tissue and to aid in distinction of different components. The most common dye combination is hematoxylin and eosin (H&E) [25]. These slides can then be viewed using light microscope and micrographs produced. Figure 2.4 shows a range of example histopathology micrographs for healthy and cancerous colon tissue.

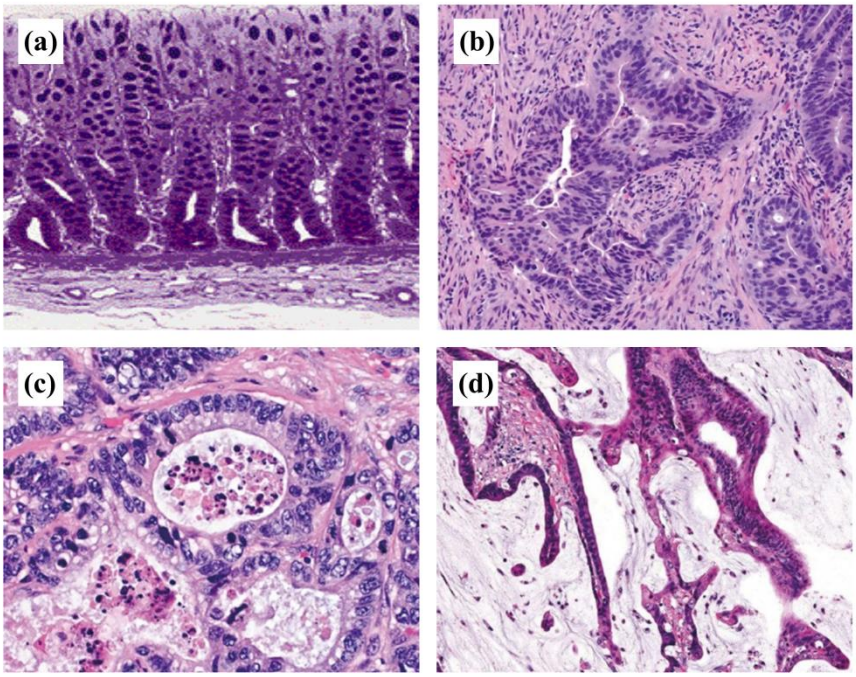

Figure 2.4: Histopathology micrographs of epithelial cells of the colon, showing (a) section of normal mucosal cells, (b) a moderately differentiated adenocarcinoma, (c) necrotic debris within lumina od adenocarcinoma glands and (d) mucinous adenocarcinoma, (image (a) adapted from [25], images (b)-(d) adapted from [14]).

2.2 Surgical intervention

Surgical oncology remains the most commonly used and most effective (in terms of cure rate) cancer therapy [21]. The success of modern surgery would not be as great if not for continual technological innovation and decades of applied research. Most notable is the advent of numerous pre-operative diagnostic techniques which have allowed for better surgical planning and more patient specific treatment. Additionally, functional changes have been seen with the introduction of Laparoscopic surgery and recently Robotically Assisted Surgery (RAS). Introduction of these factors has shown significant benefit to the patient in terms of earlier recovery of bowel function and reduced hospital stay [26]. However, some classic surgical problems remain, and new issues are apparent from the increased complexity of surgical setup.

The following sections detail the state of the art within surgery and describe some of the general themes that may be present within its future.

2.2.1 Laparoscopic surgery

Reduced access surgery, termed Minimally Invasive Surgery (MIS), was originally introduced in 1983 as a method for performing appendectomy [27]. Laparoscopic surgery is a subset of MIS and is performed by inserting specialised tools into small incisions made around the region of interest. Procedures are commonly performed laparoscopically to treat gynaecological, urological, gastrointestinal and bariatric conditions. For the example of gastrointestinal surgery, incisions are made through the patient's abdominal wall, allowing access to the tissues within the abdominal cavity. A schematic comparison of open and laparoscopic surgery is presented in Figure 2.5.

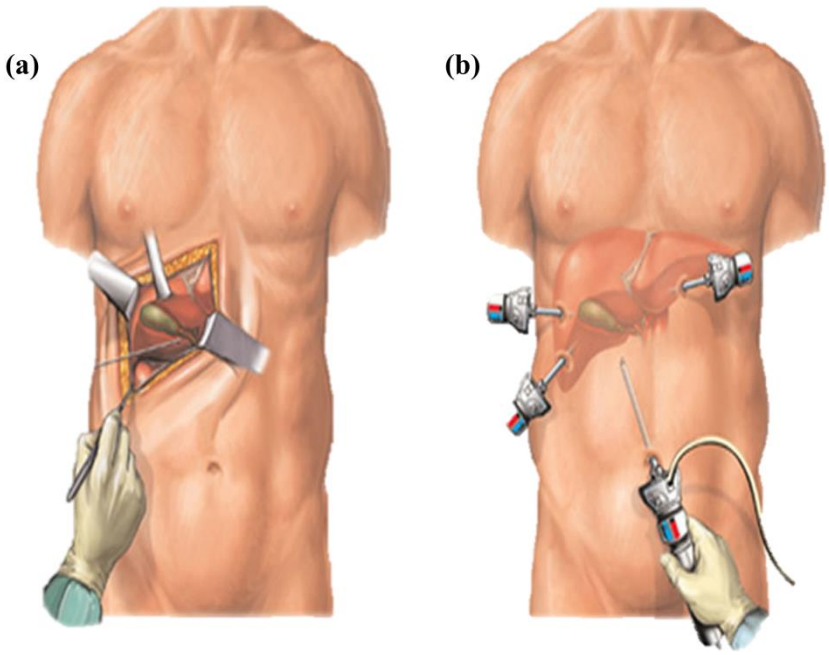

Figure 2.5: A schematic example of surgical access during a cholecystectomy (gall bladder removal) within (a) open surgery and (b) laparoscopic surgery, (images adapted from [28]).

To avoid internal injury, specialised tool ports (trocars) are manually pushed through the abdominal wall via superficial scalpel incisions [29]. This is the first of numerous practical considerations that are addressed within a modern laparoscopic procedure. Some of the other areas that have been addressed, particularly relating to procedures performed within the abdominal cavity, are:

Access: *As previously mentioned, access to the abdominal cavity is facilitated through the use of small holes in the abdominal wall. The port tool (trocar) acts to safely pierce the wall and to provide a stable access point for laparoscopic tools. Ports remain stationary relative to the tissue reducing potential trauma from tool manipulation. Access ports range from (3-30 mm), with 5 and 10 mm being most commonly used [30]. One limitation of this access method is that removal of tissues must be carried out through these same incisions.*

Manipulation: *Tissue manipulation is achieved through the use of laparoscopic tools. These typically consist of ergonomic handles attached mechanically to a distant end effector through a long thin shaft [31]. Primary tools include graspers and scissors, allowing tissue retraction and stabilisation for tasks such as cutting and suturing. Trocar ports are positioned in a triangulated pattern to allow for bimanual control, akin to open procedures. Particular issues arising from this arrangement are the inversion of movement through the trocar fulcrum and the reduction of haptic feedback [31, 32].*

Vision: *As no direct visualisation of the tissue is possible without a larger incision (laparotomy), specialised scope cameras are used to view internal structures. These scopes provide a light source as well as a 2D camera feed. Management of heat, light intensity, transmission, processing and presentation is required for a suitable image to be achieved [31].*

Intervention: *The nature of laparoscopic access necessitates that all contacting interventions be introduced through the trocar ports (or a natural orifice).Reducing the numbers of ports (and therefore incisions) has been investigated for certain procedures. Single port systems have been developed and tested, producing reduced scaring [33].*

2.2.2 Robotic surgery

The advent of robotic assistance in theatre is arguably the greatest surgical advance over the past two decades. Robotics were implemented into the operating theatre to augment surgical ability allowing precision and dexterity beyond human capability [34]. Many instances of robotic technology integration within surgery have been investigated, from needle guided brain biopsy to bone coring for hip replacement [35]. However, in modern surgery the most common

robotic assistance is delivered by the da Vinci surgical system (Intuitive, Inc., Sunnyvale, CA). The da Vinci system (Figure 2.6) is comprised of a control and vision console and a bank of robotic manipulators. One of the principle aims of the system was to allow the surgeon to remotely control the motions of the robotic arms, allowing for operating at a distance (telesurgery) [36]. However, it is the benefits of increased dexterity and movement precision that have made the system so popular within MIS procedures.

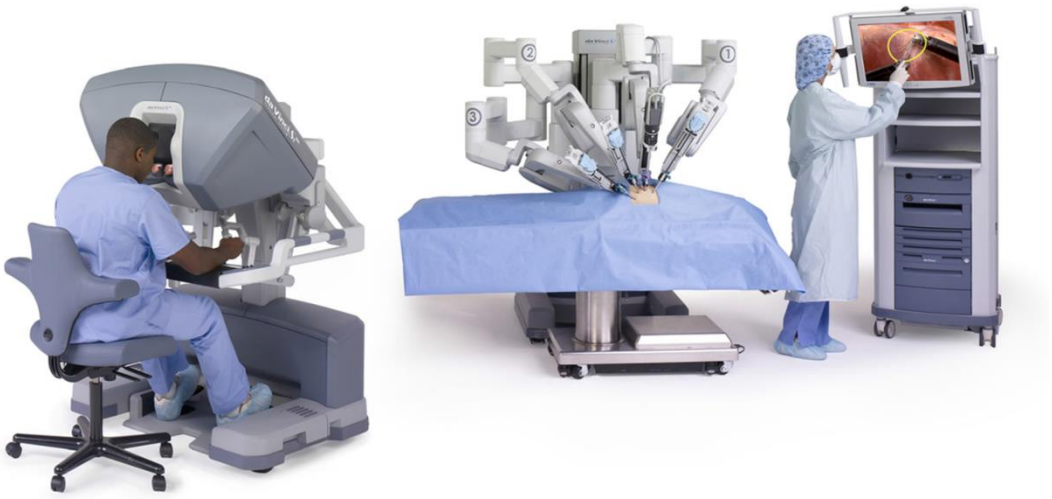

Figure 2.6: The da Vinci Si HD Surgical System, showing the surgeon at the console and the patient side cart [36].

Aside from the equipment cost and size, one issue with the da Vinci system is the lack of haptic feedback. This reduces the ability for discrimination of tissue consistency (e.g. stiffness), which can be important in identifying abnormal tissue [37]. In addition, no direct force regulation can lead to tissue damage and cause suture material breakage [38]. Although this is a limitation of current systems, separation of the surgeon from the tissues allows for integration of novel sensing and feedback modalities. This may allow the surgeon to obtain new types of data aside from, or in addition to, force/tactile data, which could give a more quantitative assessment of tissue health.

2.2.3 Future developments

Surgery in the future may become obsolete, due to improved diagnosis, radiation and drug therapies. However, there is currently no suitable replacement for surgery and much effort is still applied to its advancement. Some of the most prominent themes within surgical development are discussed in the following sections. All of which are suitable for the integration of advanced sensing, and in the case of smart theatres with robotic autonomy, improved sensing will be imperative.

2.2.3.1 Natural Orifice transluminal endoscopic surgery (NOTES)

Pure NOTES procedures are those performed with oesophageal, gastric, vaginal, colonic or urethral/vesical access only [39]. Specific surgical procedures where NOTES would be most appropriate have not been fully defined although research has mostly focused on cholecystectomy, peritoneoscopy and gastric surgery [40]. Improved triangulation and access may be achieved using a multiple orifice approach or through combination of NOTES with laparoscopic intervention [39]. The future of NOTES is not certain although it remains an active and growing research area [40].

2.2.3.2 Single Incision Laparoscopic Surgery (SILS)

As the name suggests, SILS consolidates the multiple incision points of traditional MIS procedures into a single port. This requires significant modification of laparoscopic tools to operate with restricted access. In a similar aim to NOTES, SILS looks to reduce the access trauma and scarring to improve patient comfort and recovery [39]. Problems with limited triangulation, tool clashing and tool manipulation difficulties have been reported and some adequate solutions presented [39]. SILS offers a simpler practical transition from traditional laparoscopic surgery and is a likely stepping stone on the way to pure NOTES procedures. In either modality, the benefits of better cosmesis and pain reduction must be assessed against the increase technicality, risk and cost of procedures before adoption can be supported [39].

2.2.3.3 The smart theatre

Nordlinger [41] proposes a combined approach surgical management where smart devices, the Internet of Things (IoT) and big data come together to improve surgery and reduce costs. In this scenario information from the surgical tool would be uploaded to the cloud, processed and then returned to device manufacturers and to the theatre where it can be combined with MRI or CT data in near real-time. Although this is highly conceptual, the general idea of having improved integration of technology and access to data (pre-operative and real-time) has been proposed as means of improving safety, efficiency and reducing cost of surgical procedures [42]. Kopelman et al. [42] describe some of the potential prospects for a collaboratively designed next-generation operating room. Of note are: the use of open plug-and-play standards for medical devices; the use of real-time or semi-real-time CT or interventional MRI data; and the application of augmented reality with co-registration of visual and diagnostic images [42].

With the increased frequency and range of procedures conducted with robotic assistance, there is also a real opportunity for increased autonomy. Most autonomous interventions performed to date have been within orthopaedic or neurosurgery where there is typically a stable material for stereotactic instrument orientation [43]. It is feasible that with improved sensing

and co-registration of preoperative imaging that autonomous interaction with soft tissue will be achieved (e.g. cutting, suturing and ablating).

Realisation of a smart operating theatre will require redesign of current equipment, patient management and surgical procedures. It is evident that there is a clear need for improved intraoperative sensing modalities to move towards real-time, personalised and even automated surgery.

2.3 Tissue assessment methods

Evidence suggests that the surgical resection of cancer may benefit from being personalised [3, 4]. This may allow for a reduction in the radical nature of surgery, improving outcomes for the patient. Integration of such a treatment model requires more detailed data regarding tissue health than is currently available through standard preoperative imaging techniques. In the context of cancer surgery, identification of a region of abnormal tissue can only be achieved through assessment of its properties. For identification to be confirmed, the properties examined must be compared for to those of a healthy specimen or evaluated for similarities with known disease types. This process is necessary for simple visual examination through to intricate chemical analysis of tissue cells. For a particular process to be effective at diagnosing the abnormality the targeted property should be specific to the disease type and the equipment used to measure it must allow accurate and precise evaluation of this property. The practicalities associated with the measurement site must be considered for proposed sensing modality.

Balog et al. [44] recently developed a surgical tool (iKnife) for intraoperative tissue assessment during brain surgery. The technique uses rapid evaporative ionization mass spectrometry to analyse the vapour produced during electrosurgical tissue dissection. Early stage testing has indicated a 100% (81 cases) positive identification of cancerous tissues using multivariate statistical methods [44]. Although measurements are destructive in nature, the near-real-time characterisation may allow for personalised tumour resection and help to reduce cancer recurrence.

Development of alternative intraoperative assessment techniques has been the focus of much research. Attention has been focused on direct measurement of mechanical [7] and electrical properties [8], and on imaging using passive and active agents [5, 6]. Many additional technologies have become relevant to the surgical setting, with electrochemical sensing (including biosensors) being the most prominent. Each of these areas have a wide research scope, however, the focus of this review is on those techniques that have been considered surgically appropriate in terms of tool integration, either in their current state or with advancement of enabling technologies. To this end, methods of mechanical and electrical tissue

property assessment forms the major focus of the review. In addition, discussions of biosensor technology and some new surgical imaging techniques under development have been presented.

2.3.1 Mechanical properties of tissues

Mechanical property estimation of biological tissues has been the focus of widespread research. As these properties are fundamentally based on the micro and macroscopic structure of tissue, they are influenced by changes in physiology [45, 46]. Abnormal processes, such as neoplasia of cancer cells, may therefore induce significant changes from the normal tissue stiffness range [47-49]. Medical examination of soft tissues through physical manipulation (palpation) utilises stiffness as a key indicator for making a primary clinical diagnosis. In women this is particularly prevalent for breast examination, where screening programs for cancer have contributed to the lowering mortality rate [50, 51]. In men initial diagnosis of prostate conditions including prostatic cancer are still made using physical assessment [52]. Manual palpation is, however, not always an option and remains highly subjective in nature. To this end, much research has been conducted to establish novel methods and tools for assessing the mechanical properties of soft tissues.

2.3.1.1 Mechanical modelling

Tissues respond to applied stress (σ_m) through relative motion, in a static sense this is the tissue strain (ε_m). Many assumptions are made for the mathematical analysis of tissue, often being considered *linear* (direct relation of applied stress to observed strain), *elastic* (tissue returns back to its pre-deformation state after applied load is removed), *isotropic* (mechanical properties are not orientation specific) and *incompressible* (no change in volume). Under these assumptions the stress-strain relationship is greatly simplified to the Hookean relationship of equation (2.1), where E_m is the Young's modulus of the material [53].

$$\sigma_m = E_m \varepsilon_m \tag{2.1}$$

With the assumptions of equation (5.4) the tissue can be characterised by a single number, the Young's modulus, E_m. This parameter is theoretically independent of stress conditions on the tissue and allows simple direct comparison between tissue types. However, a model under these assumptions is not generally appropriate for describing the complex relationship between tissue stress and strain. The infinitesimal deformation theories applied to metals and hard plastics for such mechanical property assessment do not translate well to soft tissues [46].

Tissues are made up from cells and intercellular structures such as collagen, elastin and connective tissues. The relative locations, distribution and orientation of these elements make soft tissues inherently inhomogeneous, and anisotropic [46]. Time dependent alterations also occur during tissue loading giving creep (change in strain with constant stress) and stress relaxation (reduction in stress under fixed strain). Advanced modelling is therefore required in order to accurately capture the complexities of soft tissues during loading.

A vast number of more comprehensive models have been developed and tested. These may account for elastic response with directional dependence (anisotropic) and/ or compressibility [45], viscoelastic behaviour with tissue creep or stress relaxation [54, 55], and in some cases poroelasticity [56]. To determine a suitable tissue property for comparison, be it the elastic modulus E_m (resistance to uniaxial stress), bulk modulus K (resistance to uniform compression), shear modulus G (resistance to shear), or indeed a time-varying viscoelastic or porous model component, it is necessary to apply a known stress condition to the tissue and measure the relative displacement (or vice versa). Many techniques have been developed to allow tissue properties to be determined. Ultimately, this is the remit of mechanical property transducers.

The essence of mechanical property measurement is the application of energy to the target material while monitoring the applied stress and spatial variation. Methods have been developed using contact force and displacement (strain) measurement, both statically and dynamically, as well as through ultrasound based imaging. These modalities have been described and some of the benefits and limitations discussed. Only literature relevant to the context of medical diagnostic devices has been considered.

2.3.1.2 Contact force measurement

Contact force measurement is arguably the simplest way to obtain information about tissue properties. The method makes use of sensors either in contact with the tissue (direct) or situated away from but linked to the tissue (indirect). The loading and therefore positional alteration of internal sensing components will cause a measureable change, often a change in electrical resistance (e.g. load cell strain gauge). When configured into appropriate external circuitry, a suitable voltage or current response is generated that can be calibrated to determine the physical force applied over a working range.

Tholey et al. describe an integrated laparoscopic tool capable of measuring grasp, longitudinal and lateral force during tissue manipulation [57]. The design makes use of a piezoresistive sensor in order to meet the size constraint involved while successfully characterising soft, medium and hard artificial tissue. This type of sensing offers a pragmatic solution to relay a level of haptic feedback during MIS, however, the localised measurement and

lack of parameterisation techniques make it less suitable for large scale assessment of soft tissues. To address this, Zbyszewski et al. [58] developed a method of measuring the stiffness distribution over a wider spatial area. Their system makes use of a roller-ball supported by a pressurised air cushion. Displacement of the ball is measured using fibre optics, allowing the measured displacement to show differences in tissue stiffness produced by abnormalities. Zbyszewski et al. [59] compared the sensor to a wheeled equivalent system with similar results being shown for both systems. Figure 2.7 shows the air cushioned system and the results obtained from testing of a silicon phantom.

The roller-ball mapping technique allows a large area to be assessed but localised measurement is not supported as in the case of the instrumented grasper. Also the roller-ball becomes an additional tool (rather than an extension of functionality of a current tool) which could require extra port incision or prolonged operating times.

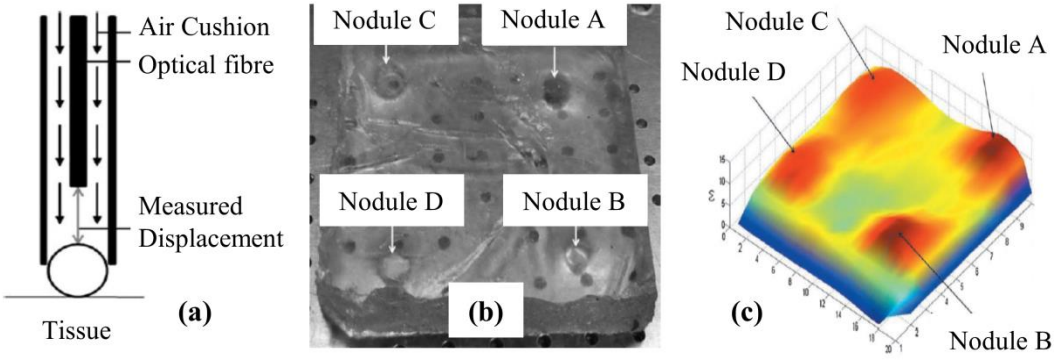

Figure 2.7: Air cushioned stiffness sensing system: (a) schematic of the sensor probe, (b) silicon phantom assessed using the tool showing stiffer nodule locations, and (c) the output voltage as a function of position, shows increased voltage around the stiffer inclusions (nodules) [59].

2.3.1.3 Dynamic palpation

An alternative approach to mechanical property characterisation of tissues was proposed by Phillips et al. [60]. The method of dynamic palpation involves the application of cyclic compressive strain to tissue while the corresponding load is monitored. Application of this technique has primarily been focused on evaluation of *ex vivo* prostatic tissues for benign prostatic disease (benign prostatic obstruction and benign prostatic hyperplasia) [60] and malignancy [49, 61], although it has also been applied to the human eye for intraocular pressure assessment [62, 63]. Typically, an amplitude ratio $|E^*| = \sqrt{E_1^2 + E_2^2}$ and phase angle $\phi = tan^{-1}(E_2/E_1)$ will be determined based on comparison of the stress and strain measurements [63]. In this case E_1 and E_2 represent the real part (storage modulus) and imaginary part (loss modulus) respectively. This is analogous to the electrical technique of Bioimpedance Spectroscopy (BIS) discussed within Section 2.3.2.2.3.

Initial dynamic palpation systems comprised of a mechanical shaker to provide tissue excitation using a hemispherical probe tip and an axial load cell [60]. This type of system is practically unsuitable for *in vivo* prostate examination. Recent work by the same research group has been focused on this aspect, developing a dynamic palpation sensing tool ('eFinger') suitable for *in vivo* prostate assessment [64]. A custom thin composite structure was produced using a multi-layer technique [65], with an integrated strain gauge and flexible membrane for tissue interaction. Membrane actuation was achieved pneumatically with a compressed air supply and electronically controlled valve [64]. Flow pressure into the device was monitored with a pressure sensor and used in conjunction with the positional response of the integrated strain gauge to determine stiffness parameters. Figure 2.8 shows the typical response of the two signals along with a fitted profile based on Fourier series analysis.

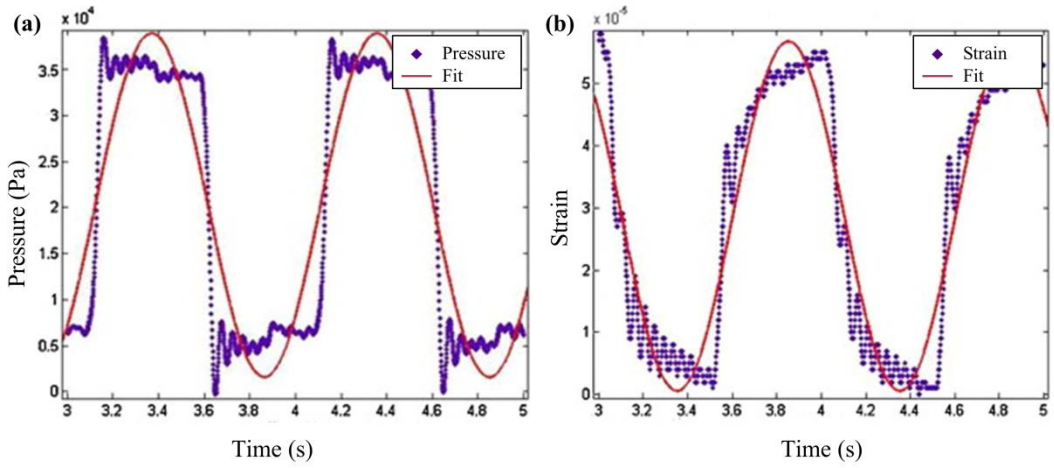

Figure 2.8: Example raw and Fourier fit dynamic palpation results obtained using the eFinger for (a) pressure and (b) strain; results adapted from [64].

It is evident that there is a significant level of noise within the system, making the fitting model highly idealised for the measurement. Assessment of cadaver tissues (bladder, prostate and smooth muscle) was performed and compared to manual digital palpation. Differentiation of the different tissue structures was evident using the eFinger, and this was in agreement with manual palpation [64]. Spatial mapping of *ex vivo* diseased prostate tissue using the eFinger at different frequencies (5, 10, 15 Hz; 0.5 bar) was also conducted and correlated with manual evaluation *in vivo* and *ex vivo*. Findings again indicated agreement with manual palpation, and show that performance is best at low frequencies [64]. This work demonstrates the complexity required for contact measurement systems aimed at *in vivo* testing. Promising results have recently been obtained using dynamic palpation. However, there is still a requirement for controlling operating conditions such as contact pressure in order to optimise the sensor performance.

2.3.1.4 Elastic imaging (elastography)

A wide range of methods have been investigated and developed with the aim of imaging the stiffness distribution of region of interest (ROI). In contrast to the mechanical property assessment techniques previously described, elastography modalities are typically based on indirect contact with the tissue of interest and deliver a spatial distribution of tissue stiffness. Some of the most promising techniques in this field have been presented in the following sections.

2.3.1.4.1 Ultrasound

Ultrasound, (US) as the name suggests, refers to waves that are above the highest human audible frequency of 20 kHz. In diagnostic medical US imaging, frequencies are generally found in the range of 1-10 MHz [66]. When pressure waves meet a boundary between two different materials a certain proportion of the wave is reflected, with the attenuated wave continuing into the second medium. The level of attenuation depends on the echogenic properties of the two materials. More specifically this depends on their relative acoustic impedance, which is calculated as the product of the material density and the speed of sound through the material. As certain biological interfaces have different acoustic impedances, US waves passing through the body will reflect and be detectable. This means that for a single scan line an amplitude against time can be produced, which can be converted to amplitude position information through assumptions regarding the speed of sound through the body. Recording multiple scan lines allows the amplitude position data to be converted to a two dimensional image [67].

The relatively low cost and portability of US scanners has given them a firm place within diagnostic imaging based solely on echogenic properties of tissue. However, over the last two decades various methods have been developed to utilise US to obtain the elastic property distribution within tissues. The motivation for this work was often to create and imaging system capable of detecting inhomogeneous lesions within tissues, such as cancers of the prostate, which often show little clarity on standard US images. The early work can be generally grouped into three methods, as described by Taylor, 2000 [68] as: vibration sonoelastography, compressive/quasi-static elastography-strain imaging, and transient elastography.

There has since been steady development of these techniques, taking advantage of the improvements to US systems and computational power. Also, a number of additional modes of elastic imaging making use of US (with the exception of Magnetic Resonance Elastography) have been introduced. Parker et al. [69] recently gave an overview of the development of elastic imaging in the form of a timeline, as shown in Figure 2.9.

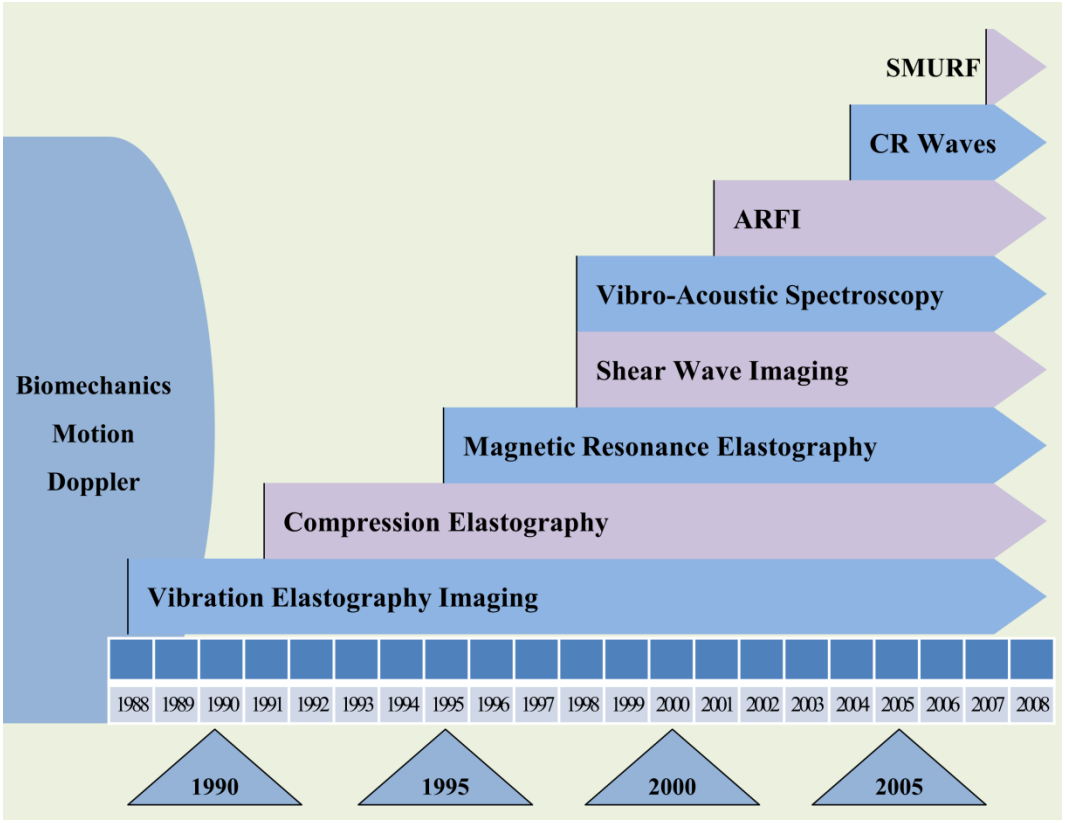

Figure 2.9: 20 year timeline of the developments in elastic imaging of biological tissues; (adapted from [69]).

2.3.1.4.2 Vibration Sonoelastography

The techniques involved in vibration sonoelastography were first implemented in a non-imaging application in 1987 by Krouskop et al. [70]. Lerner and Parker et al. [71, 72] actually coined the term "*sonoelasticity*" in early development of a qualitative tissue stiffness measurement technique. In principle, the process involves (1) subjecting tissue to continuous shear wave excitation, and (2) calculating the vibration amplitudes within the tissue ROI. Shear wave propagation is achieved through direct contact of a mechanical vibrator with the tissue. Driving frequencies applied are low (20-1000 Hz) with amplitudes of less than 0.5 mm (typically 0.1 mm). Continuously applying the driving force induces a fixed oscillation distribution within tissue. For a fixed intensity wave the amplitude of vibration inside of an inclusion of higher shear modulus will be reduced. Imaging the distribution of amplitudes indicates the relative shear modulus distribution. The method of determining the amplitudes of vibration uses a pulsed-Doppler technique, assessing the variance of the power spectrum of returned US to indicate amplitude distribution, a method described in detail in [68].

2.3.1.4.3 Compressive/quasi-static elastography-strain imaging

The quasi-static method of imaging the elastic properties of tissue requires (1) taking an image of the tissue prior to any deformation, (2) applying a load to the tissue, (3) taking an image of the deformed tissue [73]. The application of load can be applied using the US probe to manually compress tissue. Alternatively, mechanically controlling the step compression of the probe has been investigated [74], and even the use of physiological pressure changes of the vascular system to compress tissue [75]. The motions of the tissue under compression can be determined using cross-correlation techniques [76]. It is important to note that this method assumes uniform stress application and produces only images of the tissue strain, meaning the elasticity image only gives an indication of the relative elastic distribution.

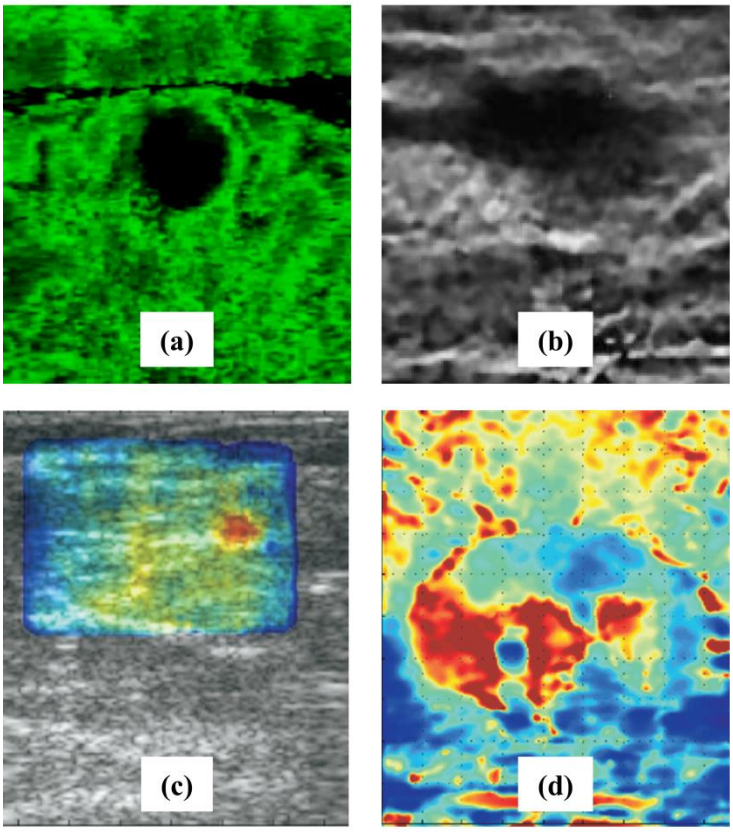

Figure 2.10: Examples of elasticity images obtained using different US based techniques, showing (a) vibration-amplitude image showing delineated stiff region within phantom model [77]; (b) invasive ductal carcinoma from breast compression based elastogram [76]; (c) small ductal carcinoma shown as stiff (red) region; image generated using Supersonic Shear Imaging [78]; and (d) elastic image of prostate *in vitro* showing two focal carcinomas, obtained using crawling wave elastography [79].

Compression elastography methods have been used in clinical trials for strain imaging of cervical lymph nodes [80]. A qualitative scoring system was used to assess nodes, leading to 73% accuracy and 83.8% specificity in detection of malignancy (results compared to those from routine fine needle aspiration for cytology). This highlights that qualitative elastography is

capable of detecting malignancy but the accuracy in identification by the observer is still too low for routine clinical adoption.

Numerous other methods have been developed using US and US transducers as a fundamental element in imaging elastic properties. Of particular note is a commercial elastic imaging device (FibroScan®, Echosens, Paris, France), developed to allow quantification of liver fibrosis non-invasively [81]. A number of review articles have been published by some of the founding researchers in the field; attention is directed toward Ophir et al. [76] or Parker et al. [69] for more comprehensive descriptions of a number of these methods. Some of the images obtained using different techniques have been presented in Figure 2.10.

2.3.2 Electrochemical and electrical properties

Measurement of the electrochemical and electrical properties of biological fluids and tissues has been the subject of research for more than a century [82]. These properties are based fundamentally on the chemistry and physiology of the cells and tissues. Therefore, much research has been conducted to assess the feasibility of measuring these in a diagnostic sense. Characterisation of this nature is a broad field with a primary division between electrochemical methods and electrical methods. However, in many cases consideration of both aspects is essential to achieve a successful measurement. This section presents relevant techniques currently used to measure and interpret electrochemical and electrical properties of biological systems.

2.3.2.1 Electrochemical characterisation

This type of characterisation is concerned with defining electrical behaviour induced by chemical reactions at the interface of an electrode [83]. The interface is the point at which the electrode (usually a solid metal) meets with the electrolyte (fluid analyte). Redox reactions within the interface region cause generation and removal of free electrons. The electrode facilitates the transfer of electrons, effectively allowing cathodic and anodic reactions to remotely influence each other. As an example, oxidation of a species at the anode will cause the production of a metal cation and at least one electron. This will be held by the metal electrode causing an accumulation of charge on the electrode. This excess of electrons may then supply a cathodic reaction at a different location on the electrode. Thus the redox reaction is completed and electrode charge is restored.

The described example is for a single electrode however, this can occur between two similar or different remote electrodes provided they are electrically and ionically (i.e. through the salt bridge) connected. The electrode reactions induce a charge separation between metal and solution phase. This is known as the electrode potential, and is specific for reactions under

chemical equilibrium [84]. The rate at which oxidation and reduction occur determines the number of electrons flowing through the metallic elements of the cell, and therefore the cell current. The performance of the cell in terms of electrode potentials and current flow can be used to infer information regarding the interface reactions and cell kinetics. Fundamentally, these characteristics are the focus of electrochemical assessment techniques.

2.3.2.1.1 Electrode potentials

In the simplest sense, assessment of electrode potentials at various tissue interfaces may show specificity for tissue condition. Any differences noted may be caused by different reactions and/or chemical equilibria. Muriel et al. [85] presented a study to determine the electrode potentials at tissue interfaces under a wide range of conditions. Silver-silver chloride electrodes were used to measure the potential between the parietal peritoneum and the tissue of interest. The primary measurements were on live guinea pigs under light ether anaesthesia. Factors of influence included age, level of anaesthesia, surface temperature, ischemia (canine tests) and time after death. The results showed that many of these factors apparently cause an altered electrode potential. However, changes were minor (< 10mV), being within healthy tissue type variation as shown in Figure 2.11. Results also showed inconsistencies with varied condition and with results from other studies. It was noted that some influences found were likely to be caused by changes in the reference tissue. This highlights that the Ag/AgCl measurement electrode used was not appropriate as it is highly non-polarisable and therefore insensitive to small changes in the tissue (interface) chemistry.

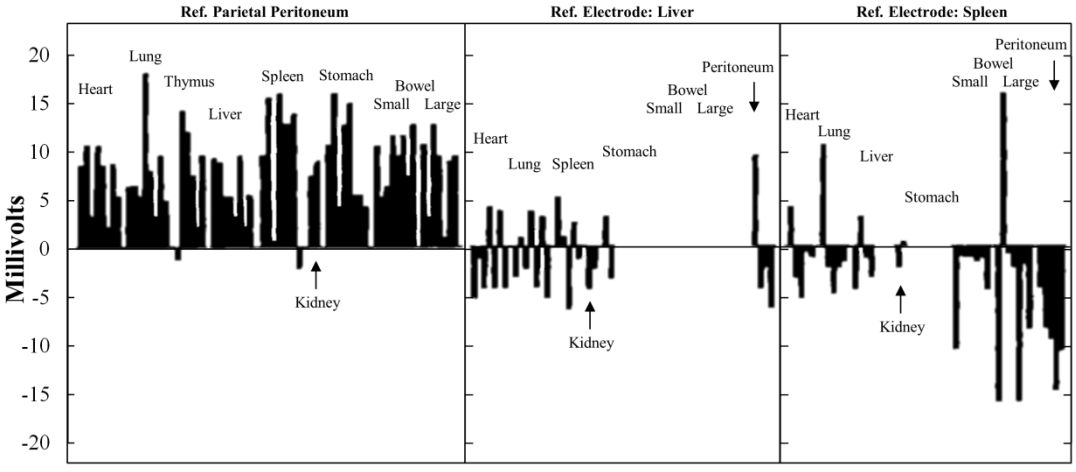

Figure 2.11: Electrode potentials for various guinea pig organs measured with three different reference tissues; (adapted from [86]).

A much greater potential shift was found by Gensler [87] when assessing would healing in plant tissue using noble metal (palladium) measurement electrodes. Transient increasing potentials were found for wound healing and re-wound healing with positive potential shifts of around 300 mV. Of more direct relevance to surgical oncology, a number of studies have looked at electrode potentials of healthy and cancerous tissues [88-90]

Morris [89] tested electrode potential assessment as a method for determining the state of breast lesions. Lesions were identified through palpation or mammography and electrode potential tests performed as part of the routine biopsy procedure. The predictive nature of the measured potential was assessed, with the technique showing only 50% accuracy. However, of three malignant lesions tested all were correctly identified. A different study examined the use of direct current stimulation as a means of tumour growth retardation [90]. The electrode potential was used as an assessment metric for comparison to an untreated control group. Although microscopic examination of the mice tumours following the treatment showed high levels of necrosis, no significant difference in electrode potentials were found.

The findings from electrode potential measurement indicate that this parameter may relate well to physiological processes and act as a specific marker for determining tissue type and health. However, the experimental setup in terms of electrode selection is critical and many factors have been shown to cause changes in potential. A suitable inference from the published work is that electrode potentials measured with standard materials (Ag/AgCl or noble metals) are susceptible to artefact bias when used within general tissue interaction. Application under more controlled conditions, modification of electrode materials or coupling with additional sensing modalities may allow for improved leveraging of this property.

2.3.2.1.2 Biosensors

The development of biosensors was a natural progression from standard electrode potential measurements, and is now arguably the most prolific research field relating electrochemical sensing of biological systems. Original bio-sensing was targeted at measuring pH, with Michaelis and Davidoff [91] analysing lysed red blood cells and Michaelis and Kramsztyk [92] measuring the pH of various mammalian tissues. Additional effort was focused on the development of a suitable electrode configuration for determining oxygen concentration [93]. A radical shift in bio-sensing technology occurred with the addition of immobilised enzymes to the electrode surface, broadening the range of possible analytes [94]. The advent of a bio-recognition component (e.g. enzyme, antibody, aptamer or cell) allowed development of sensors specific to a wide range of biological targets [93]. A schematic of the working principle of a modern electrical property based biosensor along with an example of a manufactured device is shown in Figure 2.12.

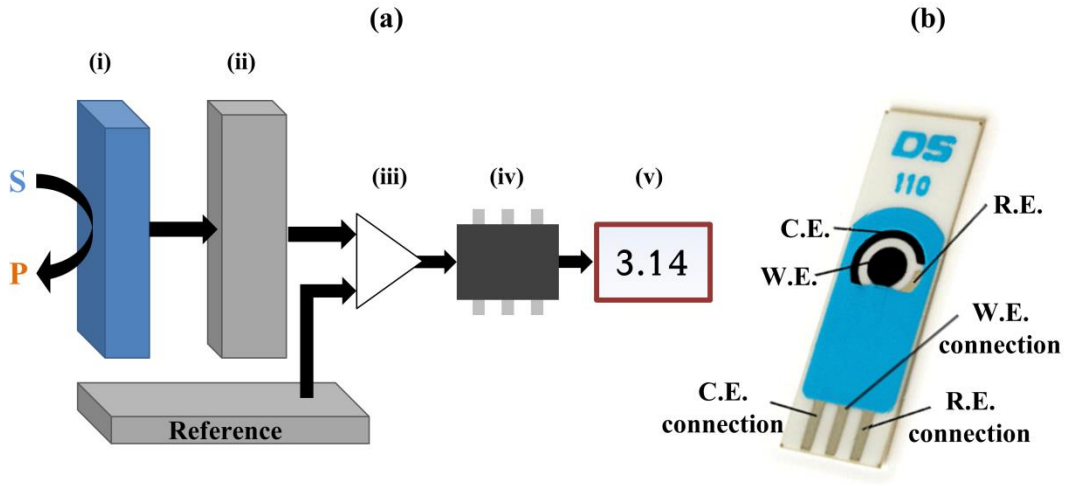

Figure 2.12: Biosensors, showing (a) a schematic of the typical components within a biosensor: (i) the bio-recognition component (substrate (S) to product (P) reaction), (ii) the working electrode (WE) transducer, (iii) electric signal conditioning elements, (iv) processor and (v) display, and (b) an example screen printed biosensor showing working electrode (WE), counter electrode (CE) and reference electrode (RE); ((a) adapted from [95], (b) adapted from [96]).

Particular attention has been devoted to the development of glucose biosensors [97], with the aim of improving the management of diabetes. Amperometric (current measurement from applied potential) methods have been widely developed and utilised in an enzymatic and non-enzymatic form. The driver for the latter being improved long-term stability relative to enzymatic systems [97].

Research has also explored the use of biosensors for the detection of cancer biomarkers [98]. Biomarkers are typically found within blood, urine or tissues and give objective indication of normal biological processes, pathogenic processes or pharmeaceutical response to therapeutic intervention [99]. Testing in this way has the potential for detection of malignancies prior to metastatic dissemination [100]. Li et al. [98] give a comprehensive review or the types of biomarkers assessed and the associated bio-sensing technology. The concentration of biomarkers expressed within tissues is noted as being of very low concentration, necessitating biosensors of very high sensitivity with a low Limit of Detection (LOD).

Assessment of the tumour microenvironment may offer a number of alternative biomarkers that can be determined using direct tissue contact bio-sensing. Vaupel et al. [101] detail a number of variable factors within the tumour microenvironment, indicating a reduced oxygen concentration (pO_2) and increased glucose consumption. For the measurement of oxygen concentration, Kieninger et al. [102] developed a measurement analysis method based on chronamperometric (potential stepping) measurement. Potential stepping is used to remove the oxide layer formed rapidly on the anode during measurement. The associated transients

noted within the current profile were characterised and removed from the signal to determine the underlying current associated with the oxygen concentration.

The ability to fabricate such small devices with high specificity means biosensors are of clear technological relevance to intraoperative sensor development. However, application of current biosensors *in vivo* offers a number of significant challenges such as biocompatibility, enzyme stability, signal transmission and power supply [103]. In addition, being specific to a single target analyte may not be appropriate for a broad surgical sensor. Measurement strategies for determining one or more of the properties associated with the tumour microenvironment may be a more suitable approach for allowing definition of tumour margins or involved lymph nodes during surgical assessment.

2.3.2.2 Electrical characterisation

Electrical characterisation is concerned with defining how a biological system behaves under current flow. This is primarily its ability to resist current flow (resistance), but extents to current storage (capacitance) and changes in current (inductance). A material's resistance is the level to which it inhibits current flow, with conductance being a measure of ease of current flow [104]. Materials are typically quantified by resistance or conductance depending on their dominating current flow characteristic. The absolute resistance of a uniform material (volume conductor) is directly proportional to length (in the direction of current flow) and inversely proportional to cross-sectional area (perpendicular to current flow direction). The constant of proportionality is called the material resistivity (ρ), measured in Ohm-metres ($\Omega.\,\mathrm{m}$), and is typically the quoted metric when quantifying materials.

The mechanism of electrical conduction through metals involves free motion of delocalised electrons in accordance with an applied potential. By contrast, conduction through ionic solutions, as found in biological materials, requires the migration of larger charged species (ions) through the solution. This mechanism is highly complex and can be modelled from multiple levels of abstraction. From a simplified mechanistic view the conductivity is related to the velocity at which the ion is able to move through the solution for a given applied potential difference i.e. the rate of charge delivery (current) per unit potential difference (voltage). Therefore the determining factors must be related to forces acting to oppose the motion of the ion. Those discussed most prominently in the literature take the form of viscous drag and dielectric friction. A simple early model is that of spheres (ions) moving through a fluid being subjected to viscous drag forces described by Stokes law (slip) [105].

$$\delta_v = 4\pi\eta_0 r_i \tag{2.2}$$

Where δ_v is the viscous drag contribution (drag coefficient), η_0 is the pure solvent viscosity and r_i the ionic radius. The applied potential across the electrochemical cell will accelerate the ion to a velocity where viscous drag balances the applied electrical force, thereby making the ionic radius of direct relevance to the conductivity of the ionic solution. The limiting ionic conductance is often referred to as the Walden product. This is the limiting ionic conductance, λ_0 multiplied by the pure solvent viscosity, η_0. Modelling limiting conductance using Stokes viscous terms only turns out to be predictive for relatively large ions but shows poor correlation to experimental results for small metal ions [106]. For this reason many alterations have been proposed to include contributions to the limiting conductance from dielectric friction [105].

It has been suggested the dielectric contribution to ion retardation stems from two possible mechanisms [107]. These are due to (1) a reaction force from the dielectric cloud surrounding the ion and (2) extra energy dissipation due to induction and relaxation of solvent polarisation. Incorporation of the dielectric models into Walden product calculations improves agreement between theory and experiment, although there is still significant disagreement between many proposed models. Figure 2.13 illustrates the level of agreement between proposed models and experimental data in terms of the calculated Walden product against inverse ionic radius. The error contained within these models can be attributed to a number of factors: (1) the statistical nature of ions and molecules on the scales in question (2) the charge carried by and an ion and specifically the influence this has on both other ions and on the solution in question and (3) the solution properties both in bulk regions and those in close proximity to the charged species; water being a particularly problematic example due to its hydrogen bonding, self-dissociation and dipolar molecular arrangement.

Arguably the most successful, accessible model is that of Chen and Adelman [105] who present a molecular model based approach allowing the description of ion motion through solution. In fact the work of Chen and Adelman aims to establish links between previous models combining the Solvated ion model where small ions are surrounded by water molecules, increasing their effective radius and viscous drag and the dielectric friction mechanism presented by Zwanzig [107]. The model presented shows good agreement with experimental data over a wide range of ionic sizes (Figure 2.13) and allows a level of prediction about the limiting conductivity of a solution.

Chen and Adelman [105] justify their model through the importance being able to relate analytic models to experimental data. In essence it forms an effective theory, allowing a simplified view of the ion conduction problem. Further abstraction toward the larger scale is also employed and justified for the same reason. A high level view of the conductivity of a biological tissue system utilises idealised electrical component analogies [108]. For even a simple piece of tissue, the fluids, cells and structures involved each form considerable challenge

for complete theoretical description, making an electrical analogy more mathematically approachable.

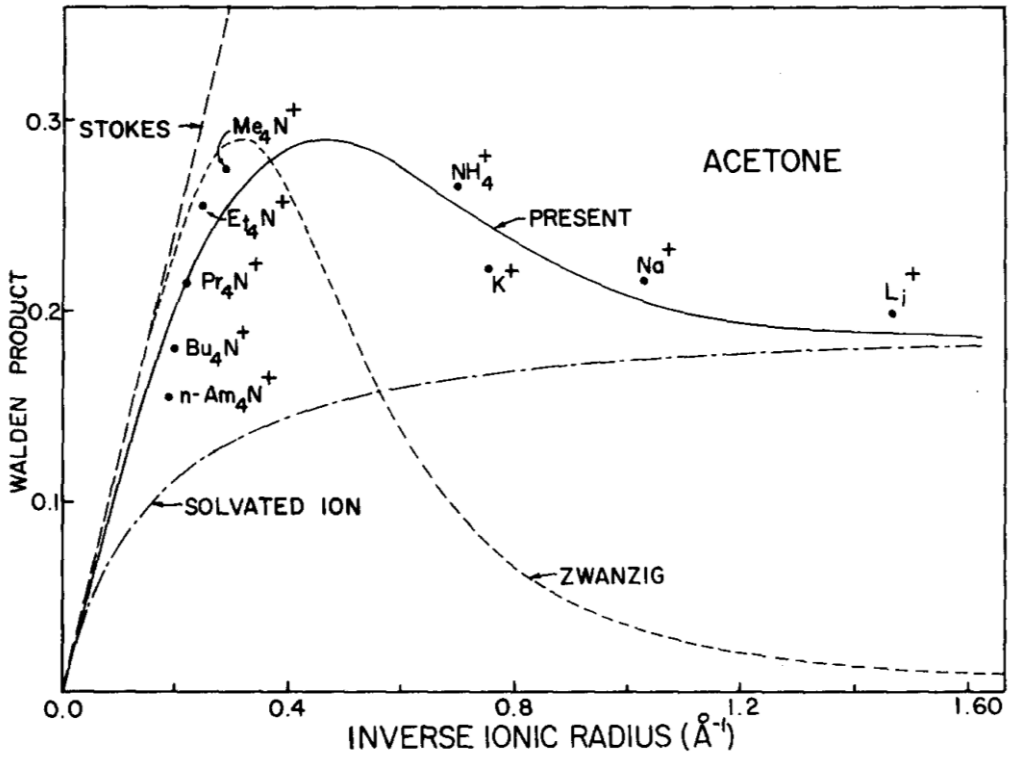

Figure 2.13: Comparison of experimental and theoretical Walden products for cations dissolved in acetone. Various proposed models are overlaid with the model of Chen and Adelman (present) showing best agreement with experiment [105].

2.3.2.2.1 DC resistance

For tissue resistance characterised in the DC case, application of a small amplitude voltage across the tissue and measurement of the corresponding current flow and cell geometry theoretically allows resistivity to be determined. In practice however, this process is somewhat complicated by polarisation at the electrode interface leading to erroneous values for the examined tissue [109]. Many methods of eliminating electrode polarisation error from AC impedance measurements have been proposed; a comprehensive summary of these is given by Kalvøy et al. [110]. Protocols involve either additional electrodes or numerical decoupling of electrode and tissue data. Most commonly, the four-electrode system is employed with separate potential and current measuring electrode pairs [82]. Accounting for cell geometry is also not straight forward when assumptions of ideal volume conductors are removed. Normalisation is therefore challenging, and aside from computational modelling and tight control over experimental conditions, there is little mitigation available.

Despite the challenges discussed above, much physiological data has been collected for both DC and AC conductivity. Table 2.1 summarises some of the published data specifically for

DC and low frequency AC measurements. It can be seen that large differences are found between hard tissue and soft tissue. This may be explained through the relatively low fluid levels in hard tissue (e.g. bone) reducing the ease of ionic conduction. Soft tissues show similar results to one another and are slightly more resistive than fluids (blood) on their own. Large variations are found between sources for the same tissue type indicating either natural physiological variation or inconsistent experimental/normalisation techniques.

Table 2.1: Resistive properties of biological tissues for low frequency AC and DC stimulation (all data determined from conductivity values).

Material	Resistivity, ρ (Ω.m)	Source
Bone, living	100	[104]
Muscle, 37°C	2.4-6.7	[104, 111]
Whole Blood	1.4-2.3	[82, 104, 109, 111]
Tumour	2.5-4	[82]
Fat	25-50	[82, 111]
Heart	2.5-17	[82]
Liver	3.4-43	[82, 111]
Lung (inflated)	11-42	[82]

2.3.2.2.2 Biogalvanic resistance

Chemical reactions at the electrode/electrolyte interfaces in an electrochemical cell induce a cell potential. Alternatively, application of a potential across electrodes may cause them to react chemically with the electrolyte [112]. The Galvanic cell is an example of the former, delivering electrical energy due to redox reactions within a cell consisting of two dissimilar metal electrodes in electrolyte solution. It was noticed as early as 1791 (by Galvani after whom the cell is named) that applying dissimilar metal electrodes to animal tissue produces an electrical stimulus [113]. In effect this phenomenon means that biological tissue has the ability to generate electrical power. Roa and Richter, 1974 initially investigated this bio-galvanic property for use as a power source to drive pace makers [114]. Due to improvements in lithium-ion batteries, the biogalvanic cell was abandoned for this application. However, recent work by Globerg et al. has reported a new potential application utilising biogalvanic cells [115].

Using a biogalvanic power source to allow measurement of the passive electrical resistance of biological tissues, Golberg et al. propose a simple means of distinguishing tissue type, or healthy from diseased tissue [115, 116]. The potential difference across a biogalvanic cell, established by placing two differing metal electrodes (zinc and copper) across a target tissue, was used to drive a measureable cell current. Modulation of cell current was achieved through application of an external resistive load. With the assumption of a constant Open

Circuit Voltage (OCV), the measured cell current, I for a specific external load, R_{EXT} can be related to the internal resistance of the galvanic cell, R_{INT} using equation (2.3). Using volume conductor assumptions where A and L are the electrode area and separation respectively, this was converted to a Galvanic Apparent Internal Resistance ($GAIR$) using equation (2.4).

$$\frac{1}{I} = \frac{R_{EXT}}{OCV} + \frac{R_{INT}}{OCV} \tag{2.3}$$

$$GAIR = \frac{R_{INT}A}{L} \tag{2.4}$$

Golberg et al. [115] reported that the $GAIR$ is a tissue-specific property that can easily be determined for biological tissues. Their research tested heart, liver and lung tissues all freshly harvested from Sprague-Dawley rats as part of a zinc/copper biogalvanic cell (Figure 2.14(a)). The resistive properties measured showed a significant difference ($p < .05$) between each compared tissue type. It was concluded that $GAIR$ is a reliable property for distinguishing between tissues. Additionally the influence of electroporated and microwave treated liver tissues showed a dramatically reduced $GAIR$ value, being around half that of healthy liver (Figure 2.14(b)). This result indicates that this method may also find application in quantifying tissue damage or diagnosing pathology.

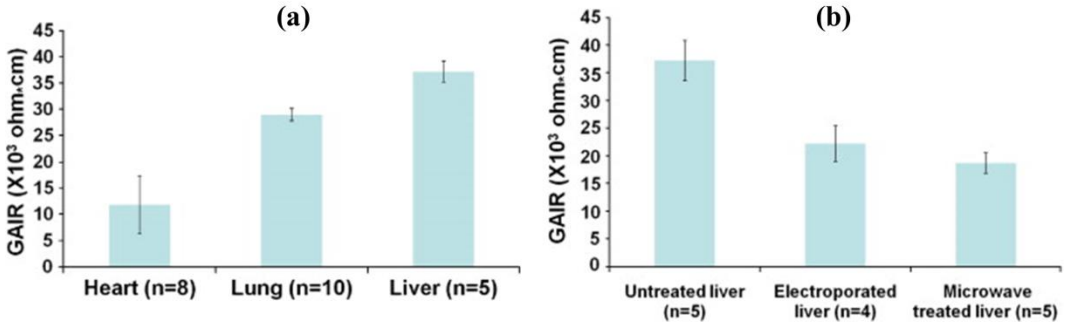

Figure 2.14: Sprague-Dawley rat tissue GAIR results for (a) various organ tissues and (b) for untreated, electroporated and microwaved liver; (adapted from [115]).

Further to this work Golberg et al. expanded the $GAIR$ technique to testing rat liver tissue *in vivo* [117]. Significant differences were found between *in vivo* $GAIR$ results and *in vitro* results previously discussed in [115]. The biogalvanic cell geometry and setup under testing conditions are shown in Figure 2.15. Results from the study indicate that *in vivo* liver tissue shows $GAIR$ value of approximately half that of the same tissue *in vitro*, with a similar level of inter-test variation. An increase in resistivity between *in vivo* and *in vitro* was in agreement with

Bioimpedance Spectroscopy (BIS) results presented by Spottorno et al. for pig liver and kidney tissue [118].

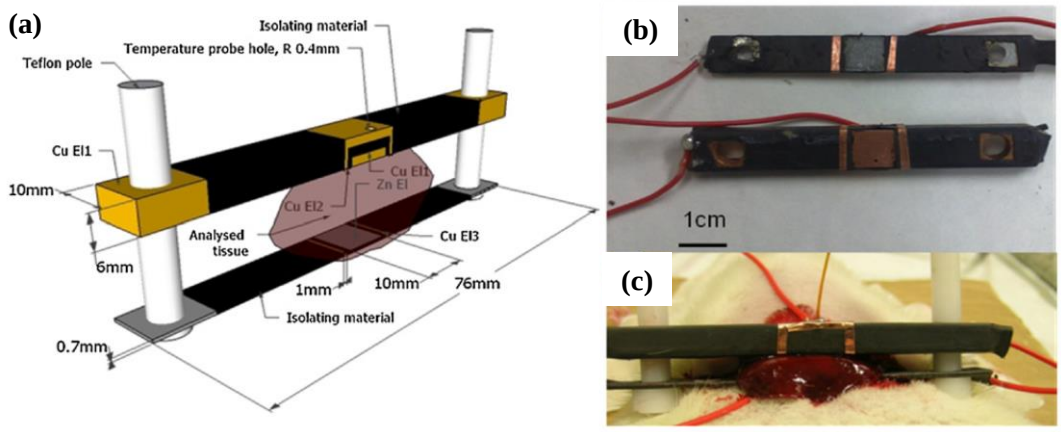

Figure 2.15: Zn/Cu galvanic testing cell setup including BIS and electroporation capabilities. (a) Schematic representation cell setup; (b) actual electrode set-up; (c) electrode positioned on rat liver, in vivo [117].

The $GAIR$ values were also evaluated against (BIS) results obtained in parallel. The comparison was made specifically with the calculated resistivity at zero frequency R_0 (DC resistivity), with similar trends being shown for all liver treatments. Reduction in $GAIR$ and R_0 due to electroporation was justified biologically as resulting from cell membrane disintegration. However, the differences between the BIS resistivity and $GAIR$ valves presented are not adequately addressed.

2.3.2.2.3 AC resistance

Impedance is the ratio of voltage to current, in accordance with Ohms law, and it is indicative of a material opposing the flow of electrical current. Impedance can account for both time variant (AC) and time invariant (DC) current flow, and bioimpedance is the specific application of impedance to biological materials, such as human tissues. Bioimpedance measurements are often frequency dependent and so assessment is commonly made over a range of AC frequencies, this is known as Bioimpedance Spectroscopy (BIS) [108]. The electrical impedance is a complex quantity, giving information about the magnitude of resistance and the relative phase between potential difference application and current flow (or vice versa). Equation (5.4) shows the general expression for impedance, where $\boldsymbol{Z}(\omega)$ is the frequency dependent complex impedance, $R(\omega)$ the resistance, $X(\omega)$ the reactance, ω the angular frequency and j the imaginary unit.

$$\boldsymbol{Z}(\omega) = R(\omega) + jX(\omega) \tag{2.5}$$

The measurement of impedance is typically performed using commercial instrumentation. For low frequency ranges (20 Hz to 110 MHz), an auto-balancing bridge circuit (Figure 2.16) will be employed [119]. This simplified diagram shows the main components involved in an impedance measurement. A source signal is generated and applied to the test specimen (sample). An operational amplifier is employed to balance the current flow through the test specimen (I_X) and the range resistor R_r (I_r). The voltages across the test specimen V_X and the range resistor V_r are then measured sequentially using a vector voltmeter which extracts the magnitude and phase elements of the two voltages. These can be combined as shown within equation (2.6) to derive the impedance of the test specimen at the source frequency. This process can be repeated across a range of source frequencies to generate the Bode or Wessel plots.

$$\boldsymbol{Z} = \frac{V_X}{I_X} = R_r \frac{V_X}{V_r} \tag{2.6}$$

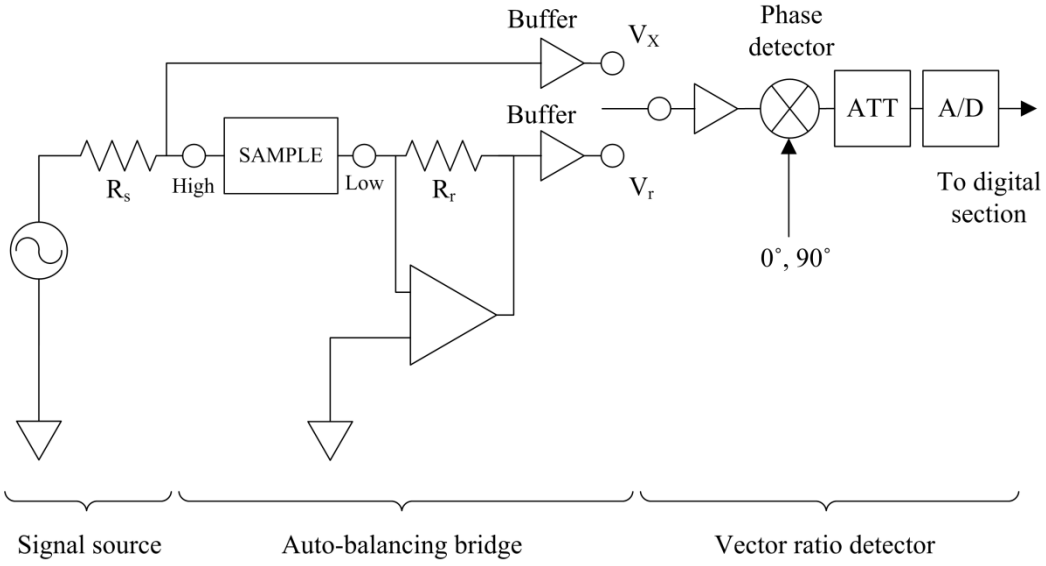

Figure 2.16: Auto-balancing bridge impedance measurement block diagram; (adapted from [119]).

Impedance parameters (resistance R and reactance X) are often normalised to the geometry of the measured tissue and presented in terms of complex resistivity ($\boldsymbol{\rho}$), made up of real and imaginary components ρ' and ρ'' respectively. The inverse case (for a conductive

specimen) may represent admittance ($Y = 1/Z$) parameters (conductance G and susceptance B) in terms of ($\boldsymbol{\sigma}$), made up of real and imaginary components σ' and σ'' respectively.

Tissue polarisation using an electric field of time varying strength or direction causes a phase shift due to the time required for charge displacement. This time-dependence is known as a relaxation and can be viewed as decaying response to a step input. Dispersion is a frequency domain version of relaxation and allows description of system (tissue) permittivity as a function of frequency [108]. For a single dispersion system (one relaxation time constant), a typical response will be two frequency independent permittivity levels (high and low frequencies) with an abrupt transition between them around a characteristic centre frequency.

As tissues are made up of many components of different scales and electrical properties, there are multiple dispersion processes over a wide frequency range. Early work by Schwan suggested three stages, namely the α- , β- and γ-dispersion as shown in Figure 2.17 [108]. Most tissue measurements are taken within the frequency range of the α- and β-dispersion phase with frequency ranges of mHz-KHz and 0.1-100 MHz respectively. These are generally associated with active cell membrane effects, intracellular structures and passive cell membrane capacitance [108]. This inevitably makes frequency range selection an important factor in assessing tissue properties.

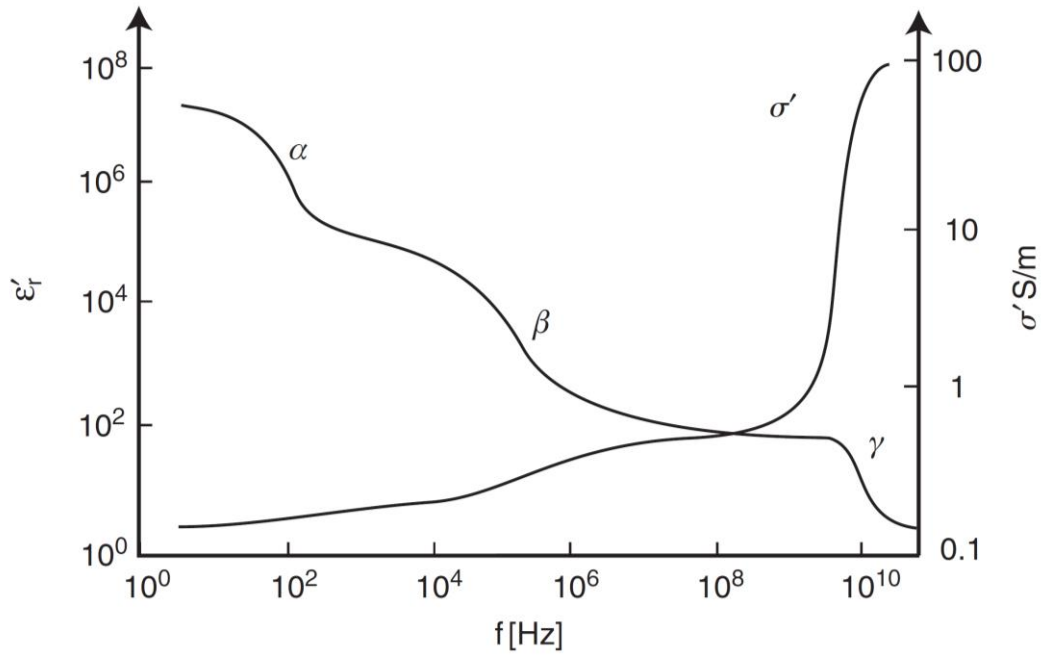

Figure 2.17: Idealised dispersion regions for tissue tested with BIS, showing permittivity and conductivity [104].

Complex tissue dispersion behaviour was demonstrated in early work by Schwan [120]. More recently, Gabriel et al. gave a comprehensive review of the available data on BIS measurement for tissue [121] and presented additional measured data across a wide frequency range (10 Hz to 20 GHz) [122].

BIS measurement has been explored as a possible diagnostic technique for determining the presence of cancer. Measurements have been taken by many groups, [123-125], with the general result showing cancer tissue to have a lower resistivity than healthy tissue. Most applications have been focused on breast cancer, with external electrode placement. However, Laufer et al. [123] presented results obtained using BIS on liver tissue with and without cancerous tumours. The typical dispersion behaviour can be seen on normal and cancerous tissue (Figure 2.18), with cancerous regions showing both reduced resistivity and increased dispersion characteristic frequency [123].

Distinction between healthy and cancerous tissues has been demonstrated in many cases, however quantifying the difference in a robust way has been the subject of many recent papers [126-128]. Most initial quantification has been based on fitting electronic circuit analogies to the data. These have the benefit of being described completely with only a few parameters. The most common model is the Cole-Cole model which is described mathematically in equation (2.7); where R_0, R_∞, α and τ_c represent the low frequency resistivity, the high frequency resistivity, fractional power and the characteristic time constant respectively.

The general representation is of a suppressed semi-circular arc when plotted on the complex plane (Wessel diagram). This method however does not always give a good fit to the measured data and differences between plots are only assessed using a few parameters. Investigation has been undertaken to assess more powerful numerical schemes for improving the statistical detection of cancer. Much of this work has been applied to skin cancer classification (most probably due to the relative ease of obtaining *in vivo* data). Methods of analysis include; (1) Principal Component Analysis (PCA), described by Aberg et al. [127], (2) Neural network by Dua et al. [128] (3) bespoke impedance data indexing developed by Blad et al. [129]. Conclusions from each method are positive, showing the applicability of analysis techniques to BIS data and how this data can be manipulated into the most simple of interpretations for the observer. These techniques also benefit from increasing statistical power as the data set available gets larger, meaning accuracy of diagnosis would improve as the wealth of trial data increases. A particular advantage of impedance (or resistance) measurement is the objective nature of the metrics obtained. If these are attained using consistent and appropriate experimental techniques then issues associated with subjective interpretation can be avoided. However, the large variability of conditions, particularly with BIS makes obtaining consistent data difficult.

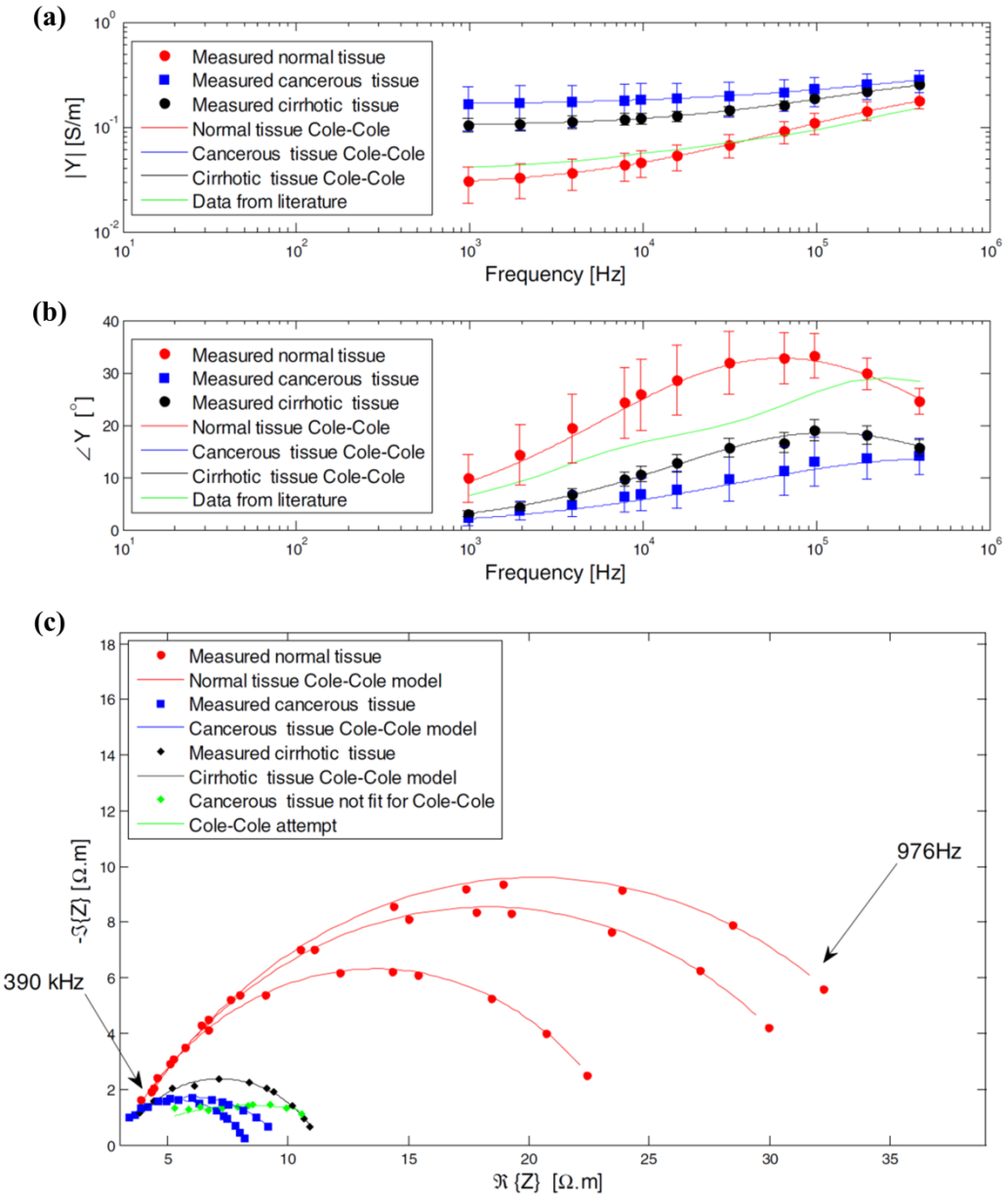

Figure 2.18: BIS results for normal, cancerous and cirrhotic liver tissue with Cole-Cole model fitting, showing (a) average admittance amplitude, (b) average admittance phase, and (c) the corresponding Wessel impedance plots; (adapted from [123]).

$$Z(\omega) = R_\infty + \frac{R_0 - R_\infty}{1 + (j\omega\tau_c)^\alpha} \tag{2.7}$$

2.3.2.2.4 Electrical characterisation commercially

There are now many electrochemical and electrical based sensors that have matured into commercial products. Biosensors have been manufactured commercially for monitoring of analytes, and now play a significant role in medicine, agriculture/food, environmental and industrial monitoring [130]. Adapted electrical characterisation techniques have also been

utilised within commercial devices. The TearLab device (TearLAB, San Diego, CA) has been developed as an EIS based tool for assessment of dry eye syndrome [131, 132], and the ZedScan™ (Zilico, Sheffield, UK) for objective real time assessment of cervical epithelial tissue [133].

As the ZedScan™ device delivers real time contact assessment of tissues it is highly relevant to a surgical sensing application. The system utilises patented bioimpedance measurement techniques and a Cole-Cole model to generate metrics relating to the health state of cervical tissues [134, 135]. Early publications describe the use of a pencil shaped probe (5.5 mm diameter) with 4 gold electrodes, designed for assessment of cervical intraepithelial neoplasia (CIN), a precursor lesion to cervical cancer. Clinical results showed a reduced low frequency resistance with the progression of CIN which was related to the associated increase in extracellular space [135]. However, a high (56 %) measurement rejection rate was also reported, potentially indicating the difficulties of using BIS to obtain reliable measurement data.

2.3.3 Optical properties (surgical imaging)

During surgery visual information is crucial for the surgeon to perform the required tasks. This is even more pertinent when the kinaesthetic and tactile sensations are reduced during laparoscopic procedures. Augmentation of the visual field has been proposed to help improve cancer surgery [136, 137]. Considerable evidence suggests that contrast agents can aid in the detection of small metastases and delineation of tumour margins [138]. Imaging typically involves the delivery of a contrasting agent to the tissue, its excitation with electromagnetic radiation of appropriate wavelength and measurement and processing of the contrast agent response (returned wavelength and spatial intensity). This process has been detailed schematically for fluorescence based imaging using indocyanine green (ICG) in Figure 2.19(a). Additionally, the principle of photoacoustic based imaging has been presented in Figure 2.19(b).

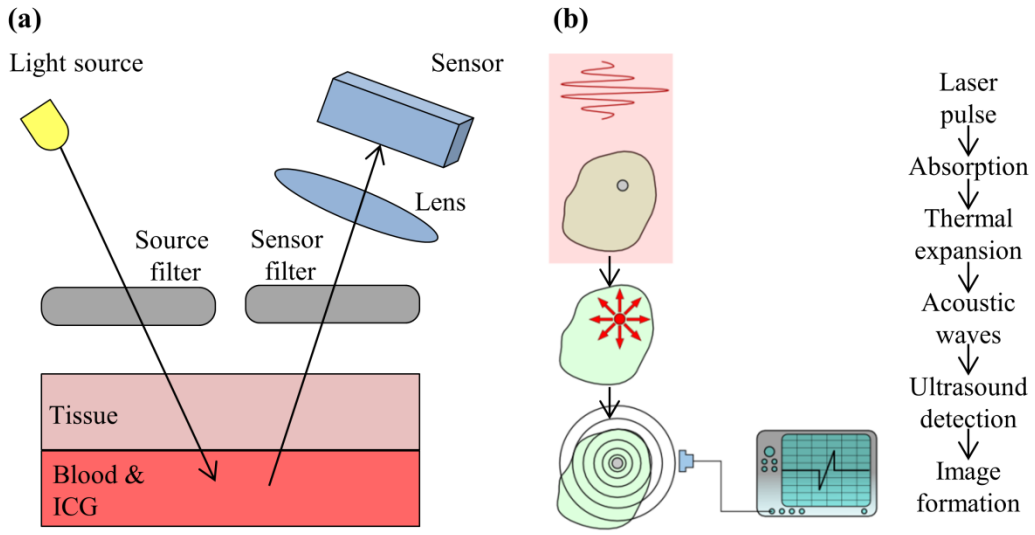

Figure 2.19: Intraoperative imaging techniques, showing (a) the principle of fluorescence imaging, and (b) principle of photoacoustic imaging; ((a) adapted from [139], (b) adapted from [140]).

Within fluorescence imaging a number of organic dye molecules have been approved for human use including indocyanine green (ICG), fluorescein, photofrin and 5-aminolevulinic acid (5-ALA). Many other candidates are available although are not widely used due to lack of Food and Drug Administration (FDA) approval. In the field of surgical oncology, ICG and 5-ALA have therefore been the most commonly used contrast agents [136, 141-143]. The peak absorbance of ICG (~800 nm) makes it possible to image deeper into tissues, and its low autofluorescence delivers a higher signal to background ratio [141]. ICG has therefore been used for medical diagnostic imaging in a number of regions including sentinel lymph node mapping in breast tissue and in brain, liver and colorectal tumour delineation. Figure 2.20 shows examples of fluorescence imaging using ICG as a contrast agent.

As an alternative contrast agent, 5-ALA has also been utilised as a means of delivering tumour imaging. 5-ALA is a non-fluorescent pro drug, however it induces cellular accumulation of fluorescent porphyrins as it is metabolised [5]. It is therefore reliant on the increased metabolism of cancerous cells. In 2006, Strummer et al. [5] published results from study examining the effect of using 5-ALA in fluorescence image guided cancer surgery on the resection radicality, progression-free survival, overall survival and morbidity. The study concluded that the use of 5-ALA led to more complete resections of tumours (65 % vs 36 %) leading to improved progression-free survival in patients with malignant glioma [5]. The drug has also been used for the diagnosis of malignant and pre-malignant lesions during fluorescence colonoscopy [143] and detection of peritoneal metastasis [142], with significant improvement with respect to standard assessment reported in both case.

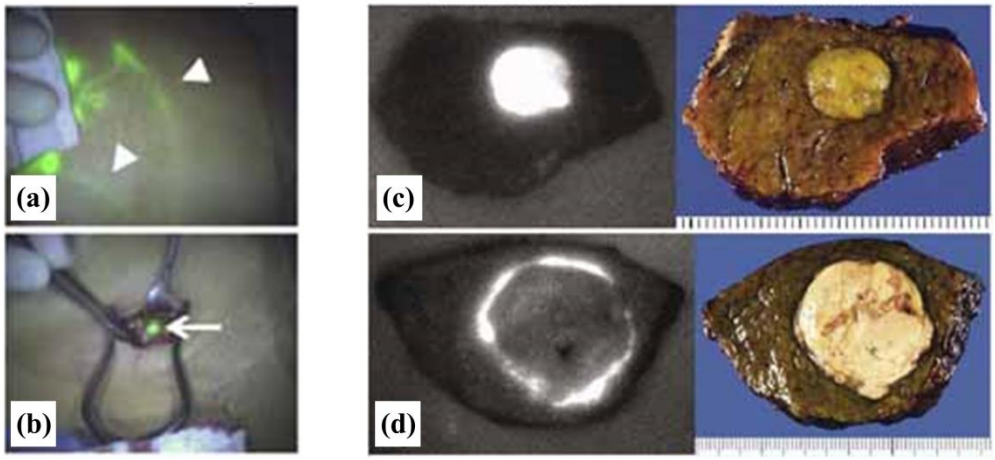

Figure 2.20: Imaging using ICG, showing (a) combined colour and fluorescence image of the lymphatic channels (arrows indicate injection site), (b) sentinel lymph node, (c) ICG retention in a well-differentiated hepatocellular carcinoma, fluorescence image (left) and gross image (right) shown, and (d) ICG retention in a poorly-differentiated hepatocellular carcinoma, fluorescence image (left) and gross image (right) shown; (images adapted from [141]).

Particular issues with fluorescence imaging techniques are the penetration depth of the excitation wave and the issue of complete imaging of heterogeneous tumours [137]. Alternative imaging techniques with improved penetration depth, such as photoacoustic imaging, are concurrently under investigation [136, 144]. This technique uses laser light excitation to induce thermal expansion in a target molecule. The rapid heating causes broadband acoustic waves to be produced that can be detected using an ultrasound transducer (Figure 2.19(b)) and thus imaged [137]. To improve delineation between target and surrounding tissues, contrast agents are often used. These may be small molecules or larger nanoparticles (e.g. nanorods, nanoshells and nanocages) [145]. The latter can give much higher contrast and be easily tuned over the near infrared spectrum. Surface modification is also possible for these particles, allowing for attachment of cancer specific targets. Although photoacoustic imging offers a practically attainable imaging solution, there remain some long term safety concerns with the use of nanoparticles in the body [145].

Improvement in the applicability and efficacy of augmented surgical imaging using the discussed techniques is typically considered to require cancer-specific functionalised contrast agents [141]. As a consequence, delay in quantifying the safety of these probes will slow the progression to the clinic [136, 144]. Additionally, exposure of the surgeon to numerous imaging modalities may enforce the reliance on their interpretation of subjective data to make the best clinical decisions.

2.4 Summary of the literature

There have been many significant advances in the diagnosis, management and treatment of cancer patients over the past few decades. However surgery, at least in the short term, will likely remain as the primary choice for the treatment of cancer. For colorectal cancer surgery, excessive removal of tissue can lead to complications with recovery and a reduced quality of life for the patient. There is a desire, therefore, to more towards more personalised procedures where resections are optimised to reduce unnecessary morbidity. This ultimately requires improved real-time intraoperative sensing.

Availability of quantitative intraoperative diagnostic techniques is scarce and prognosis is often made post operatively [14]. The literature reviewed has described a wide range of sensing modalities and methods that have the potential to be developed into a surgical sensing tool. Broadly, these can be divided into methods of assessing mechanical, electrochemical, electrical or optical properties of tissues. Some of the strengths and weaknesses of these methods in the context of surgical sensing have been summarised in the following sections.

2.4.1 Mechanical approach

Mechanical property assessment is arguably the most relatable approach within surgery due to its association with traditional palpation techniques. The simplicity of contact force measurement makes it directly applicable for surgical integration, as demonstrated in the atraumatic grasper of Tholey et al. [57]. However, this localised force measurement is aimed at delivering haptic feedback to the surgeon for subjective assessment rather that for quantifying tissue health. Extension to spatial imaging through the use of a specialised tool, such as that of Zbyszewski et al. [58] (Figure 2.7) could deliver more quantitative tissue assessment. However, the unidirectional loading could prove to be problematic for *in vivo* measurement of soft tissues and integration with existing tools offers significant challenges.

Some important developments have been achieved in the last two decades regarding elastic imaging. Qualitative elastography has been shown to be capable of detecting malignancy [80], but the accuracy in identification by the observer is still too low for routine clinical adoption. This could be due to malignancy not being expressed directly as alteration in tissue stiffness in all cases. Palmeri and Nightingale, 2011 [146] review the level of clinical adoption of elastography and present the current challenges. Ultrasound based techniques will be likely to provide an effective clinical tool in specific areas, such a prostate examination and intervention monitoring [147]. However, the current size and system complexity offer challenges for laparoscopic integration as a general tissue assessment device.

2.4.2 Electrochemical approach

Exploitation of tissue electrochemistry has been described as a method of health assessment for over fifty years [148]. The simple measurement of electrode potentials can offer information about the relative state of different tissues, including damage, temperature, and presence of anaesthetic [85, 87]. Influence from such a wide range of parameters means that electrode potential measurement may lack the required specificity for cancerous tissue assessment. However, with the advent of a bio-functional element to the working electrode there has been a rapid rise in the research and development of biosensors with high specificity.

The use of electrochemical properties appears to offer a robust and yet specific means of testing for low concentrations of analytes. Most of the established medical diagnostic techniques focus on processing and analysing fluid samples taken from the patient. This process is not directly applicable to the surgical sensing application. However, the electrode development and small-scale electronics are highly relevant for this application area.

2.4.3 Electrical approach

DC resistance techniques formed the basis of early tissue characterisation tests. However, the use of DC was short-lived as the induced electrode polarisation was an undesirable measurement artefact. The principle of DC is straight forward but the measurement approach was found to be problematic. A modern DC approach of determining a galvanic apparent internal resistance (GAIR) as a tissue characterisation parameter was recently proposed by Golberg et al. [115]. Initial limited trials on rat models showed the method to be capable of tissue differentiation and exhibited significant changes due to cell damage from electroporation [115]. These results have been partially verified through comparison to BIS measurements although some unexplained differences remain [116]. Due to being simple and scalable, biogalvanic cell testing is a prime candidate for integration into a surgical device. Additionally, the technique effectively combines electrochemical and electrical information, which could allow for a bi-modal sensor. However, for the GAIR approach to be considered as a surgical sensing method, tests describing the behaviour of the cell under varied conditions, evaluating reliability and repeatability are required. Additionally no known work on healthy human tissue has been conducted, and the influence of cancerous tissue on the GAIR value has not been determined.

AC tissue resistance assessment (BIS) replaced DC techniques early on and has remained the prominent electrical technique. However, although well established, the techniques within BIS are challenging. Consideration of the terminology alone makes BIS error prone within mathematical manipulation and reporting. Significant care and diligence is required to record a reliable and meaningful measurement. Additionally, data comparison is difficult without

application of a model, and defining which model is suitable and relating it to the complex nature of tissue is a significant challenge. Freedom of model selection and the associated metrics makes it easier to extract statistically distinct data from measurements. However, this potentially limits the use of BIS to very specific applications, as seen with the commercial ZedScan tool (Zilico, Sheffield, UK).

Even with these challenges there have still been some significant findings for healthy vs cancerous tissue, suggesting that looking into electrical tissue properties in a diagnostic sense may be fundamentally sound. The development of a commercial device for cancer screening using BIS is encouraging and there is an active research community supporting the development of BIS technology.

2.4.4 Optical approach

Some of the most promising future surgical technologies are those of real-time imaging. There are many modalities under investigation, with each looking to exploit different optical properties of tissues. The major benefits of imaging tissues are the broad assessment field and integration with standard imaging. This makes the experience very intuitive for the surgeon and therefore augments the procedure without adding significant complication. It is likely that enhanced real time imaging will form part of future surgical procedures. However, problems with penetration depth, stability, duration and toxicity may need to be addressed prior to routine uptake. Intensity images presented to the surgeon currently rely on subjective interpretation to make surgical decisions. Improved image processing may allow for objective metric extraction, although it may be necessary to move toward a multimodal approach where optical data and data from contact measurements are combined to quantify the presence of cancer.

2.5 Conclusions

Nearly all of the presented sensing modalities rely on measurement of the side effects of cancerous tissue growth rather than targeting cancer specific cells. Although this is not the ideal measurement scenario, the efficacy of this approach has been demonstrated within diagnostic imaging such as CT and US and will be likely to form the basis of the next generation of cancerous tissue sensing techniques.

To achieve cancerous tissue delineation, elastic imaging may prove to be a suitable technique. However, the associated system complexity makes elastic imaging impractical for surgical tool integration. The use of biosensors offers specificity but typically only for single samples thereby lacking the practicality (e.g. repeated use) required for an *in vivo* surgical sensor. The robustness and repeatability required may be best achieved through electrical tissue

assessment, where the majority of techniques are based on AC measurements. Commercial application of BIS techniques suggest that it may allow for cancerous tissue discrimination. However, the complexities of performing reliable measurement and of extracting suitable metrics are not trivial.

Based on the reviewed literature, the biogalvanic characterisation approach appears to offer the most appropriate method for investigation. This technique is new with a limited number of publications around the topic [115, 116, 149]. However, it is relatively simple in terms of EC components, measurement equipment and characterisation procedures. Additionally, the technique is suitably scalable to allow for device integration. The DC nature makes it possible to include exploitation of electrochemical processes or maintain a purely electrical assessment. This flexibility makes it an ideal candidate for exploration as a surgical sensing modality.

The initial work presented in this thesis will focus on development and testing of a biogalvanic based sensing system. This will aim to independently assess the efficacy of the technique over a range of operating conditions. Adaptation of the sensing methodology will then be made together with further validation in a surgical context.

Chapter 3
A biogalvanic characterisation system

This chapter details the development and validation of a biogalvanic characterisation system. The systems presented were developed to allow examination of the biogalvanic tissue characterisation method proposed by Golberg et al. [115]. Design and development of cell electrodes, electronic circuitry, control software, and characterisation protocols are presented. Section 3.1 details some of the important and fundamental considerations of the systems developed. Sections 3.2-3.7 detail the specific components developed for contacting, controlling, measuring and characterisation of tissue samples. Testing protocols were developed to evaluate the performance of the completed systems. This validation process is presented within Section 3.8.

3.1 System Requirements

For successful evaluation of the biogalvanic characterisation technique, suitable measurement equipment was required. Developments were made with consideration of the equipment specification and the practicalities of tissue work. In general, the system can be divided into two aspects: (1) equipment at the tissue interface, and (2) equipment away from the tissue interface. Constraints on each are independent, and as such have been considered separately. This section details the general considerations and specific requirements necessary for achieving the aim of developing a biogalvanic characterisation system. The work was performed in relation to attaining a number of specific objectives:

Objective 3.1: *To define the required elements (formal requirements) for the tissue interface, control, measurement and analysis equipment.*

Objective 3.2: *To explore the available equipment options for performing the required biogalvanic characterisations on tissue samples.*

Objective 3.3: *To develop a suitable method for electrode manufacture and delivery to tissue surfaces.*

Objective 3.4: *To develop and validate an adjustable biogalvanic measurement and control system.*

Objective 3.5: *To develop and assess characterisation methods for extracting comparative metrics from biogalvanic measurements.*

The following sections detail work conducted to define the system requirements for the various elements to therefore meet Objective 3.1.

3.1.1 Systems overview

In consideration of Objective 3.2, two measurement systems were explored and compared. The measurement systems tested were: (1) a custom biogalvanic system (c.f. Section 3.5.1 & 3.6), and (2) the commercially available CompactStat (Ivium Technologies) in standard load control mode (c.f. Section 3.5.2). For the purpose of clarity, these will be referred to as the Biogalvanic system and CompactStat system respectively in the following sections. The Biogalvanic system is a combination of numerous bespoke subsystems. In contrast, the CompactStat system offers a small EC measurement and control device. Figure 3.1 gives an overview of the various elements involved in development of a successful biogalvanic testing system. These subsystems are

applicable to one or both of the measurement systems described and are the focus Sections 3.2-3.7 in this chapter.

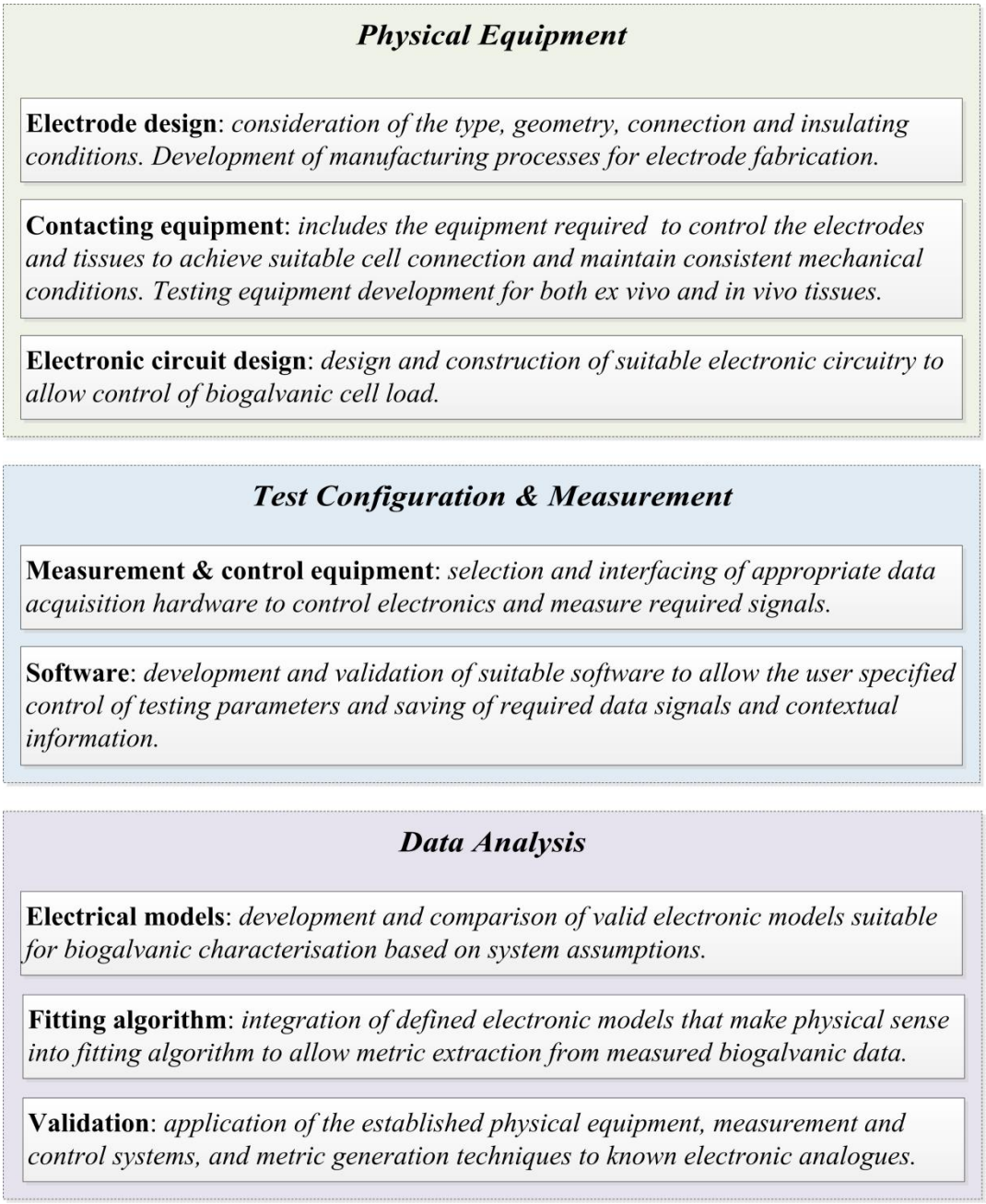

Figure 3.1: An overview of the elements considered in the development of a biogalvanic characterisation testing system.

3.1.2 Tissue interface equipment

Tissue interfacing equipment was considered as: (1) equipment that is in direct contact with the test materials, and (2) equipment that is required to deliver direct contacting elements to the test material under the desired conditions. The former is primarily the electrodes and any insulating surface materials. The electrodes themselves can take varied contacting geometry and be

constructed from many materials, forming a huge potential for variability. The use of pure metal electrodes constrains the attainable material sizes. Commercially available pure metals are only available in finite forms and sizes and machining capability is practically limited. The selected electrode materials need to be connected to the control electronics and so require wire connection through solder, weld, clip or conductive glue. Each of these processes has equipment and size limitations, and should be selected as to not induce permanent change in the material or add excessive series resistance. The considerations of electrode production have been formally summarised within Requirement 2.1.

Requirement 2.1: *Produce metal electrodes with: repeatable surface conditions; insulated electrical connection to measurement equipment; and optional insulated contacting boundaries.*

The contacting conditions at the electrode-tissue interface are fundamental to the assumptions made in the characterisation models (c.f Section 3.7.1). Consideration of how the electrodes are applied to the tissue surface is therefore essential. Specifically, the geometric arrangement, tissue thickness and applied load/strain may alter the cell performance away from that of the characterisation model. The design aim was to address and control these issues, while considering the limitations of the surrounding environment available for electrode manipulation. The specific considerations for the contacting equipment have been defined as Requirement 2.2.

Requirement 2.2: *Allow delivery of manufactured electrodes to the tissue interface on ex vivo and in vivo organs, with repeatable control of contacting strain or load.*

3.1.3 Remote equipment

Elements remote to the surface interface are comprised of the control, configuration, measurement and processing aspects of the characterisation. Electronic systems need to give reliable connection to the EC cell without inducing additional noise or unintentional resistance. Additionally, the switching between external loads should be rapid as to not invalidate the model fitting assumptions of discrete external loads proposed by Golberg et al. [115]. External load values should also be changeable and the control of the switching mechanism should be easily adjustable, allowing external load values and switching rates to be altered readily. A disconnect from the external loads is also desirable to allow measurement of the true open cell voltage. The system requirements specific to the load control system have been formalised as:

Requirement 2.3: *Develop an electrical load control system to connect to the biogalvanic cell directly without introducing additional noise and resistance.*

Requirement 2.4: *Allow connection of discrete external loads, configured to the model arrangement presented by Golberg e al. [115].*

Requirement 2.5: *Permit transition across multiple, variable loads with the aim of controlling the transition times and therefore induced transients [83].*

Software used should allow the user to adjust the resistor range and switching intervals selected, along with their switching rate and the measured voltage parameters. In addition, the collected data from tests should be recorded to file and include raw values along with the test configuration. For useful metrics to be obtained the software should apply a selected model to the measured data and save the output to file. A high level of autonomy is desirable for this type of system as it reduces the risk of human error, although is a secondary concern at the initial testing stage. As such the requirements pertaining to software for control, measurement and model fitting were defined as:

Requirement 2.6: *Measurement of the external load and cell voltages should be conducted with a device of high resolution, reducing quantisation error to <1 mV. This value is based on expected minimum voltage transitions seen for previous biogalvanic work [115, 149].*

Requirement 2.7: *Biogalvanic system software should interface with measurement and control sub systems, allow the user to configure test settings of external resistor range and switching rate, and allow configuration of voltage measurement rates. Measured voltage-time data along with the test configuration should be saved to file for post-processing.*

Requirement 2.8: *Biogalvanic characterisation models to be defined, implemented into fitting algorithms and applied to measured data for validation. Characterisations should allow for simple post-processing of measured data.*

The design, generation and testing of the subsystems outlined within Figure 3.1 has been detailed within Section 3.2-3.7. Each section specifies the work conducted to meet the requirements stated within this section and the broader chapter objectives.

3.2 Galvanic Electrodes

This section describes the metal electrodes designed to meet Requirement 2.1. As numerous electrode arrangements were employed throughout the tests described in subsequent chapters, a specific nomenclature was developed and is described within the following section.

Electrodes are the first point of electrical contact at the tissue surface, and are inherent within any measurement of electrochemical systems. The types available and their potential arrangement options are vast. The most prominent electrode variables have been described:

Material: A wide range of *electrode materials have been used in electrochemical measurement systems [83, 84, 108, 150]. For a suitable galvanic cell the materials should create sufficient potential difference under aqueous conditions to allow measurement of the voltage transitions across the range of external cell loading.*

Geometry: *The electrode geometry covers the size, shape and relative positioning of the anode and cathode. For the biogalvanic system, the model assumptions have previously been based on axially aligned electrodes with contact areas and separation used in the definition of GAIR (volume conductor theory, [108]).*

Surface: *The surface of the electrode is in direct contact with the tissue. It is integral in generating current through redox reactions and carrying current as a conductor. The surface of the electrode will influence the reaction type, cell potential and cell resistance. Modification through chemisorption of compounds may be conducted to improve electrode performance within a given application [150]. Conversely, modification to the surface during measurement can occur through passivation, leading to alterations of the EC cell and measurements of it [84]. For the presented system, pre-conditioning of the electrode surfaces through mechanical abrasion was deemed appropriate for the short duration of testing conducted.*

Connection: *An ideal connection to the electrode will add no additional resistance and cause no influence on the electrochemistry of the galvanic cell. Typical methods involve mechanical coupling of wires through screws or clamps; direct connection through solder or weld; or adjoining wire with the aid of a conductive cement.*

To establish a suitable galvanic cell and allow direct comparison to the work of Golberg et al. [115, 116, 149], copper and zinc were selected as the electrode materials. Investigation was instead focused on the contacting conditions at the electrode-tissue interface. To this end a number of different geometries were developed and have been described within Table 3.1.

Electrode arrangements were aligned either in axial, parallel-needle, or co-planar arrangements, with additional variation of the boundary isolation with or without the use of a non-conducting resin (Varidur^{TM}, Buehler, USA). Cylindrical metal was used in all arrangements with three diameters employed. Insulated copper wire was soldered onto the back of the electrodes at locations away from the tissue interface. For the largest electrode set, direct solder onto the electrode was not possible; therefore conductive cement (CW2400 Epoxy, Circuitworks, USA) was used to complete the electrical connection.

The electrode arrangement and size has a direct influence on the model assumptions, and is particularly pertinent to any conversion of characterised resistance to a resistivity ($GAIR$, equation (2.4)). An electrode nomenclature was developed to allow a simple means of identifying the arrangement used in a reported test. For example a test of the X_{D-R} electrode set would be in configuration X with electrode diameter D; the subscript R indicates that the electrodes were set in resin. For the needle configuration information regarding the exposed electrode lengths and separations was required. The electrode configurations and corresponding codes are detailed in Table 4.1.

Table 3.1: Electrode geometries and nomenclature employed throughout testing.

Configuration of electrodes	Test Diameters (mm)	Representative Code
Axially aligned	12	A_{12}
	6	A_6
Parallel-needle	1	N_1
Co-planar	1	C_1

A number of processes were involved in the manufacture of a particular electrode set. Raw material in the form of pure zinc and copper round (99.9%) was machined to the required diameter. Attachment of connecting wire was then implemented using the techniques previously described. For electrodes requiring boundary insulation, the machined electrodes were place into a resin mould and filled with resin. Set electrodes were then removed and mechanically polished with 1200 grit and cleaned with distilled water. Figure 3.2 illustrates the involved steps and shows an example of the manufacturing steps in producing a A_{12-R} zinc electrode.

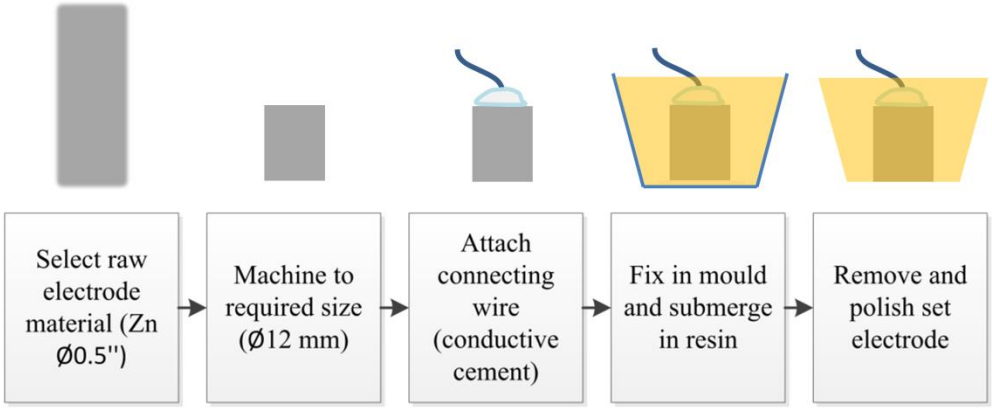

Figure 3.2: Electrode manufacturing steps for the production of an A_{12-R} zinc electrode.

3.3 Contacting equipment

To obtain robust data from *ex vivo* or *in vivo* tissue samples and to meet Requirement 2.2 a number of parameters were considered in the development of contacting equipment:

Platform: *A stable level platform is required to support the target tissue specimen to allow stable connection of test electrodes.*

Alignment: *The biogalvanic characterisation model assumptions are based on concentric alignment of opposing electrode faces. For axial electrode experiments, the contacting equipment should produce and maintain this condition.*

Access: *For repeat testing there is a need to manipulate and change tissues. Contacting equipment should give enough space to practically achieve this and to allow replacement or cleaning of the test electrodes.*

Loading: *The mechanical stress applied to tissue and the corresponding strain is likely to produce a significant influence on the measured internal resistance. The contacting equipment should therefore allow application of load to the tissue and measurement of thickness and strain.*

A testing rig was constructed to allow laboratory based tissue testing of *ex vivo* samples. The Testing platform, shown in Figure 3.3(a), was made using adjustable aluminium sections (Rexroth, Bosch Group, Germany) with electrode housing sleeves machined from acetal polymer (Delrin®, Ensinger, Germany). Sleeves were manufactured to support either A_6 or A_{12} electrodes held vertically. The lower electrode is fixed into position and the upper electrode

locked to a desired position using a grub screw or held under a constant load using the upper applicator.

For conducting biogalvanic characterisation tests on *in vivo* tissue, a surgical clip was developed. The Surgical clip is more appropriate for testing in the confined space of the operating theatre. The Surgical clip shown in Figure 3.3(b) allows tissue to be clamped between electrodes of fixed separation while measurements are taken. The discrete position locking mechanism however offers less control of the load/strain conditions compared to the Testing platform. The final device was 3D printed in polyamide and painted with PVA to reduce porosity.

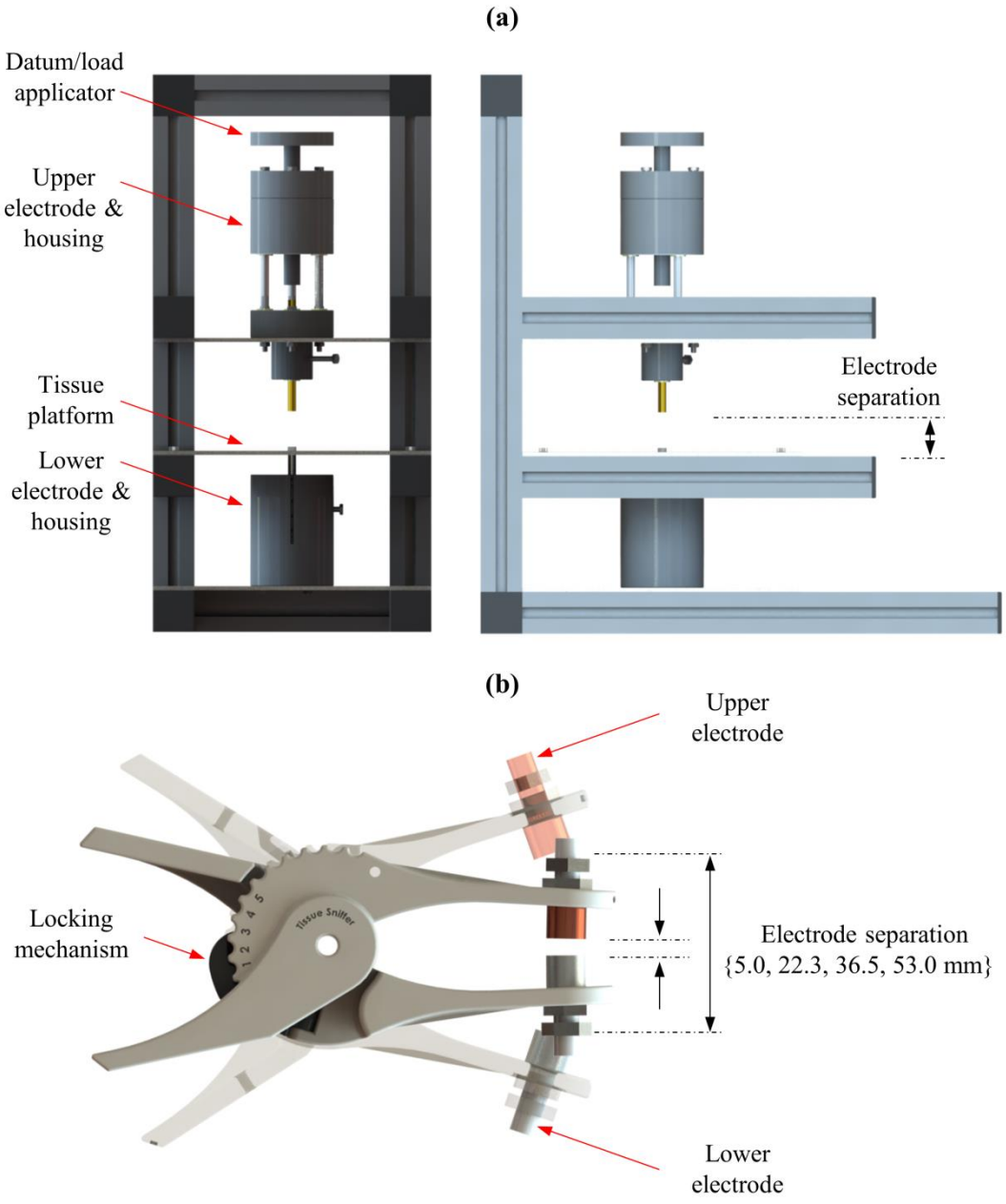

Figure 3.3: Galvanic cell testing systems, with: (a) Testing platform design for fixed strain/separation tests, and (b) Surgical clip design, allowing fixed separation tests.

3.4 Electronic Circuit Design

To meet the criteria of Requirements 2.3 - 2.5 a circuit board was designed with circuit CAD software (Eagle PCB). To reduce additional series resistance and allow fast transitions between external loads, electromechanical relays (G6A-234P, Omron Corporation, Japan) were employed. These were switched through the use of transistors which were controlled with digital level logic. This allowed the development of digitally controlled switching units, as shown in Figure 3.4(a). When a high digital signal is present, each unit adds a mounted fixed resistance (e.g. R1 shown in Figure 3.4(a)) between the cathode and anode. With a digital low signal, each unit acts as a connector to the adjacent switching unit. The output of the final switching unit must be connected to the anode to complete the circuit. Combining a number of switching units allows a binary number based digital logic output to control the effective external resistor value. A 7-bit system was developed with the first digital channel being assigned to switching the galvanic cell into series with the external resistors, allowing the effective resistance and OCV to be measured. Figure 3.4(a) shows a schematic of the cell connection switch and a single switching unit. Each switching unit contained a relay, transistor, indicator LED (not shown for simplicity), diode, current control resistor and external load precision resistor. This structure was employed to allow unit testing prior to integration of the complete system, with the potential for simple expansion to a larger testing system with more loads. Figure 3.4(b) shows the final printed circuit board including soldered components. The principle of operation of this circuit is shown diagrammatically within Figure 3.5.

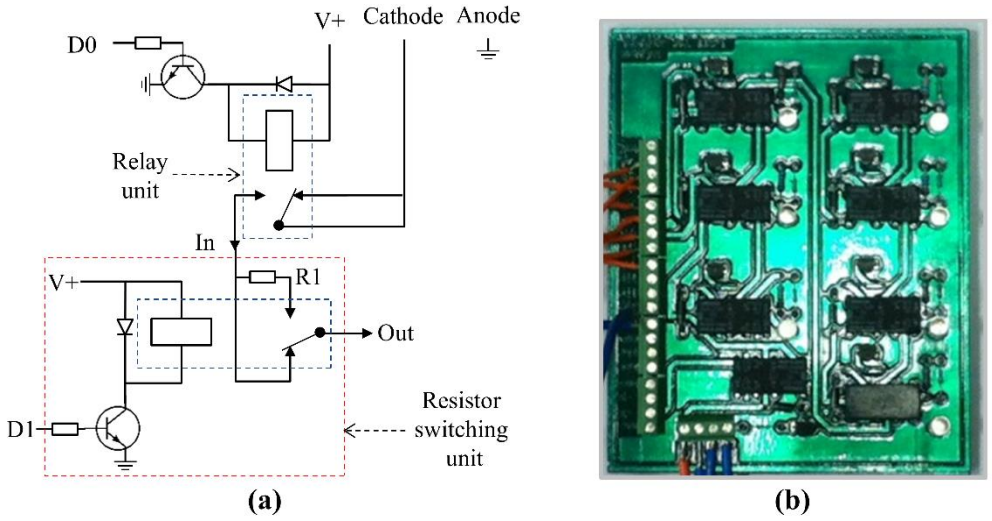

Figure 3.4: (a) Switching unit schematic for external load control electronics, and (b) printed board containing soldered components.

The effective series resistance value is determined by the summed values of the fixed resistors soldered into the circuit along with any contribution from circuit connections. Initial

board development made use of resistors starting from 5 kΩ and doubling for each subsequent relay, ending with 320 kΩ for a maximum effective resistance of 635 kΩ. This arrangement gives a large range that can be linearly addressed with respect to binary input number with a resolution of 5 kΩ. In practice, the errors and availability of standard fixed resistors moved the actual circuit slightly away from this ideal but was corrected for by sequential resistance measurement prior to testing. Initial testing with this resistor range showed insufficient coverage at the low end resistance to achieve suitable characterisations with Model B (c.f. Section 3.7). The resistor set was therefore adjusted to provide suitable coverage of the low resistance region. Appendix A, Table A.1 details the values achieved for binary input number for the two resistor sets, subsequently referred to as Resistor set 1 and Resistor set 2 for the linear set and low range set respectively.

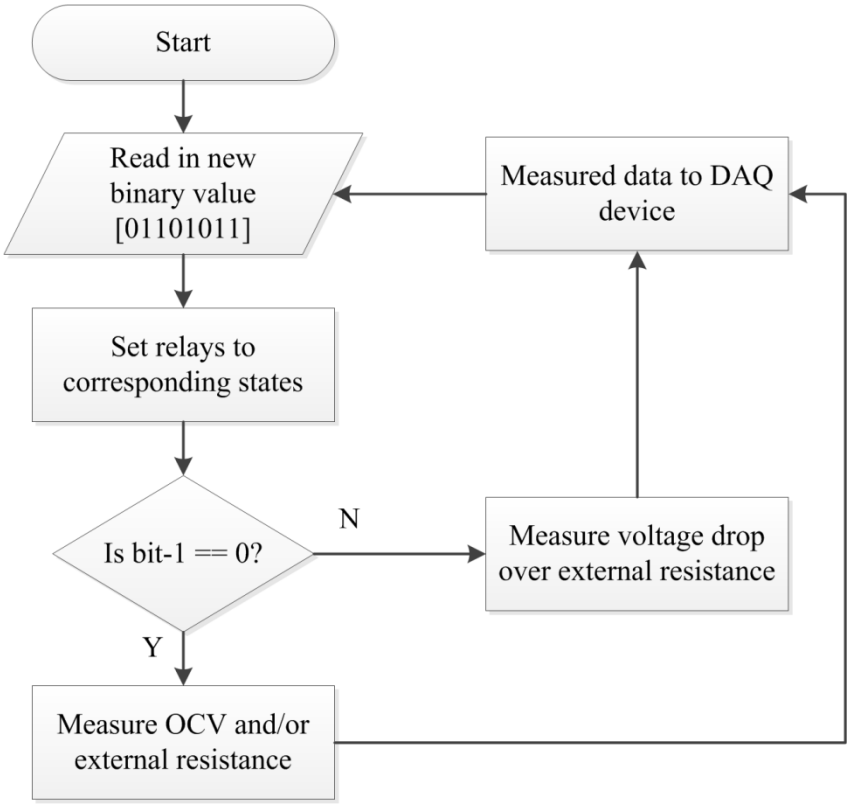

Figure 3.5: Flow chart illustrating the principle of operation of the designed electronics.

3.5 Measurement & Control Equipment

To meet Requirement 2.6, specialised hardware was required to control the external load and measure the corresponding voltage drop. Two systems were employed to achieve this: (1) the NI myDAQ (National Instruments, USA), and (2) the Ivium CompacStat (Ivium Technologies, the Netherlands). The former was used in conjunction with the electronics described within

Section 3.4, and programmed through custom software (LabVIEW, National Instruments, USA). Development with the NI myDAQ was conducted due to the limitations of the settings with the CompactStat. Through the use of this hardware, the Biogalvanic System was able to be made specific to the type of testing and flexible to the focused testing variables.

The CompactStat was used to perform two functions in the described tests, firstly as a Zero Resistance Ammeter (ZRA) to record current response of the myDAQ based biogalvanic system, and secondly as a standalone load control system for comparative characterisation. The following sections describe the utilised hardware in more detail.

3.5.1 NI myDAQ

The NI myDAQ (National Instruments, USA) is an inexpensive device that allows control and measurement of analogue and digital signals. The configuration is highly customisable through the accompanying software (LabVIEW, National Instruments, USA). The hardware specification for the myDAQ data acquisition device is given within Table 3.2. For the biogalvanic characterisation system, the device was configured to generate digital outputs for each of the relays on the custom PCB described within Section 3.4. In addition, a time-coded recording of the voltage drop across the external resistance was established. The accompanying control software for the myDAQ is described within Section 3.6.

Table 3.2: NI myDAQ specifications adapted from [151].

Parameter	Value
Manufacture	National Instruments
Model	myDAQ
Number of analogue input channels	2
Analogue input range	+/- 10 V, +/- 2 V
ADC resolution	16 bits
Number of digital IO channels	8

3.5.2 Potentiostat

Potentiostats allow the control and measurement of electrical signals in electrochemical systems [83]. The CompactStat (Ivium Technologies, the Netherlands) is a portable, small form-factor potentiostat with the power and precision to conduct simple electrochemical measurements. The platform can be powered from USB and is easily configured through native software (IviumSoft, Ivium Technologies), enabling equipment to be moved from lab to clinical setting. Some of the important specifications are presented in Table 3.3.

Figure 3.6 shows a diagram of a typical potentiostat (potential control) / galvanostat (current control) device. The electrochemical cell is connected to the electronic circuitry through standard external connector leads. These are labelled working electrode (WE), counter electrode (CE), reference electrode (RE), sense (S) and ground (G). During operation, the potential is measured between RE and S and the current is measured between CE and WE, i.e. through the electrochemical cell. When the cell is connected, the control amplifier drives the potential (polarisation) of the CE relative to the WE. The level of polarisation is controlled using potential feedback from RE-S (potentiostat mode) or current feedback from WE (galvanostat mode). The respective feedback signal is compared to the desired driving signal and the resulting error used to modulate the polarisation of CE appropriately. The device connectors can be reconfigured to give various modes of operation that have specific use in electrochemical testing.

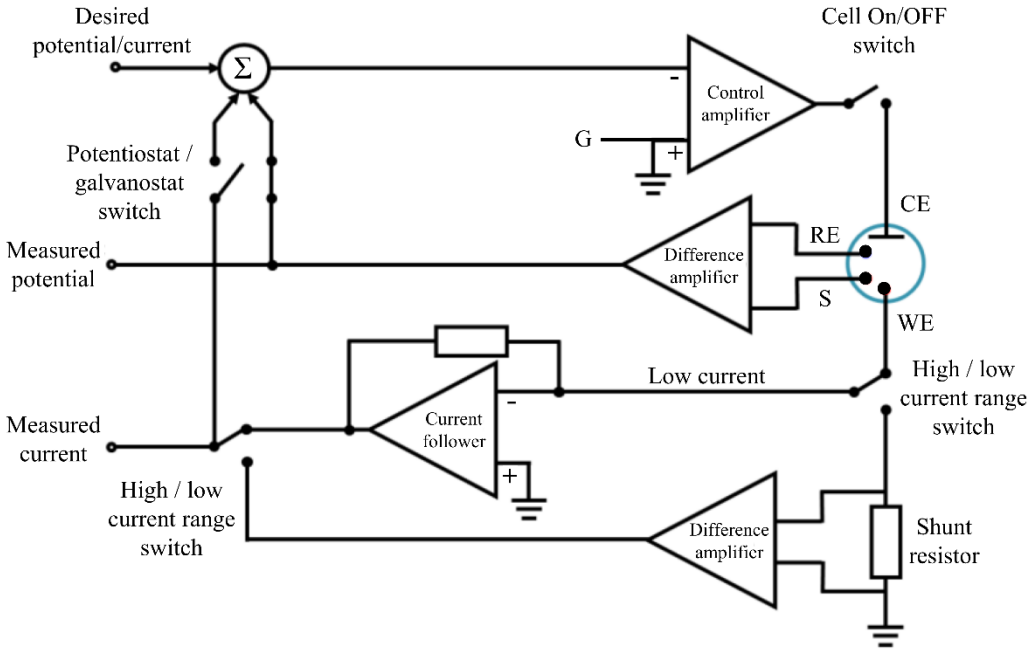

Figure 3.6: Diagram of the electronic configuration of a typical potentiostat/galvanostat, (image adapted from [152]).

Through disconnection of the cell and connection of G to the counter electrode of the electrochemical cell, the cell current can be accurately measured without augmenting cell potentials. This Zero Resistance Ammeter (ZRA) arrangement was used with the CompactStat to allow accurate measurement of cell current during characterisation with the myDAQ based biogalvanic characterisation system. Figure 3.7(a) shows schematically the how the ZRA was applied to the biogalvanic characterisation system.

Table 3.3: Ivium CompactStat specifications adapted from [153].

Parameter	Value
Manufacture	Ivium Technologies
Model	CompactStat
Current range	1 pA – 1 A
Voltage range	1 mV - 10 V
Time resolution	10 µs
Scan rates	1µ V/s – 10,000 V/s

The CompactStat was also used to develop an appropriate testing method for comparison. A two electrode polarisation cell was first established through coupling of the WE and S connectors and the CE and RE connectors respectively. The native software (IviumSoft, Ivium Technologies, the Netherlands) allows the cell potential and current to be regulated in accordance with a simulated external resistive load. The electrode and wiring configuration for this type of test is shown within Figure 3.7(b) [152]. Theoretically, this system offers external load control with a fully configurable resistor range. However, two issues are apparent: (1) the current limitations of the device limit the available low end resistance, and (2) the current range must be adjusted manually to allow testing in specific resistance ranges resulting in the need for multiple software configuration files to run a single test. Section 3.8 describes the comparison tests conducted using the CompactStat and the custom biogalvanic system.

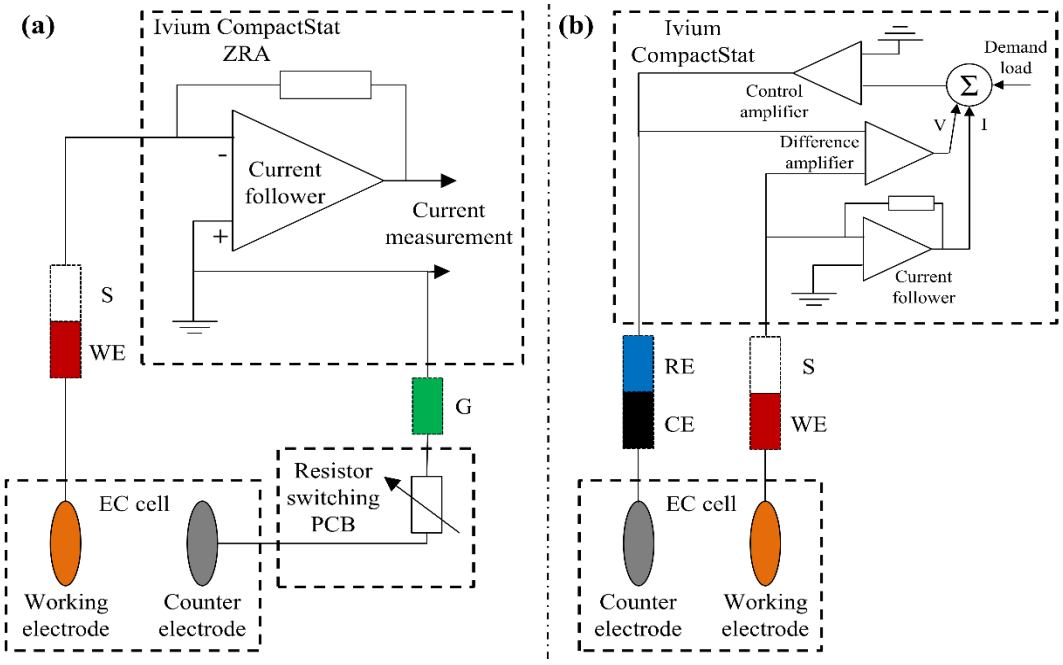

Figure 3.7: Biogalvanic testing system configured with the Ivium CompactStat Zero Resistance Ammeter (ZRA); allowing accurate current measurement during myDAQ based characterisation.

3.6 Software

This section describes the development of software to meet Requirement 2.7 with the use of the Biogalvanic system. The primary function of the developed software was therefore to send digital outputs to control the PCB relays autonomously while measuring, displaying and logging the corresponding voltage drop and resistor values. Additional functionality was added to allow programmatic control of the resistor range, switching rate, data averaging and repeat settings.

The software architecture was selected and implemented to allow simple configuration of testing protocols. Figure 3.8 shows the main user interface (UI) as well as the front panel of the test measurement program. Figure 3.9 shows schematically the program behaviour for running a configured test. A number of user selectable options were made available from the main user interface. The functionality of each has subsequently been described:

Watch Digital: *Allows monitoring and manual control of the digital channels of the myDAQ device. This can be used to apply specific external loads manually and to check electronic functionality.*

Watch Resistance: *Allows monitoring of the resistance external load currently switched in to the cell. This can only be measured when the cell is disconnected from the galvanic electrodes.*

Watch Voltage: *Allows monitoring of the voltage drop over the selected external loads. While the cell is disconnected this also allows for direct measurement of the OCV.*

Change IO: *Allows reconfiguration of the myDAQ channels. This is used only to meet physical alterations of the electronics system.*

Monitor Data: *Combines control of the digital channels with measurements of the corresponding voltage drop. This can be used to manually monitor cell performance prior to running automated tests.*

Configure & Run: *Loads the configuration interface where the user can select the desired test parameters of: switching rate, switching direction, resistor range, voltage averaging options and repeat options. Following completion of these fields the user may run the tests. This will automatically cycle through the defined tests and save the corresponding data.*

Review Data: *Generates a review interface where saved raw data files can be loaded and processed using the desired model fitting options.*

Stop: *Closes connection to the myDAQ device and stops the software.*

Figure 3.8: Main LabVIEW program UI (top) and testing measurement program UI (bottom).

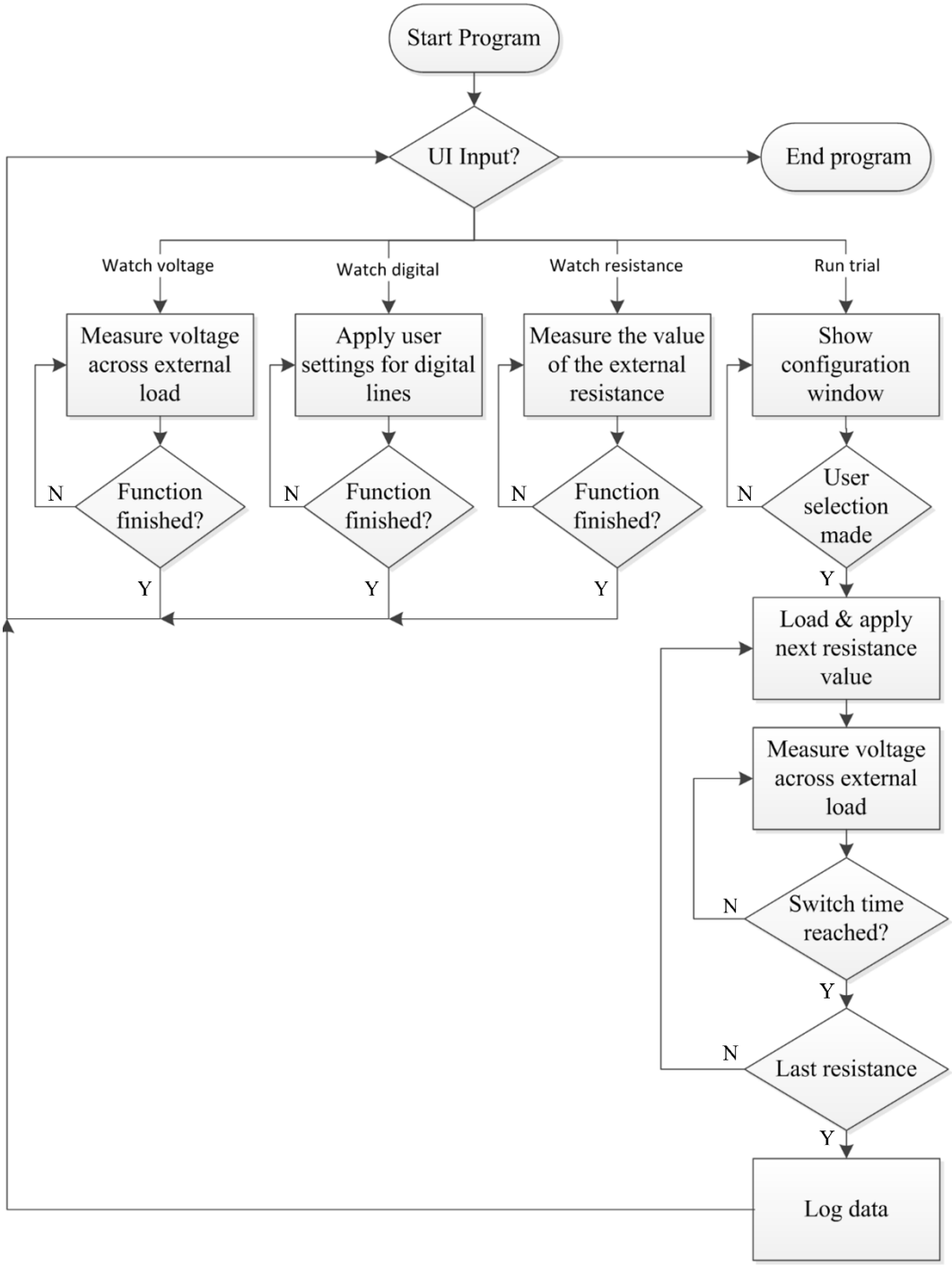

Figure 3.9: Flow chart schematic of the software architecture, illustrating program behaviour.

3.6.1 Steady state voltage measurements

The described software was configured to measure the steady state voltage of the individual cell-external load combinations. With the assumption of the transient behaviour of the cell behaving as a first order system, it is possible to define steady-state mathematically [154]. Equation (5.4) is representative of a first order system with a decaying exponential voltage (V) response. In this case V_0 represents the voltage prior to application of the new external load, τ is

the time constant specific to the system and t represents time. For times equal to multiples of τ it is possible to determine the percentage of signal decay, therefore allowing definition of steady state based on a specific percentage threshold. For example a decay time of 5τ would give a decay to less than 1% of the original voltage V_0.

$$V = V_0 e^{-\frac{t}{\tau}} \tag{3.1}$$

Although this method clearly gives a quantifiable means of establishing steady state, it was not practically selected. As the time constant for the system would be dependent on the test conditions and potentially the external load values, the suitable decay time would be variable. This removes experimental repeatability from the system and adds additional complexity to the analysis. An alternative method was utilised to make measurement times more consistent. Application of external loads was controlled for a fixed, specified time depending on the switching rate. To obtain a steady state voltage measurement, the arithmetic mean of a specified percentage of the data acquired prior to the next switch was taken.

A trade-off in the percentage of the signal chosen exists between removing noise and attaining a value most representative of steady state. Figure 3.10 illustrates how the average voltage reading is selected from measured data. It is evident that the accuracy relative to the true steady state value is dependent on the switching time and the time constant of the system. For a small τ, a fast switching rate will achieve an accurate steady state value, while the same switching rate applied to a system with a large τ will induce significant inaccuracy in the average voltage achieved. Application of this method is therefore at the discretion of the user and estimations of the system behaviour are required to make appropriate switching rate selections.

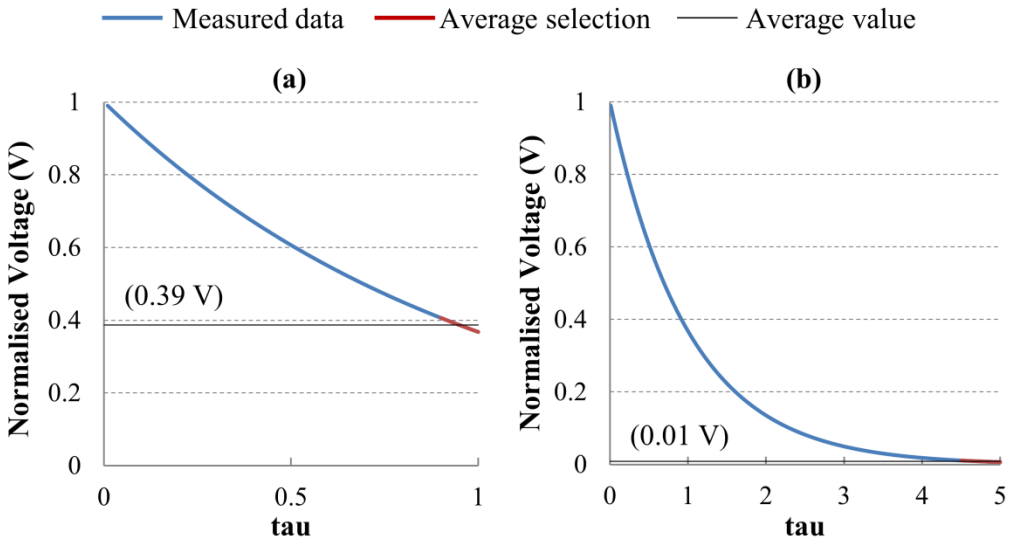

Figure 3.10: Illustration of the steady state averaging technique employed for determining voltage values corresponding to external loads. Shows a 10% data selection applied with a switching time equal to (a) τ and (b) 5τ.

3.7 Model Based Characterisation & Parameterisation

To determine useful metrics relating to the biogalvanic cell it is necessary to utilise a representative model. Models may be selected to fit to measured data in the most optimal fashion, or may use constitutive equations to relate measurements to the physical characteristics of the system. The following sections detail the electrical model and fitting strategies implemented within the biogalvanic characterisation process to meet Requirement 2.8.

3.7.1 Electrical models

A representative model of the biogalvanic system is shown in Figure 3.11. Based on this configuration it is possible to derive many theoretically valid characterisation approaches, including that proposed by Golberg et al. (equation (3.2)) [115]. In this case, a point-wise characterisation based on the independent current flow at one external resistance value is employed. Internal resistance (R_{INT}) can be determined for any external resistance as long as the OCV is known.

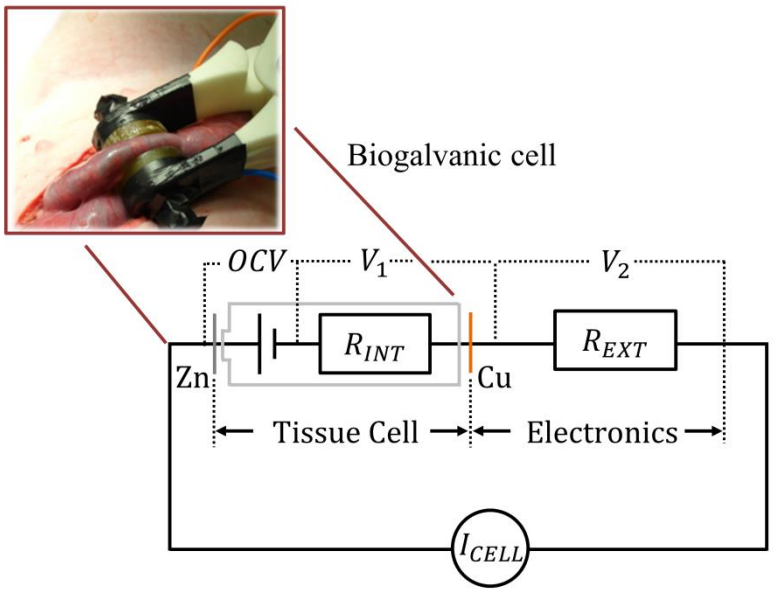

Figure 3.11: Electrical equivalent model of the biogalvanic system (insert: clamped tissue specimen).

3.7.1.1 Point-wise method

A point-wise characterisation may be performed through application of a single external load and measurement of the corresponding voltage drop. Based on equation (3.2), the OCV is also required. For comparison of the performance of this method to those proposed in the following sections, averaging across multiple external resistance values was conducted. The point-wise values were calculated for each external resistor in the characterisation set, based on equation

(3.2). For electronic model validation described in Section 3.8, these values were determined using the known value of OCV. The averages were then determined for the resistor set used, and compared to values attained with the alternative models.

$$\frac{1}{I} = \frac{R_{EXT}}{OCV} + \frac{R_{INT}}{OCV} \tag{3.2}$$

3.7.1.2 Model A

The expression of equation (3.2) is based on Ohm's law and an idealised electrical circuit analogy. Manipulation of this expression was employed to develop two model fitting schemes for characterising the measured data. The first (Model A) is given in equation (3.3), and offers a simple graphical method for determining the internal resistance (R_{INT}) and the equivalent Open Circuit Voltage (OCV). Determination of the relationship between the external resistor and inverse current flow using linear regression gives the internal resistance R_{INT} and the OCV; represented by the negated ordinate-intercept and gradient respectively. Figure 3.12(a) illustrates a typical Model A characterisation, and indicates how alteration of R_{INT} and OCV affects the plot.

(Model A) $$R_{\mathrm{EXT}} = \mathrm{OCV}\frac{1}{I} - R_{\mathrm{INT}} \tag{3.3}$$

3.7.1.3 Model B

The second model (Model B) uses an alternative expression relating the measured voltage (V_2) to the internal resistance and OCV for a given external load. The developed model is again based on the electrical analogy of Figure 3.11 and is expressed as equation (3.4). This was also extended into vectorised form as shown in equation (3.5), where $\boldsymbol{V}$ represents the vector of measured (V_2) voltages for the external resistor set ($\boldsymbol{R}$). This allows relation of a full measured dataset to a single internal resistance. Figure 3.12(b) shows the typical Model B plot on a logarithmic external resistor scale, again indicating how variation in R_{INT} and OCV influence the plot.

(Model B) $$V_2 = IR_{EXT} = \frac{OCV}{(R_{EXT}+R_{INT})}.R_{EXT} \tag{3.4}$$

$$\boldsymbol{V} = \frac{OCV}{(\boldsymbol{R} + R_{\mathrm{INT}})}\boldsymbol{R} \tag{3.5}$$

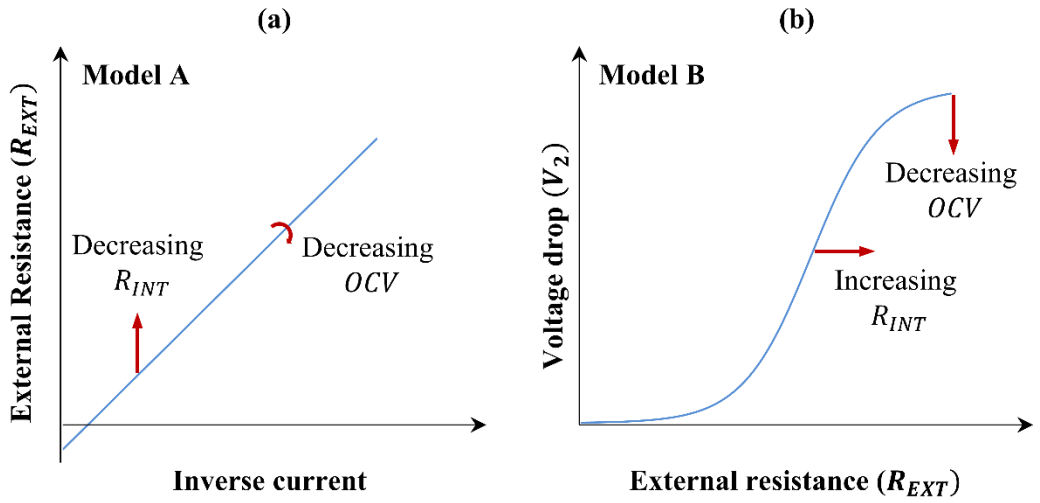

Figure 3.12: Typical model fits over a range of external resistor, showing influence of OCV and R_{INT} variation on (a) Model A, and (b) Model B.

3.7.2 Model fitting methodology

As alternatives to the point-wise internal resistance characterisation method of Golberg et al. [115, 116], the two electrical models developed were incorporated to allow all measured voltages over the R_{EXT} range to be used in determining a single value of R_{INT}. Model A and Model B, equations (3.3) and (3.4) respectively, were employed in two fitting algorithms to allow extraction of the desired internal resistance and OCV metrics.

3.7.2.1 Model A fitting

To fit to Model A, the LabVIEW Linear Fit function (National Instruments, USA) was used to generating a linear best fit for discrete measured V_2 and R_{EXT} data. Based on the relationship of equation (3.3), the internal resistance and OCV were extracted. Figure 3.13(a) shows a typical fit achieved using this fitting method with data measured from an electronic simulation cell described within Section 3.8.

3.7.2.2 Model B fitting

An alternative approach was required for application of Model B. The model, described by equation (3.5), was applied to the measured data using a Levenburg-Marquardt [155] algorithm (commonly employed for fitting of BIS data [116, 123]). This was employed in LabVIEW (National Instruments Ltd., TX), allowing minimisation of the sum of squares (S) determined by equation (5.4). In this case V_i is the voltage measured across the external resistance R_i and m represents the vector length determined by the number of external resistors employed. The vector of model coefficients to be optimised is $\boldsymbol{\beta}$ which in this case represents the OCV and R_{INT}. A single value for each element of $\boldsymbol{\beta}$ is determined for each dataset for the converged

minimum error fit. Figure 3.13(b) shows a typical output fit to measured data from the electronic simulation of Section 3.8.

$$S(\boldsymbol{\beta}) = \sum_i^m [V_i - f(R_i, \boldsymbol{\beta})]^2 \tag{3.6}$$

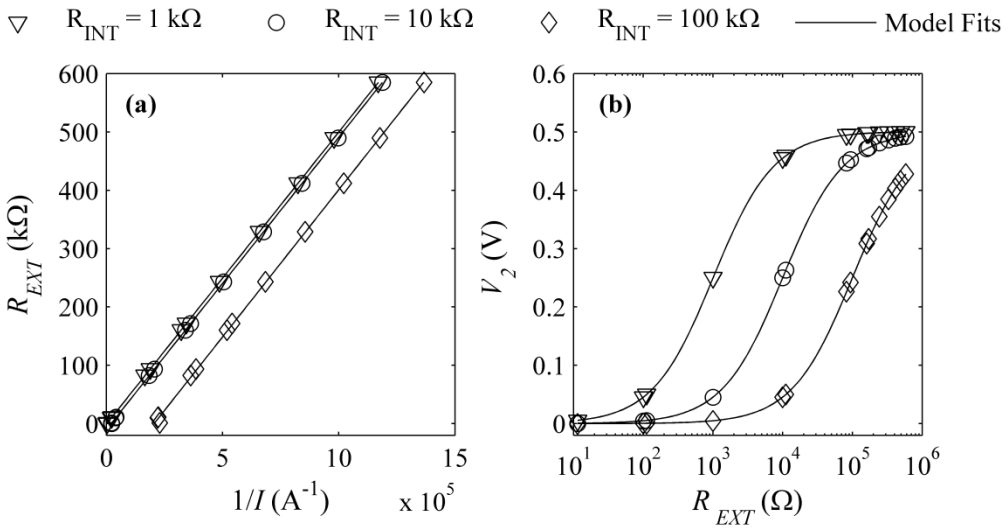

Figure 3.13: Typical optimised model fits to data measured using an electronic simulation of 1, 10 and 100 kΩ fixed resistors at 0.5 V OCV in conjunction with the custom biogalvanic measurement system, for (a) Model A, and (b) Model B.

The model fitting methods described in this section offer alternatives to internal resistance through a point-wise application of equation (3.2). The use of a complete dataset acts to reduce the variability associated with a point-wise scheme. In addition, the flexibility to determine an effective OCV value also removes the need for it to be measured directly under open cell conditions, or for it to be assumed for the specific test. The following section describes validation of the measurement systems described, and the proposed model fitting methods.

3.8 Validation

To validate the test systems developed, measurement and characterisation of electronic components was performed. Identical test procedures were carried out using both the Biogalvanic system and the CompactStat, allowing head-to-head comparison of the measurement system performance. In addition, characterisations were performed using the point-wise, Model A and Model B techniques described within Section 3.7 to allow comparison of the models and fitting methods. The validation methodology and results are detailed within

Section 3.8.1 and Section 3.8.2 respectively. Section 3.8.4 gives a summary of the important outcomes from the validation process.

3.8.1 Methodology

Validation was conducted through the use of an electronic cell model. Each model cell was comprised of a calibrated power supply (EL302RD, AIM-TTI Instruments, UK) in series with a fixed resistor. These components were configured to simulate the OCV and internal resistance of a biogalvanic cell respectively. A series connection with the measurement system under test was subsequently made, as illustrated within Figure 3.14. Measurements were conducted with a 0.5 V simulated OCV and simulated internal resistance values of 1, 10 and 100 kΩ. These values were representative of the range found from preliminary tissue measurements. The measurement systems employed were: (1) the Biogalvanic system (c.f. Section 3.5.1 & 3.6), and (2) the CompactStat in standard load control mode.

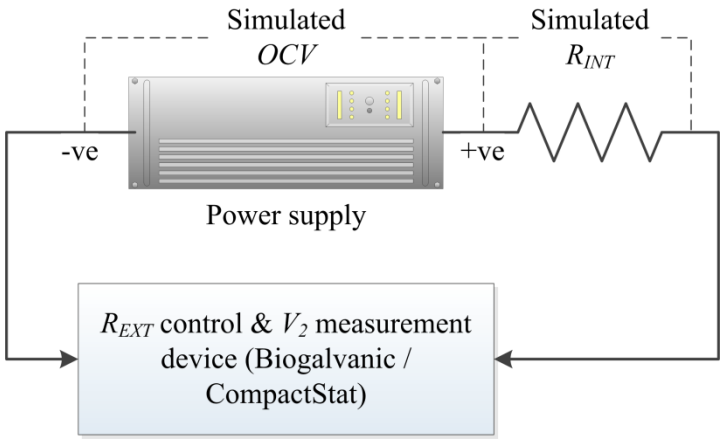

Figure 3.14: Schematic of the electronic simulation arrangement during connection to the external load control and voltage measurement device.

All output metrics were considered as an average of 10 repeat characterisations. Fifteen external resistance levels were used on both systems, ranging from 11.5 Ω to 585 kΩ with approximately even logarithmic spacing. Characterisation of the measured data was conducted using the point-wise method of Golberg et al. [115], as well as through application of Model A and Model B, as described within Section 3.7.1. Influence of resistor range on the model fit predictions was also analysed as part of the study. Figure 3.15 illustrates the characterisation methodology employed to extract the metrics required for the validation study.

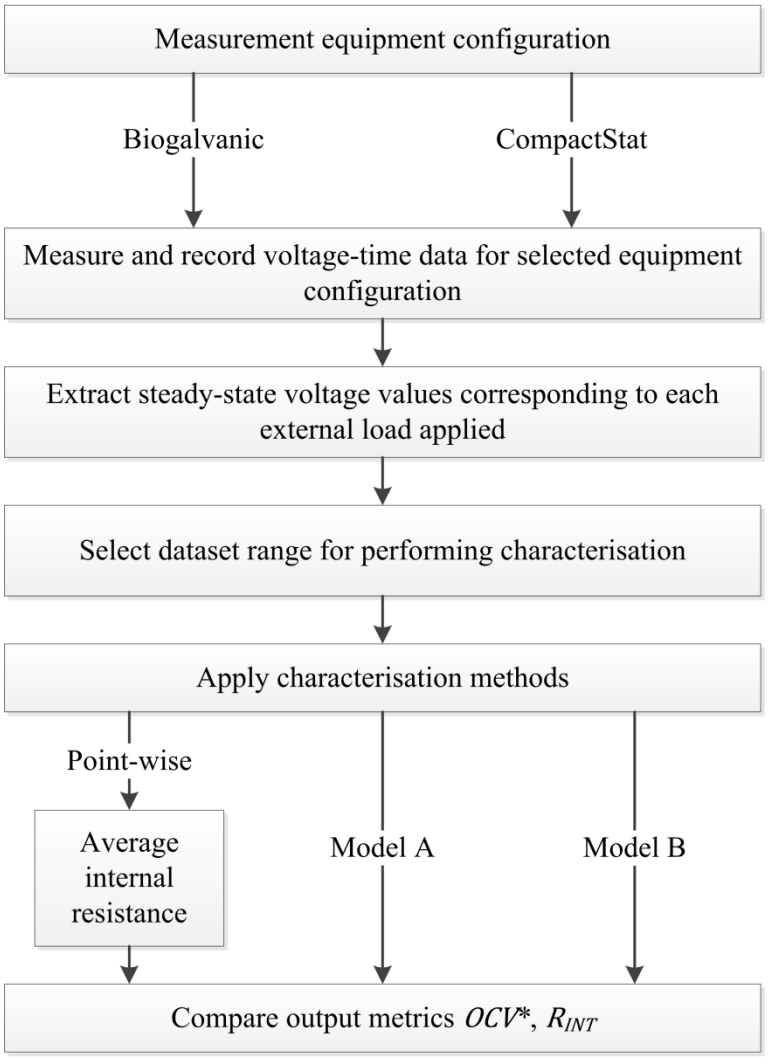

Figure 3.15: Methodology sequence used for validation of the measurement equipment and characterisation strategies (*OCV assumed for point-wise method).

3.8.2 Results

Example voltage-time traces recorded during a typical characterisation of an electronic test cell using the two measurement configurations are shown within Figure 3.16. The responses are as expected for electronic analogues, with sharp transitions at external load switching points. Deviations between the measurement configurations can be seen at external loads above 10 kΩ for characterisations of the larger internal resistances.

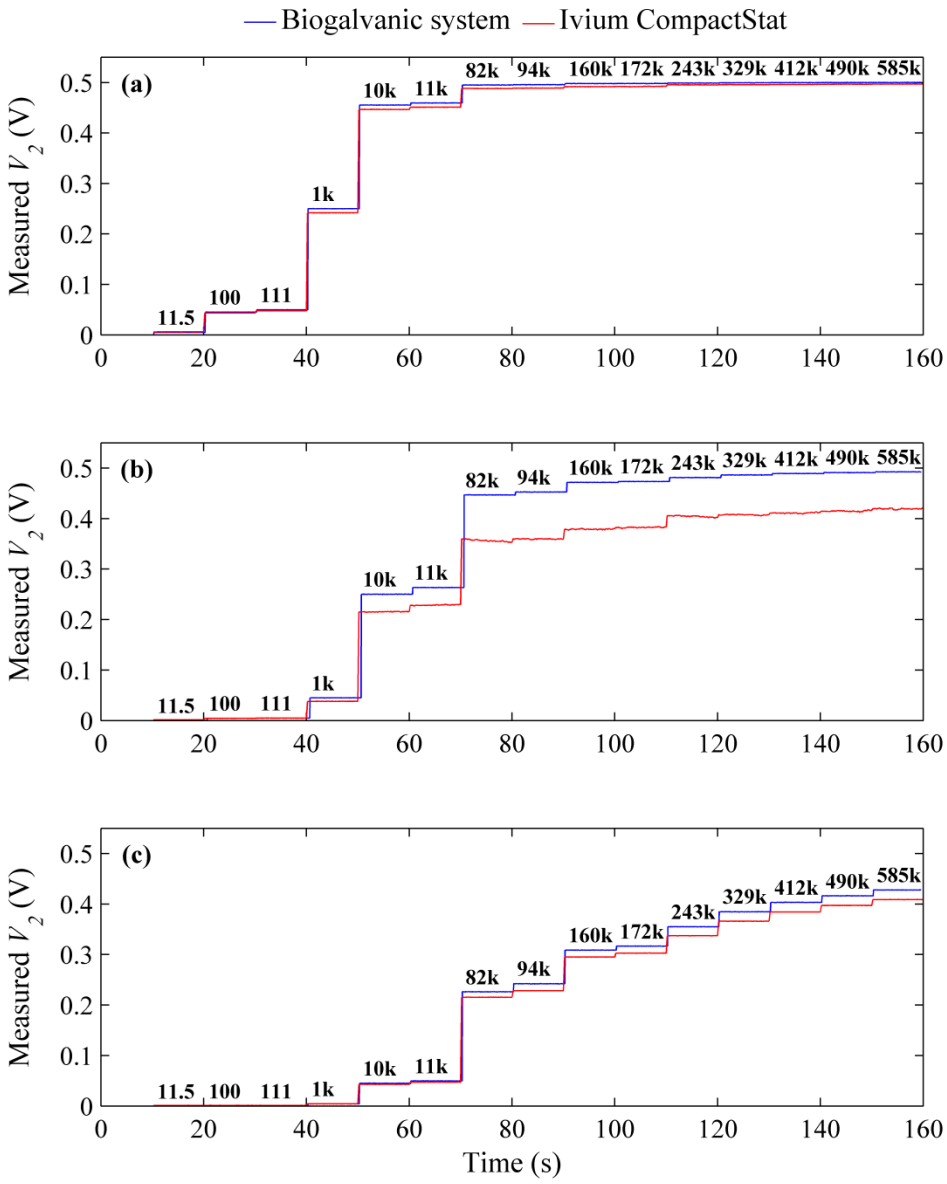

Figure 3.16: Example measured voltage (V_2) traces for electronic model characterisation of (a) $R_{INT} = 1$ kΩ, $OCV = 0.5$ V, (b) $R_{INT} = 10$ kΩ, $OCV = 0.5$ V and (c) $R_{INT} = 100$ kΩ, $OCV = 0.5$ V. Data shown from the Biogalvanic system and the Ivium CompactStat configured to load control mode; corresponding external resistance values are also shown (in Ohms).

The steady state voltages for each of the external loads were extracted from the voltage-time data. Two comparative metrics were calculated from each dataset: internal resistance and OCV. These were obtained using the three characterisation methods described within Section 3.7. The characterisation graphs obtained for application of Model A and Model B are presented within Figure 3.17 and Figure 3.18 respectively.

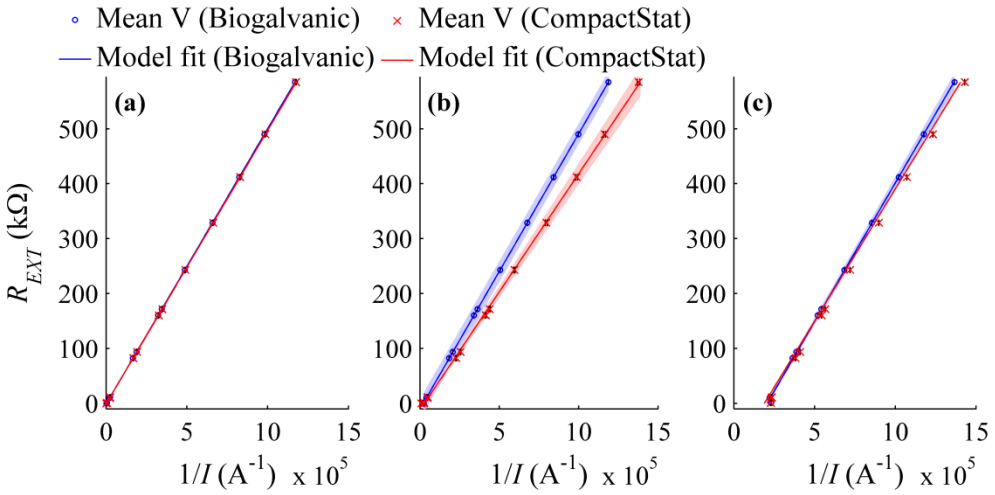

Figure 3.17: Mean measured V_2 (represented as $1/I = R_{EXT}/V_2$) and characterisation fit values for Model A fitting to electronic simulations of (a) $R_{INT} = 1$ kΩ, $OCV = 0.5$ V, (b) $R_{INT} = 10$ kΩ, $OCV = 0.5$ V, (c) $R_{INT} = 100$ kΩ, $OCV = 0.5$ V. Shaded region represents 1 standard deviation of the mean model fit. In order to improve clarity data presented in (b) and (c) are from resistor sets of 14 and 11 elements respectively; complete resistor range values are presented within Table 3.5.

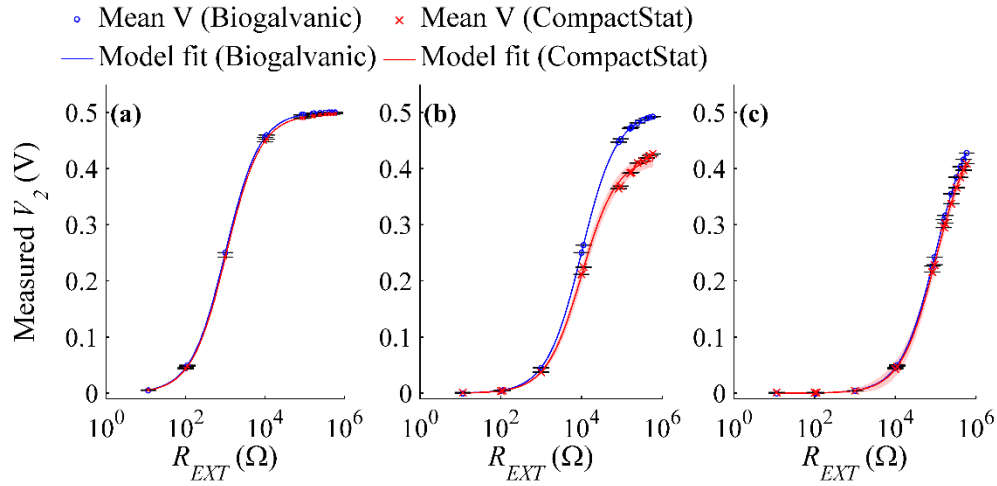

Figure 3.18: Mean measured V_2 and characterisation fit values for Model B fitting to electronic simulations of (a) $R_{INT} = 1$ kΩ, $OCV = 0.5$ V, (b) $R_{INT} = 10$ kΩ, $OCV = 0.5$ V, (c) $R_{INT} = 100$ kΩ, $OCV = 0.5$ V. Shaded region represents 1 standard deviation of the mean model fit.

Table 3.4, Table 3.5 and Table 3.6 show the characterised values obtained through point-wise, Model A and Model B respectively. In addition, this tabulated data contains the fitting results for external resistor set sizes ranging from 15-10. As error was primarily induced from the low end resistors this data was obtained through sequential removal of the lowest external load within the data set followed by re-fitting with the respective characterisation method.

Table 3.4: Point-wise data (Average (±SD)) for electronically simulated R_{INT} and OCV models ($1, 10$ and 100 kΩ at 0.5 V); including influence of resistor range selection on characterisation (n=10). All values determined using an assumed OCV of 0.5 V.

$R_{INT} = 1\ k\Omega, OCV - 0.5\ V$							
Resistor Range (size)		All (15)	2:15 (14)	3:15 (13)	4:15 (12)	5:15 (11)	6:15 (10)
myDAQ	$R_{INT}\ (k\Omega)$	0.629 ±0.020	0.591 ±0.022	0.559 ±0.023	0.521 ±0.025	0.477 ±0.028	0.427 ±0.030
CompactStat	$R_{INT}\ (k\Omega)$	1.887 ±0.052	1.954 ±0.056	2.023 ±0.060	2.103 ±0.065	2.197 ±0.071	2.299 ±0.078
$R_{INT} = 10\ k\Omega, OCV - 0.5\ V$							
Resistor Range (size)		All (15)	2:15 (14)	3:15 (13)	4:15 (12)	5:15 (11)	6:15 (10)
myDAQ	$R_{INT}\ (k\Omega)$	-71.04 ±241.21	9.792 ±0.018	9.666 ±0.020	9.540 ±0.023	9.484 ±0.024	9.435 ±0.027
CompactStat	$R_{INT}\ (k\Omega)$	41.85 ±1.146	44.52 ±1.251	47.01 ±1.372	49.91 ±1.509	53.33 ±1.656	57.33 ±1.837
$R_{INT} = 100\ k\Omega, OCV - 0.5\ V$							
Resistor Range (size)		All (15)	2:15 (14)	3:15 (13)	4:15 (12)	5:15 (11)	6:15 (10)
myDAQ	$R_{INT}\ (k\Omega)$	-53.42 ±174.2	-56.58 ±186.6	-29.18 ±204.7	100.7 ±0.096	99.39 ±0.031	99.24 ±0.025
CompactStat	$R_{INT}\ (k\Omega)$	99.48 ±0.356	106.2 ±0.363	110.7 ±0.286	115.7 ±0.039	115.9 ±0.039	116.9 ±0.054

Table 3.5: Model A fit data (Average (±SD)) for electronically simulated R_{INT} and OCV models ($1, 10$ and 100 kΩ at 0.5 V); including influence of resistor range selection on characterisation (n=10).

$R_{INT} = 1\ k\Omega, OCV - 0.5\ V$							
Resistor Range (size)		All (15)	2:15 (14)	3:15 (13)	4:15 (12)	5:15 (11)	6:15 (10)
myDAQ	$R_{INT}\ (k\Omega)$	1.017 ±0.008	0.998 ±0.008	0.995 ±0.010	0.991 ±0.012	0.987 ±0.014	0.984 ±0.018
	$OCV\ (V)$	0.501 ±0.000	0.501 ±0.000	0.501 ±0.000	0.501 ±0.000	0.501 ±0.000	0.501 ±0.000
CompactStat	$R_{INT}\ (k\Omega)$	1.273 ±0.027	1.316 ±0.031	1.359 ±0.036	1.418 ±0.043	1.502 ±0.054	1.609 ±0.067
	$OCV\ (V)$	0.498 ±0.000	0.498 ±0.000	0.498 ±0.000	0.498 ±0.000	0.498 ±0.000	0.498 ±0.000
$R_{INT} = 10\ k\Omega, OCV - 0.5\ V$							
Resistor Range (size)		All (15)	2:15 (14)	3:15 (13)	4:15 (12)	5:15 (11)	6:15 (10)
myDAQ	$R_{INT}\ (k\Omega)$	-17.860 ±58.502	10.404 ±0.014	10.228 ±0.014	10.036 ±0.011	10.002 ±0.012	9.998 ±0.016
	$OCV\ (V)$	0.439 ±0.151	0.502 ±0.000	0.501 ±0.000	0.501 ±0.000	0.501 ±0.000	0.501 ±0.000
CompactStat	$R_{INT}\ (k\Omega)$	11.841 ±0.189	13.020 ±0.232	13.450 ±0.291	14.035 ±0.383	14.916 ±0.500	16.393 ±0.698
	$OCV\ (V)$	0.430 ±0.002	0.431 ±0.002	0.432 ±0.002	0.432 ±0.002	0.433 ±0.002	0.435 ±0.002
$R_{INT} = 100\ k\Omega, OCV - 0.5\ V$							
Resistor Range (size)		All (15)	2:15 (14)	3:15 (13)	4:15 (12)	5:15 (11)	6:15 (10)
myDAQ	$R_{INT}\ (k\Omega)$	-139.76 ±34.88	-150.79 ±36.97	-153.93 ±52.21	103.92 ±0.24	100.52 ±0.09	100.28 ±0.08
	$OCV\ (V)$	0.115 ±0.083	0.112 ±0.082	0.116 ±0.094	0.505 ±0.000	0.502 ±0.000	0.501 ±0.000
CompactStat	$R_{INT}\ (k\Omega)$	68.746 ±0.884	82.140 ±1.076	90.911 ±0.921	103.29 ±0.139	101.60 ±0.164	101.57 ±0.146
	$OCV\ (V)$	0.444 ±0.001	0.459 ±0.001	0.468 ±0.001	0.481 ±0.000	0.480 ±0.000	0.480 ±0.000

Table 3.6: Model B fit data (Average (±SD)) for electronically simulated R_{INT} and OCV models ($1, 10$ and 100 kΩ at 0.5 V); including influence of resistor range selection on characterisation (n=10).

$R_{INT} = 1\ k\Omega, OCV - 0.5\ V$							
Resistor Range (size)		All (15)	2:15 (14)	3:15 (13)	4:15 (12)	5:15 (11)	6:15 (10)
myDAQ	R_{INT} $(k\Omega)$	1.009 ±0.000	1.009 ±0.000	1.008 ±0.000	1.007 ±0.000	1.002 ±0.002	1.005 ±0.002
	OCV (V)	0.501 ±0.000	0.501 ±0.000	0.501 ±0.000	0.501 ±0.000	0.501 ±0.000	0.501 ±0.000
CompactStat	R_{INT} $(k\Omega)$	1.061 ±0.001	1.061 ±0.001	1.062 ±0.001	1.063 ±0.001	1.119 ±0.009	1.126 ±0.010
	OCV (V)	0.497 ±0.000	0.497 ±0.000	0.497 ±0.000	0.497 ±0.000	0.497 ±0.000	0.497 ±0.000
$R_{INT} = 10\ k\Omega, OCV - 0.5\ V$							
Resistor Range (size)		All (15)	2:15 (14)	3:15 (13)	4:15 (12)	5:15 (11)	6:15 (10)
myDAQ	R_{INT} $(k\Omega)$	10.039 ±0.004	10.038 ±0.004	10.037 ±0.004	10.036 ±0.004	10.028 ±0.004	10.038 ±0.007
	OCV (V)	0.501 ±0.000	0.501 ±0.000	0.501 ±0.000	0.501 ±0.000	0.501 ±0.000	0.501 ±0.000
CompactStat	R_{INT} $(k\Omega)$	10.054 ±0.291	10.054 ±0.290	10.054 ±0.290	10.054 ±0.290	10.046 ±0.297	10.501 ±0.275
	OCV (V)	0.421 ±0.003	0.421 ±0.003	0.421 ±0.003	0.421 ±0.003	0.421 ±0.003	0.422 ±0.003
$R_{INT} = 100\ k\Omega, OCV - 0.5\ V$							
Resistor Range (size)		All (15)	2:15 (14)	3:15 (13)	4:15 (12)	5:15 (11)	6:15 (10)
myDAQ	R_{INT} $(k\Omega)$	100.2 ±0.064	100.2 ±0.064	100.2 ±0.064	100.2 ±0.064	100.2 ±0.064	100.1 ±0.066
	OCV (V)	0.500 ±0.000	0.500 ±0.000	0.500 ±0.000	0.500 ±0.000	0.500 ±0.000	0.500 ±0.000
CompactStat	R_{INT} $(k\Omega)$	101.4 ±0.161	101.4 ±0.161	101.4 ±0.161	101.4 ±0.161	101.4 ±0.161	101.4 ±0.159
	OCV (V)	0.479 ±0.000	0.479 ±0.000	0.479 ±0.000	0.479 ±0.000	0.479 ±0.000	0.479 ±0.000

Data in Table 3.4, Table 3.5 and Table 3.6 show the characterised metrics and the actual electronic simulation values across reducing external resistance set sizes. Figure 3.19 and Figure 3.20 present this information as a percentage characterisation error in R_{INT} and OCV for the three characterisation models using the Biogalvanic and CompactStat systems respectively.

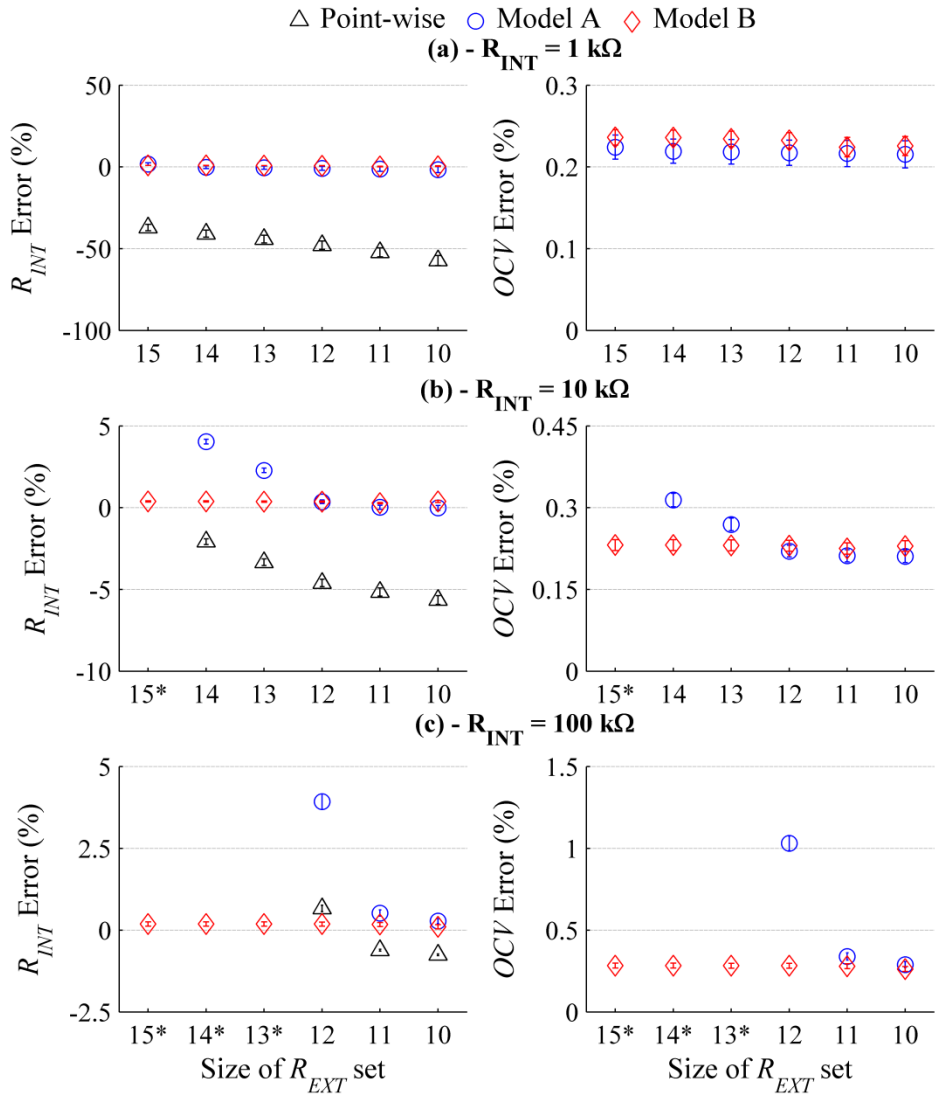

Figure 3.19: Percentage error from electronic model characterisation using data measured with the custom Biogalvanic system; indicating metric outputs from Point-wise, Model A and Model B characterisations. The influence of the input measured dataset size on the characterised internal resistance and OCV is shown for electronic models (a) $R_{INT} = 1$ kΩ, $OCV = 0.5$ V, (b) $R_{INT} = 10$ kΩ, $OCV = 0.5$ V, (c) $R_{INT} = 100$ kΩ, $OCV = 0.5$ V. *Indicates where data points have been omitted due to magnitude of error, values for these points may be found within Table 3.5, Table 3.6 and Table 3.4.

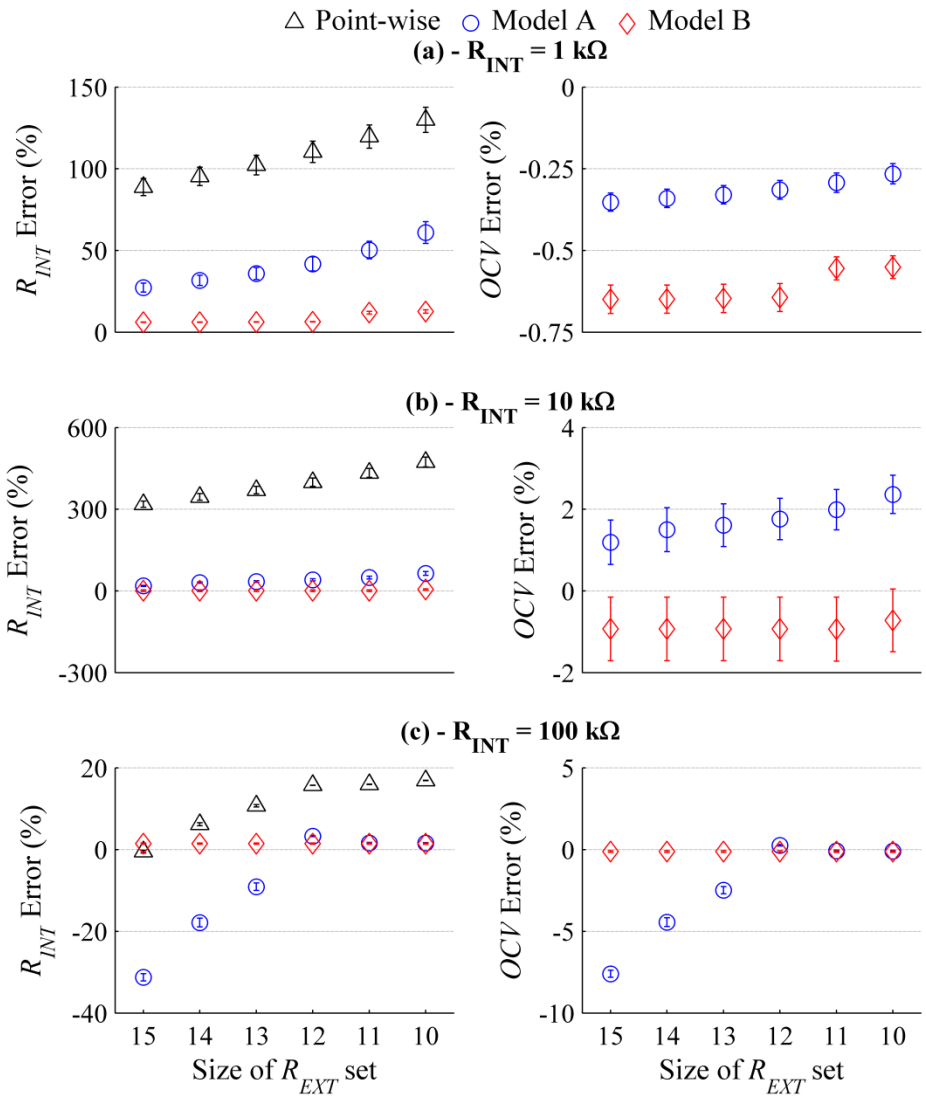

Figure 3.20: Percentage error from electronic model characterisation using data measured with the Ivium CompactStat; indicating metric outputs from Point-wise, Model A and Model B characterisations. The influence of the input measured dataset size on the characterised internal resistance and OCV is shown for electronic models (a) $R_{INT} = 1$ kΩ, $OCV = 0.5$ V, (b) $R_{INT} = 10$ kΩ, $OCV = 0.5$ V, (c) $R_{INT} = 100$ kΩ, $OCV = 0.5$ V.

Figure 3.21 shows the error in internal resistance determined using the point-wise method for the electronic simulation as a function of the external resistor used within the calculation (equation (3.2)). For these calculations the OCV was input as that measured on the power supply as well as values ±1% of this, representing the influence of small variations in OCV as seen in biogalvanic systems [114].

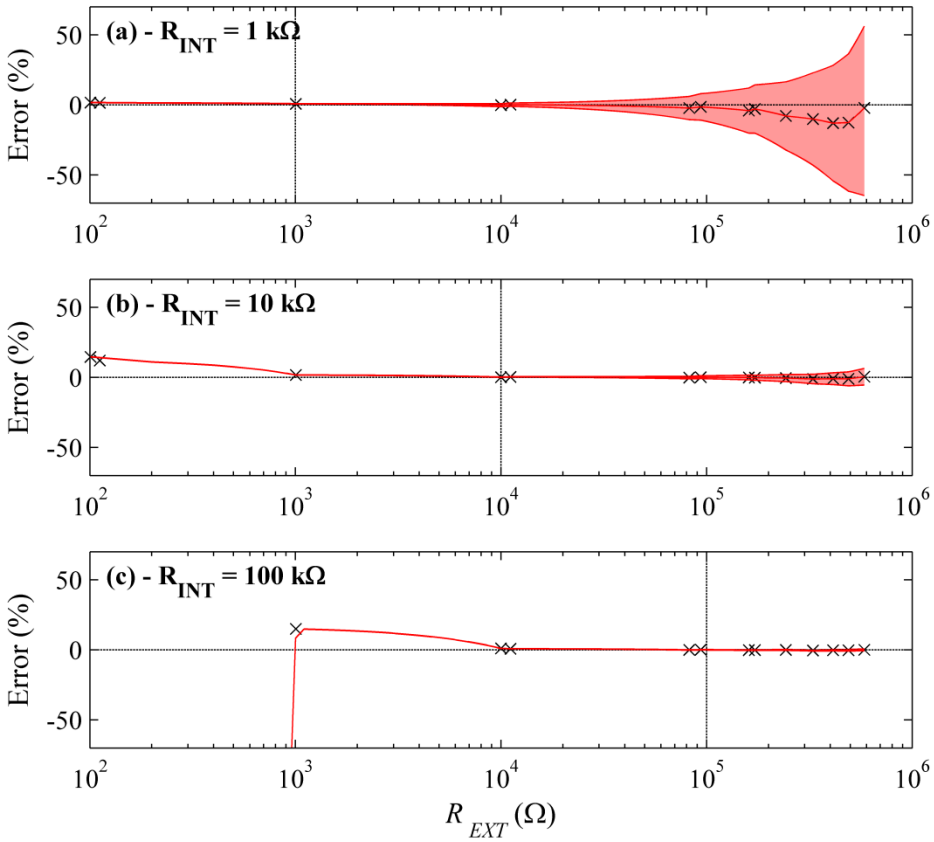

Figure 3.21: Error (%) in determined R_{INT} values using point-wise method, as a function of R_{EXT} used in calculation; (x) represent determined R_{INT} using correct OCV, error range from ±1% variation of correct OCV shown as the shaded region. Data measured using the Biogalvanic system on electronic simulations of (a) $R_{INT} = 1$ kΩ, $OCV = 0.5$ V, (b) $R_{INT} = 10$ kΩ, $OCV = 0.5$ V, (c) $R_{INT} = 100$ kΩ, $OCV = 0.5$ V.

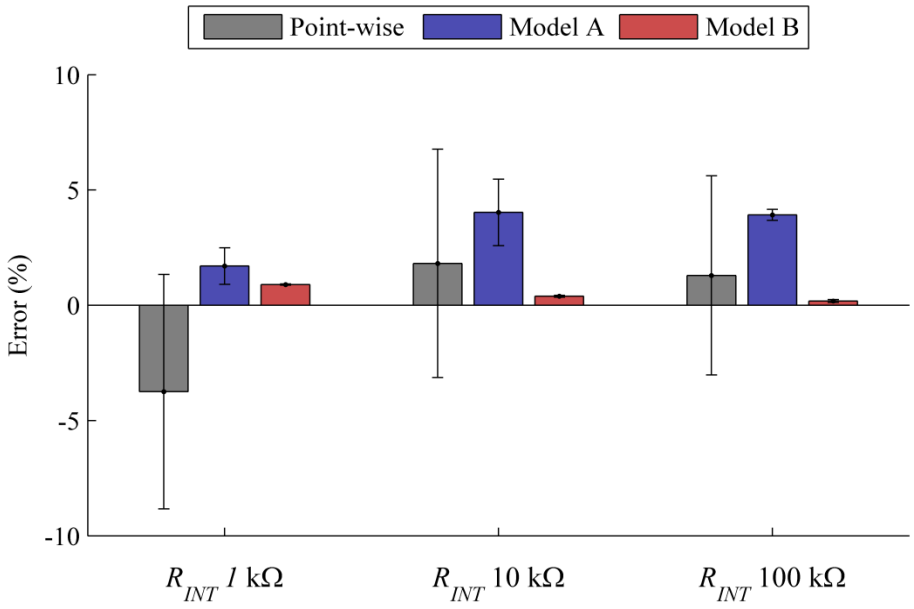

Figure 3.22: Mean error (%) ± 1SD (n = 10) in determined R_{INT} for point-wise, Model A and Model B characterisation methods, performed with data measured using the Biogalvanic system on electronic simulations of $R_{INT} = 1, 10$ & 100 kΩ $at\ OCV = 0.5$ V. Model A error at 10 and 100 kΩ shown for resistor sets of 14 and 11 respectively.

3.8.3 Validation discussion

The validation study performed shows variability with the control and measurement systems selected for testing as well as the model and fitting approach used for metric generation. The following sections detail and discuss main findings from the study and give justification for the testing systems used within initial tissue and salt solution testing described within Chapter 4 and Chapter 5 respectively.

3.8.3.1 Control & measurement systems

Two systems were employed in the presented validation study. These were the Biogalvanic system and the Ivium CompactStat configured to load control mode. Figure 3.16 shows representative voltage-time traces for the two systems. It can be seen that for internal resistance values simulated at 10 and 100 $k\Omega$ there are significant differences. This is most prominent with the 10 $k\Omega$ test, where voltages are of the order of 100 mV lower using the CompactStat at high external loads. Differences in the voltage traces are persistent through the characterisation processes and lead to much higher errors within the characterised R_{INT} and OCV values, as illustrated through comparison of Figure 3.19 and Figure 3.20.

This ultimately brings the performance of the CompactStat under these conditions into question. It should be noted, however, that the reason for many of these significant errors is likely due to the challenge of configuring the potentiostat to conduct load control experiments over the desired testing range (an unusual application of the CompactStat device). Indeed, incorrect matching of measurement current range and external load with the simulated R_{INT}, OCV combination can lead to current saturation, inducing an incorrect voltage reading. The complexity of addressing this configuration issue was deemed outside of the scope of early stage testing and therefore initial parametric testing of Chapter 4 and Chapter 5 was conducted using the custom Biogalvanic system. For later stage testing it was necessary to utilise the CompactStat to perform load control experiments, and so these issues were revisited as part of the work presented in Chapter 6.

3.8.3.2 Characterisation technique comparison

Three characterisation techniques were utilised in the presented validation study. These were point-wise calculation using equation (3.2) with the assumption of a fixed OCV, linear regression fitting to the developed Model A of equation (3.3), and least-squares fitting to the developed Model B of equation (3.4). Figure 3.17 shows the model fits achieved using Model A for the electronic simulations tested. It is evident that the data fit well to the linear model of equation (3.3). However, the presented data for 10 and 100 $k\Omega$ shows results from reduced external loads set sizes. This is due to the large fitting error induced by the low external

resistance voltage reading under these simulations. This is particularly evident within the characterisation error (%) presented within Figure 3.19 and Figure 3.20. For the larger resistor sets used, characterisation error with Model A was found to be large. This increased error was more prominent in the larger simulated external loads and in the Biogalvanic system. The latter is likely due to the improved resolution of the CompactStat device.

Figure 3.18 shows the model fits achieved using Model B for the electronic simulations testing. The least-squares fitting method presented in Section 3.7.2 allows equation (3.4) to be applied to the measured data with minimal error. Figure 3.19 and Figure 3.20 show that the characterisation error (%) achieved when using Model B compares favourably to the alternative methods. Not only is the error typically lower than other methods, but it remains widely consistent through alteration of the external load range used and the simulated internal resistance. This robustness to variation of input data is particularly relevant to tissue testing, where the resistance being characterised is not known at the time of the measurement and therefore a wide range of external loads, particularly at the low end is required.

The use of a point-wise technique, offers the simplest approach to resistance measurement. However, it can be seen within Figure 3.19 and Figure 3.20 that the error (%) is often large and particularly sensitive to the resistor range testing, even with the use of averaging over the full resistor range. Figure 3.21 illustrates the error (%) caused as a function of the external load selected for the calculation and for accurately known OCV. For R_{EXT} values greater than the internal resistance, error increases linearly with increasing R_{EXT}. For R_{EXT} values smaller than R_{INT}, errors become large due to the resolution of the voltage measurement system. Variations in the OCV used also exaggerates these errors, making point-wise characterisation accurate only with R_{EXT} values similar to the internal resistance. For the case of tissue assessment, the internal resistance will be unknown at the time of measurement therefore selection of a similar external load would be challenging. With this method there is also an additional need for measurement or assumption of the cell OCV prior to each characterisation. The consequence on the characterisation error for small inaccuracies (±1 %) in this value is shown within Figure 3.21. The overall sensitivity in resistance characterisation makes it a poor choice for assessment of biogalvanic characterisation as a whole.

3.8.4 Validation summary

Figure 3.22 compares errors produced by point-wise, Model A and Model B characterisation of R_{INT} for the electronic simulations tested. Errors associated with the point-wise data and the linear regression fit of Model A are comparable and larger than those for the least squares characterisation of Model B. Characterisation errors for Model B range from 0.9% to 0.19% with increasing simulated R_{INT}. This is much lower than the errors presented with the other two

methods, which have a range of ±4%. More significantly, the variability seen within repeats is negligible for Model B compared to the point-wise and Model A characterisations which show standard deviation of up to ±5%. Improved characterisation accuracy and precision, coupled with reduced sensitivity to external resistor range and OCV indicate that the least squares fitting method of equation (5.4) using Model B is more robust than the point-wise and Model A methods. The validation study presented has also highlighted the challenging nature of performing load control experiments using the CompactStat. For these reasons the subsequent characterisation data reported within Chapter 4 and Chapter 5 have been attained using the Biogalvanic system in conjunction with model B fitting.

3.9 Chapter Summary

In meeting Objective 3.1, the requirements for the development of a practical system for performing biogalvanic characterisation have been considered. Based on these findings suitable systems were developed, allowing the contact, measurement and analysis of tissue samples. Presented solutions take the form of the Biogalvanic system, a bespoke software controlled electronic measurement system, and a commercial potentiostat (CompactStat, Ivium Technologies) configured to allow external load control. The exploration and development of these systems pertain to Objectives 3.2 and 3.4 respectively. In accordance with Objective 3.3, manufacture of suitable biogalvanic electrodes has been described (Section 3.2), with applied testing reported within Chapter 4.

For application to the measured data collected using these systems, a range of model fitting algorithms were explored, realising Objective 3.5. The findings from the system validation suggest that fitting across a full range of measured data to produce and single internal resistance and OCV may reduce the sensitivity of the system to external load selection. The combination of the Biogalvanic system and least squares fitting of Model B (equation (3.4)) has been verified as the most appropriate selection for application to tissue models. This has therefore been utilised in the work of the following chapters where appropriate.

Chapter 4
Biogalvanic tissue testing

This chapter describes the first stage of tissue testing with the biogalvanic characterisation system described in Chapter 3. A parametric investigation into the contacting conditions and the sensing configuration has been undertaken. Primarily, the testing described was conducted on *ex vivo* porcine tissues, although additional results from *in vivo* porcine tissue and *in vitro* and *ex vivo* human tissue are also presented.

The results indicate that modelling a galvanic tissue system as a fixed Open Circuit Voltage (OCV) and internal resistance (R_{INT}) in series corresponds well with measured data both *ex vivo* and *in vivo*. Through application of the proposed measurement technique and the model fitting methods described in Chapter 3, repeatable determination of these two parameters is possible.

Results show that internal resistance is sensitive to tissue type, thickness and mechanical strain conditions. Additionally, the external resistor switching rate and direction have been shown to influence the characterised resistance. In combination these results demonstrate that the simplicity of the model proposed does not allow for complete capture of the resistive properties of tissues. In contrast, variability found in the determined OCV due to test conditions was found to be less than for R_{INT}. This parameter also showed specificity to tissue type, and based on a single test on diseased *ex vivo* rectum tissue, showed a difference with tissue health.

4.1 Testing Aims

The desired application of the biogalvanic characterisation system is as a contact measurement device incorporated into a surgical tool for MIS. As such the biogalvanic method of tissue characterisation requires testing under appropriate conditions. The primary aim of the testing presented is to assess the performance of the technique under contact with tissue; defining the validity of the test equipment and model assumptions employed. In addition, it is an aim of the study to determine the significant influencing parameters on the characterisation process that may affect application in surgery. The following objectives were defined to allow realisation of the chapter aims:

Objective 4.1: *To assess the efficacy of the custom biogalvanic characterisation system developed in Chapter 3.*

Objective 4.2: *To investigate the model assumptions and findings presented by Golberg et al. [115, 116]. Specifically, evaluate the applicability of normalising the biogalvanic resistance to GAIR.*

Objective 4.3: *To utilise the developed Biogalvanic characterisation system to perform parametric investigation into the influence of tissue thickness and strain, and external resistance switching rate and direction.*

Objective 4.4: *To explore the applicability of the technique on both ex vivo and in vivo tissues.*

4.2 Testing Conditions

A wide range of tissue tests were performed in order to meet the objectives outlined in Section 4.1. This section details the testing conditions for the various experiments described. Conditions for *ex vivo* porcine tissue, *in vivo* porcine tissue, *in vitro* human tissue and *ex vivo* human tissue are described within the following sections respectively.

4.2.1 Porcine tissue *ex vivo*

Measurements were conducted on fresh *ex vivo* porcine tissues (liver and colon). Animals used were bred and sacrificed in accordance with UK Home Office regulations (Animals [Scientific Procedures] Act 1986). Porcine colon and liver were dissected immediately after death to obtain fresh tissue. Tissue was transported to the University of Leeds and experiments were carried out

at least four hours after death. All tissue samples were handled, transported, stored and discarded in accordance with The University of Leeds tissue protocol. Figure 4.1(a) shows typical testing conditions for *ex vivo* porcine colon tests using the Testing platform described within Section 3.3.

4.2.2 Porcine tissue *in vivo*

Tests were conducted on female white pigs under UK Home Office regulations for animal experimentation. Access to the organs (colon, rectum and liver) was facilitated via a large abdominal incision (laparotomy). Biogalvanic characterisations and galvanic current measurements were performed on the exposed porcine tissues. Alignment of testing electrodes was achieved through the use of the Surgical clip described within Section 3.3. Figure 4.1(b) shows a typical biogalvanic characterisation test performed on porcine colon tissue *in vivo*.

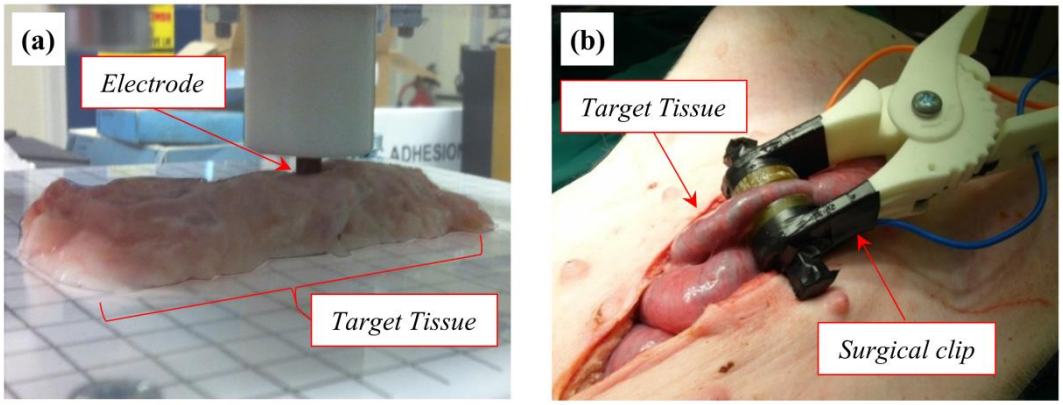

Figure 4.1: Typical contacting conditions for biogalvanic porcine tissue testing, showing (a) ex vivo porcine colon tissue testing with A_{12} electrodes under minimal strain using the Testing platform, and (b) application of A_{12-R} electrodes to porcine colon *in vivo* using the Surgical clip.

4.2.3 Human tissue *in vitro*

This study describes a single experiment performed on cadaveric tissues *in vitro*. Measurements were performed on liver tissues exposed in the abdomen of a human cadaver. The cadaver experimentation was conducted in accordance with the National Research Ethics Service Committee Yorkshire and the Humber – Leeds East (REC reference: 12/YH/0063). Galvanic current measurements were performed on liver tissue under a number of electrode configurations described within Section 4.5.1.

4.2.4 Human tissue *ex vivo*

This study describes a single experiment performed on excised, diseased human rectal tissue. Freshly excised human rectal tissue was obtained in accordance with NHS and Leeds Teaching Hospital ethics procedures. Biogalvanic measurements were performed on abnormal (adenocarcinoma) and contrasting healthy tissue identified by the surgeon. Test results have been presented within Section 4.5.2.

4.2.5 Biogalvanic characterisation

Experimentation documented in this chapter primarily consists of biogalvanic characterisation tests performed on various tissue types. The following sections detail the measurement setting ranges and electrode configurations used.

4.2.5.1 Measurement settings

From the validation study performed in Section 3.8, the Biogalvanic system was selected for performing initial tissue testing. This was based on the demonstrated current saturation errors found for high internal resistance tests when using the CompactStat (c.f. Section 3.8.3.1). All biogalvanic characterisation tests described within this chapter were performed using this system. Due to the developmental nature of the testing conducted some of the characterisation settings were adjusted between investigations. However, all voltage readings were sampled at 25 Hz with steady state values taken as the arithmetic mean of the final 10% of samples recorded prior to external load switching. External resistor switching rate was set to 0.05 Hz unless otherwise stated. Two resistor sets were employed for testing (specific values detailed in Appendix A, Table A.1), defined as:

Resistor set 1 *31 approximately linearly spaced resistors ranging from 5-635 kΩ.*

Resistor set 2 *15 approximately logarithmically spaced resistors ranging 10-5.85×10^5 Ω.*

4.2.5.2 Electrode configurations

Characterisation of *ex vivo* porcine liver and colon tissue was conducted using A_6 and A_{12} copper and zinc electrode pairs manufactured as described within Section 3.2. Electrodes were connected to the resistor network using copper wire. Tissues were contacted with the wet ground (1200 grit) end faces of the electrodes in axial alignment. Application of the electrodes to tissues was achieved using the Testing platform for *ex vivo* work and the Surgical clip for *in vivo* work, as shown in Figure 4.1. The testing platform allowed conformation to tissues of

varied thickness and control of the applied mechanical tissue strain. The Surgical clip allowed *in vivo* tissues to be held with a fixed strain and reliable contact during measurement.

4.2.6 Galvanic current measurements

As the current demand on a galvanic cell is increased, a maximum value is achieved. This is indicative of the current limiting mechanism of the cell. Based on the characterisation model assumptions (Section 3.7) this should be related to the internal electrical resistance of the cell. In addition, under a closed cell condition the rate of reaction at both electrodes will be at a maximum, driving any passivation (electrode fouling) processes to occur as fast as possible. Testing of this property was therefore carried out to assess how various electrode configurations influence the measured closed cell current.

4.2.6.1 Measurement settings

Each measurement was performed through insertion of the electrode pair directly into the target medium. A ZRA (CompactStat, Ivium Technologies) was employed to monitor the galvanic current flow under closed cell conditions for a period of 10 min (600 s). For comparison, steady state galvanic currents were taken as the average of the measured current over the final 200 s of each test.

4.2.6.2 Electrode configurations

Needle electrodes were manufactured using (Ø1 mm) zinc and copper wire (Goodfellow, UK) to have a range of separations and exposure lengths. Figure 4.2 shows the important electrode geometry and an example of a complete electrode pair. Table 4.1 details the full range of needle electrode pairs constructed and the corresponding codes used for their identification.

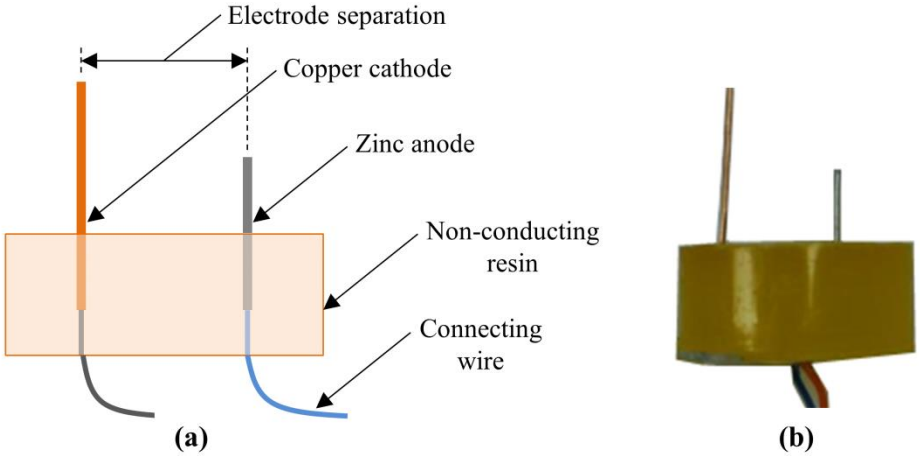

Figure 4.2: Needle electrode construction showing (a) schematic of electrode geometry, (b) example of physical manufactured electrode (electrode N_I shown).

Table 4.1: Geometries of the needle electrode range manufactured for closed cell current testing.

Anode length (mm)	Cathode length (mm)	Separation (mm)	Corresponding Code
10	10	7	N_A
10	10	14	N_B
10	10	20	N_C
10	10	24	N_D
10	10	30	N_E
20	20	20	N_F
30	30	20	N_G
10	15	20	N_H
10	20	20	N_I
10	25	20	N_J

4.3 Porcine (*ex vivo*) Experiments

This section describes *ex vivo* porcine tissue experiments performed to assess the influence of various parameters on the biogalvanic characterisation process and its associated metrics. In particular, variation with the tissue parameters of position, thickness, area and strain has been examined. Additional investigation into the influence of exposure time and switching rate has also been described.

4.3.1 Repeats and positional variation

An initial set of testing was conducted to establish the variation of the characterised resistance with position across a tissue surface. Tests were performed on *ex vivo* colon and liver with dissected sections giving 10 cm of working length. Seven 1 cm spaced test locations were identified across the surface of the two tissue types. A set of A_6 electrodes were positioned into contact with the tissue under minimal strain prior to each test; this electrode separation value was used as a measure of tissue thickness. Resistor set 1 was employed for biogalvanic characterisations and the measured data was fit using Model A. Three repeat measurements were taken at each of the test locations using an external resistor switching rate of 0.5 Hz. Figure 4.3 shows the average data for each location on the colon and liver tissue, along with the corresponding average Model A linear fit.

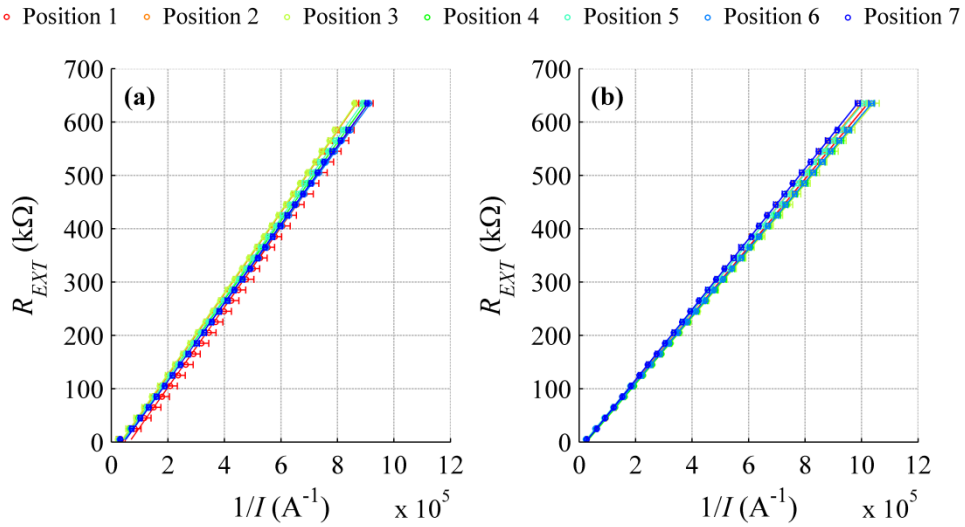

Figure 4.3: Mean measured V_2 (represented as $1/I = R_{EXT}/V_2$ ± SD (n=3)) and Model A characterisation fits for varied positions across (a) *ex vivo* porcine colon, and (b) *ex vivo* porcine liver.

Through characterisation of the measured data using Model A, the R_{INT} and OCV for each position was extracted. Table 4.2 and Table 4.3 show the average data from these characterisations for the locations across colon and liver tissues respectively. The measured thickness and electrode geometry was applied to equation (2.4) and the corresponding $GAIR$ values calculated. These output metrics have been presented graphically in Figure 4.4.

Table 4.2: Model A characterisation results for positional variation across an *ex vivo* colon surface, including calculated $GAIR$ values.

Colon							
Location	1	2	3	4	5	6	7
OCV (V)	0.749 ±0.005	0.764 ±0.002	0.762 ±0.005	0.737 ±0.003	0.747 ±0.003	0.725 ±0.001	0.734 ±0.002
R_{INT} $(k\Omega)$	46.81 ±17.31	27.88 ±1.638	24.48 ±5.891	27.71 ±2.008	28.85 ±1.624	29.97 ±0.989	32.47 ±5.274
Thickness (mm)	16.6	17.5	17.9	19.5	18.8	19.4	19.6
$GAIR$ $(\Omega.m)$	79.58 ±29.44	45.09 ±2.65	38.63 ±9.29	40.17 ±2.91	43.44 ±2.44	43.70 ±1.44	46.93 ±7.63

The OCV values determined for each tissue type shows intra-tissue variation of up to 30 mV. Between types there is a significant ($p < .05$) difference between the mean values of 0.745 ±0.014 V and 0.639 ±0.013 V for colon and liver tissue respectively; determined through a two tailed Student's t-test. Similarly, differences in the internal resistances were found for the two tissue types. Colon and liver tissues also gave statistically different ($p < .05$) mean ±SD

characterised internal resistance values of 31.17 ±7.31 and 14.99 ±1.82 respectively. Conversion of internal resistance values to $GAIR$ does not yield consistent values for each tissue type. The $GAIR$ metric shows a dependence on tissue thickness, indicating that it is a potentially different metric from tissue resistivity.

Table 4.3: Model A characterisation results for positional variation across an *ex vivo* liver surface, including calculated $GAIR$ values.

	Liver						
Location	1	2	3	4	5	6	7
$OCV\ (V)$	0.637 ±0.004	0.651 ±0.008	0.625 ±0.014	0.629 ±0.009	0.643 ±0.006	0.626 ±0.007	0.660 ±0.004
$R_{INT}\ (k\Omega)$	16.42 ±3.497	16.19 ±1.661	16.02 ±1.164	16.14 ±0.255	11.62 ±1.097	13.36 ±0.708	15.15 ±1.422
Thickness (mm)	18.0	17.4	17.7	14.8	12.8	7.2	6.0
$GAIR\ (\Omega.m)$	25.79 ±5.49	26.31 ±2.70	25.59 ±1.86	30.83 ±0.49	25.67 ±2.42	52.47 ±2.78	71.41 ±6.70

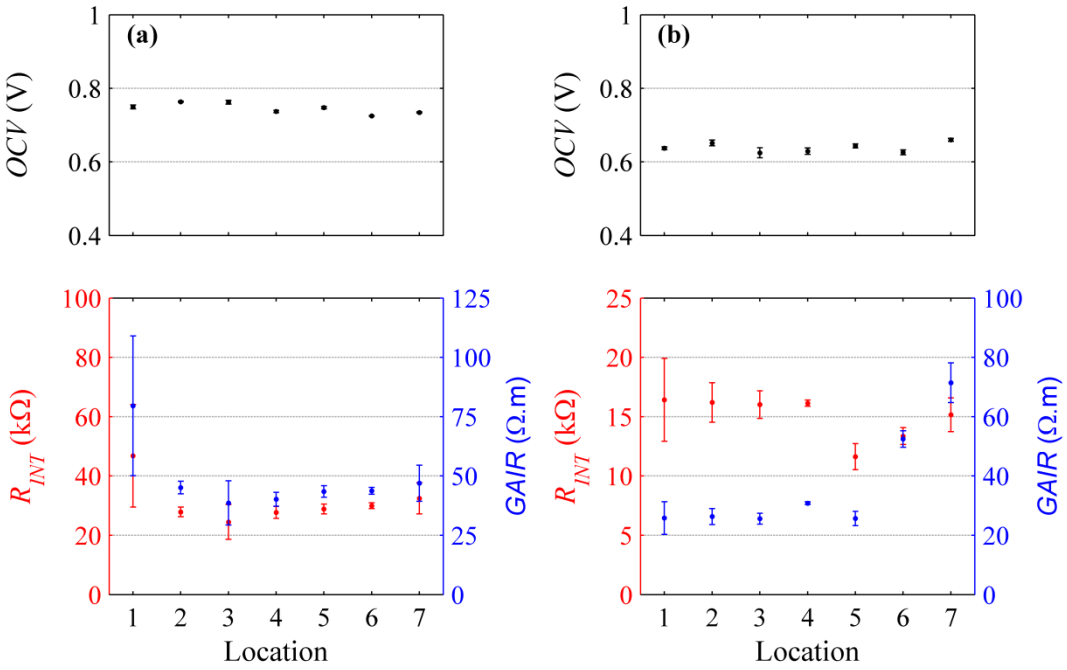

Figure 4.4: Mean (±SD, n=3) characterised OCV, R_{INT} and $GAIR$ values determined using Model A for varied positions across (a) *ex vivo* porcine colon, and (b) *ex vivo* porcine liver.

4.3.2 Exposure time

Exposure time relates to the duration of electrode contact with the tissue as well tissue contact with the atmosphere. Understanding this parameter is essential as it is an unavoidable consequence of all measurements. The testing protocol involved setting electronic, tissue and electrode variables to a fixed starting condition followed by measurement at set time intervals over a specified time period. Exposure time is interlinked with the measurement procedure as each reading takes a finite length of time to complete. Therefore the values obtained represent an effective average for that time range. Each measurement was conducted using Resistor set 1 and a switching rate of 0.5 Hz. Testing was carried on a section of *ex vivo* porcine liver (approximately 40x40 mm) which was wetted using deionised water prior to testing. An A_6 electrode set was contacted with the tissue under minimal strain. The upper and side surfaces of the tissue were left exposed to the atmosphere throughout the experiment.

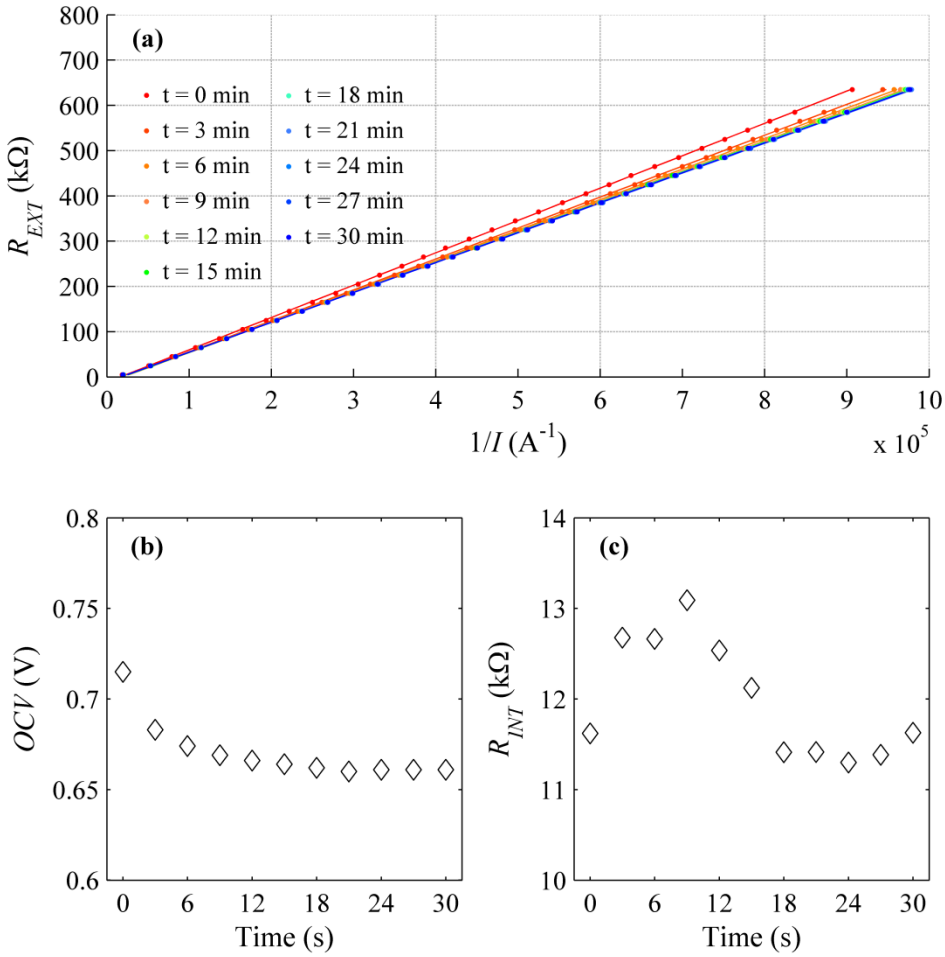

Figure 4.5: Influence of exposure time on the biogalvanic characterisation properties, showing (a) measured V_2 (represented as $1/I = R_{EXT}/V_2$), and Model A characterisation fit; (b) characterised OCV values as a function of time; and (c) characterised R_{INT} values as a function of time.

Figure 4.5(a) shows the external resistance against inverse current for all of the measurements taken. Characterisation through linear Model A fitting shows the OCV parameter (Figure 4.5(b)) to follow an exponential decay as a function of time, dropping from 0.72 – 0.66 V. Characterised internal resistance, shown in Figure 4.5(c), has an average (mean ± SD) value of 12.3 ± 0.7 kΩ with sporadic variation shown but no time dependant trend. The decline in OCV, and its lack of correlation to internal resistance changes, suggests that there are significant changes in the ion concentrations at the tissue-electrode interfaces. This may be due to changes in tissue properties or as a result of the disruption caused by the measurement technique. A significant drop in OCV would suggest a drop in the cathode (copper) potential or an increase in the anode (zinc) potential. Discussions presented within Chapter 5 indicate that this phenomenon may be linked to a reduction in the oxygen concentration at the copper cathode.

4.3.3 Controlled thickness

Tissue thickness is a direct parameter in the conversion constant relating R_{INT} to $GAIR$ (equation (2.4)). Investigation into the influence was performed through the dissection of *ex vivo* porcine liver tissue to sequentially smaller thicknesses. A 'thick' section of liver tissue was identified and isolated. Cuts were then made into the tissue to create test pieces of varied thickness, from 5.5-15.8 mm. Each section was tested over three repeats using Resistor set 1 at a switching rate of 0.5 Hz. An A_{12} electrode set was employed for testing.

Figure 4.6 shows the characterisation of the measured data along with the output metrics from Model A fitting. Figure 4.6(b) shows the OCV values determined as a function of tissue thickness. No clear correlation can be seen between these variables. The values presented for R_{INT} and $GAIR$ (Figure 4.6(c)) both decrease with increasing tissue thickness. The large variation in $GAIR$ indicates that either the resistivity of the tissue is not consistent between tests or the conversion assumptions are incorrect.

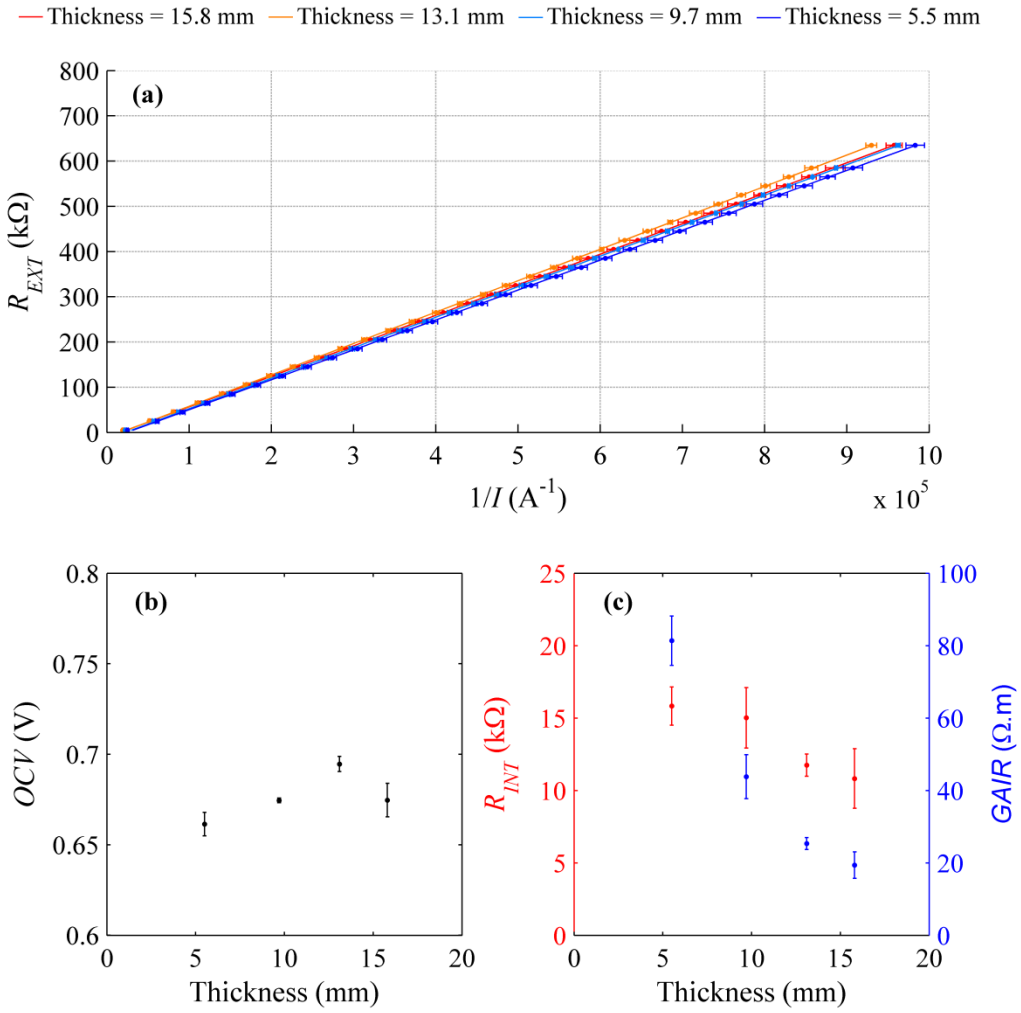

Figure 4.6: Influence of controlled liver thickness on the biogalvanic characterisation properties, showing (a) measured V_2 (represented as $1/I = R_{EXT}/V_2$), and Model A characterisation fit; (b) characterised OCV values; and (c) characterised R_{INT} and $GAIR$ values.

4.3.4 Controlled area

In addition to tissue thickness, the contact area is directly considered in the conversion of R_{INT} to $GAIR$ (equation (2.4)). A simplistic view of the system may assume that this area is equal to the electrode contact area. However, a tissue medium offers more freedom for current pathways thereby breaking this assumption. Investigation into the influence the tissue area was performed through the successive dissection of *ex vivo* porcine liver tissue to sequentially smaller areas. Three test areas were extracted from a single liver specimen and each section tested over three repeats. Square sections with areas of 2.25, 6.25 and 12.25 cm^2 were obtained; specimen thicknesses were 3.30, 3.35 and 3.35 cm respectively. An A_{12} electrode configuration was used. Electronics and measurement setup was identical to that described within Section 4.3.1.

Figure 4.7(a) shows the characterisation of the measured data using Model A. Figure 4.7 (b) shows the OCV values determined as a function of tissue area. No clear correlation can be

seen between these variables. However, Figure 4.7(c) shows a reduction in R_{INT} with an increase in tissue area. Conversion of resistance to $GAIR$ assumes a constant electrode area in equation (2.4). However, the results of Figure 4.7(c) indicate that the area of the tissue impacts the characterised resistance, and if neglected may introduce error in the conversion to $GAIR$.

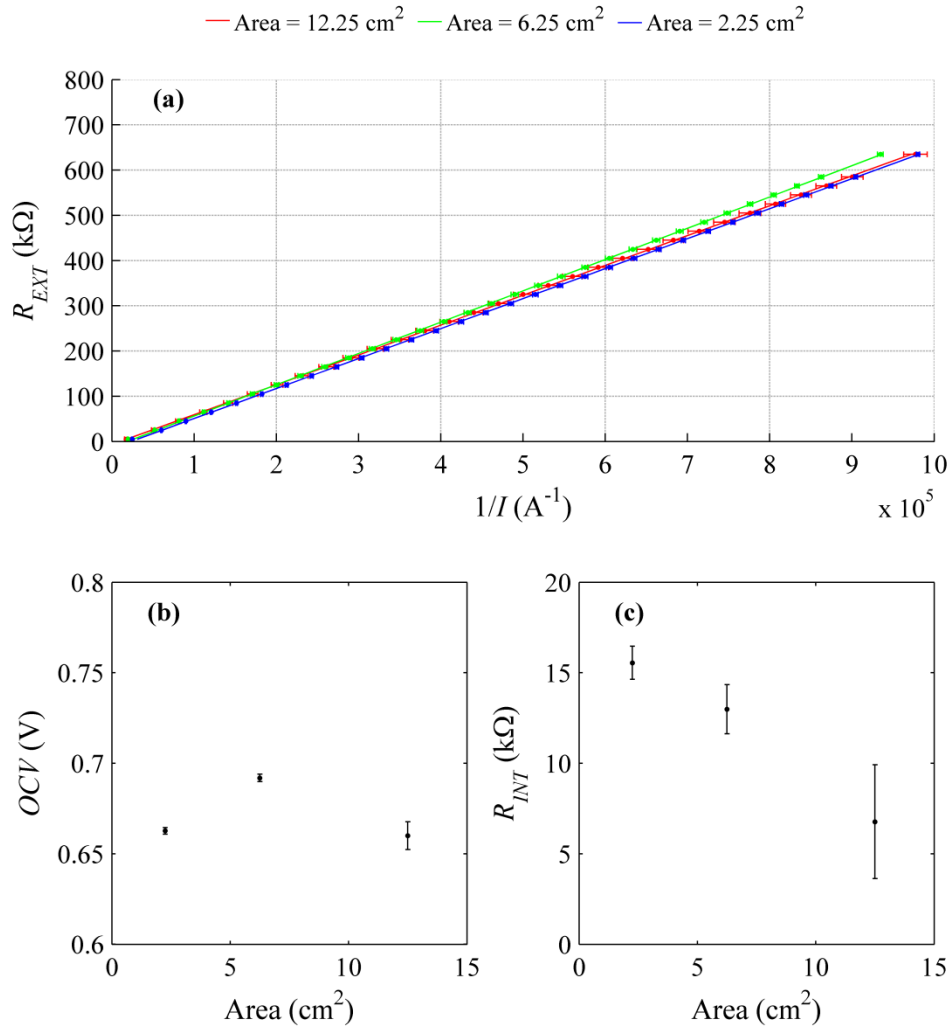

Figure 4.7: Influence of tissue area on the biogalvanic characterisation properties, showing (a) measured V_2 (represented as $1/I = R_{EXT}/V_2$), and Model A characterisation fit; (b) characterised OCV values; and (c) characterised R_{INT} values.

4.3.5 Strain and natural thickness

To assess the influence of tissue strain, the testing platform (Figure 3.3(a)) was used to apply varied strain to tissue samples. Five repeat tests were conducted on thick liver (28.3 mm), thin liver (9.7 mm) and closed colon (9.1 mm) tissue under two mechanical strain conditions (0% nominal contact and ~50% strain). Figure 4.8 shows how the mechanical contacting conditions were achieved. The actual mechanical strain ε_m achieved was calculated as $(x - x^*)/x$, where x is the zero strain thickness and x^* is the strained thickness. Reported strain values have been

represented as percentage strain. Repeat tests for each tissue type were conducted using the same tissue sample, taken from a single animal. An A_{12}electrode set was employed to conduct the measurements and apply the tissue strain. At this stage of tissue testing, Model B had been developed and was found to show improved accuracy over Model A. Characterisation of each dataset was therefore performed using Model B. Resistor set 2 was used for conducting characterisations with a switching rate of 0.2 Hz.

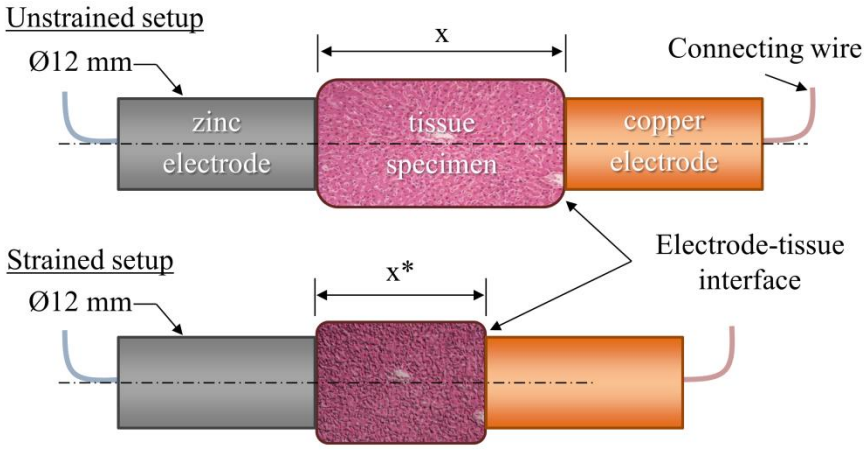

Figure 4.8: Schematic illustration of tissue strain conditions for strain and thickness testing showing zero strain thickness x and strained thickness x^*.

Figure 4.9 shows the mean measured data points for each *ex vivo* test case, presented alongside the mean Model B fit. The influence of application of ~50 % strain has been indicated, showing a shift to the left (reduced R_{INT}) with strain for liver tissue and minimal change for colon tissue. Figure 4.10 shows the distribution of characterised internal resistances and OCV values for repeat tests of each tissue configuration. A two-tailed Student's t-test with equal variance (n=5) was applied to the two strain cases for each tissue configuration and output metrics.

Figure 4.9 indicates that measured data under all experimental configurations tested conforms to the Model B profile and can therefore be continuously approximated using equation (3.4). The internal resistances in Figure 4.10(a) show interdependence on tissue type, thickness and strain. Tests on both thick and thin porcine liver sections show a significant ($p < .05$) decrease in the determined internal resistance for an increased strain level. However, application of mechanical strain to colon tissue does not show a significant influence on the characterised internal resistance. The relative internal resistances for thin liver tissue under both strain cases are much higher relative to thick liver tissue, indicative of different resistivity ($GAIR$) in the same tissue type. It is also evident that colon tissue shows increased variation in internal resistance when strained without significant change in magnitude.

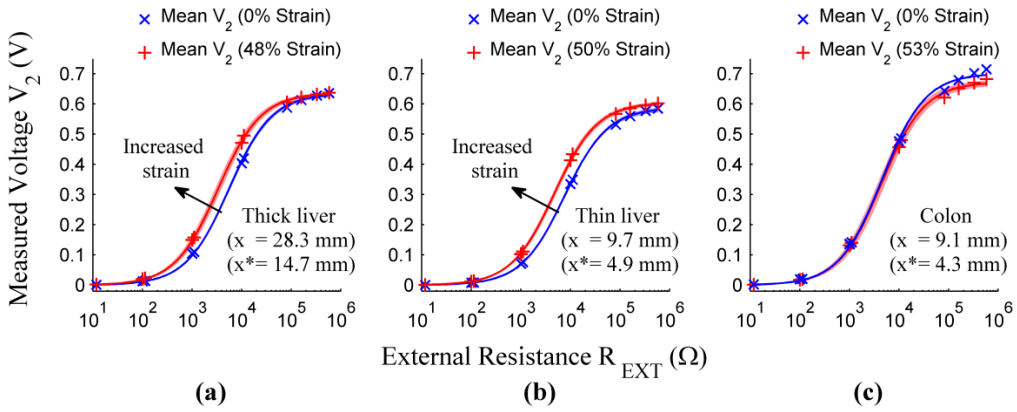

Figure 4.9: Mean measured data and model fits for nominal and high strain for (a) 'thick' liver tissue, (b) 'thin' liver tissue and (c) closed colon tissue; shaded region representing 1 SD of mean (n=5). Repeat measurements taken from a single tissue sample.

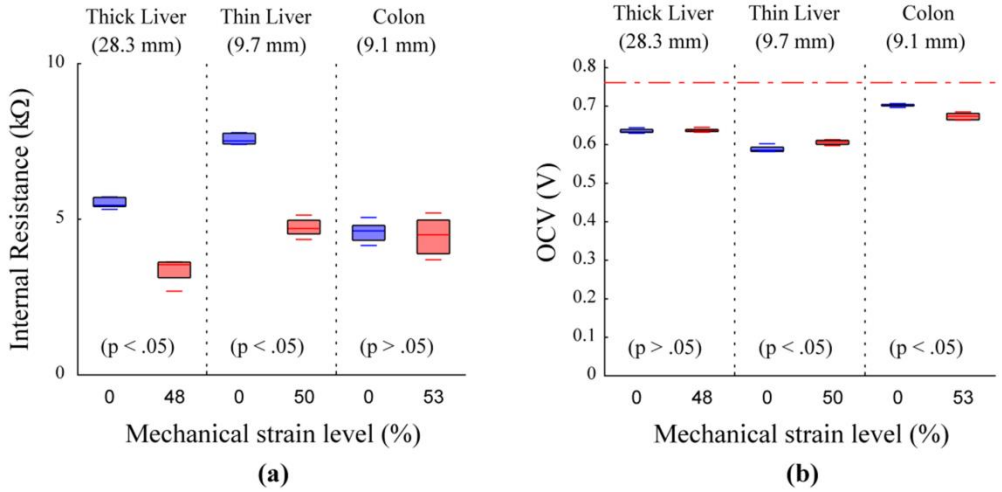

Figure 4.10: Box plots of characterized parameters from *ex vivo* porcine tests on single sections of liver and colon tissue with strain levels indicated; showing (a) determined internal resistance, and (b) OCV. Potential line (red dashed) corresponding to standard conditions also shown. Levels of statistical significance between strain levels (two-tailed Student's t-test, equal variance (n=5)) are shown; statistical significance taken as $p < .05$.

Determined OCV values for liver tissue, shown in Figure 4.10(b) are lower than those for colon tissue, with all values being below the standard electrode potential of equation (5.3). Statistically significant differences in OCV with tissue strain was found in thin liver and closed colon, although only slight change in magnitude were recorded (+200 mV and -300 mV respectively). A change in cell OCV is indicative of interface electrode potential fluctuations, which is associated with altered reaction species concentrations. The applied strain has likely caused the relative concentrations to change. This is discussed further in Section 5.5.

4.3.6 Electrode area

As discussed in Section 4.3.4, the conducting area is directly involved in conversion of R_{INT} to $GAIR$. The electrode area is assumed to be equal to the conducting area for the purpose of calculation. Although the findings from Section 4.3.4 suggest that this assumption is potentially incorrect, the electrode area may still directly influence the characterised internal resistance. Assuming a homogenous reaction process, electrode area scales the magnitude of current for a given redox reaction at a specific current density. In addition, an increased current will be distributed over a wider salt bridge medium area. This effectively reduces the internal resistance of the cell, which should be reflected in the biogalvanic characterisation.

Figure 4.11 shows characterised OCV and R_{INT} values collated across the varied tests for the two axially aligned electrode areas. The included data are only from tests conducted under minimal strain conditions. Tests for liver and colon tissues have been combined to allow indication of the general influence of the electrode area on the characterisation metrics. Figure 4.11(a) and Figure 4.11(b) shows box plots of the collated OCV and R_{INT} data respectively. It is evident that the electrode area alters the characterised biogalvanic parameters. A small reduction in OCV and a large reduction in R_{INT} are seen with an increase in electrode area. Statistical comparison (one-tailed Student's t-test with unequal variance (28.3 mm^2: n=28; 113 mm^2: n=53) indicates that these differences are significant ($p < .05$). Based on the arithmetic means, the internal resistance is 3.1 times smaller for a 4 times increase in electrode area.

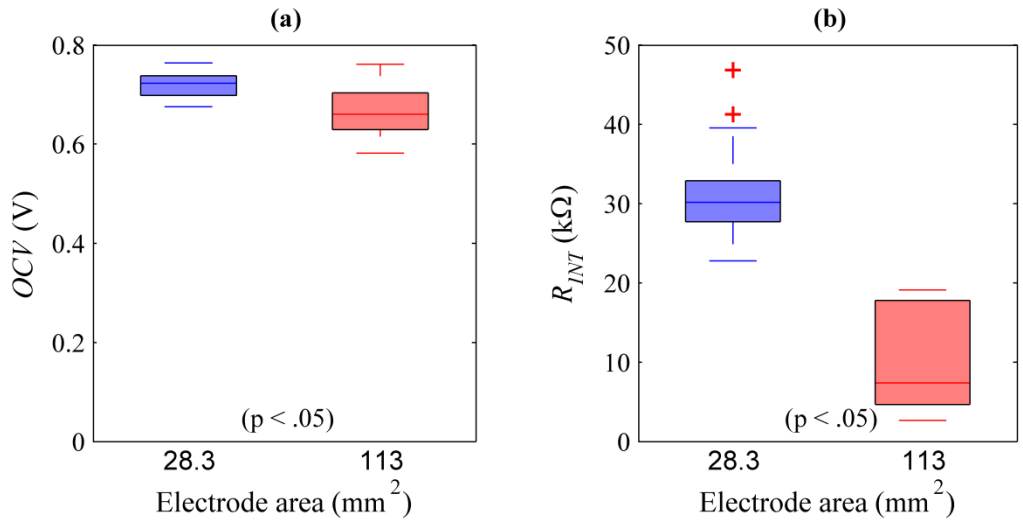

Figure 4.11: Collated biogalvanic characterisation results as a function of electrode area across all reported tissue testing under minimal strain; distribution of (a) OCV and (b) R_{INT} shown. Statistical significance indicated (one-tailed Student's t-test with unequal variance (28.3 mm^2: n=28; 113 mm^2: n=53).

4.3.7 Switching rate

Investigation into the influence of switching rates was performed on a single porcine colon specimen. The test location was contacted with an A_{12} electrode set under minimal strain conditions. Electrode separation was measured at 8.65 mm. Biogalvanic characterisations were performed using Resistor set 1, loaded in an increasing order. The switching rate employed was varied from 0.1 – 1.5 Hz in a random testing sequence, with 30 sec between each test. Each dataset was subsequently characterised using Model A and a linear regression model fitting method.

Figure 4.12(a) shows the measured data points for each switching rate tested, presented alongside the Model A fit. A clear decrease in the model fit gradient can be seen as the switching rate is increased. Figure 4.12(b) and Figure 4.12(c) contain the output metrics of OCV and R_{INT} respectively as a function of switching rate. It is evident that there is a decrease in the determined OCV and a minimal increase R_{INT} as the switching rate is increased.

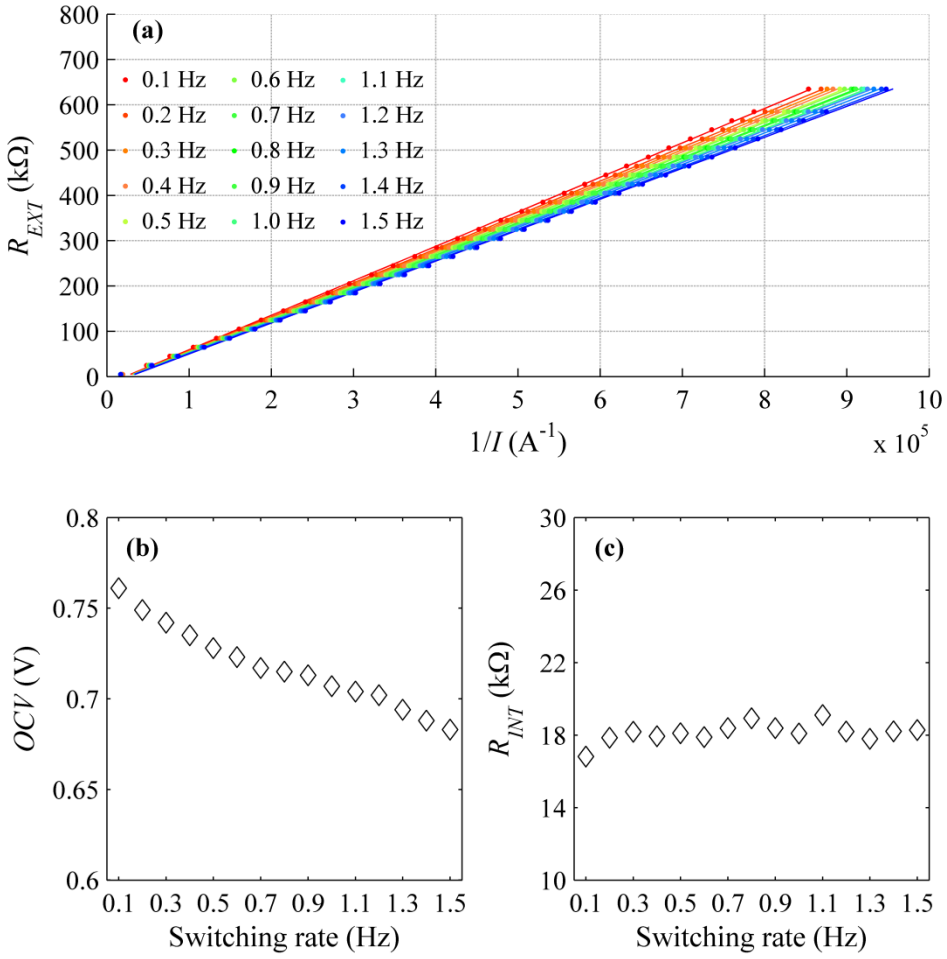

Figure 4.12: Influence of external resistor switching rate on the biogalvanic characterisation properties, showing (a) measured V_2 (represented as $1/I = R_{EXT}/V_2$), and Model A characterisation fit; (b) characterised OCV values; and (c) characterised R_{INT} values.

4.4 Porcine (*in vivo*) Experiments

Biogalvanic characterisation and galvanic current testing was performed on porcine tissues *in vivo.* For biogalvanic testing, electrodes (A_{12-R}) were set in non-conducting resin, wet ground (1200 grit) and mounted in the jaws of the Surgical clip to provide fixed axial alignment and separation of 9.2 mm. Figure 4.1(a) shows the typical contact conditions obtained during the testing. In addition, tests were performed to assess the closed cell maximum galvanic current. For these tests, parallel-needle electrodes of various anode and cathode lengths were inserted directly into the tissue region of interest. Needle electrodes were selected to allow easier variation of electrode separation and relative cathode length. Additionally, needle electrodes allowed for pre and post-testing within NaCl(aq) analogues, to compare establish the influence of tissue interaction of the closed cell current. Figure 4.2 shows an example of the parallel-needle electrodes.

4.4.1 Resistor direction

Tests were conducted on a single anesthetised 30kg female white pig under UK Home Office regulations for animal experimentation. Investigation was made into the influence of resistor switching direction i.e. the value of external resistance either increases or decreases during testing. Five resistor sweeps were made for increasing and decreasing resistor switching respectively at three different tissue locations (colon, rectum and liver). Resistor switching rate was fixed at 0.2 Hz and measurement points taken as the mean of the last 10 samples prior to resistor switching. Electrodes were rinsed with distilled water between each set of repeats. Influence of resistor switching direction on each tissue configuration was assessed using a two-tailed Student's t-test. To determine if internal resistance or OCV are specific to tissue type a ranked statistical comparison (Kruskal-Wallis test) was conducted.

Figure 4.13 shows the mean measured data and the mean Model B fit for each *in vivo* test case. The data spread is illustrated through the shaded region which represents the standard deviation produced by the characterisations. Figure 4.14 (a) and (b) show boxplots for the characterised internal resistance and OCV respectively.

Figure 4.13 illustrates the agreement between measured data and the model of equation (3.5) for all tissue types tested. This is apparent in both resistor switching directions, demonstrating that the complete electrochemical system can be modelled as a single resistance. The direction of resistor switching highlights model fit hysteresis within individual tissue types. This is clearly evident in the characterised internal resistance values of Figure 4.14(a), where differences are statistically significant ($p < .05$) for all tissue types. Statistical analysis (Kruskal-Wallis test) also shows the internal resistance to be significantly different ($p < .05$) between tissue types.

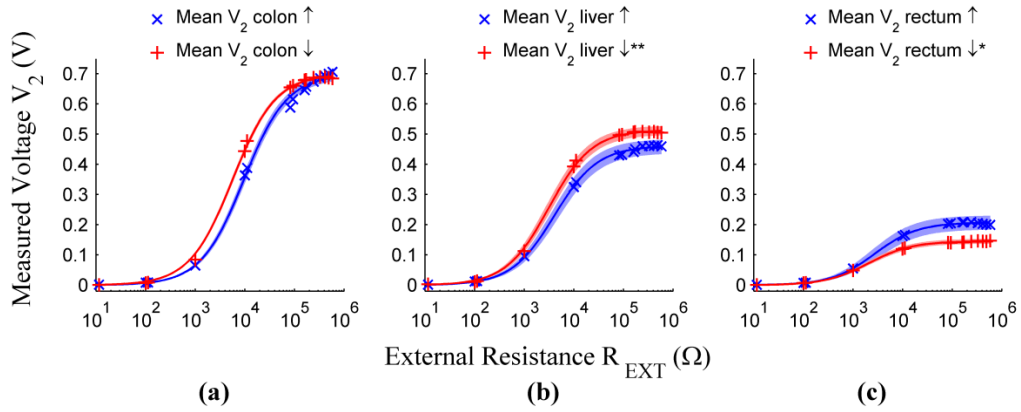

Figure 4.13: Average measured data and model fits for *in vivo* porcine tests with increasing (↑) and decreasing (↓) external resistor switching, on (a) colon, (b) liver, and (c) rectum; shaded regions represent ±1 SD of mean (n=5). *(n=4), **(n=3).

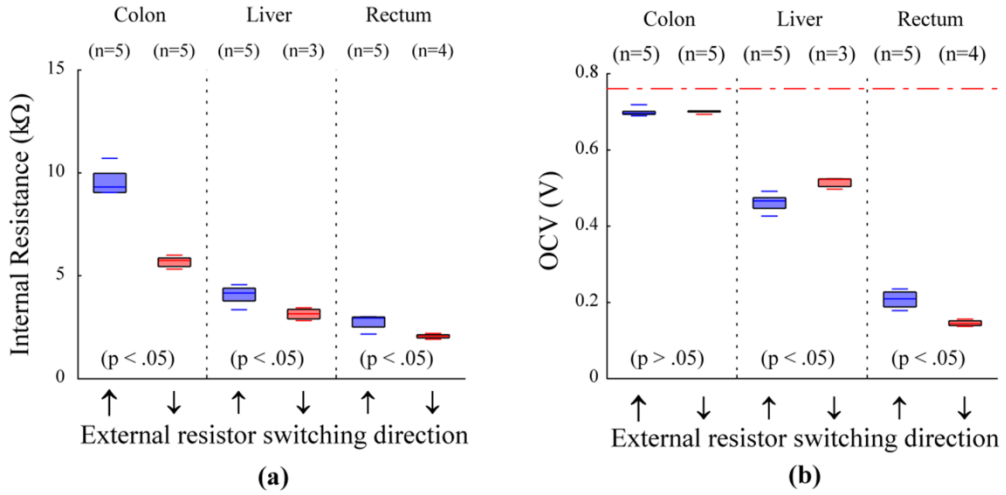

Figure 4.14: Box plots of characterised parameters from *in vivo* porcine tests on colon, liver, and rectum tissue with increasing (↑) and decreasing (↓) external resistor switching; showing (a) determined internal resistance, and (b) OCV, potential line (red dashed) corresponding to standard conditions also shown. Sample size (n) and statistical significance between resistor switching direction tests (two-tailed Student's t-test, equal variance) are shown.

Resistor switching direction shows no influence on OCV for colon tissue. However, rectum and liver tissue OCV values are significantly altered by the direction of external resistor switching. It can be seen in Figure 4.13 that the measured voltage values at high external resistor values (toward OCV) differ markedly between the three tissue types. In all cases the values are below the standard potential difference predicted by the proposed reaction (equation (5.3)). Figure 4.14(b) shows comparatively the characterised OCV for each test case. Statistical analysis (Kruskal-Wallis test) shows significant differences between tissue types ($p < .05$) for characterised OCV. This result is consistent for testing with either resistor switching direction.

4.4.2 Galvanic current

Tests were conducted on a single anesthetised 25kg female white pig under UK Home Office regulations for animal experimentation. Investigation was made into the reusability of electrodes as well as galvanic current performance as a function of electrode lengths (anode and cathode) and separation.

4.4.2.1 Electrode reusability

The variability of an electrode pair is a potentially influencing factor within the biogalvanic system. Tests were therefore conducted to assess how the current flow properties through an electrode pair vary with use. A single N_C electrode pair was used to record five repeat galvanic current tests under three scenarios: (1) 154 mM (0.9 wt%) NaCl – pre-test, (2) porcine liver tissue in vivo, and (3) 154 mM (0.9 wt%) NaCl – post-test. Between each repeat the electrode were removed from the test location, disconnected for 60s and then replaced under connection. The time-varying galvanic currents were measured using the Ivium CompactStat (Ivium Technologies) in closed cell (zero load) mode. The average galvanic current trace for the three test conditions is shown along with the full measured data range in Figure 4.15(a) and Figure 4.15(b). The galvanic current recorded over the final 200 s for each repeat test was averaged and is presented in Figure 4.15(c). A summary of the means for each test location across all five repeats is given in Figure 4.15(d).

The galvanic current measured in tissue was found to be significantly lower than in NaCl. Specifically, the average galvanic tissue current presented in Figure 4.15(d) is only 21% of that the NaCl pre-test. Repeat NaCl testing after tissue measurements is again much larger, with galvanic tissue currents being 18% of the NaCl post-test current. Statistical analysis (Student's t-test, two-tailed equal variance) show the NaCl post-test current to be significantly ($p < .05$) larger than for the NaCl pre-test.

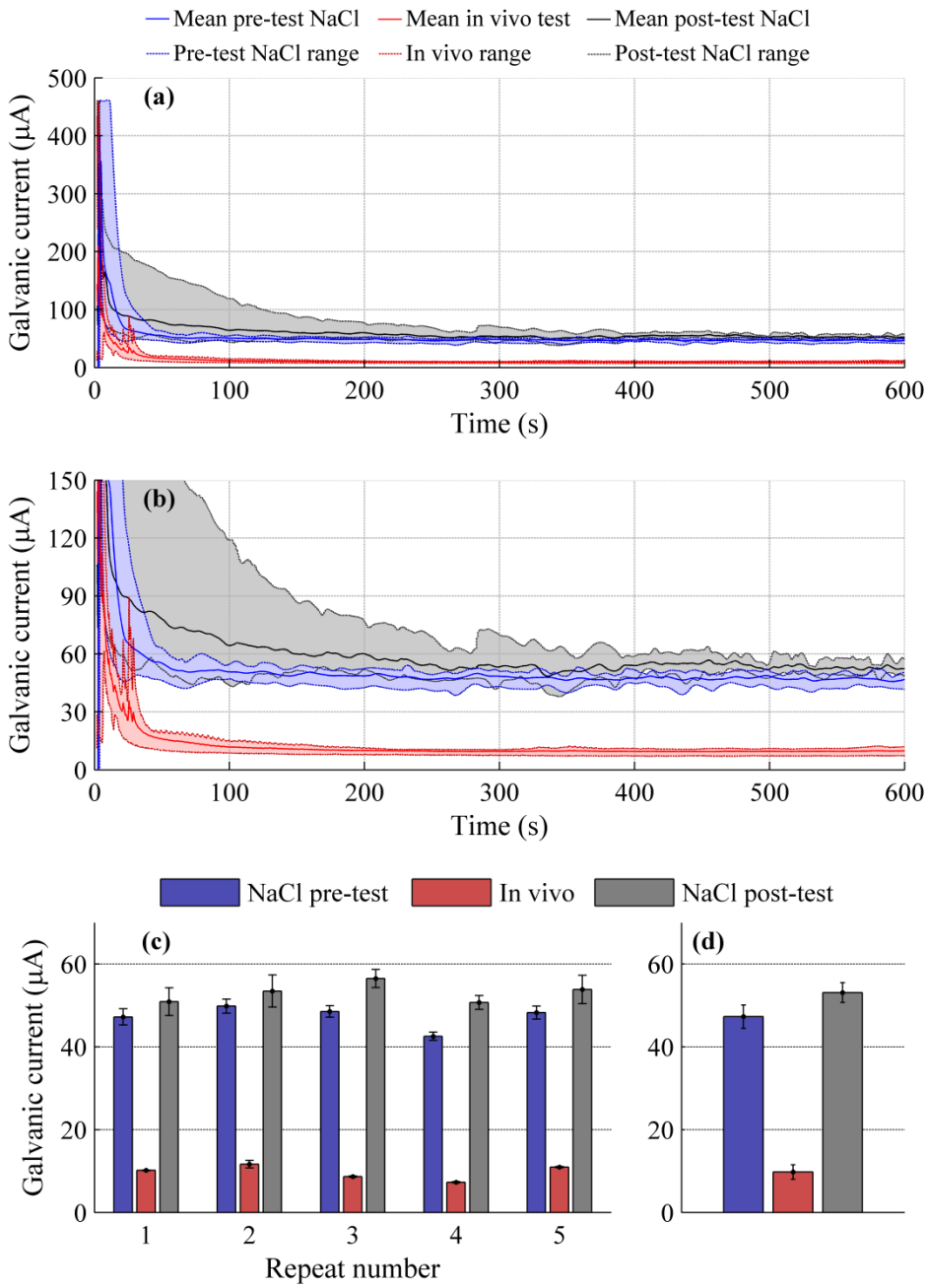

Figure 4.15: Galvanic current test data for pre and post-test NaCl and *in vivo* porcine liver measurements, showing (a) mean galvanic current and data range (shaded region), (b) mean galvanic current and data range (shaded region) on a scaled ordinate axis, (c) mean ± SD galvanic current as a function of repeat number, and (d) overall mean ±SD for all repeats.

4.4.2.2 Electrode separation

Assuming a simple geometric arrangement (as is the case for needle electrodes), the spacing between galvanic electrodes is significant as it directly influences the distance of the current pathway. For a homogeneous salt bridge medium, a larger potential drop will occur to maintain current flow over the pathway. Current limited conditions will be a function of the rate of the supporting redox reactions or the internal resistance of the salt bridge medium. Testing was

conducted to assess how increasing the salt bridge resistance in tissue tests affects the limited current value. Five electrode pairs (N_A, N_B, N_C, N_D and N_E) were manufactured and tested, with 1mm diameter zinc and copper wire set to a 10 mm exposure. The separation between electrodes was varied from 6–30 mm in approximately 5 mm increments. Each electrode pair was pre-tested in 154 mM NaCl solution prior to tissue tests. Electrode pairs were inserted into clear regions of the liver and the closed cell galvanic current measured for 10 minutes using the Ivium CompactStat (Ivium Technologies) in closed cell (zero load) mode.

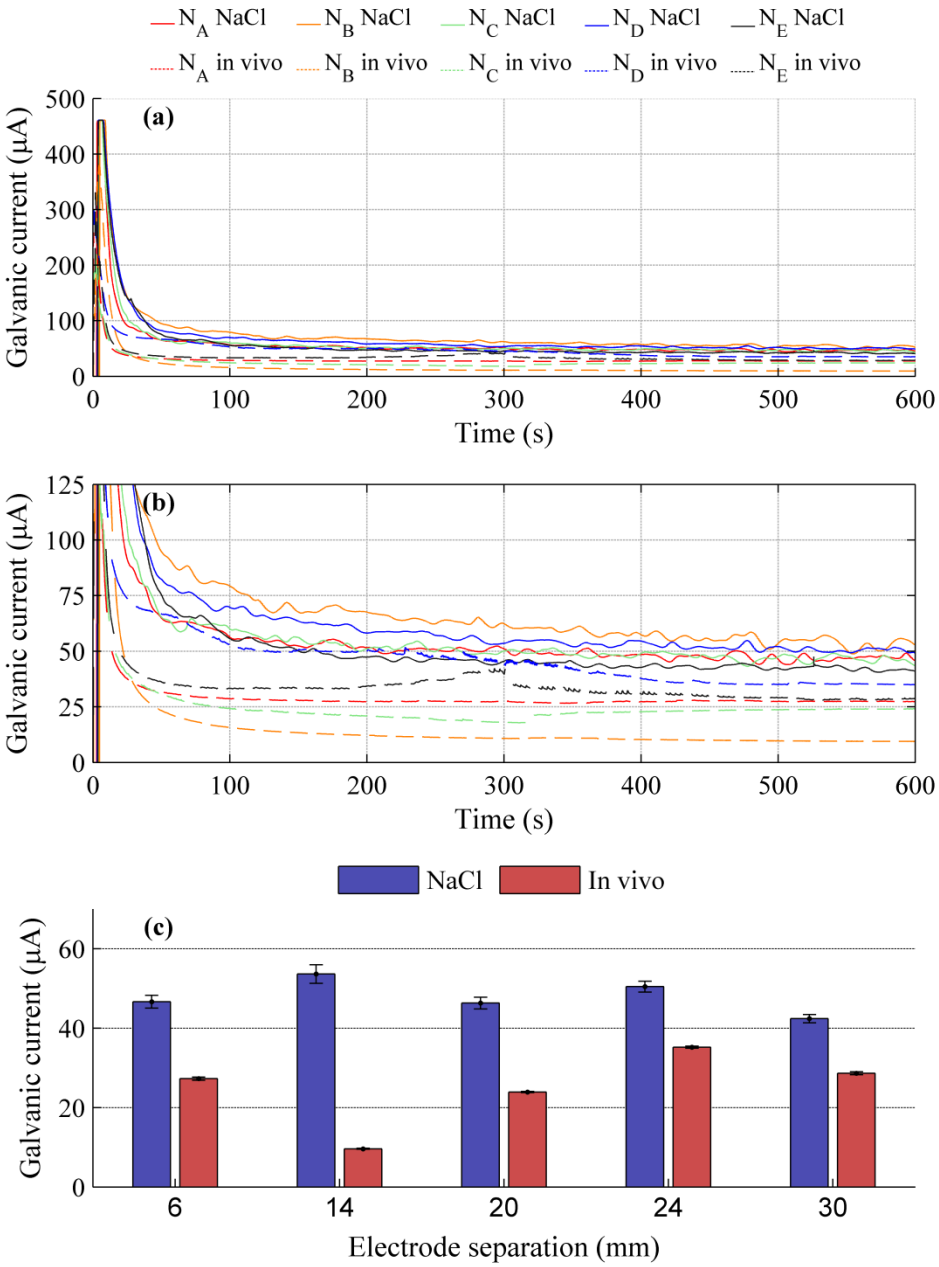

Figure 4.16: Galvanic current test data for pre-test NaCl and *in vivo* porcine liver measurements, showing (a) mean galvanic current and data range (shaded region), (b) mean galvanic current and data range (shaded region) with a scaled ordinate axis, and (c) mean ±SD galvanic current as a function of electrode separation.

Figure 4.16(a) and (b) shows the current trace obtained for each electrode in NaCl and porcine liver tissue. A typical galvanic current decay is shown in all tests, with current values settling to approximately steady state after 400 s. The mean current ±SD for the last 200 s for each electrode separation is shown in Figure 4.16(c). It is again evident that NaCl tests show significantly ($p < .05$; Student's t-test, two-tailed equal variance) higher mean steady state currents than *in vivo* porcine liver tests. The electrode separation does not show an influencing trend on the steady state current, implying that the current limiting mechanism is not that of the salt bridge resistance under closed cell conditions.

4.4.2.3 Relative electrode area

Current limiting mechanisms are discussed in more detail in Chapter 5, with electrode kinetics and internal resistance being the controlling mechanisms in galvanic cells, [83]. The slower kinetics of the reduction reaction at the copper cathode is a potentially limiting step under closed cell conditions. Testing was therefore conducted to assess how increasing the relative area of the cathode would influence the closed cell galvanic current. Four electrode pairs (N_C, N_H, N_I and N_J) were manufactured and tested, with 1mm diameter zinc and copper wire set to a 20 mm separation. The cathode lengths were varied from 10-25 mm in 5 mm increments. Each electrode pair was pre-tested in 154 mM NaCl solution prior to tissue tests. Electrode pairs were inserted into clear regions of the liver and the closed cell galvanic current measured for 10 minutes. Time-varying current through the closed galvanic cell was measured using the Ivium CompactStat (Ivium Technologies) in closed cell (zero load) mode.

Figure 4.17(a) and (b) shows the current trace obtained for each electrode in NaCl and porcine liver tissue. A typical galvanic current decay is shown in all tests, with current values settling to approximately steady state after 400 s. The mean current ±SD for the last 200 s for each electrode separation is shown in Figure 4.17(c). It is again evident that NaCl tests show significantly ($p < .05$; Student's t-test, two-tailed equal variance) higher mean steady state currents than *in vivo* porcine liver tests. For NaCl tests, a longer cathode increases the measured galvanic current suggesting that the current limiting mechanism is under cathodic control. For equivalent porcine liver tests this trend is not as clear for the shorter cathode lengths although a larger galvanic current is seen for the longest cathode.

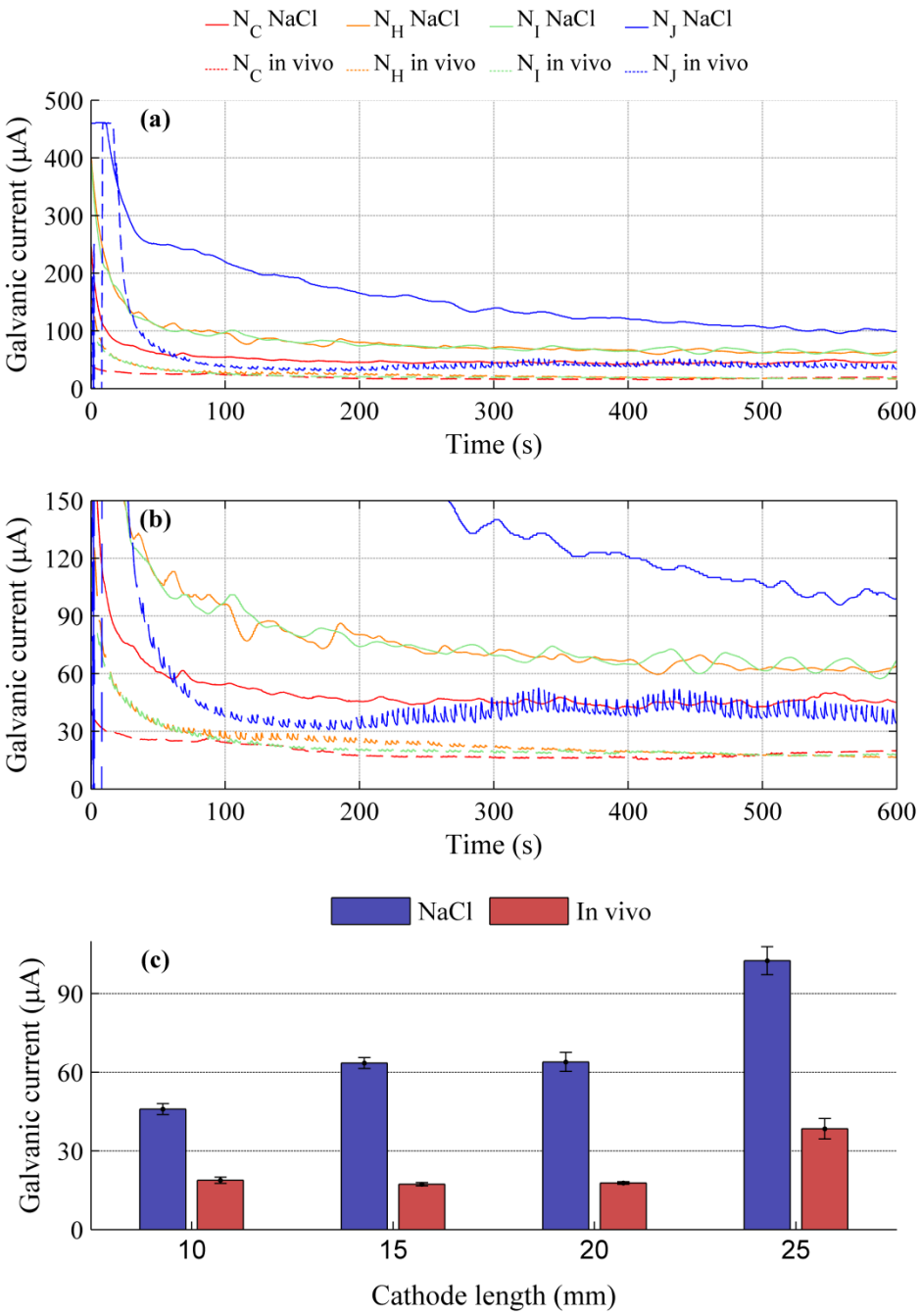

Figure 4.17: Galvanic current test data for pre-test NaCl and *in vivo* porcine liver measurements, showing (a) mean galvanic current and data range (shaded region), (b) mean galvanic current and data range (shaded region) with a scaled ordinate axis, and (c) mean ±SD galvanic current as a function of cathode length.

4.4.2.4 Electrode configuration

Comparison was made between galvanic current tests using needle and axial electrode arrangements. Steady state galvanic current tests were measured using an axial electrode set A_6 ($exposed\ area\ =\ 28.3\ mm^2$), and a needle electrode set N_C ($exposed\ area\ =\ 31.4\ mm^2$). Axial electrodes were clamped into position on the exposed liver at a separation of 20 mm using

the Surgical clip (c.f. Section 3.3) and the time-varying galvanic current measured for 10 minutes using the Ivium CompactStat (Ivium Technologies) in closed cell (zero load) mode. The same process was performed using the needle set inserted into a fresh liver region. For comparison, the same galvanic current tests were performed in 154 mM NaCl, with five repeat measurements for each electrode configuration.

Figure 4.18 shows the current traces obtained for the two configurations *in vivo* and in NaCl. It is evident that the NaCl tests generate a significantly larger steady state current than the equivalent test conducted on porcine liver tissue. In addition, the N_C needle electrode pair produces a significantly larger galvanic current when compared to the axial A_6 electrode pair. Table 4.4 contains the average steady state currents calculated as the mean of the last 200 s of the test. The electrode configurations were selected to have similar electrode exposure areas with N_C having 11 % greater exposure than the A_6 pair. However, the needle electrodes show 2.7 times and 9 times the average steady state current in NaCl and liver tissue respectively.

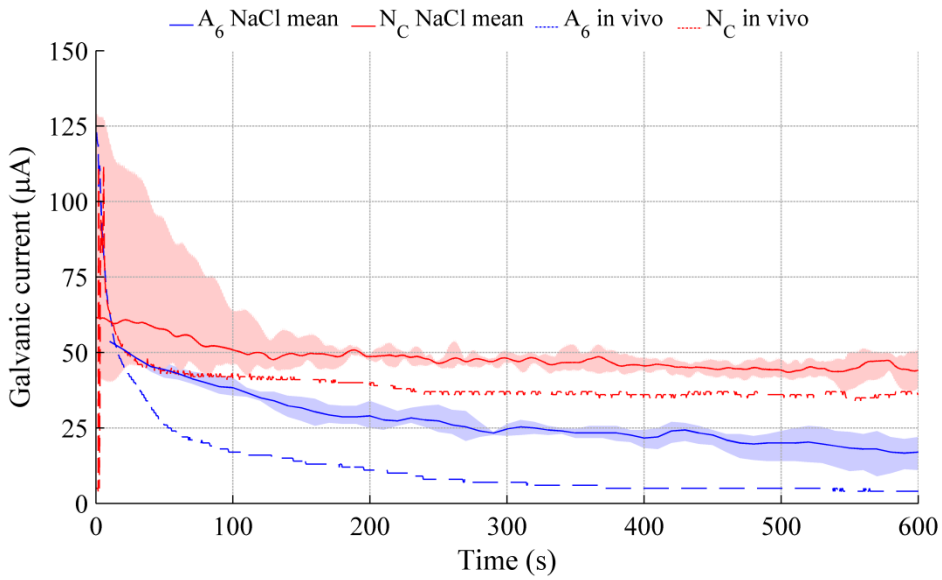

Figure 4.18: Galvanic current test data for axial and needle electrode types tested in NaCl (n=5) and on *in vivo* porcine liver (n=1).

Table 4.4: Average steady state current for axial and needle electrodes tested in 154 mM NaCl and on *in vivo* porcine liver; variation (±SD) shown for NaCl tests.

Axial electrodes (A_6)		Needle electrodes (N_C)	
154 mM NaCl	*Porcine liver*	*154mM NaCl*	*Porcine liver*
16.78 (±3.15)	4.00	44.95 (±2.09)	36.30

4.5 Human Tissue Experiments

This section describes two experiments conducted with human tissue. The first was performed to obtain data on regarding the biogalvanic current of human tissues under closed cell conditions. This was performed on a human cadaver with the use of two electrode configurations. The second experiment describes biogalvanic characterisation performed on freshly excised human rectum containing a disease element (adenocarcinoma).

4.5.1 Galvanic current (Cadaver)

Tests were conducted on a cadaveric specimen to examine the galvanic current from cell connection to steady state. An A_{6-R} electrode set was clamped directly onto the liver with a resulting separation of 12.5 mm, as shown within Figure 4.19(a). In addition, a similar galvanic current test was performed using an N_C needle electrode set (∅1 mm), as shown in Figure 4.19(b). The time-varying current through the closed galvanic cell was measured using the Ivium CompactStat in closed cell (zero load) mode. The cell current was monitored for 10 min (600 s), allowing for settling of transient aspects.

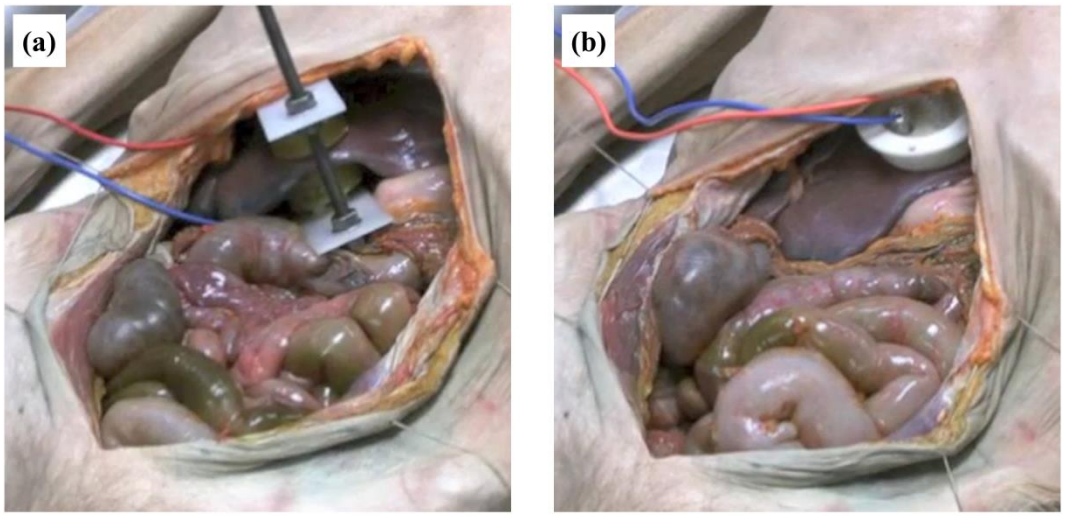

Figure 4.19: Images of electrode configurations used during cadaveric galvanic current experiments; showing (a) A_{6-R} arrangement (12.5 mm separation) and (b) N_c needle electrodes with 10 mm insertion depth at 20 mm separation.

Figure 4.20 shows the galvanic current trace for the two test electrode configurations. It can be seen that in both cases a large current spike is present upon cell connection. Current levels decay in an exponential manner as time progresses, tending to a steady current level as illustrated within Figure 4.20(a). Closer examination of the data indicates that even in the

apparent steady state region, the galvanic current is continuing to fall. Figure 4.20(b) shows a current drop-off of 47% and 11% for the axial and needle electrode configurations respectively.

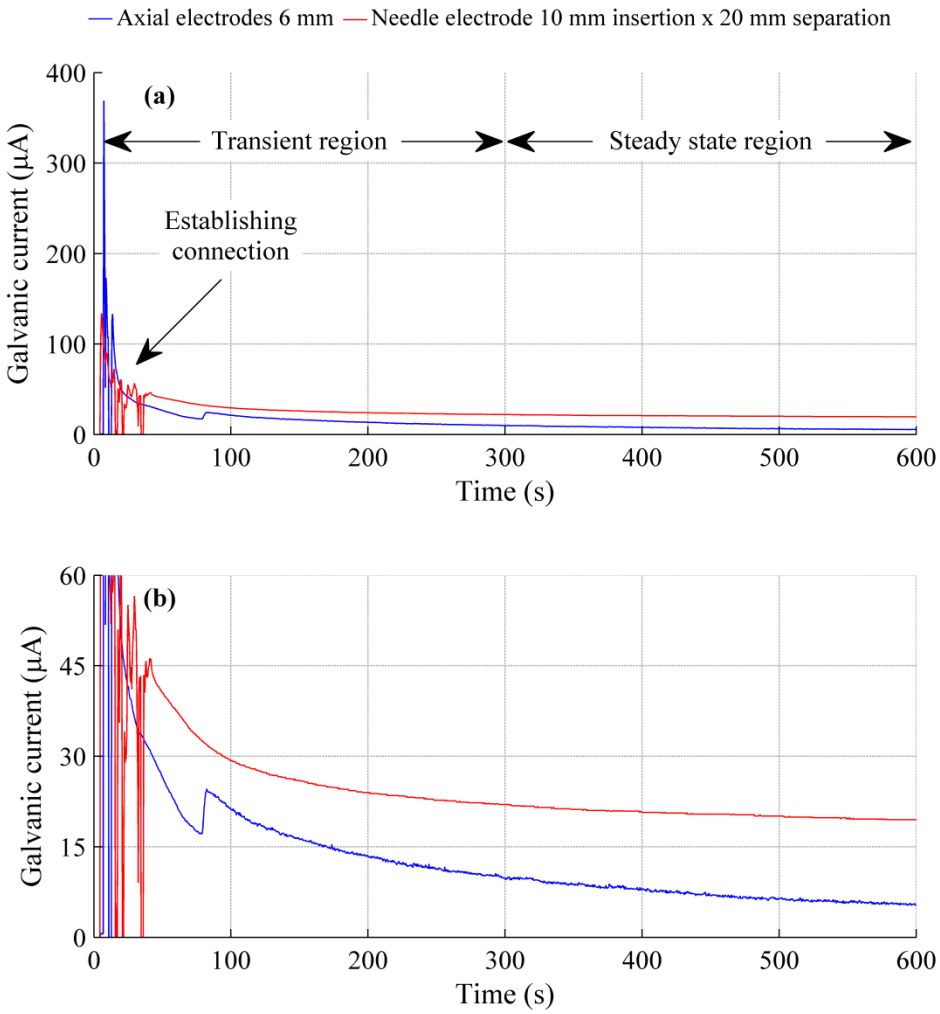

Figure 4.20: Galvanic current traces from cadaveric liver tissue tests using axial and needle electrode, showing (a) full scale data, and (b) zoomed y axis for clarity of steady state region.

4.5.2 Tissue health

A single set of tests were carried out to investigate the influence of tissue health on biogalvanic characterisation. Tests were carried out on freshly excised human colon tissue with an abnormal region (adenocarcinoma). The test was conducted to obtain data for healthy and abnormal colon tissue, and to assess the proficiency of the Testing platform and Surgical clip under clinical conditions. Axially, aligned electrodes (A_{12}) were contacted with the abnormal and healthy tissue regions under minimal strain conditions using the testing platform (Figure 4.21(a)). Similar alignment conditions were also achieved using the surgical clip (Figure 4.21(b)), set to clip setting 2 (Figure 3.3(b)) in both cases, leading to approximate strains of 28% and 23% on

the healthy and abnormal regions respectively. Both sets of contacting equipment were tested under the same characterisation conditions. Resistor set 1 was employed with a switching rate of 0.5 Hz. The faster switching rate was selected due to time constraints on the measurement procedure. Three repeats were performed for healthy and abnormal tissue regions for electrode contact maintained with the Testing platform and Surgical clip. Model fitting to the measured data using Model A and Model B was performed and compared. Statistical analysis (Student's t-test, two-tailed unequal variance) was performed to compare healthy and abnormal tissue results. Figure 4.21(a) shows the tissue under test (including abnormality) using the Testing platform. Figure 4.21(b) shows the tissue under test (healthy region) using Surgical clip.

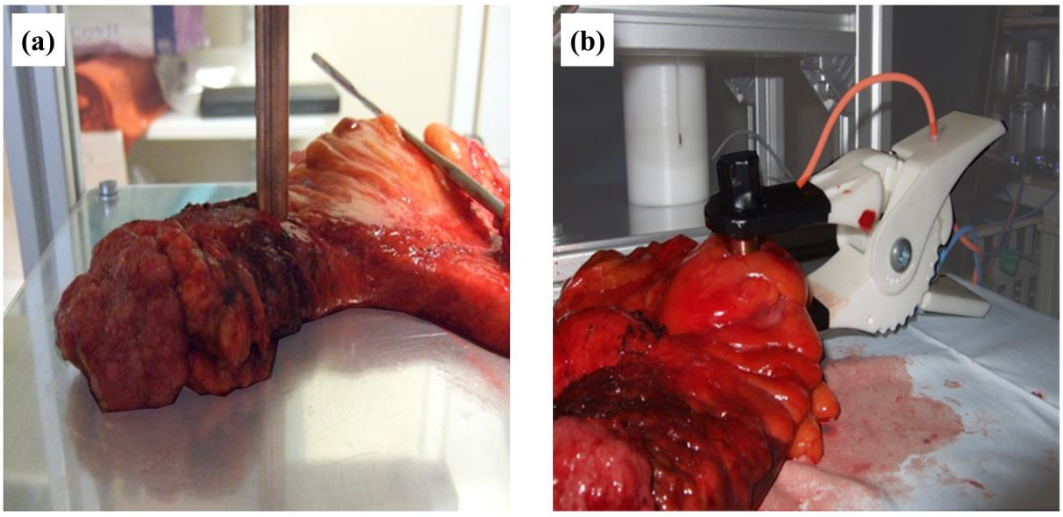

Figure 4.21: Freshly excised human colon tissue with abnormality under test with a) testing rig, and b) with the surgical clip.

Figure 4.22 shows the average measured data for healthy and abnormal tissue data recorded using the two test configurations. Model fitting using Model A and Model B has been also presented. Application of Model A to the data produces a good quality fit, as can be seen within Figure 4.22(a) and Figure 4.22(b). The measured data gives a highly linear trend, with small variability with repeat measurements. Figure 4.22(c) and Figure 4.22(d) show that the linear resistor set used pushes the weighting of the Model B fit to the upper voltage range and away from the critical transition point around R_{INT}. This is caused by the resistor range not driving the cell to high enough current to cover the full cell voltage range, ultimately reducing the quality of the fit.

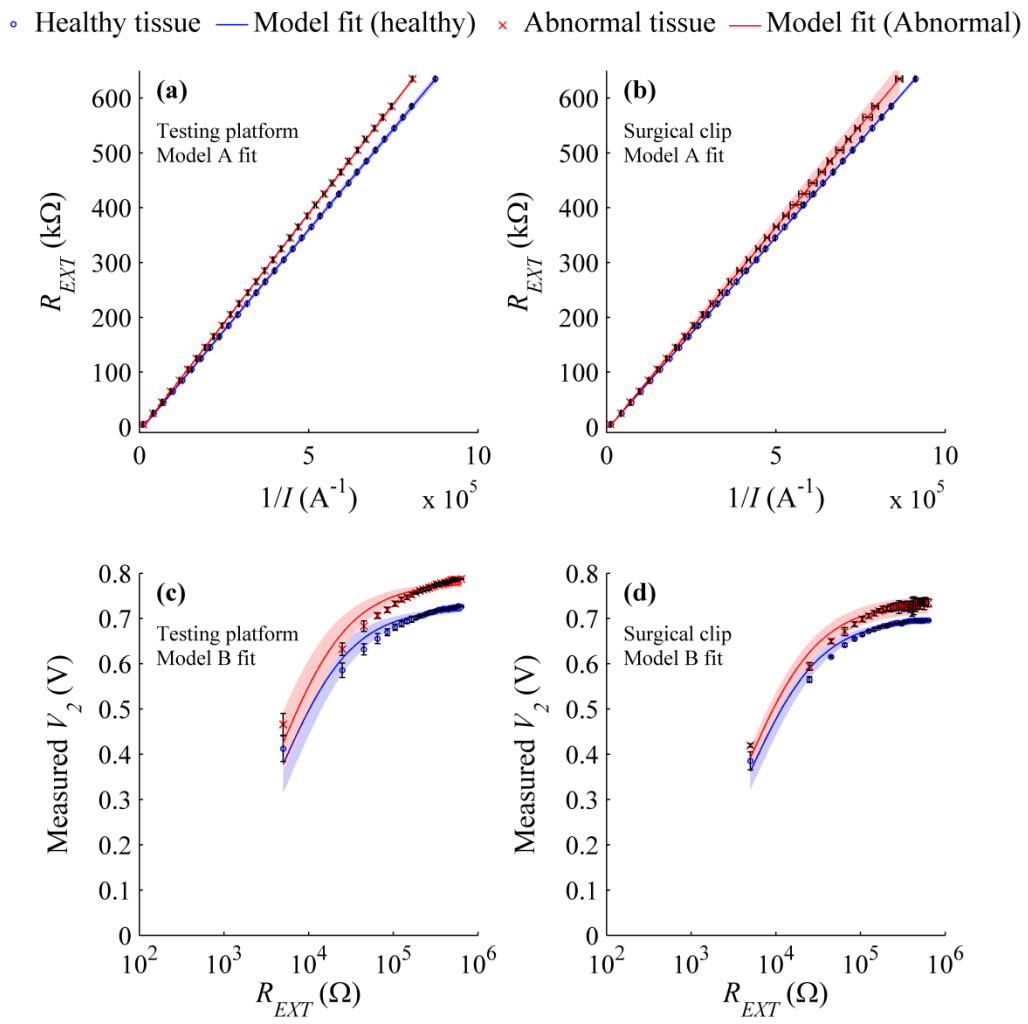

Figure 4.22: Average biogalvanic characterisation measurements on healthy and abnormal (adenocarcinoma) human colon tissue *ex vivo*, showing: (a) testing platform measurements (minimal strain) characterised with Model A; (b) surgical clip measurements (fixed strain) characterised with Model A; (c) testing platform measurements (minimal strain) characterised with Model B; and (d) surgical clip measurements (fixed strain) characterised with Model B. Error bars and shaded regions indicate ±1 standard deviation (n=3) for the measured data and model fits respectively.

The average R_{INT} and OCV results (mean±SD) are presented in Table 4.6. Small differences can be seen for the mean values of healthy and abnormal tissue using both model fitting methods. For Model A the internal resistance is shown to increase slightly with abnormality, while with Model B a small reduction is seen. For abnormal tissue the OCV values increase for both models. Inclusion of the standard deviation of the measured data results in insignificant ($p > .05$; Student's t-test, two-tailed unequal variance) differences in the determined R_{INT} for both models. However, significant differences ($p < .05$; Student's t-test, two-tailed equal variance) were found in the determined OCV values using both models. Figure 4.23 and Figure 4.24 illustrate these findings graphically for R_{INT} and OCV respectively.

Comparison of the Testing platform and Surgical clip indicates that both allow similar differentiation of healthy and abnormal tissues. The differences seen in R_{INT} may be as a result of the strain conditions on the tissue. Discrete fixing points on the surgical clip give fixed separation, variable strain condition (c.f. Section 4.3.5) whereas the testing platform allows fixed strain, variable separation.

Tests on both tissue types produced OCV values consistent with *ex vivo* and *in vivo* porcine colon testing. Characterised OCV values were noted to show a reduction with repeat measures. This is likely to be related to the influence of tissue exposure time as discussed in Section 4.3.2.

Table 4.5: Determined average (mean ±SD, n = 3) results (model B) for healthy and abnormal human colon using test rig and surgical clip.

Testing configuration	Tissue type	Model A R_{INT} (kΩ)	Model A OCV (V)	Model B R_{INT} (kΩ)	Model B OCV (V)
Testing platform	Healthy	7.857 ±1.168	0.735 ±0.002	4.559 ±0.828	0.723 ±0.002
Testing platform	Abnormal	8.601 ±0.813	0.796 ±0.001	4.168 ±0.576	0.780 ±0.002
Surgical clip	Healthy	5.491 ±0.429	0.703 ±0.001	4.644 ±0.517	0.699 ±0.001
Surgical clip	Abnormal	6.158 ±0.479	0.742 ±0.011	4.366 ±0.169	0.735 ±0.010

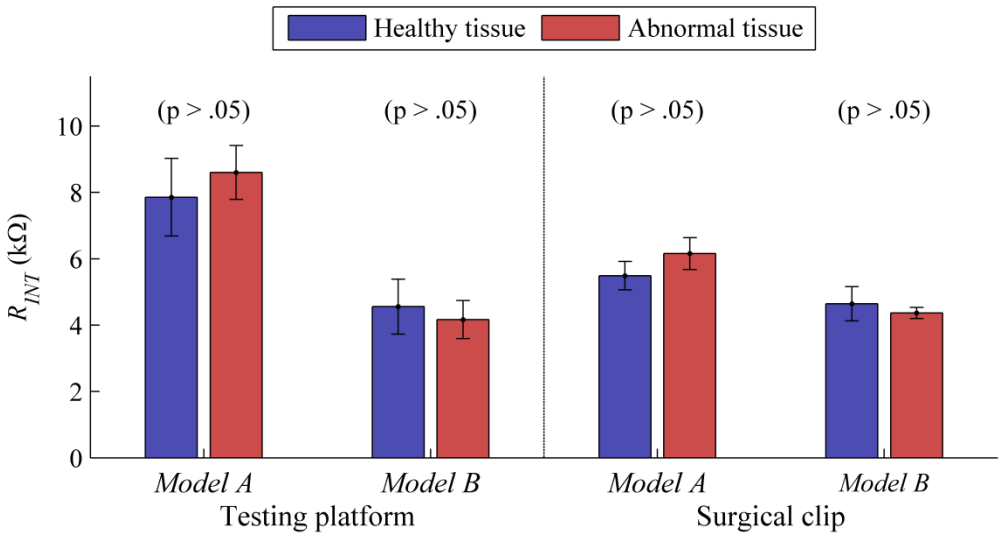

Figure 4.23: Mean ±SD model fit metrics obtained for healthy and abnormal *ex vivo* human colon tissue using the testing platform and surgical clip. Output metrics R_{INT} for Model A and Model B are presented.

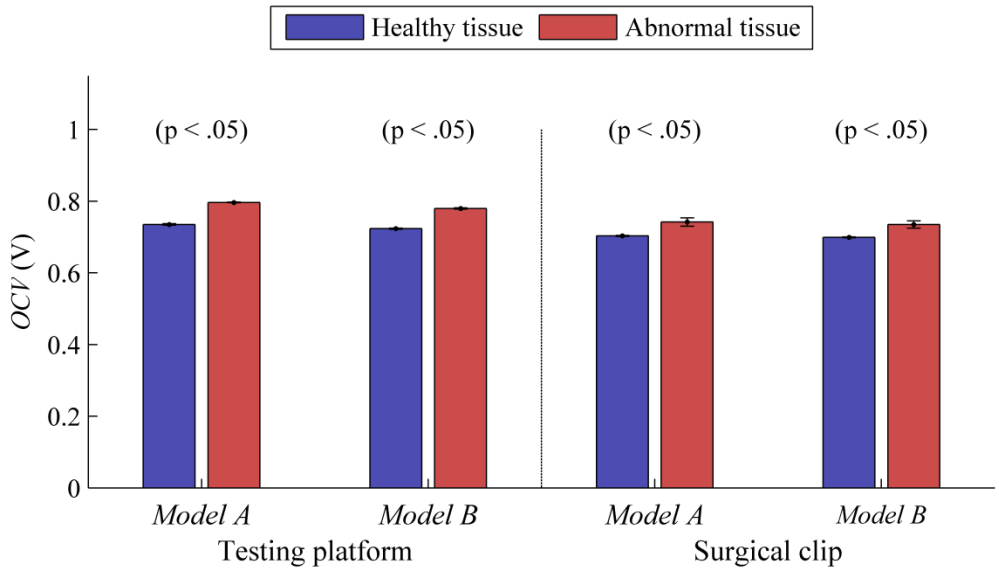

Figure 4.24: Mean ±SD model fit metrics obtained for healthy and abnormal *ex vivo* human colon tissue using the testing platform and surgical clip. Output metrics OCV for Model A and Model B are presented.

4.6 Discussion

It is evident from the presented results that biogalvanic characterisation is a complex process showing great variability under the examined testing conditions. In summary, Table 4.6 contains the findings from the initial parametric experimentation described in this chapter.

Table 4.6: Examined parameters and their influence on the biogalvanic tissue characterisation metrics under galvanic conditions; (✓- influence, ✗ - no influence, ↔ - mixed results).

Electronic variables			
Variable	Model fit	Influence on R_{INT}	Influence on OCV
Resistor range	A,B	✓	✓
Switching rate	A	✓	✓
Switching direction	B	✓	↔
Tissue variables			
Variable	Model fit	Influence on R_{INT}	Influence on OCV
Tissue type	A,B	✓	✓
Tissue health	A,B	✗	↔
Tissue area	A	✓	✓
Tissue thickness	A,B	✓	↔
Tissue strain	B	↔	↔
Positional variation	A,B	↔	↔
Exposure time	A	↔	✓
Electrode variables			
Variable	Model fit	Influence on R_{INT}	Influence on OCV
Contact area	A	✓	✓
Exposure time	A,B	✓	✓
Geometry	-	-	-

It has been indicated in Table 4.6 where variability was found with one or both output metrics during manipulation of the testing parameter. Where separate tests on the same parameter showed variability and invariability, a mixed result has been indicated. In relation to Objective 4.1, the range of experimentation conducted has successfully demonstrated the efficacy of the Biogalvanic characterisation system. Two resistor set configurations have been utilised, and two models (Model A and Model B) have been shown to fit well to data collected on *ex vivo* and *in vivo* tissues. Through the application of electronic models, the variability in system parameters of R_{INT} and OCV has been examined.

4.6.1 Model assumptions and GAIR

Objective 4.2 required examination of the model assumptions presented by Golberg et al. [115, 116] (c.f. Section 3.7). In addition, examination of the mathematical conversion of the characterised internal resistance to a normalised resistivity of $GAIR$ was required. On initial inspection, accurate model fitting and production of consistent internal resistance values within the same tissue specimen suggest the appropriateness of the proposed biogalvanic model. That is to say that the measured data conforms well to the assumption of a fixed internal resistance. However, application of a $GAIR$ correction does not lead to tissue specific resistivity, and tissues have shown significant variation in the characterised OCV.

4.6.1.1 Internal resistance

From the model assumptions, the relationship between internal resistance and $GAIR$ should be linked by contact area and cell thickness (for an axial system). Indeed, such a model should show linear scaling of internal resistance with thickness and electrode area variation. Sections 4.3.3 and 4.3.6 show that there is some influence on internal resistance with these parameters, although linear scaling was not found in both cases.

Figure 4.6 demonstrates a reduction in R_{INT} with an increase in tissue thickness. This leads to an exaggerated rate of $GAIR$ reduction with increasing thickness, which contradicts the model assumption. The influence of electrode area presented in Figure 4.11 shows better model agreement, with a 3.1 times reduction in R_{INT} with a 4 times increase in electrode area. However, these data represent an average across a wide range of testing, and have large variability.

Manipulation of the tissue area presented in Section 4.3.4 also showed influence on resistance. Figure 4.7 illustrates an increase in R_{INT} with a reduction in tissue area, suggesting that current pathways are not necessarily constrained to within the cylindrical volume projected by the electrode faces.

The significant variability shown with converted $GAIR$ values can only be explained via inaccuracy of the model or tissue inhomogeneity. Based on the magnitudes of variability and from comparison to published tissue resistivity data (Table 2.1), model inaccuracy is likely to be the dominating factor in these findings.

4.6.1.2 Open Circuit Voltage

A second assumption of the model presented by Golberg et al. [115] is that of a constant OCV equal to the standard redox equation (5.3). It is particularly evident across the performed tests that there is significant variation in the characterised OCV. Equation (5.3), demonstrating the predicted potential difference of the cell based of standard half-cell reduction reactions, suggests an expected OCV of 0.76 V. Measured values are all lower than this, ranging from 0.75 to 0.25 V across tissue types and test conditions. This indicates that the reaction conditions at the electrode-tissue interface differ significantly from those used in predicting the standard galvanic potential difference.

4.6.2 Parametric investigation

This chapter reports extensive parametric investigation of the biogalvanic characterisation process, in accordance with Objective 4.3. The following sections detail the main findings from the presented work. Table 4.6 offers a specific summary of the presented testing.

4.6.2.1 Influence of time

Electrochemical systems are typically subject to variation with time. This is inherent in the physical phenomena that develop with the measurement of a galvanic cell. The influencing parameters have been considered as those that cause influence to the measured signals but do not alter the properties of the cell components (electrodes, tissues and connecting electronics), and those that cause a permanent change to the properties of the cell. The former includes the time-dependent properties of electrode-tissue interface perturbed by external load switching and time varying ion concentrations, controlled by diffusion, convection and electrical migration. These may cause great temporal influence on the measured signals but will not fundamentally change the physical properties of the cell. In contrast, permanent cell changes may occur through processes of electrode surface passivation and tissue drying. An assumption was made that these processes will occur on two different time scales. The former has been assumed to be inherent within individual characterisations and the latter in longer term repeated measures testing.

To investigate the influence of time on the biogalvanic characterisation process, three preliminary tests were performed. These were: external load switching rate; external load

switching direction; and tissue exposure time. These parametric studies were also considered to have practical importance within the desired sensing application.

Influence of external resistor switching rate was investigated in Section 4.3.7. Figure 4.12 shows the characterisation results as switching rate was varied from 0.1-1.5 Hz. A significant decrease in OCV is seen for increasing rate. Transient settling of the measured voltage signal is less likely to be reached with a faster switching rate. As a result the stead-state voltage value extracted will not be a true representation of the system (c.f. Section 3.6.1). Over a full characterisation this will lead to an under prediction of the OCV. The characterised internal resistance also shows variation with switching rate, although no clear trend is evident.

Section 4.4.1 presents a comparison between increasing and decreasing external load switching directions. Clear hysteresis is evident with loading direction, and leads to a statistically significant alteration of the characterised internal resistance across all tissue types tested. The OCV shows less variability with direction, although two of the three tissue types still show a statistical difference. The disparity between the R_{INT} and OCV hysteresis suggests that processes beyond inaccurate steady state voltage extraction are present. Independent influence on the characterised internal resistance may be expected if the limiting processes at high current flow are not purely attributed to the electrical resistance of the tissue. Closed cell galvanic current experiments presented in Section 4.4.2 show that the maximum current is indeed not linearly dependent on tissue resistance scaling (Figure 4.16), but is significantly increased through application of larger cathodic reaction site (increased cathode length, Figure 4.17).

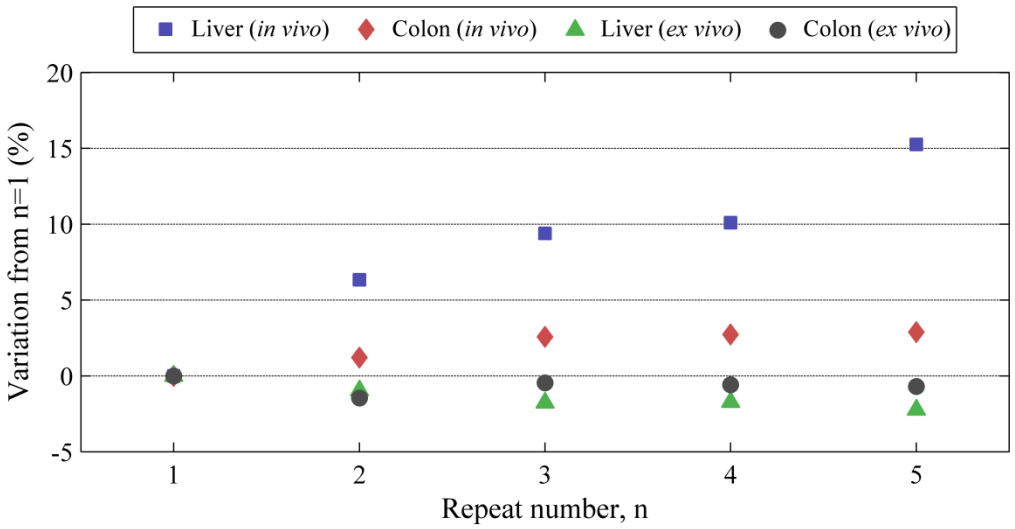

Figure 4.25: Percentage variation in OCV with repeat number (n) normalised to repeat 1 (n_1) for liver and colon tissue tested under *ex vivo* and *in vivo* conditions.

Figure 4.5 showed an exponential decay for the characterised OCV as a function of exposure time. The internal resistance however shows more spurious variation with this

parameter. As a consideration of the influence of the longer time scales involved in repeat testing, Figure 4.25 shows the normalised variation with repeat number for measurements on liver and colon tissues *in vivo* and *ex vivo*. Based on the presented data, OCV influence direction appears to be opposite for *ex vivo* and *in vivo* tests.

The demonstrated time-dependent system behaviour may be explained through a number of factors. On shorter time scales, the settling time between switching may be significant in altering the characterised resistance and OCV, when the selected switching rate is not appropriate. For longer time scales reaction species depletion (e.g. O_2), tissue drying and electrode fouling are all factors that should be considered.

4.6.2.2 Geometric considerations

Geometric considerations include the influence of electrode area, tissue thickness, tissue area and tissue strain. Section 4.6.1 discussed the influence of the first three parameters, including how they relate to the model assumptions and $GAIR$ conversion. Section 4.3.5 described testing involving alteration of tissue strain. Application of approximately 50% strain to liver tissues resulted in a statistically significant reduction in characterised internal resistance. This is as would be expected based on model assumptions and a reduced thickness. However, the magnitude of reduction and a lack of change when applied to colon tissue indicate a more complex process. For an axial based sensing system, strain is likely to be an unavoidable consequence of tissue measurement. It therefore forms an important parameter for consideration.

4.6.2.3 Tissue condition

The following sections detail and discuss the main findings from the investigations of this chapter pertaining to tissue variation.

4.6.2.3.1 *Ex vivo* vs *in vivo*

Objective 4.4 required biogalvanic characterisation to be performed with *ex vivo* and *in vivo* tissues. Direct comparisons cannot however be made between *ex vivo* and *in vivo* results due to inherent differences in test temperatures and mechanical contact conditions. However the R_{INT} values all fall within the same order of magnitude and show similar levels of variation. The OCV values for *ex vivo* tissues are similar to those recorded *in vivo*, although the former shows marginally higher values for both tissue types. A more exaggerated difference between colon and liver tissue was found for tests *in vivo*. This suggests that living tissue has a greater influence on the interface conditions within the galvanic cell and therefore the relative potentials between electrodes in an open cell. Figure 4.25 supports this, showing that *in vivo*

experimentation delivers a greater and positive influence on OCV over repeat measuremnets, while *ex vivo* tissue show a consistent drop in OCV.

4.6.2.3.2 Tissue type

The presented testing has been focused primarily on liver and colon tissue types. The results across all testing generally show colon tissue to have a higher internal resistance and OCV. These findings may be related to the tissue structures, with consideration of the homogeneity and fat content of the respective tissue types. These factors are likely to influence the resistivity of the tissue and therefore the characterised Biogalvanic resistance. The variation in OCV is associated with the redox reactions sustained at the galvanic electrodes. For colon tissue, a more separate potential is achieved leading to an increased OCV. Implications of ion concentrations and the specific cell reactions on this characterised metric are discussed further within Chapter 5. Findings presented in Figure 4.14 show specificity for colon, liver and rectum tissues *in vivo* for both characterisation metrics. This finding suggests that there is significant influence on the biogalvanic cell from the tissue. However, the additional findings of the chapter suggest that there may not a simple relationship with tissue resistivity.

4.6.2.3.3 Tissue health

Similar differences between the Testing platform and the Surgical clip shown in Figure 4.22 and Figure 4.23 indicate that relative measurement may be sufficient for health discrimination. The most significant differences relating to health can be seen between the OCV values shown in Figure 4.24. Assuming negligible temperature differences between healthy and abnormal tissue, the OCV is determined by the relative ion activities (concentrations) as described in the Nernst equation [83]. Measured differences may be due to physiological alterations to the ion concentrations in the respective tissue regions, making OCV a potential tissue health descriptor.

4.7 System-Relevant Findings

The work presented in Chapters 3 & 4 has focused on the development and testing of an internal resistance characterisation system for tissues under galvanic cell conditions. Motivation for working in this area has been in part due to the promising results presented by the founders of the technique, Golberg et al. [115]. Additionally, the technique is simple and scalable which are often overlooked attributes in development of surgically appropriate sensing systems. Much work has been performed in an attempt to develop a testing system and to establish appropriate testing protocols. The developed Biogalvanic system and testing protocols have allowed

repeatable data to be obtained on an appropriate time scale. The central chapter findings pertaining to biogalvanic characterisation have been summarised:

Biogalvanic system: *The developed Biogalvanic characterisation system and model fitting methodologies were validated in Chapter 3. Application to tissues across a wide range of conditions has shown similar data to that measured by Golberg et al. [115]. Model fitting has produced good agreement with measured data and allowed extraction of condition specific R_{INT} and OCV metrics.*

Model assumptions: *The model assumptions of biogalvanic characterisation were assessed through alteration of the influencing variables. Tissue thickness and area both showed influence on R_{INT} although not in agreement with model predictions. The implications of these findings are that the characterised resistance is not solely from the tissue and that normalisation of data to a $GAIR$ value is therefore inappropriate.*

Tissue specificity: *Findings from investigation of the model assumptions suggest that tissue resistance is only part of the characterised R_{INT} value. However, testing across tissue types in vivo has shown specificity based on this metric. In addition, the characterised OCV was also found to be specific to tissue type and was less sensitive to the measurement settings.*

Temporal variation: *Time dependence of the biogalvanic cell was made evident through investigation of external load switching conditions (rate and direction) and through repeated measures over an extended time period. Findings indicate that for fast switching an under prediction of OCV is produced based on incorrect steady state voltage readings. This theory was not shown to extend directly to testing of external resistor direction, where non-linear artefacts at high current levels have been proposed as the cause of some of the hysteresis shown. Longer time scale processes such as electrode passivation and tissue drying have also been identified as important considerations for a biogalvanic tissue system.*

Geometric variation: *Nominal strain geometric variations were found to cause significant influence on internal resistance. Under mechanical strain of approximately 50% the internal resistance of liver tissue was found to reduce. However, similar testing on colon tissue induced no change in resistance.*

4.8 Chapter Summary

Results presented in this chapter have demonstrated that tissues show behaviour comparable to the electronic model presented in Figure 3.12. The developed Biogalvanic testing system has allowed measurement and characterisation of *ex vivo* and *in vivo* tissues of different types, meeting Objective 4.1. The results demonstrate that biogalvanic tissue systems can be modelled as a fixed internal resistance and open circuit voltage.

Results and discussion related to the investigation of the model assumptions of the biogalvanic technique and Objective 4.2 have been presented. Although measured data can be modelled as a single fixed internal resistance, the findings have suggested a greater complexity to the biogalvanic system. Additional parametric investigation conducted in accordance with Objective 4.3 supports this suggestion, indicating that the characterisation metrics are dependent on a wide range of variables (c.f. Table 4.6).

Testing has been performed across a range of tissue conditions. In relation to Objective 4.4, *ex vivo* and *in vivo* testing have shown similar values for R_{INT} and OCV although tissue specificity was found to be greater during *in vivo* testing. Results have also shown sensitivity tissue health and strain, and to external resistor loading conditions. These have not always been in accordance with expectation, and the influences are not always repeatable. Some justification and implication of these findings has been discussed in the context of development of a surgically appropriate sensing tool.

Chapter 5
Electrochemical investigation of the biogalvanic system

Extensive biogalvanic tissue testing presented in Chapter 4 demonstrated significant variability in characterisation metrics for a wide range of parameters. Some specificity to tissue type and condition was shown, positioning biogalvanic measurement as a potential method for obtaining health-specific tissue information. However, there is a dearth of understanding in the biogalvanic literature regarding the underlying galvanic cell, electrode reactions and their controlling factors which limits application of the technique. This chapter, therefore, describes relevant background information (Section 5.2) followed by electrochemical investigation of the system, implemented to make improved assessment of the galvanic cell and characterisation process.

Section 5.3 presents a parametric electrochemical investigation into a zinc-copper galvanic system using salt (NaCl) solution analogues at physiologically-relevant concentrations (1.71, 17.1 & 154 mM). The potential difference at open cell, closed cell maximum current and the internal resistance (based on the characterisation method of Chapter 3 and 4) were measured. Additionally, independent and relative polarisation scans of the electrodes were performed to improve understanding of the system. Section 5.4 presents an investigation into the influence of temperature on the closed cell current, included as a supplementary study.

The findings, discussed in Section 5.5, suggest that the prominent reaction at the cathode is that of oxygen-reduction, not hydrogen-evolution. Results indicate that cell potentials are influenced by the concentration of dissolved oxygen at low currents and maximum closed cell currents are limited by the rate of oxygen diffusion to the cathode. Characterised internal resistance values for the salt solutions did not correspond to theoretical values at the extremes of concentration (1.71 and 154 mM) due to electrode resistance and current limitation. Section 5.6 describes how these findings are related to the biogalvanic system and how alterations to the equipment and model may be employed to improve performance.

5.1 Testing Aims

The primary aim of the presented study is to gain information relating to the biogalvanic system (electrodes, salt-bridge medium and characterisation process) using electrochemical techniques. Ultimately, this information is to be used to improve understanding of the findings from Chapter 4 and to inform any future applications of the biogalvanic technique. The following objectives were defined in order to allow realisation of the chapter aims:

Objective 5.1: *To develop a suitable analogue testing arrangement to allow parametric control and variation of resistivity, temperature and geometry.*

Objective 5.2: *To define a suitable selection of relevant electrochemical measurements to apply to the developed analogue.*

Objective 5.3: *To investigate the influence of salt-bridge resistance (NaCl concentration) on the defined electrochemical tests and the biogalvanic characterisation process.*

Objective 5.4: *To relate the chapter findings to the biogalvanic characterisation system and explore the implication on previous results and suggest adaptations for future testing.*

5.2 Background information

For biogalvanic characterisation, a zinc and copper galvanic cell is established and used as the current generating power source. The cell current is passively regulated using external resistors, which reduces measurement system complexity, as external power supply and additional current control electronics are not required. This simplicity makes the biogalvanic method an attractive sensing modality. However, the findings presented in Chapter 4 showed that the system is removed from the simple model assumptions described in Chapter 3 [115, 156]. Application to porcine tissues *ex vivo* and *in vivo* showed sensitivities to mechanical contact condition (strain levels) and time-dependent behaviour. In addition, and crucially, little is known of the electrochemistry that governs the characterisation process. This section presents some electrochemical and corrosion considerations that relate to the biogalvanic system. The developed salt solution system analogue has also been described and justified in this section.

5.2.1 Relevant electrochemical theory

For the copper and zinc galvanic cell proposed, information presented by Golberg et al. [115, 116] suggests the primary standard electrode reactions of:

$$Zn^{2+}(aq) + 2e^- \rightarrow Zn(s) \qquad E^0 = -0.76\,V \text{ (SHE)} \qquad (5.1)$$

$$2H^+(aq) + 2e^- \rightarrow H_2(g) \qquad E^0 = 0.00\,V \text{ (SHE)} \qquad (5.2)$$

Giving the predicted full cell reaction and galvanic potential difference under standard conditions of:

$$Zn(s) + 2H^+(aq) \rightarrow Zn^{2+}(aq) + H_2(g) \quad \Delta E^0 = 0.76\,V \qquad (5.3)$$

The actual half-cell reaction potentials are influenced by the cell conditions in accordance with the Nernst equation (5.4), where the actual reduction potential, $E_{red}$is a function of the standard half-cell reduction potential E^0 and the chemical activity of the reducing agent, a_{red} and the oxidising agent, a_{ox}. For dilute solutions the activity coefficient tends to unity leaving the chemical activity interchangeable with ionic concentration. For the hydrogen evolution reaction (equation (5.2)) to be thermodynamically favourable at pH7, a potential more negative than -0.41 V (SHE) is required at the cathode. The measured Open Circuit Potential (OCP) of copper under comparable conditions, and measured in this study is +0.1 V (SHE), making hydrogen evolution unfavourable [157]. The oxygen reduction reaction (equation (5.5)) at pH7 is however thermodynamically feasible at potentials lower than +0.81 V (SHE), suggesting that this is the primary reaction at the copper cathode under open cell conditions. Therefore the full cell reaction within the galvanic cell would be that of equation (5.6).

$$E_{red} = E^0 - \frac{RT}{zF} ln \frac{a_{red}}{a_{ox}} \qquad (5.4)$$

$$2H_2O + O_2 + 4e^- = 4(OH)^- \quad E^0 = +0.4\,V \text{ (SHE)} \qquad (5.5)$$

$$Zn + H_2O + \tfrac{1}{2}O_2 \rightarrow Zn^{2+} + 2(OH)^- \quad (\Delta E^0 = 1.16V) \qquad (5.6)$$

Biogalvanic characterisation within the range of expected tissue resistivity (0.2-50 $\Omega.m$ [158]) using the proposed external resistance range will necessitate moving the cell from near open cell conditions toward short circuit. For high current levels the electrode potential must shift away from the equilibrium potential by an amount ΔV, in accordance with the Tafel equation (5.7). The term α represents the charge transfer coefficient and the terms F, R and T represent the Faraday constant, the universal gas constant and absolute temperature respectively [159]. The sign in equation (5.7) indicates the reaction type with positive representing an anodic process and a negative representing a cathodic process. It is possible that the required potential shift for the cathodic reaction supporting the anodic dissolution of the zinc metal will become sufficient to cause change from solely oxygen-reduction to a mixed system also including hydrogen-evolution.

$$I \propto exp\left[\pm\frac{\alpha F}{RT}\Delta V\right] \tag{5.7}$$

5.2.2 Corrosion considerations

The measurement system is fundamentally based on the corrosion of zinc metal. As such, the corrosion mechanisms for zinc dissolution as well as the supporting cathodic reactions should be considered. Electrochemical studies have been conducted looking at zinc and copper in isolation, and as part of a galvanic cell. In neutral and basic solutions the anodic polarisation of zinc produces oxides and hydroxides, although passivation of the electrode is not achieved [160]. García-Antón et al. [161] suggest that these oxide regions may cause reduced reaction kinetics for the zinc oxidation reaction. This could lead to increasing resistance of the zinc electrode with time. However, shorter time scales and surface treatment between tests should mitigate or at least reduce the effect of this potential issue. Cathodic polarisation of copper in neutral aqueous solution will be dominated by the reduction reactions of water and of dissolved oxygen; equation (5.2) and (5.5) respectively. In particular, the rate of the oxygen-reduction reaction, equation (5.5), has been shown to be limited at a high overpotential by the mass transport of dissolved oxygen to the electrode surface [162]. As part of a Zn-Cu galvanic couple, the copper electrode has been shown to be highly polarisable with respect to the zinc electrode [163]. Therefore the behaviour of the copper electrode under cathodic polarisation will be likely to dominate the behaviour of the galvanic cell.

5.2.3 NaCl solution model

To characterise the electrochemical properties of the system, tests were conducted within salt solutions (NaCl (aq)). This offers improved control over the system parameters in comparison

to testing with biological tissue. In particular, a salt solution model allows control over the salt bridge conductivity giving meaningful validation to the biogalvanic characterisation system. The applicability of using an aqueous sodium chloride system is based on a number of assumptions: (1) the primary tissue current pathway is through extracellular fluid, (2) the dominant ionic components of extracellular fluid are Na^+ and Cl^-, and (3) the electrochemistry is dominated by the NaCl medium and the electrode properties. It is common within BIS characterisation to consider biological cells in a capacitive nature, due to their non-conductive lipid bilayer cell membrane [164, 165]. At low frequency the current pathway will therefore be predominantly through the extracellular fluid surrounding the cells. The major ionic species within extracellular fluid are Na^+ and Cl^- making the use of NaCl solution an appropriate model [164, 166].

Initial comparisons between the NaCl solution and tissue results were made within the presented study to understand further the efficacy of this model. The analysis of a salt solution system can thus help to validate the biogalvanic system and demonstrate the influence of electrochemical factors that may need to be addressed for reliable use in tissue characterisation. Specific testing of the OCV, closed cell currents and transition currents was undertaken. The influence of salt solution conductivity within a physiological range on these independent aspects of the galvanic cell is presented within this chapter. Additionally, comparisons have been made between the independent electrochemical findings and the applied characterisation process, with reference made to published tissue data.

5.3 Experiment 1: Concentration of NaCl

This section presents the testing methodology and results for investigation into the influence of salt concentration on the galvanic cell and its constituent parts. Salt concentration was selected as the primary variable for investigation due to its direct relation to resistivity (resistance), which is the principal biogalvanic characterisation metric.

5.3.1 Preliminary investigation

Preliminary testing was performed in order to establish typical current behaviour of various types of cells during the biogalvanic characterisation process. The current was measured using a Zero Resistance Ammeter (ZRA) (Compact Stat, Ivium Technologies) during a biogalvanic characterisation of 17.1 mM NaCl solution. The system was tested using 15 fixed external loads (Resistor set 2) switched in descending order at 100 second intervals. In addition, identical characterisation of an electronic model with an OCV of +0.8 V and internal resistance of 10.2 kΩ, was performed and the current monitored as a function of time. The resistance value used in

this model is within 1 % of the theoretical resistance of 17.1 mM NaCl solution under the test geometry.

For comparison a current profile attained during a single biogalvanic characterisation of *ex vivo* human rectum was performed. Freshly excised human rectal tissue was obtained in accordance with NHS and Leeds Teaching Hospital ethics procedures. The biogalvanic characterisation was performed over 20 fixed external load values switched in descending order at 10 second intervals. The current trace during the characterisation was recorded for comparison to the salt solution tests.

5.3.2 Measurements

Tests were conducted in isolation from mechanical considerations through the use of an aqueous sodium chloride electrolyte. Salt solutions of 1.71, 17.1 & 154 mM (0.01, 0.1 & 0.9 wt% respectively) NaCl were prepared through volumetric combination of analytical grade NaCl (Fisher Scientific) with distilled water. These concentrations represent a conductivity range spanning across that of soft tissues [158]. Test solutions were maintained at 25+/-1 °C for all tests using a temperature-controlled hotplate (MR Hei-Standard, Heidolph). Axially aligned flat faced copper and zinc 12 mm diameter cylindrical electrodes were set in non-conducting resin and connected to external control and measurement equipment through copper wire. Electrode surfaces were wet ground to 1200 grit and rinsed with distilled water prior to each test. Figure 5.1 shows the geometric arrangement and experimental setup used for galvanic testing in salt solutions.

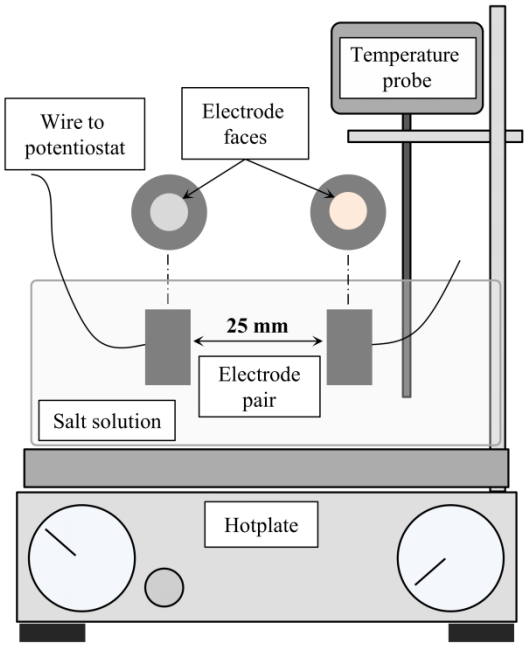

Figure 5.1: Geometric arrangement and test setup for the axially aligned galvanic test cell.

5.3.2.1 Open circuit voltage

The OCV was determined using two separate techniques. Firstly, individual OCP values were measured for each electrode relative to a Ag/AgCl reference electrode (Thermo Scientific). Subsequently the difference between the individual electrode potentials was calculated to give the expected OCV for the galvanic couple. Secondly, the OCV was measured directly from the galvanic couple through external connection of a high resistance voltmeter. To test the OCV, each electrode/electrode-pair was placed into the test solution and allowed to stabilise for 30 minutes. The OCP/OCV measurements were then conducted using a precision potentiostat (CompactStat, Ivium Technologies). Each measurement recorded the potential for 30 minutes with the determined OCV being calculated using average potentials over this period. Statistical analysis of the influence of concentration on the galvanic OCV was conducted using a single-factor analysis of variance (ANOVA) test (n=5).

5.3.2.2 Closed cell current

In order to measure the current levels produced under closed cell conditions a Zero Resistance Ammeter (ZRA) (Compact Stat, Ivium Technologies) was connected in series with the cell. Upon closing the galvanic cell through the ZRA a large initial transient was typically present. To determine the steady state closed current the system was monitored for 1 hour with data from the final 30 minutes used to obtain steady-state average values. Figure 5.2 shows the transient behaviour seen when establishing the closed cell current along with the steady-state variation seen in the final 30 minutes of testing. The variation of closed cell current with concentration was assessed statistically through application of a single-factor ANOVA test (n=5).

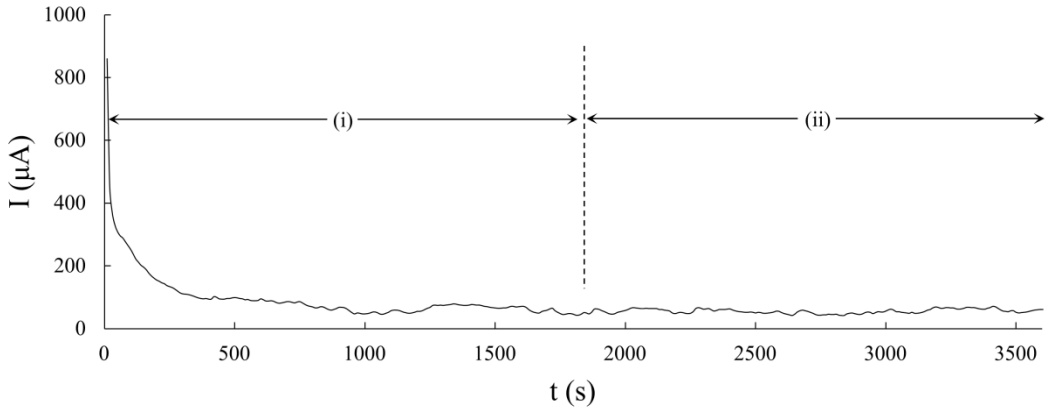

Figure 5.2: Typical closed cell current trace showing (i) initial transient settling period and (ii) region used to determine average steady state closed cell current.

5.3.2.3 Galvanic characterisation

For typical galvanic cell characterisation, the electrode pair was submerged in the test solution and connected as an open cell for 30 minutes prior to resistor switching. External resistor values were then switched every 100 seconds from high resistance to low resistance over 15 fixed values. An external resistor switching time of 100 seconds was implemented in order to allow transient voltages caused by discrete switching to settle before being used to determine internal resistance. The system was connected in series with the ZRA to allow measurement of current during this period. The resistor switching pattern and typical resultant current trace can be seen in Figure 5.3(a). The internal resistance of the cell was determined using the model and fitting method described by Chandler et al. [156].

5.3.2.4 Polarisation

Polarisation scans were undertaken using the individual electrodes of the galvanic cell as the working electrode in a typical three-electrode cell. A combination Ag/AgCl reference and Pt counter electrode (Thermo Scientific) was employed. Polarisation was undertaken after a 30 minute OCP settling period. The zinc and copper electrodes were polarised from OCP in the anodic (increasing) and cathodic (decreasing) potential directions respectively. A scan rate of 0.5 mV/s was employed in all tests. Each polarisation was conducted to 1 V against OCP in the test direction specified. Five repeat tests were conducted for each electrode at each NaCl concentration.

5.3.2.5 Relative polarisation

Relative polarisation of the galvanic cell was conducted through cathodic polarisation of the copper electrode against a zinc counter/reference electrode of the same geometry. Consequently, data more representative of the galvanic cell under internal resistance characterisation could be obtained. The copper potential was controlled from OCV to closed cell value (0V), with corresponding current response being measured. Five repeat tests were conducted for each of the test solution concentrations. Additionally, a relative polarisation scan was conducted on freshly excised human colon tissue for comparison to the salt solution data. Tissue was obtained in accordance with NHS and Leeds Teaching Hospital ethics procedures.

5.3.3 Results

5.3.3.1 Preliminary investigation

The current-time trace from biogalvanic characterisation of 17.1 mM NaCl solution is shown in Figure 5.3(a). It can be seen that numerous standard features are present, these are identified as: (i) the established Open Circuit Voltage (OCV) at open cell conditions (no current flow between

electrodes); (ii) transition currents showing no transient behaviour; (iii) transition currents with significant transient behaviour; and (iv) established maximum current under closed cell conditions. Figure 5.3(a) also shows the current response for characterisation of an electronic model. The two systems show similar current behaviour for stages (i) and (ii). However, discrepancies are seen at higher current levels where the transient behaviour and limited maximum current are seen to be typical only of the salt solution.

The current profile attained during biogalvanic characterisation of *ex vivo* human rectum tissue is shown in Figure 5.3(b). The profile shows that the outlined features seen within the NaCl model are also apparent in the biological tissue test. In particular, similarities in the transient behaviour and limitation at high current are shown. This indicates that the present characterisation model assumption of a pure internal resistance is not appropriate over the full testing range for pure salt solution or biological tissue.

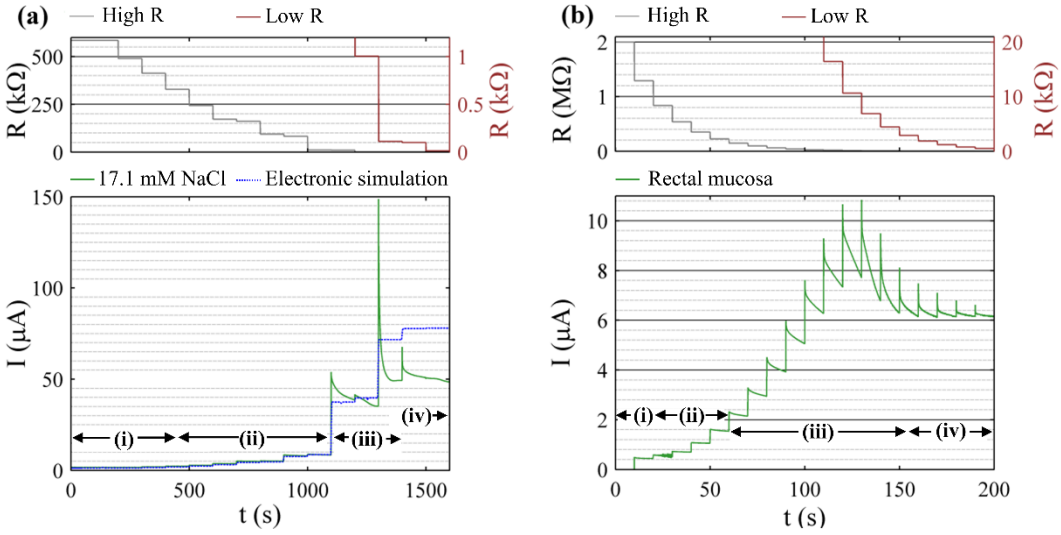

Figure 5.3: Current-time profiles during biogalvanic characterisation of: (a) 17.1 mM NaCl at 25°C (green line); and an equivalent electronic simulation of R_{INT} = 10.2 kΩ and OCV = 0.8 V (blue dashed line), and (b) human rectum tissue ex vivo. External resistor values as a function of time are also shown above each current trace. A secondary ordinate axis (right) has been used to show the low external resistance values. The identified features for salt solution and tissue data are: (i) low current towards open cell; (ii) current level step transitions at low current; (iii) transient behaviour occurring at higher currents after switching; and (iv) closed cell maximum current.

5.3.3.2 Open and closed circuit

Figure 5.4 shows the averaged OCV values and data range for varied salt solution concentrations; obtained using two different methods. OCV values range from 0.8-0.9 V, with statistically significant differences ($p < .05$) being shown between mean values, determined using a galvanic couple. For comparison, Figure 5.4 also presents *in vivo* OCV results obtained in a separate study [156]. These values represent the mean and range of five repeats tested on a

single porcine specimen at three different tissue locations. The OCV values for a tissue salt bridge are all lower than for aqueous NaCl. Additionally, the values span from 0.3-0.7 V and are specific to the tissue type tested.

Figure 5.5 shows the average steady state maximum current obtained for varied solution concentration. No statistical significance ($p < .05$) between average closed cell currents at varied test concentrations was found. However, the average current for the 1.71 mM NaCl solution is lower than either of the more concentrated solutions. Variability in results is large for all concentrations, with standard deviations ranging from 4-8 μA.

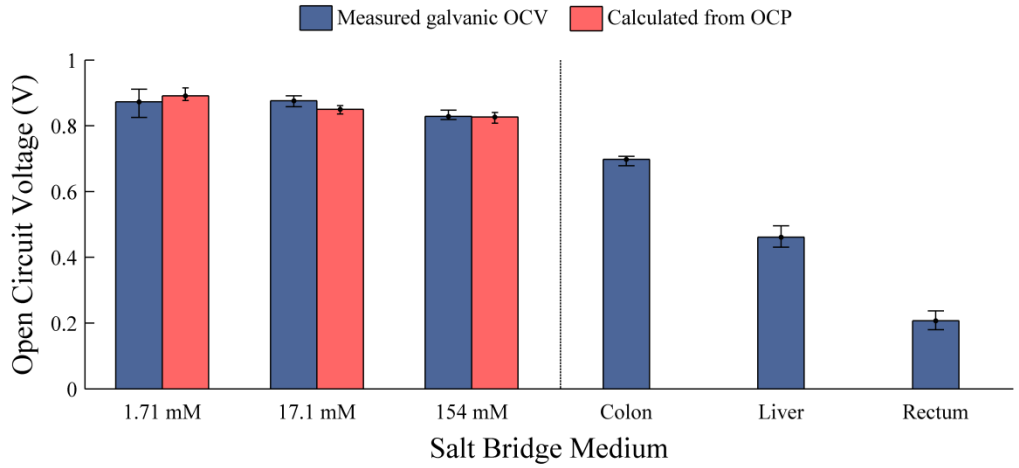

Figure 5.4: Averaged OCV determined for solutions of varied [NaCl] using galvanic determination and calculated from independent electrode OCP measurements; full data range indicated (N=5). OCV values from *in vivo* porcine tissue tests also shown for comparison [156].

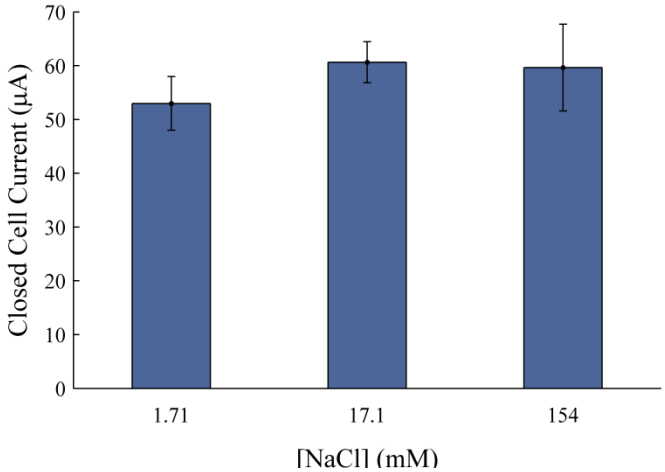

Figure 5.5: Average closed cell current for varied [NaCl]; showing +/- 1SD (N=5).

5.3.3.3 Galvanic characterisation

Figure 5.6 shows the characterised internal resistance values determined for the varied salt solution concentrations. The internal resistance values measured using the galvanic method

follow the trend of the theoretical data, although errors are seen to be large at the extremes of solution concentration. For the lowest NaCl concentration (1.71 mM), the galvanic method gives resistance values much lower than theory, and shows a high degree of variability for repeat tests. The 17.1 mM concentration gives measured values in line with theory, with the mean internal resistance being 6 % larger and with low repeat variation. For the highest concentration (154 mM), measured resistance values were consistently greater than theory with a high degree of variability.

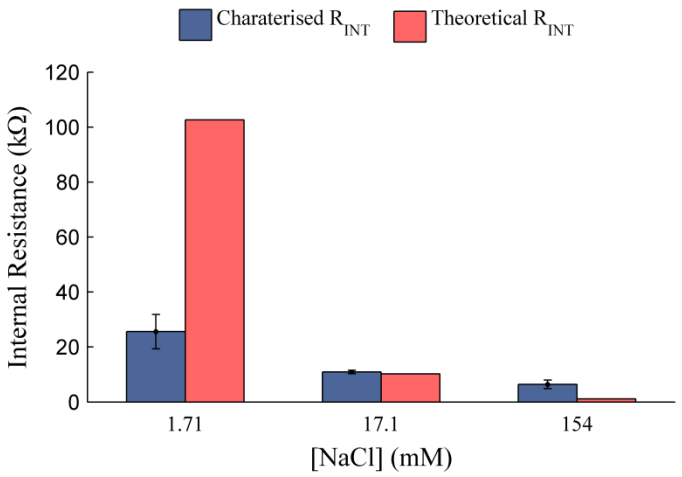

Figure 5.6: Averaged internal resistance ± standard deviation, determined using: the galvanic characterisation method, and from theory using conductivity data.

5.3.3.4 Polarisation

Figure 5.7 shows the current profile produced by polarisation of each electrode for the three concentrations tested. The mean polarisation curves are represented by solid lines with the range from five repeats indicated via the corresponding shaded boundary. The anodic polarisation of the zinc electrode shows a typical exponential potential-current response for an electrode under charge transfer control; as described by equation (5.7). The range of zinc polarisation profiles is small for all concentrations, indicating that polarisation of this electrode is highly repeatable. The NaCl concentration has the influence of altering the potential-current response. Specifically, for the same overpotential the current is higher for a higher NaCl concentration. This is likely due to a reduction in the losses associated with uncompensated solution resistance as the solution resistance drops. In contrast, the cathodic polarisation of copper breaks from linear behaviour at potentials more negative than 0.1 V from OCP, showing influence from mass transport kinetics. This is exemplified by the large range of polarisation profiles seen from repeat tests; particularly in more concentrated solutions. The OCP values of the copper electrode are more negative for increasing NaCl concentration. The point of equal current for the anodic and cathodic profiles of the galvanic cell has been indicated for each concentration. This is

predictive of the maximum current attainable by the cell, although the influence of polarisation scan rate and internal resistance losses are not accounted for.

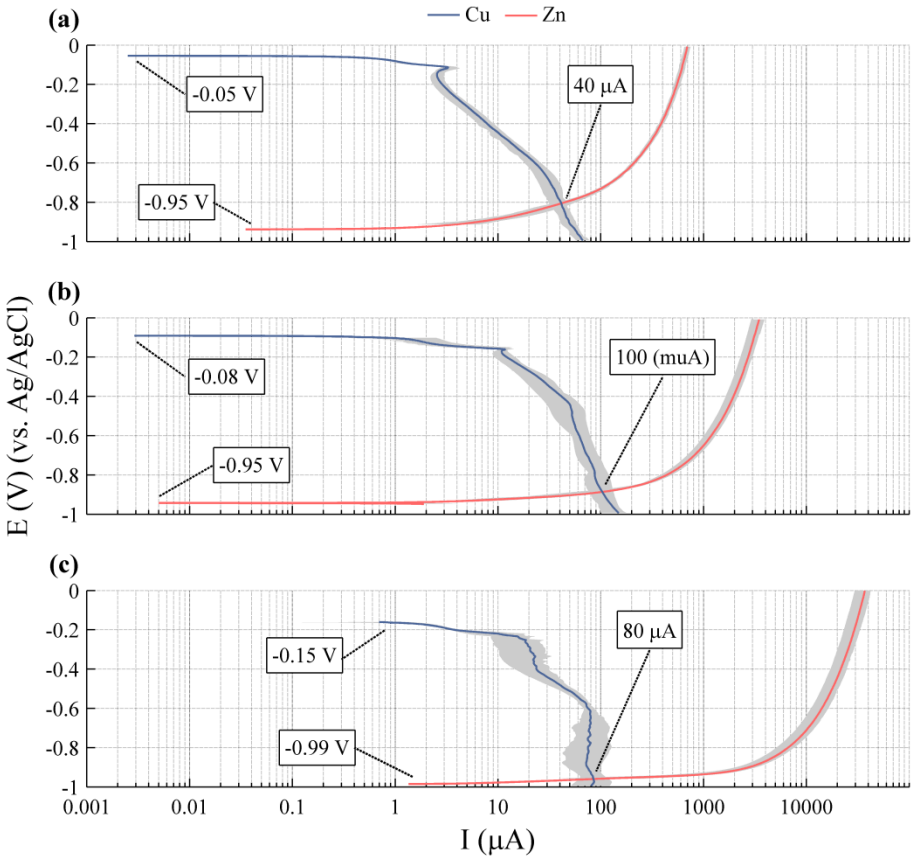

Figure 5.7: Average polarisation data (N=5) for axial electrodes tested in (A) [NaCl] = 1.71 mM, (B) [NaCl] = 17.1 mM, and (C) [NaCl] = 154 mM; zinc and copper polarised in the anodic and cathodic direction by 1 V from OCP respectively. The range seen within repeats is shown for each test case as the shaded region. Predicted average closed cell current and individual electrode OCP values are indicated.

5.3.3.5 Relative polarisation

Figure 5.8(a)-(c) shows the polarisation of the copper electrode against a zinc counter for three NaCl concentrations. The current profile produced shows a combination of the features seen within the individual polarisation curves of Figure 5.7 All concentrations tested tend towards a similar limiting current, similar to the closed cell current results of Figure 5.5. Increased non-linear potential-current behaviour is seen with increased concentration. The profiles demonstrate three distinct regions: (1) activation-controlled response at potentials close to the OCV, where small potential changes cause large changes in current; (2) an approximately linear increase in current with increase in potential; and (3) mass transport limited regime where current becomes independent of potential. The duration of each stage varies for each of the test concentrations. The relative polarisation data for a cell connected through *ex vivo* human colon tissue is shown

in Figure 5.8(d). The profile produced shows cell features predicted from salt solution tests, with large activation controlled and current limited regions. These features were also predicted from the biogalvanic current trace in Figure 5.3(b).

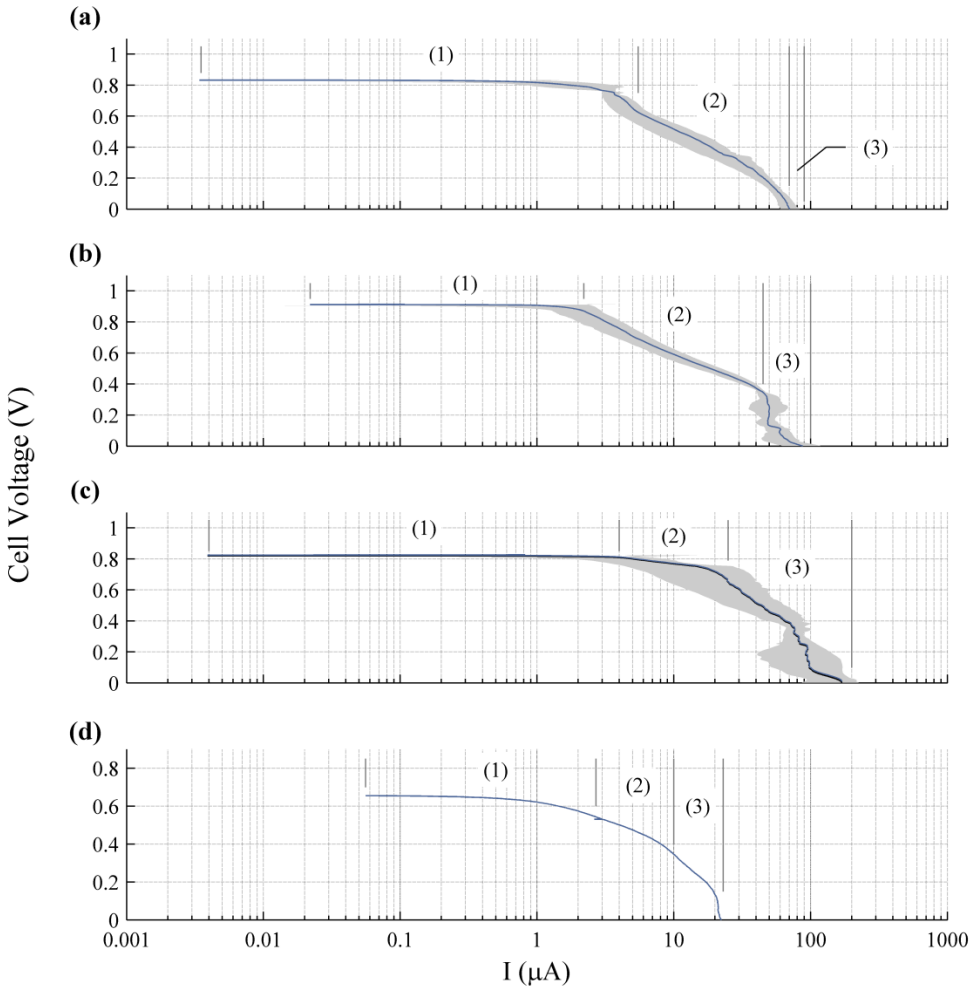

Figure 5.8: Average relative polarisation data (n=5) for axial copper electrode against a zinc counter & reference for salt bridge mediums of (a) [NaCl] = 1.71 mM, (a) [NaCl] = 17.1 mM, (c) [NaCl] = 154 mM, and (d) human rectal mucosa (ex vivo). Copper polarised in the cathodic direction from OCV; (a-c) show repeat testing range shown as shaded region (N=5). Potential current control methods annotated as: (1) activation control, (2) internal resistance control, and (3) mass transport control.

5.4 Experiment 2: closed cell galvanic current

This section reports the findings related to current measurement under closed cell conditions. The relevance of this parameter to the biogalvanic system is presented along with an investigation into the influence of temperature on the closed cell current. A summary of the closed cell current tests perform is also presented.

5.4.1 Relevance to biogalvanic characterisation

The closed cell galvanic current represents a specific point in the biogalvanic characterisation procedure. This point is where the external load on the cell is sufficiently low that it does not restrict current, which is instead limited through internal mechanisms. This was selected for investigation as it offers an easily achievable test condition, removed from a number of the influencing variables of the biogalvanic characterisation process (c.f. Chapter 4). Measurement under this condition on *in vivo*, and *in vitro* tissues is presented within Section 4.4.2 and Section 4.5.1 respectively. This section reports closed cell galvanic current results from testing under varied electrode geometry, temperature and salt solution concentrations.

5.4.2 Influence of temperature

During measurement of the closed cell current in salt solution systems, controlled to temperatures above room temperature, significant transients were noticed. Figure 5.9 shows a typical current profile found during closed cell galvanic current testing. This cyclic process was also evident for varied concentrations and electrode geometries, as shown in Figure 5.10.

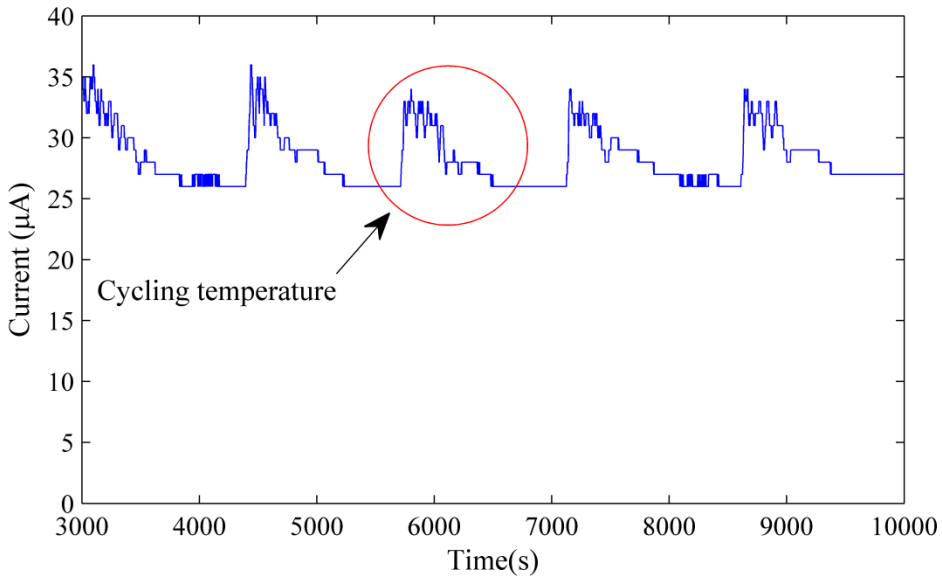

Figure 5.9: A typical closed cell galvanic current trace recorded during a temperature controlled investigation with electrode set N_C in NaCl(aq) (1.71 mM), showing cyclic current variation.

The cyclic nature of the current trace was deemed to be caused by either interface phenomena such as build-up and clearing of reaction product, or a complex passivation cycle, or due to alteration of the cell temperature induced through non-ideal control. The effect of temperature fluctuation offered a simpler testing process. As such, testing was conducted through sequential alteration of the cell temperature. In addition, a system was developed to allow time-synchronised measurement of current and temperature.

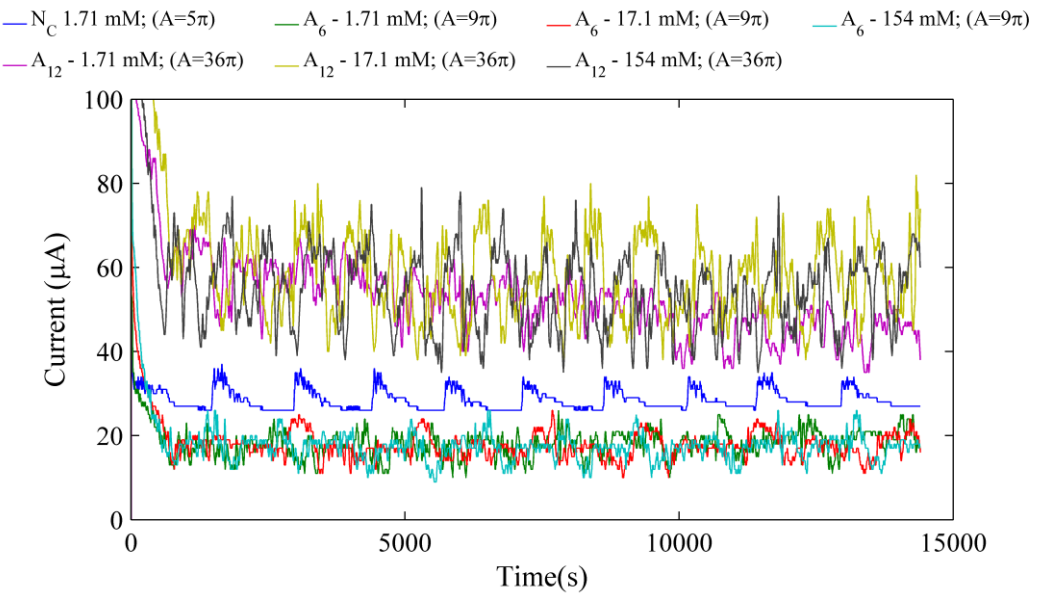

Figure 5.10: Cycling phenomenon and steady state values shown for closed cell galvanic current measurements across cell geometries and salt solution concentrations.

5.4.2.1 Methods

Tests were conducted to investigate the influence of temperature on the closed cell galvanic current. A range of solution temperatures were employed for testing, while the corresponding closed cell galvanic current was recorded. In addition, external monitoring of the temperature was used to investigate the steady-state control of the system.

5.4.2.1.1 Temperature monitoring

The salt solution temperature was monitored during testing using a second temperature sensor. A temperature sensing element (Pt1000 for MR Hei-Standard, Heidolph) from a hotplate controller of the same specification was used for monitoring the cell temperature. The sensor is a Resistive Temperature Detector (RTD), meaning a variation in resistance with temperature. A Pt1000 has a resistance of 1000 Ω at 0 ˚C, and over small temperature range its resistance varies in an approximately linear fashion, in accordance with equation (5.8), [167]. This equation shows that for a positive temperature coefficient of resistance (α_t), a linear increase in resistance of the RTD will be expected for an increase in temperature (T ($^{\circ}C$)). The temperature coefficient of resistance for platinum, as in the Pt1000, is 0.0039 ($/^{\circ}K \equiv /^{\circ}C$) [167].

The resistance change across a 50˚C range was therefore calculated as shown in equations (5.9)-(5.11). For a variable resistance sensor, it is typical to use a bridge resistor network configuration to convert resistance change into a measurable potential difference [167]. Using the theoretical resistance values of the RTD across the testing temperature range, the expected output voltage across a Wheatstone bridge was determined using equation (5.12). The

assumption of an ideal sensor with a balanced bridge at 0 ˚C was made, giving the voltages at 0 and 50 ˚C in equations (5.13) and (5.14) respectively.

$$R_{RTD} = R_0[1 + \alpha_t T] \tag{5.8}$$

$$R_0 = 1000[1 + (0.0039 \times 0)] = 1000\,\Omega \tag{5.9}$$

$$R_{50} = 1000[1 + (\alpha \times 50)] = 1195\,\Omega \tag{5.10}$$

$$\Delta R = 1195 - 1000 = 195\,\Omega \tag{5.11}$$

$$V_G = \left(\frac{R_{RTD}}{R_3 + R_{RTD}} - \frac{R_2}{R_1 + R_2}\right) V_s \tag{5.12}$$

$$V_0 = \left(\frac{1000}{1000 + 1000} - \frac{1000}{1000 + 1000}\right) 5 = 0\,V \tag{5.13}$$

$$V_{50} = \left(\frac{1197}{1000 + 1197} - \frac{1000}{1000 + 1000}\right) 5 = 0.224\,V \tag{5.14}$$

To achieve optimal resolution for the voltage range expected across 0-50˚C, amplification to 0-10 V was employed. A differential amplifier was used to amplify the potential difference across the bridge. The full sensing electronics configuration is shown in Figure 5.11. The resistor values for the differential amplifier were selected to give an approximate gain of 40. With the selected settings a calibration against a second Pt1000 (MR Hei-Standard, Heidolph) calibrated to ±0.05˚C was conducted. Figure 5.12 shows the temperature sensing system calibration data. The calibrated system was utilised in the galvanic current testing to achieve synchronised time-coded temperature data.

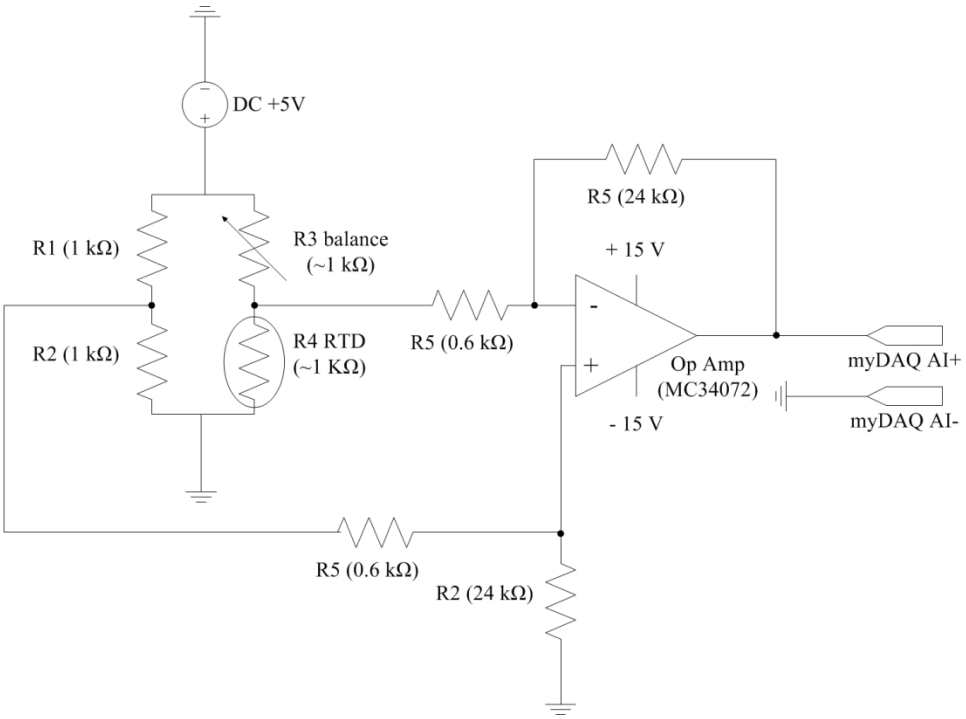

Figure 5.11: Circuit diagram for Pt1000 RTD based temperature measurement.

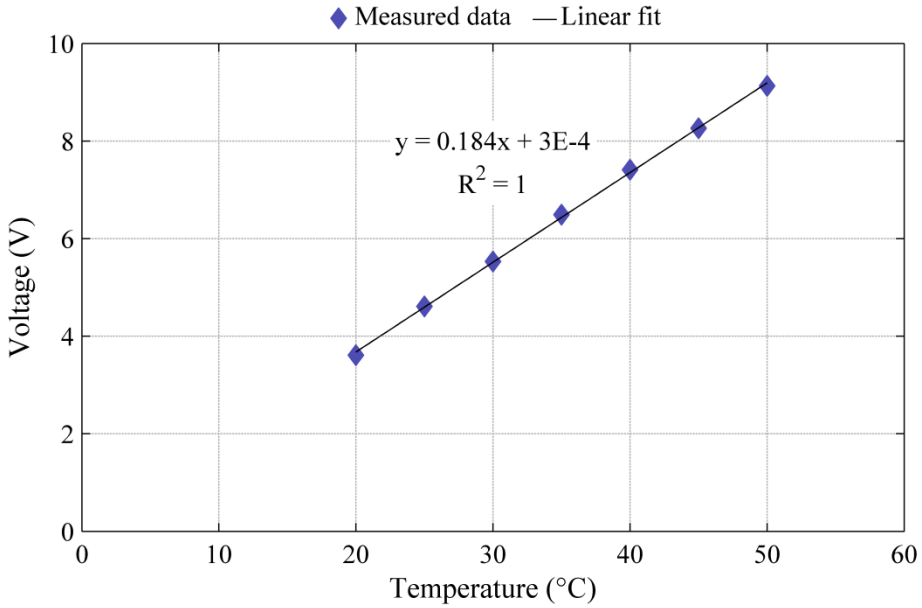

Figure 5.12: Calibration results for custom temperature sensing system over the proposed testing range of 20-50 ˚C.

5.4.2.1.2 Temperature variation

Temperature variation testing was conducted using an N_C needle electrode pair (1mm diameter with 10 mm indentation and 20 mm separation). The electrode pair was held submerged in 500 ml of 1.71 mM NaCl solution in 150 mm diameter beaker centred on a magnetic stirring hotplate (MR Hei-Standard, Heidolph). The hotplate control was set to a fixed temperature

(setpoint), with the 'manual' temperature set to 100˚C. Closed cell galvanic current was measured using a ZRA (Compact Stat, Ivium Technologies) for 1 hour at each temperature. Temperature setpoints ranging from 20-50˚C in 5˚C intervals were tested in a randomised order, with three repeats recorded at each temperature. The average galvanic current for each temperature was determined as the arithmetic mean current over the final 30 min of testing. Current and temperature data were qualitatively investigated through graphical comparison of synchronised data.

5.4.2.2 Results

The mean closed cell galvanic current as a function of solution temperature is shown in Figure 5.13. A positive linear relationship can be seen for temperatures up to 40˚C, with the relative increase in closed cell current being less at temperatures above this value. This drop in linearity may be associated with changes in the electrode kinetics arising from electrode passivation at higher temperatures. Figure 5.14 shows how the solution temperature and closed cell galvanic current vary with time. Significant hysteresis in the hotplate controller, causing a fluctuation of ±1˚C around the temperature setpoint, is evident within the trace. Crucially, the heating element generates electronic noise that is picked up by the electrodes, and causes an abrupt rise in the closed cell current signal of approximately 6 µA when switched on. The cyclic heating pattern is picked up in the measured current trace. Although the temperature fluctuation of a tissue system is likely to be considerably slower than for the hotplate, Figure 5.14 illustrates how temperature can have a significant influence on the cell current and therefore biogalvanic resistance characterisation.

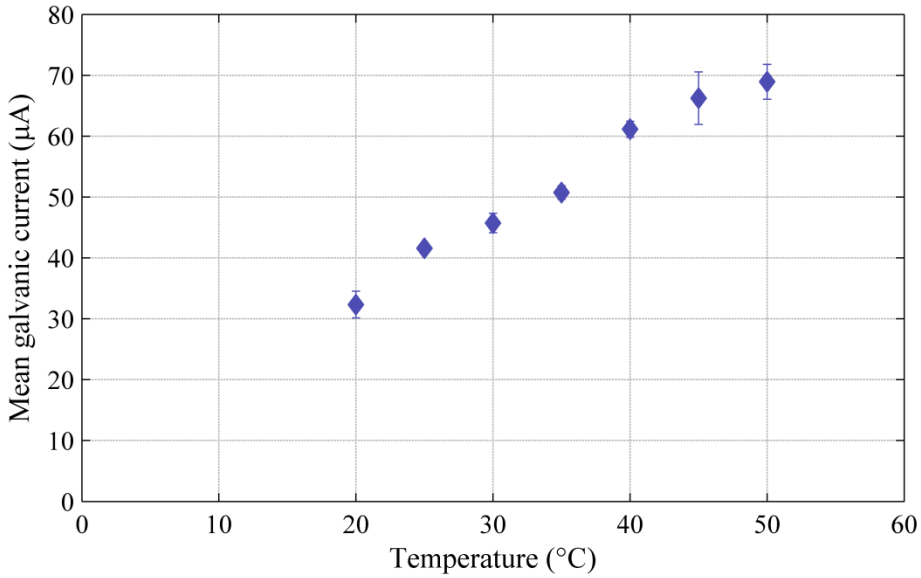

Figure 5.13: Mean±SD (n = 3) closed cell galvanic current as a function of solution temperature for N_C electrode set.

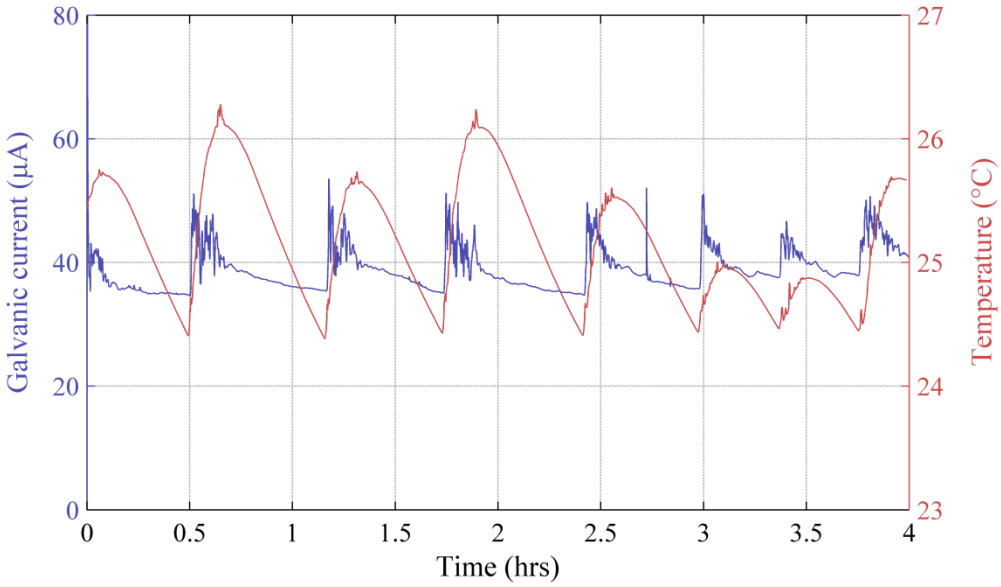

Figure 5.14: Galvanic current and solution temperature as a function of time for 1.71 mM NaCl at 25˚C.

5.5 Discussion

5.5.1 Open circuit voltage

Average OCV values measured from the galvanic couple show statistical significance for varied NaCl concentration. Salt ion concentrations within physiological range alter the standard electrode potentials, generating a range of OCV values varying by 0.1 V (from 0.8-0.9V). Variations in electrode potentials can be accounted for through temperature and local ion concentration fluctuation, in accordance with the Nernst equation. Salt solution results are markedly different to OCV values measured *in vivo* on porcine tissues [156]. Tissue results are presented for comparison in Figure 5.4. A much larger range spanning from 0.2-0.8 V is shown, with differences between tissue types being statistically significant. The much lower OCV values seen *in vivo* may be related to altered reaction mechanisms. In particular, the lower OCV may be caused by a lower open circuit potential at the copper electrode. For an aqueous system with a low dissolved oxygen concentration, the electrode potential at the cathode may become more negative to thermodynamically support the hydrogen-evolution reaction of equation (3). If tissues have type specific dissolved oxygen concentrations, then specific OCV values for zinc-tissue-copper galvanic cells would be expected. Carreau et al. [168] showed that there is significant variation in the oxygen partial pressure (pO_2) between tissue types, specifically indicating a lower pO_2 for liver tissue compared to intestinal tissue. The influence of oxygen can also be seen within the salt solution system (Figure 5.7); where the OCP at the copper

electrode becomes more negative as the oxygen solubility is reduced by higher NaCl concentrations. For NaCl concentrations from 0-171 mM the solubility of oxygen reduces from 8.22-7.79 mg/l (~5 %) [169].

5.5.2 Closed cell current

5.5.2.1 Influence of concentration

Figure 5.5 shows the closed cell current to be insensitive to the concentration of NaCl. No statistically significant differences in steady state current values are shown between concentrations. This suggests that at maximum current the system is not limited by the resistance of the salt bridge. It can be seen directly in Figure 5.3(a) that for an electronic model of equivalent internal resistance, the current at low external resistor values is higher than that produced in the galvanic cell. Therefore, at high current levels the characterisation method is no longer influenced by the solution resistance but by a limited reaction rate. Additionally, the fluctuations at maximum current are large (as shown in Figure 5.10) indicating instability of the current limiting mechanism. In particular the fluctuations were noted to be sensitive to temperature and agitation which are typically associated with a mass transport limiting, diffusion controlled processes [162, 170].

5.5.2.2 Influence of temperature

Temperature showed a significant influence on the closed cell galvanic current. The results shown in Figure 5.13 indicate an approximately linear increase in current with temperature, suggesting that the mechanisms of current limitation are directly proportional to temperature. Temperature is therefore an important consideration for steady-state current tests as well as biogalvanic characterisation. The cycling influence of the solution temperature shown in Figure 5.14 also acts to demonstrate the sensitivity of the system to this value.

5.5.3 Galvanic characterisation

The internal resistance values predicted using the biogalvanic characterisation method show discrepancies with theoretical values determined using conductivity data for the corresponding solution concentrations. For the 1.71 mM solution, the measured internal resistance is much lower than theory (25 %). This is due to the method of characterisation not being specific to the internal resistance, and thereby measuring the influence of electrode activation. For the 154 mM solution, internal resistance values were measured as being larger than those predicted theoretically. This can be accounted for through the mass transport limited current under closed cell conditions being a dominant factor over the solution resistance. In addition the characterised resistance is highly variable within the same conductivity of solution which corresponds with

the fluctuation seen at closed cell current levels. The resistance of the electrodes are also not accounted for within the characterisation model which will inevitably lead to a larger prediction of internal resistance if the system is assessed over the full current range. The internal resistance determined of the 17.1 mM solution shows agreement with theory, and also indicates little variation with repeat testing. Figure 5.6 indicates that the galvanic characterisation method is inadequate at determining effective solution resistances for extremes of NaCl concentration. Inaccuracies may be caused by factors influencing the characterisation process such as mass transport limitations at the cathode, large relative resistance of the cell electrodes, and the discrete external resistor range not allowing even characterisation over the full current range. However, the relative pattern follows that of the theoretical resistance values and predicted values at 17.1 mM are within 7 % of the theoretical value, indicating that the system may be accurate when sufficiently optimised to the test case.

5.5.4 Polarisation

Polarisation tests allow the individual electrode current response to be examined over the range of possible potentials experienced during galvanic characterisation. From Figure 5.7 it can be seen that the polarisation involved during galvanic characterisation necessitates the anodic and cathodic polarisation of the zinc and copper electrode respectively. For the same electrode areas the zinc electrode requires a much smaller overpotential than the copper electrode to achieve the maximum current of the closed galvanic cell. This indicates that the system is particularly dominated by the cathodic polarisation of the copper electrode. For the 17.1 and 154 mM NaCl solution, a near vertical current response is seen in Figure 5.7 at potentials more negative than -0.4 V from the OCP of the copper electrode. For the same concentrations under relative polarisation (Figure 5.8), large mass transport limited regions are also evident. This current saturation is associated with the diffusion limited oxygen reduction reaction of equation (5.5), commonly seen in the cathodic polarisation of copper in aqueous solution [162, 171].

The value of the maximum current for a system under this type of control is determined by a number of factors, described by equation (5.15) [83]. The current (I) is controlled by the charge transferred per mole (nF), electrode area (A), diffusion coefficient (D), concentration of the diffusing species in the bulk solution (c_b), and the diffusion layer thickness (δ). For the system in solution the values can all be considered constant with the exception of the diffusion layer thickness. The diffusion layer thickness for a static (unstirred) system will be time varying in accordance with an expanding concentration gradient as the reaction proceeds. For a planar electrode, this is typically modelled as equation (5.16) [83], where t represents time. This model predicts an ever expanding diffusion layer which, in conjunction with equation (5.15), would propose a current tending to zero. It can be seem from Figure 5.2 that this was not found

experimentally; instead the system appears to fluctuate around a steady state value. The non-zero current results from natural convection resupplying electrolyte of bulk concentration to the depleted diffusion layer. An effective limit is reached on the diffusion layer thickness which is dependent on the natural convection within the system. Tobias et al. [172] advise that the often quoted diffusion layer thickness of 0.5 mm can lead to erroneous predictions of limiting currents under natural convection, and actual thickness values are highly system specific.

$$I = \frac{nFADc_b}{\delta} \tag{5.15}$$

$$\delta = \sqrt{\pi Dt} \tag{5.16}$$

This diffusion limiting mechanism is of critical pertinence to the characterisation method. Dropping the external resistance to a level where the current demanded becomes greater than that of the diffusion-limited current will cause the system to operate in a non-linear regime, inconsistent with the proposed characterisation model. Effectively, an additional resistance becomes dominant within the system, thereby restricting determination of the internal salt bridge (tissue) resistance.

5.5.5 Relative polarisation

Control of the potential across the galvanic cell using polarisation of copper against zinc is most representative of the system during biogalvanic characterisation. Utilising a slow potential transition mitigates the influence of large transient potentials caused by the discrete external resistor switching. Comparison of Figure 5.7 with Figure 5.8 indicates that the galvanic system behaves as a combination of the two polarised electrodes, with the copper dominating the current response. The diffusion limited oxygen-reduction reaction is again evident in the response for higher concentrations, indicating that it will be present during internal resistance characterisation. An activation controlled region is also present at potentials close to OCV. This indicates that at the extremes of the current range, phenomena at the electrode will dominate, thereby reducing the efficacy of internal resistance determination.

The relative influence of the various cell phenomena is proposed as being qualitatively associated with the accuracy of the internal resistance characterisation. The profiles can be divided into three distinct regions: (1) activation controlled potential-current response, at potentials close to the OCV; (2) a steep drop in potential for a small increase in current caused primarily by the internal resistance; and (3) mass transport limited regime where current becomes independent of potential. These regions have been highlighted in Figure 5.8 to allow

for compassion between concentrations. It is proposed that, when using the current characterisation method, accurate determination of internal resistance can only take place when region (2) is dominant and the external resistor range generates currents primarily spanning this region. It can be seen that for the 17.1 mM NaCl solution the activation control region is small and the onset of mass transport limitation is close to the closed cell condition. Therefore, for the majority of the potential-current profile the system is under internal resistance control, leading to more accurate characterisation. In contrast, galvanic polarisation of 154 mM NaCl shows a very early onset of mass transport limited behaviour at cell voltages of less than 0.7 V, while internal resistance control is only seen at voltages between 0.8-0.7 V. As a result, the internal resistance characterisation will pick up primarily on the effective resistance of the mass transport limiting mechanism. This may be responsible for the over prediction of the salt bridge resistance seen in the 154 mM solution. For the low resistance system of the 1.71 mM NaCl solution, the galvanic polarisation shows little influence of the mass transport limitation (cell voltages < 0.2V). This exposes a large region of internal resistance (0.6-0.2V) which should allow for accurate characterisation. However, the system also shows a large portion of the profile under activation control (0.8-0.6V). In conjunction with the fixed range of external resistances, it is postulated that the characterisation of internal resistance in this solution is dominated by this activation region, leading to an under prediction of internal resistance.

Figure 5.8(d) shows the response for relative polarisation of the cell connected through tissue. Electrochemical features seen during NaCl tests are again present here with large activation potential losses and mass transport limited current. The tissue system is subject to the same phenomena seen in NaCl, demonstrating that the salt solution model is appropriate for examining the system's electrochemical properties. However, the specific potential-current relationship may not be exactly captured within a particular NaCl system and tissue data should also be examined independently when making biogalvanic characterisations.

5.6 System-relevant findings

The primary aim of the biogalvanic characterisation method is to determine an accurate measurement of tissue resistance. This study has shown that the biogalvanic characterisation method is subject to a number of confounding factors caused by the electrochemistry of the system. Firstly, the dissolved oxygen concentration will change with the variable salt concentration of different tissues. As the oxygen concentration is directly related to the potential of the copper cathode, the cells OCV will be influenced by tissue type. However, the use of appropriate model to fit to the measured data can account for this variation, making it a useful metric in conjunction with the internal resistance. Secondly, and of more significance, is the

electrode resistance inherent in the biogalvanic system due to the use of only two electrodes. All measurements will contain contributions from losses at the electrodes along with those within the tissue. This will cause an additional resistance to be present in the system, contributing to the characterised internal resistance. If the electrode resistance is constant and small relative to that of the tissue medium then this systematic error would not preclude the measurement of a specific tissue resistance, although the accuracy will be reduced. Electrode resistance will be influenced by the material type, geometry and current test range, making choice of these parameters important. Finally, for high current demands through the cell, it has been shown that the system becomes limited by the rate of diffusion of oxygen to the copper anode. This non-linear behaviour will cause an additional error in the characterisation. This process has been shown to be present during tissue testing (Figure 5.3(b)) but may vary due to the range of oxygen concentrations expected. Mitigation of this during biogalvanic characterisations could be achieved by restricting tests to lower cathodic overpotentials (and therefore lower current densities) through the adjustment of the relative electrode areas. Although significant potential errors are present within the biogalvanic characterisation system it is feasible that these can be minimised or mitigated through careful equipment and experimental design, allowing the method to deliver representative tissue resistances. This is supported by the accuracy and repeatability achieved during 17.1 mM NaCl characterisation.

5.7 Chapter Summary

In accordance with Objective 5.1 a salt solution tissue analogue was developed and justified (c.f. Section 5.2.3). Assessment of copper-zinc galvanic cells using typical (OCP and polarisation scans) and atypical (closed cell current, internal resistance characterisation, and relative polarisation) electrochemical measurements, defined as part of Objective 5.2. This has improved the understanding of the biogalvanic system. Specifically, it has been shown to be predominantly controlled by processes at the copper electrode. The proposed reaction of hydrogen-evolution is thermodynamically unfavourable relative to the oxygen reduction reaction at the measured cathode OCP. Under tested conditions the oxygen reduction reaction is occurring and persists as the cathode potential becomes more negative. The OCV of the galvanic cell is proposed to be sensitive to the concentration of dissolved oxygen in the system. This may explain the significant variation in OCV values seen between porcine tissues *in vivo* [156].

From investigation into the influence of salt-bridge resistance (Objective 5.3), it is evident that previous work reporting biogalvanic characterisation [115, 116, 156] may have underestimated the system complexity. In particular, the assumption of a sole internal resistance is an oversimplification. Galvanic polarisation has shown that electrode activation behaviour at

high cell potentials (low current) and transport limitations of oxygen to the cathode at lower cell potentials (high current) may skew the characterisation metric, leading to inaccurate predictions of tissue resistance. These findings have been discussed in Section 5.5.3, in accordance with Objective 5.4.

There are potential benefits to biogalvanic characterisation although application of this modality requires repeatable and accurate results across a range of operating conditions. Mitigation of the issues demonstrated may be achieved through optimisation of the characterisation system, specifically selection of electrode material and geometry, and through appropriate system modelling and improved control of external resistive loads. Additionally, inclusion of the OCV parameter during assessment may yield more reliable metrics pertaining to tissue health, as this parameter is linked to the known variations in tissue oxygen concentrations.

Chapter 6
Biogalvanic system modelling

Work presented in Chapters 4 and 5 detail the systematic testing of the biogalvanic system within tissues and salt solutions. Findings from these tests have illustrated the complexity of the biogalvanic system and the potential errors apparent during characterisation. This chapter summarises exploratory work conducted with the aim of offering methods of reducing these errors, and improving the characterisation system as a whole. Due to the limited resistor selection range of the custom Biogalvanic system, Section 6.2 describes the development of a testing protocol to allow the use of the commercial CompactStat (Ivium Technologies) in the subsequent work.

The subsequent sections detail investigation into biogalvanic system modelling. Section 6.3 presents a time-dependent analytic model, with the aim of reducing the influence of the external load switching rate on the characterisation metrics. Section 6.4 describes collaborative work conducted in conjunction with the School of Computing, University of Leeds to develop a more rigorous system model, with inclusion of cell geometry and electrode polarisation effects. Section 6.5 details the findings and limitations of the modelling work presented. The chapter is concluded with a general review of the feasibility of biogalvanic characterisation as a sensing system.

6.1 Chapter objectives

A number of limitations of the biogalvanic characterisation method have been highlighted through the results presented in the preceding chapters. The simple model assumptions upon which the method is based are not adequate for dealing with the complexity of the galvanic cell during full polarisation (open cell to closed cell). This chapter presents a number of exploratory studies performed to investigate the feasibility of overcoming these limitations through the use of improved system models. The work objectives associated with this chapter are:

Objective 6.1: *To produce a more flexible external load controlling tool to allow improved parametric investigation into electronic and measurement variables.*

Objective 6.2: *To examine the inclusion of the time-dependent elements into the characterisation model to allow separation of electrode and tissue resistance values from measured data.*

Objective 6.3: *To evaluate the biogalvanic system through numerical modelling of the system.*

Objective 6.4: *To summarise the findings from this and previous chapters relating to biogalvanic characterisation, and assess its feasibility as a sensing modality within MIS.*

6.2 Improved Galvanic Cell Load Control

In Chapter 4, electronic and measurement parameters were shown to have a significant influence on the characterised biogalvanic resistance of tissues. Tested parametric variation included external resistor switching direction and rate, and the influence of resistor range was also shown to be an essential consideration (c.f. Section 4.5.2). It is for these reasons that it becomes an essential requirement for improved control of these parameters. The presented Biogalvanic testing system (Chapter 3) has the limitation of utilising fixed resistor vales over a 7-bit configuration. This significantly limits the range, resolution and flexibility of potential external load test configurations. The following sections detail the integration of a commercial potentiostat (CompactStat, Ivium Technologies) into a software reconfigurable biogalvanic measurement system.

6.2.1 CompactStat software and testing protocol

The Ivium CompactStat has been described in Section 3.5.2. The native software (IviumSoft, Ivium Technologies) allows the device to be configured into load (resistance) control, while current and voltage are measured. The electrode and wiring configuration for this type of test is shown within Figure 3.7(b), [152]. Theoretically, this system offers external load control with a fully configurable resistor range. However, two issues are apparent: (1) the current limitations of the device limit the available low end resistor, and (2) the current range must be adjusted manually to allow testing in specific resistance ranges resulting in the need for multiple discrete measurement software configurations to complete a single measurement. Section 3.8 describes the comparison tests conducted using the CompactStat and the Biogalvanic testing system. Software was developed to remove the need for manual reconfiguration of the IviumSoft software.

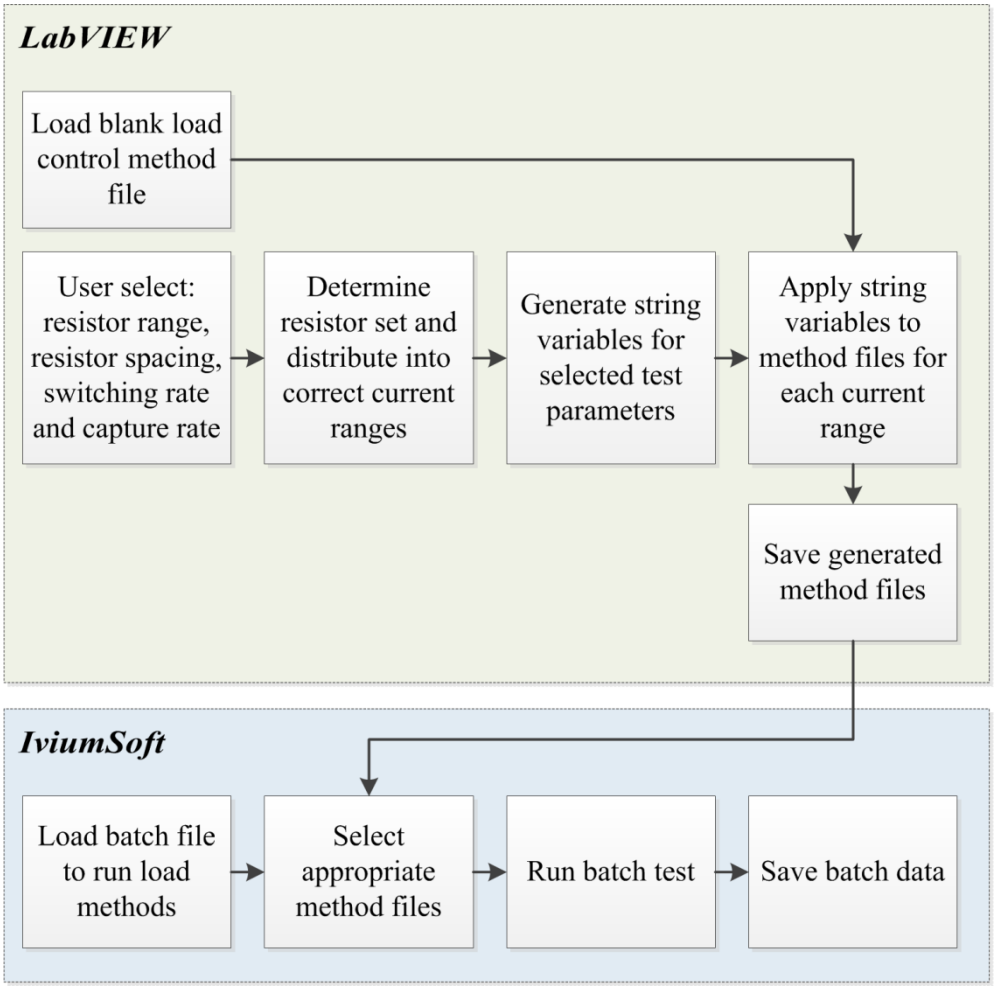

Figure 6.1: Developed software and protocol steps to allow the CompactStat to function as a biogalvanic measurement system.

Due to the power limits of the CompactStat, specific external load ranges require a specific device current range. Adjustment of this current range can only be achieved through adaptation of the testing method which cannot be performed at runtime. A solution to this was implemented through a combination of customised method files sequenced within IviumSoft Batch mode. Figure 6.1 illustrates the process developed to allow for the CompactStat to be used as a biogalvanic measurement system. Each method file could be configured to the specific external load and current range for a particular test section. Using multiple method files therefore allows the full range of external loads to be tested while not causing current saturation during measurement.

To allow for software reconfiguration of the test settings, a custom LabVIEW (National Instruments) program was written. The function of this program is illustrated in Figure 6.1. Principally, the software allows the user to select the desired testing parameters of external load range, number of loads, and switching rate. These values are then integrated into the format of an Ivium method file (.imf) to be read by the IviumSoft batch controller.

The developed system allows simple reconfiguration of the control and measurement system to test a wide range of external load configurations. However, a number of caveats to the system were identified during its testing:

Method file selection: *Batch mode transitions between method files as each is complete. Each transition requires the cell to be temporarily disconnected. This may cause signal peaks at transition points although the influence on characterisation appeared to be limited.*

Current range selection: *By default, the IviumSoft groups the external load and current ranges together. This aims to give suitable resolution for the external load testing range. However, the cell current measured is dependent on the resistance of the test cell. Therefore these default current range-external load combinations may occasionally result in current saturation. It is essential to check for current saturation during testing and to adjust these ranges in the LabVIEW software as appropriate.*

6.3 Analytic transient modelling

Biogalvanic characterisation aims to allow measurement of the passive electrical resistance of biological tissues using a biogalvanic power source, [115, 116]. The proposed simplicity of the technique make it a potential candidate for integration into surgical tools to relay real-time

information to the surgeon regarding tissue health. Investigation into the relevant electrochemistry of the galvanic cell was performed as part of Chapter 5, and has been reported by the author, [173]. The generation of tissue resistance metrics are dependent on the assumption and application of suitable electronic model. With the assumption of a constant Open Circuit Voltage(OCV), Golberg et al. [115] related the measured cell current, I for a specific external load, R_{EXT} to the internal resistance of the galvanic cell, R_{INT} using equation (6.1). The author, [156] proposed fitting the vector of voltages, $\boldsymbol{V}$ measured across the corresponding external resistances, $\boldsymbol{R_{EXT}}$ to an electrical model of the cell in accordance with equation (6.2). Fitting in this way was developed as a means of improving the accuracy and precision of the determined internal resistance and to avoid the assumption of a fixed OCV. However, results still showed significant hysteresis in the characterised internal resistance between increasing and decreasing external load switching directions [156]. In addition, the influence of switching rate on the characterised resistance of the tissue was demonstrated in Chapter 4. This adds uncertainty to a measurement and makes relation of data collected at different rates inaccurate.

$$\frac{1}{I} = \frac{R_{EXT}}{OCV} + \frac{R_{INT}}{OCV} \tag{6.1}$$

$$\boldsymbol{V} = \frac{OCV}{(\boldsymbol{R_{EXT}} + R_{INT})}\boldsymbol{R_{EXT}} \tag{6.2}$$

The load direction hysteresis and switching rate dependence shown are primarily due to transient behaviour noted between external load switching points [173]. Two possible sources of this phenomenon are: (1) the diffusion of ions at the electrode-tissue interface, and (2) electrical losses caused by resistive and capacitive nature of the electrode-tissue interface. A potential solution to this is to reduce the switching rate to such a level that any time-dependent decay has occurred. However, this is impractical for two reasons: (1) over extended periods the potential of the galvanic electrodes and the tissue resistance are likely to drift, leading to errors in the characterisation; and (2) the required settling time is such that measurement time may become impractical within a surgical setting.

Under certain conditions the current within electrochemical (galvanic) systems can be controlled by the rate of reaction at either the cathode or anode [83]. This may be determined by the rate of charge transfer or the mass transport of active species to/from the reaction interface. For a mass-transport limited system the diffusion of active species can lead to significant time varying currents within measured data [83]. Alternatively, transient currents may be associated with the electrical properties of the electrode interface. Specifically, the electrical resistance

associated with charge transfer and the capacitive properties of the Electrical Double Layer (EDL) may act in combination to produce transients with specific time constants [83]. Measurement and characterisation of these properties is a goal of techniques such as Electrochemical Impedance Spectroscopy (EIS) [174], and transient based DC techniques [175].

Section 6.3.1 reports on adaptation of the biogalvanic characterisation model of equation (5.4) to account for transient behaviour associated with electrical losses at the tissue-electrode interface. A subsequent study was performed to compare the influence of external load switching rate on the determined internal resistance of *ex vivo* porcine colon tissue using the two characterisation methods. Application of the transient model was also extended to measurements taken from *ex vivo* healthy and cancerous human rectal tissue. The efficacy of the technique is discussed in the context of application within surgical sensing.

6.3.1 Time-dependent model

The established fitting method [156] utilises a single resistance in series with the galvanic power source and external load, expressed in equation (6.2). Inclusion of time-dependent electrode interference can be achieved through a more comprehensive model, where aspects of the electrode impedance are included. Figure 6.2 shows the developed model, where potential losses across the electrode (V_{dl}) are accounted for through a parallel resistance (R_{CT}) and capacitance (C_{DL}) associated with the charge transfer resistance and EDL capacitance respectively.

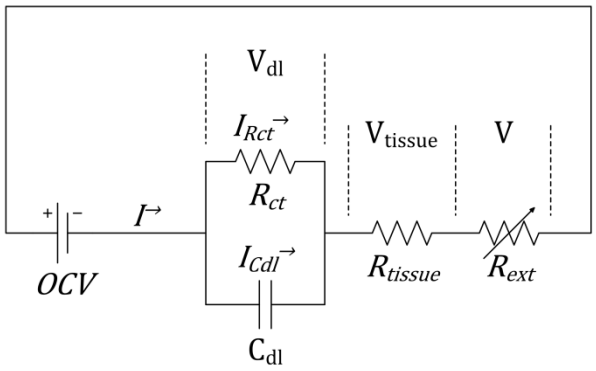

Figure 6.2: Electronic equivalent model of the biogalvanic cell including time-dependent electrode interface parameters.

The cell can be considered as discrete voltage losses across the EDL (V_{dl}), tissue resistance (V_{tissue}) and external resistance (V) in accordance with equation (6.3). The voltage drop across the EDL forms the most complex aspect of the model, with the response given by equation (6.4), with the time-constant (τ) being the product of the charge transfer resistance and EDL capacitance. The steady-state current for a particular external load R_{ext}^{i}can be calculated using equation (6.5). The current step for subsequent loads (ΔI) is therefore determined as the

difference in steady-state currents for sequential external loads. Equation (6.6) gives the voltage response across a specific external resistance. Individual voltage responses for a set of external loads can be summed to give the full voltage-time response. A Levenburg-Marquardt algorithm [155] was implemented in software (LabVIEW, National Instruments) to optimise $OCV, R_{ct}, C_{dl},$ and R_{tissue} parameters to the measured voltage-time data based on known external load values and switching rate.

$$OCV = V_{dl} + V_{tissue} + V \tag{6.3}$$

$$V_{dl} = IR_{ct}\left(1 - e^{\frac{-t}{\tau}}\right) \tag{6.4}$$

$$I^i = \frac{OCV}{(R_{ct} + R_{tissue} + R^i_{ext})} \tag{6.5}$$

$$V^i_{(t)} = OCV - \Delta IR_{ct}\left(1 - e^{\frac{-t}{\tau}}\right) + \Delta IR_{tissue} \tag{6.6}$$

6.3.2 Methods

Measurements were conducted on a single piece of *ex vivo* porcine tissue from the mid-colonic spiral and tested under laboratory conditions (20˚C) within 4 h of slaughter. The animal used was bred and sacrificed in accordance with UK Home Office regulations (Animals (Scientific Procedures) Act 1986). Test electrodes (12 mm diameter Zn & Cu) were set in non-conducting resin, wet ground (1200 grit) and clamped in axial alignment (separation 5.2 mm) under minimal strain onto the colon tissue, as illustrated in Figure 6.3. The CompactStat (Ivium Technologies) was configured using the methodology detailed within Section 6.2 to control the external load on the cell across 10 logarithmically spaced resistance values ranging from 1 MΩ - 336 Ω. The rate of external load switching was varied from 1 – 0.02 Hz in a random test order (determined using a computer generated simple randomisation) to decouple the influence of tissue degradation from any rate dependence. The voltage-time response for each rate was recorded at 100 Hz. Each voltage response was characterised using the models of equation (6.2) and (6.6) and the representative tissue resistance values of R_{INT} and R_{tissue} determined respectively.

Freshly excised human colon tissue was obtained in accordance with NHS and Leeds University Teaching Hospital Trust ethics procedures. The tissue specimen was removed as part of a right hemicolectomy, with subsequent histopathology being performed after testing. Five repeats were taken within a healthy tissue region and five from the location of the tumour (identified by the surgeon). The electrode configuration was arranged as shown in Figure 6.3.

Testing was performed using the same external resistor range as with porcine testing, with switching rate fixed at 0.1 Hz. The time-dependent response from each test was analysed using the developed transient model and compared to characterisation using a single fixed internal resistance (equation (6.2)). For each model an independent samples t-test was conducted to compare the resistance of healthy and cancerous tissue.

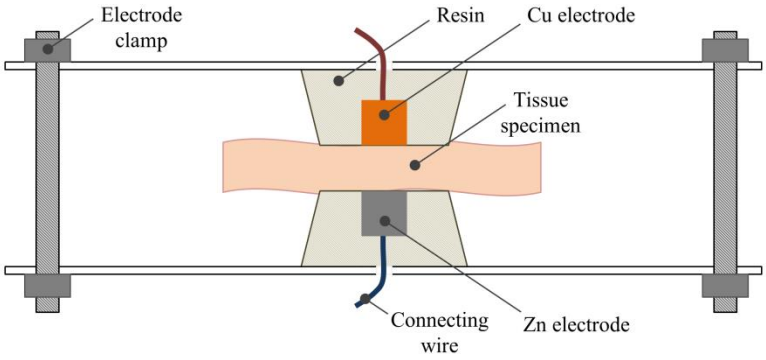

Figure 6.3: Testing configuration for axially aligned biogalvanic characterisation cell.

6.3.3 Results

Figure 6.4 shows the voltage measured across the external load as a function of time for the different switching rates employed. It is evident from the data that there is significant time dependence within each rate test. Voltage profiles between external load switching show an approximate exponential decay in most cases. External load switching rate therefore shows significant impact on the voltage measured prior to transition, as used in the characterisation model of [156]. It is evident that for longer duration tests that there is more deviation from the pure exponential decay under certain load conditions.

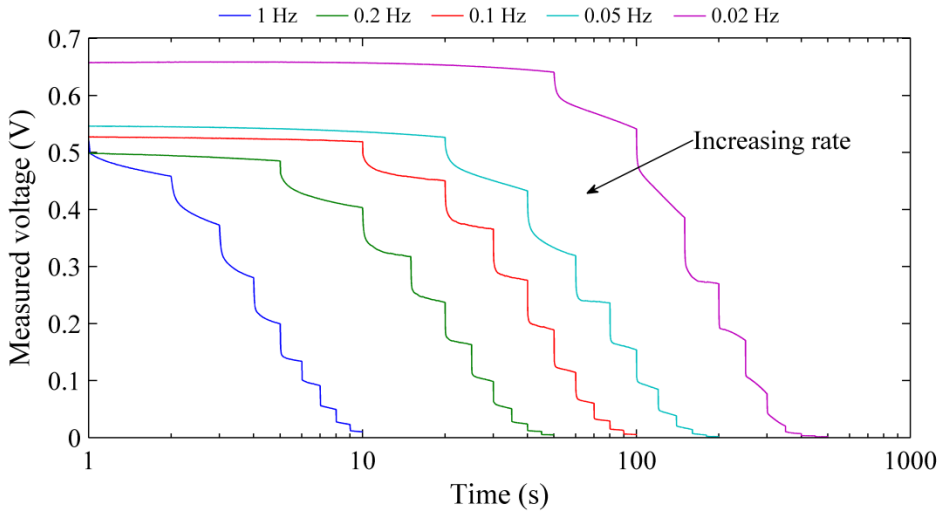

Figure 6.4: Voltage profiles from biogalvanic characterisation of porcine ex-vivo tissue for a range of external load switching rates.

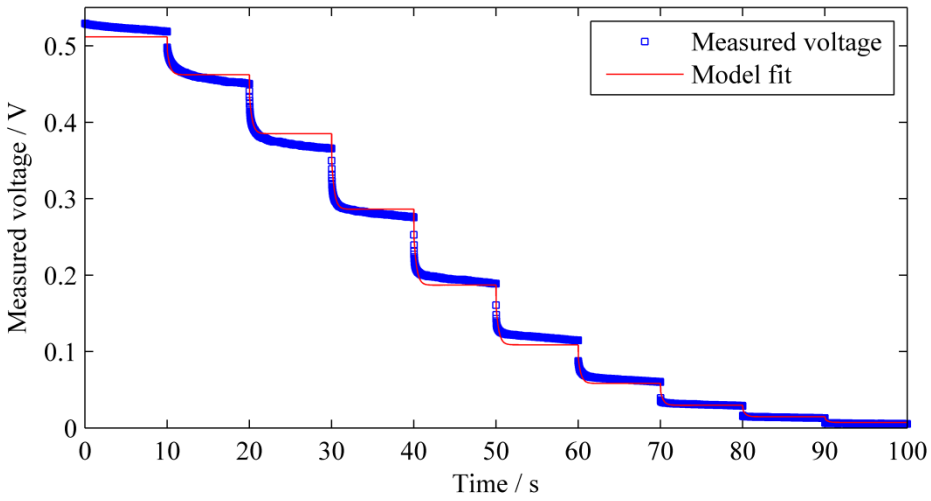

Figure 6.5: Example of model fitting result for 0.1 Hz external resistor switching rate, where the parameters of OCV, R_{ct}, C_{dl}, and R_{tissue} have been optimised to match to the measured data using equation (6.6).

Application of the transient model fitting method to the measured data allowed characterisation of the different rates tested in terms of the four fitting parameters. An example of the fitting result is shown for the median rate (0.1 Hz) in Figure 6.5. The quality of the fit is not completely consistent across the full load range of the test possibly suggesting parameter variation with cell potential. In this case, the model fit parameters may be considered as an average over the data range. Of the fit parameters, the tissue resistance has been used for direct comparison to the internal resistance of equation (6.2). Figure 6.6(a) shows the characterised resistance values for the two methods as a function of external load switching rate. Variability with rate is clear in both cases but is significantly reduced through the implementation of the transient model. This is demonstrated further by the reduction in standard deviation of the mean also presented. Resistance values obtained using the transient model are lower as the EDL resistance is decoupled and removed from the total cell resistance.

Histological analysis of the human tissue specimen reported a well differentiated caecal adenocarcinoma. Figure 6.6(b) shows repeat characterisations of this region along with a corresponding healthy tissue region using a single internal resistance model as presented in equation (6.2). On average, the characterised resistance using equation (6.2) was lower for healthy tissue (M = 62.7, SD = 12.8 kΩ), than for cancerous tissue (M = 67.2, SD = 5.2 kΩ). This difference, -4.5 kΩ, BCa 95% CI [-15.5, 8.6], was not significant $t(8)$ = -0.73, p = 0.475; this represented a small-sized effect, d = 0.35. With the single fixed resistance model approach (equation (6.2)), the overlapping responses and their high variability makes discrimination of tissue health impossible for the sample tested. In contrast, application of the transient model to the voltage-time data (Figure 6.6(c)) shows lower tissue resistance values with reduced

variability for the respective tissue condition. The average characterised resistance using this model showed a higher resistance for healthy tissue (M = 4.5, SD = 0.5 kΩ), than for cancerous tissue (M = 0.95, SD = 0.16 kΩ). This difference, 3.56 kΩ, was highly statistically significant $t(8) = 15.2$, $p < .001$; this represented a large-sized effect, d = 7.1. This indicates that, for the single sample tested, only the proposed model is capable of statistically differentiating between healthy and cancerous tissue.

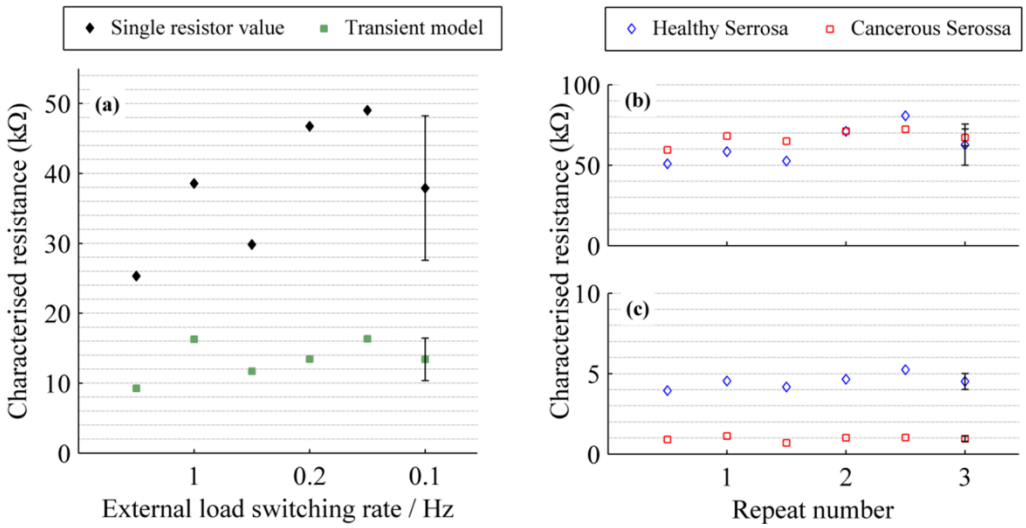

Figure 6.6: (a) Resistance characterisation results using a single fixed internal resistance model (equation 2) and the proposed transient model of equation (6) for ex vivo porcine colon as a function of external resistor switching rate. Biogalvanic characterisation repeat results for healthy and cancerous rectal tissue using (b) the single internal resistance model, and (c) the proposed time-dependent model. The mean ±1SD is also shown.

6.3.4 Discussion

The external load switching rate has a significant impact on the measured voltage-time response. Due to the complex nature of the electrochemical system this influence is not exclusively due to resistive and capacitive phenomena at the electrode interface but also due to current fluctuations as diffusion of ion species impacts on galvanic reaction rates. Diffusion related drift in the voltage response appears more clearly over larger time-scale tests, particularly prior to load switching stages in the 0.02 Hz test shown in Figure 6.4. This inevitably reduces the accuracy of the proposed model fitting method although it is evident from Figure 6.5 and Figure 6.6 that fitting to the model of equation (6.6) gives a good approximation to the system and yields meaningful data in terms of tissue resistance and electrode-tissue interface parameters. In particular, Figure 6.6(a) shows the results from resistance characterisation using implementation of equation (6.2) and the proposed transient model of equation (6.6). Significant dependence on the switching rate is shown for the former leading to a larger error in the mean resistance across all test conditions. Implementation of the transient

model reduces this variability, through removal of the electrode parameters from the system. A lower average tissue resistance is produced with much less variability with switching rate. For application in surgery the measurement system should allow optimisation through control of the external load switching rate. With the proposed model of equation (6.6), it is feasible that the switching rate be increased to allow faster characterisation, without causing large errors associated with electrode phenomena in the output metrics. Additionally, this use of the time-dependent model would allow comparison between resistance values characterised using different external load switching rates.

The characterised internal resistance values in Figure 6.6(b) show poor specificity for healthy and cancerous tissue. This may be as a direct result of the relatively large and variable influence of the electrode resistance. However, application of the time-dependent model fit allows some separation of these electrode properties from the tissue resistance of interest. Figure 6.6(c) shows how the application of the proposed model gives much less variability and generates a clear distinction between the healthy and cancerous tissue tested. The values of tissue resistance are much lower than those predicted using a single fixed internal resistance. Statistical analysis (independent samples t-test) indicates no significance ($p > .05$) when the model of equation (6.2) is implemented, while a significant difference ($p < .05$) is present upon application of the proposed model, equation (6.6). This result supports the use of the proposed model for biogalvanic determination of a tissue resistance. However, further repeated measures are required for assessment of the clinical efficacy of the technique.

It was evident from previous work, [156] that the biogalvanic technique is practically suitable for integration into surgical tools for transmural tissue assessment. However, the sensitivity of technique to external loading rate and direction posed limitations to its application. The presented model adaptations offer a simple means of reducing the influence of these factors and move the technique a step closer to being suitable for surgical integration.

Improvement to the proposed model could be achieved by allowing variation of the fitting parameters over the range of external loads tested. In addition, diffusion processes may be accounted for through inclusion of more complex electrical elements within the model. These adaptations may prove to increase the accuracy of the technique. However, the added complexity and a move from representative parameters would make interpretation significantly more challenging. A secondary approach could look to exploit the electrode-tissue interface, where modification of the electrode surface may produce additional tissue information. This could be extracted when separated from tissue resistance using the proposed model. In effect, this could lead to a bi-modal device without increasing the complexity of the characterisation.

6.3.5 Conclusion

Assessment of the voltage-time response during biogalvanic tissue characterisation shows parameter dependency, particularly in the case of external load switching rate. This variability propagates through to the characterised tissue resistance and is due to the properties of electrode-tissue interface. This work demonstrates this phenomenon and proposes the use of a more comprehensive time-dependent model to account for and separate electrode-tissue-interface and bulk tissue parameters. Model development and fitting processes have been described and tests have shown reduced variation in characterised tissue resistance with external load switching rate. The proposed model has been demonstrated as a potential means of improving the repeatability of biogalvanic tissue resistance characterisation through isolation of a tissue specific parameter. This may allow for differences between healthy and cancerous colon tissue resistance to be statistically separated, as shown in the single case evaluated. Based on the findings presented, the adjusted biogalvanic characterisation model may allow faster measurements to be taken without influence on the determined tissue resistance. This may allow for biogalvanic tissue sensing to be practically implemented within surgical applications.

6.4 Numeric biogalvanic modelling

As previously discussed, the biogalvanic technique including the existing model of equation (3.4) is overly simplistic, and does not account for the influence of the cell electrodes on the measured voltages. Section 6.3 has presented one approach to improving the quality of the model based on the time-dependent nature of the electrode-tissue interface. The work presented within this section offers a more comprehensive model of the galvanic system during characterisation, focusing on the steady-state electrode polarisation and the geometric influence. The presented spatially-extended finite element model has been used to examining how the operating conditions of the system are reflected in the characterisation process. In addition, the model has been used to improve analysis, allowing for more accurate characterisation under the conditions expected with tissue measurements. The model development and presented study were conducted in collaboration with the School of Computing (University of Leeds). The numerical model and solver were developed in the School of computing (University of Leeds). The Author contributions were in the development of the system model, supply of experimental data, model validation and analysis.

6.4.1 Numerical modelling overview

The existing method for biogalvanic characterisation determines tissue resistance R_{INT} through application and fitting of the model expressed in equation (6.2) to the measured voltages $\boldsymbol{V}$ and

corresponding external loads $\boldsymbol{R_{EXT}}$ [156]. This model assumes that the losses in potential are attributed only to the internal tissue resistance (itself assumed proportional to the volume strictly between the electrodes) and the external load. Additional considerations are required for integration of the resistive properties of the cell electrodes, and for lateral currents through the tissue.

Previously published results using the biogalvanic characterisation method [156, 176] have used cell electrodes in axial alignment. This condition is most pertinent to a laparoscopic surgical grasping tool, where the electrodes would contact either side of the target tissue for assessment to be made. An axially aligned geometry was therefore used as the case study of the presented work, including numerical modelling and physical measurement. For comparison to be made between the existing resistance method and the presented numerical model, tests were initially applied to salt solution (NaCl) analogues of know conductivity. Comparisons were subsequently extended to tissue resistance values determined from biogalvanic measurements made on healthy and diseased human colon tissue.

6.4.2 Computational biogalvanic model

The galvanic cell was modelled as a closed circuit consisting of the tissue, two electrodes in axial alignment, and a variable external resistance, all placed in series. Voltage-current relations for each component were derived independently (see below), and solved numerically using Brent's method [177], under the constraints of a constant current I, and total voltage drop equal to the open current voltage (OCV).

6.4.2.1 Geometric-dependent tissue resistance

The tissue was treated as a homogeneous conducting medium located between two opposing circular electrodes as shown in Figure 6.7, where the local current density $\boldsymbol{i}(\boldsymbol{x})$ is related to gradients in the electric potential $\phi(\boldsymbol{x})$ *via* $\boldsymbol{i} = -\sigma\boldsymbol{\nabla}\phi$ with σ a uniform conductivity [178, 179]. Steady state is assumed, and the lack of net electrical charge in the tissue means $\boldsymbol{\nabla}\cdot\boldsymbol{i} = 0$ and the Laplace equation $\nabla^2\phi = 0$ is recovered. This is discretized using a linear Galerkin finite element scheme on an adaptive triangular mesh with increased resolution near each electrode surface. This is solved iteratively using GMRES [180] within a Newton solve, necessary to accommodate the nonlinear Dirichlet boundary conditions, under the assumption of a cylindrically symmetric solution. A voltage difference V was applied across the electrodes and the net current I measured, giving a linear, geometry-dependent V-I relation for the medium. The lateral spatial extent R was increased until it had negligible effect (<2%) on the results. Results were validated by fit-free agreement with theoretical predictions for $L \ll r$ and $L \gg r$ (see Supplementary Information Appendix B).

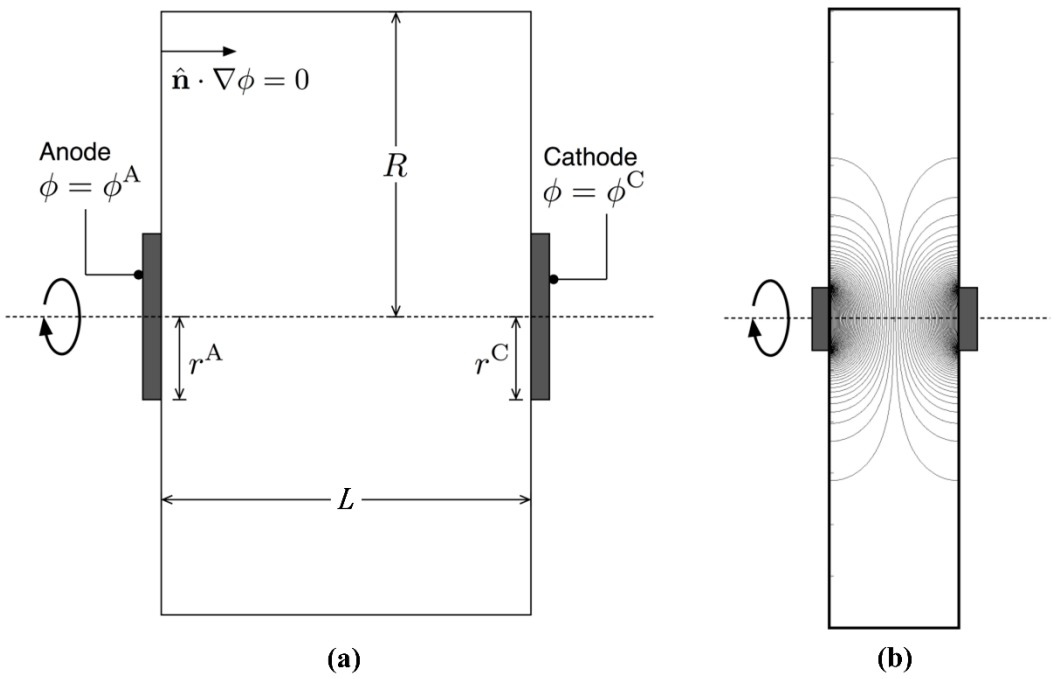

Figure 6.7: (a) Schematic of the model geometry for the medium (tissue) conductivity. The medium residues between the two electrodes held at fixed electric potentials, and there is zero current through all other boundaries. Cylindrical symmetry about the axes shown is assumed, so each electrode presents a circular surface. (b) Example of simulation output for a typical geometry (R = 60 mm, L = 25 mm and r = 6 mm). Contour lines correspond to 1% changes in ϕ. Only one half-plane was actually solved for, the full solution was recovered by rotation about the axis.

6.4.2.2 Electrode and external resistance

Each electrode was modelled by the non-linear Tafel equation (6.7) for the overpotential ΔV due to electrode resistance [181], where the superscripts A, C refer to anode and cathode parameters, respectively. The net current I through each electrode was found by multiplying each $i^{A,C}$ by the corresponding electrode's surface area. The external resistance was modelled as ohmic with known R_{EXT}.

$$i^{A,C} = i_0^{A,C}\left(e^{\Delta V/\alpha^{A,C}} - e^{-\Delta V/\beta^{A,C}}\right) \tag{6.7}$$

6.4.2.3 Fitting procedure

The exchange current densities i_0 and Tafel voltages α, β for each electrode, along with the open circuit voltage (OCV) and the medium conductivity σ, derive from the underlying electrochemistry [181], but since this is unknown they are treated as fit parameters. The tissue geometry parameters r^A, r^C, R and Z were treated as known and fixed. Fitting model predictions to data was performed by the Levenberg-Marquardt least-squares algorithm [177].

6.4.3 NaCl testing

Testing within aqueous sodium chloride (NaCl) was conducted to allow validation of the proposed model. Volumetric combination of analytical grade NaCl (Fisher Scientific) and distilled water was performed to give solutions of 1.71, 17.1 and 154 mM (0.01, 0.1 and 0.9 wt% respectively) NaCl. Cylindrical zinc and copper specimens of 12 mm diameter were fixed in non-conductive resin to leave only the circular end face of the metal exposed. Prior to testing, each sample was wet ground to 1200 grit and cleaned using distilled water.

6.4.4 Polarisation scans

Tests were initially performed to determine suitable ranges of Tafel parameters for application in the modelled system. Polarisation scans were performed using each electrode individually as the working electrode within a typical three-electrode cell. A combination Pt counter and Ag/AgCl reference electrode (Thermo Scientific) was used to complete the cell. All electrodes were submerged in a temperature controlled salt solution for 30 min at open circuit prior to polarisation. Polarisation scans were performed for the established Open Circuit Potential (OCP) to 300 mV in the anodic (increasing) direction for zinc electrode and the cathodic (decreasing) direction for copper. Five scans were performed for each metal using a scanning rate of 0.5 mV/s.

6.4.5 Biogalvanic characterisation

Biogalvanic characterisation measurements were performed using a zinc and copper galvanic cell connected within 1.71, 17.1 and 154 mM NaCl solutions. Solutions were stirred and maintained at 25+/-1 °C using a temperature-controlled magnetic stirring hotplate (MR Hei-Standard, Heidolph). Zinc and copper test electrodes were arranged axially within salt solution of appropriate concentration. Electrode spacing was adjusted to achieve a face separation of 25 mm, matching the configuration of the model system in Figure 6.7. The external load on the cell was controlled through the use of a commercial potentiostat (CompactStat, Ivium Technologies). The external load was controlled in a reducing manner across 20 evenly log-spaced discrete loads ranging from 1 MΩ – 10 Ω. A switching rate of 0.1 Hz was employed for all tests, matching the configuration used within previous studies within NaCl [176].

6.4.6 Tissue tests

Biogalvanic characterisation of human colon tissue containing a cancerous tumour (adenocarcinoma) was performed. Freshly excised (right hemicolectomy) human colon tissue was obtained in accordance with NHS and Leeds University Teaching Hospital ethics procedures. Five repeat biogalvanic characterisation measurements were performed at the

location of the tumour and within a healthy region (identified by the surgeon). Biogalvanic characterisations were performed using a commercial potentiostat (CompactStat, Ivium Technologies), with external loads controlled in a decreasing manner. External loads ranged from 110 kΩ – 4 Ω and were switched at a rate of 0.1 Hz for all tests.

6.4.7 Results

Salt solution and tissue testing data along with associated model fits using the described numerical model have been presented in the following sections

6.4.7.1 Model parameter space

The biogalvanic system was initially simulated to allow for investigation over a wide range of parameters. For clarity, symmetric systems were considered, where the anode and cathode have the same radii and electrochemical parameters, and both Tafel voltages α and β are equal. Dimensional analysis reduces parameter space to just two dimensionless variables, permitting systematic variation and easy visualisation of results. These two variables were denoted a and b, defined as equation (6.8) and (6.9) respectively, and express all voltages and currents in units of α and $\pi r^2 i_0$ respectively. Since the voltage drops across the electrodes and the medium are modelled separately, it is straightforward to calculate the fraction of the total voltage drop that is due to the medium alone. For large currents the medium always dominates, as the voltage drops across the electrodes are exponentially suppressed according to the Tafel expression, but for small currents both medium and electrode-dominated regimes occur as plotted in Figure 6.8. Fitting to an Ohmic internal resistance only works for the medium-dominated regime (Figure 6.8C & D); for large b, the exponential variation of the Tafel equation dominates and the fit becomes measurably poorer (Figure 6.8A & B).

$$a = \frac{Z}{r} \tag{6.8}$$

$$b = \frac{\sigma\alpha}{r i_0} \tag{6.9}$$

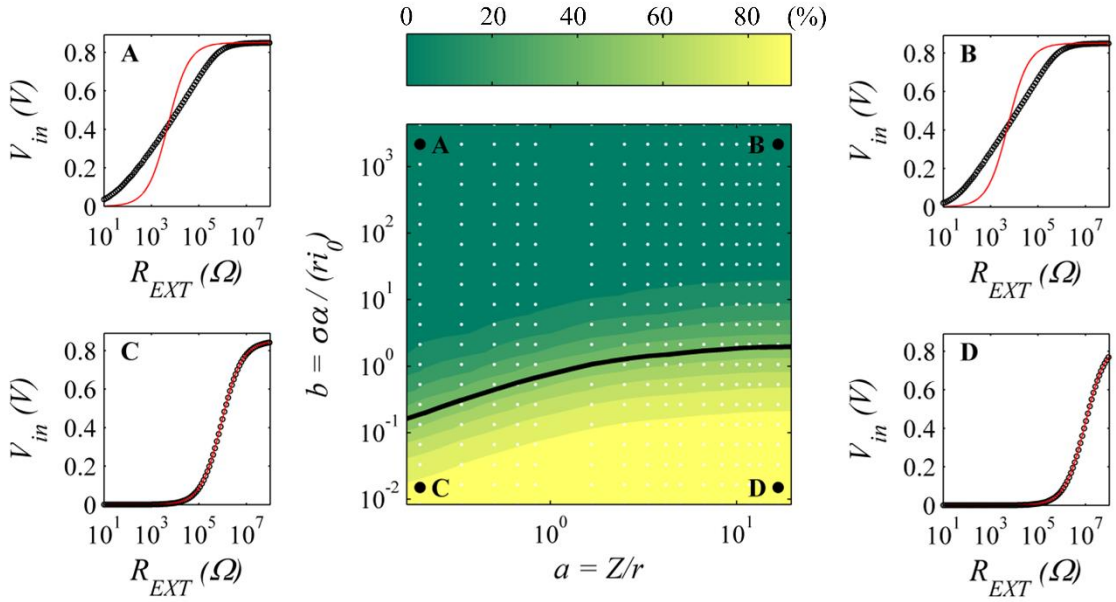

Figure 6.8: Contour plot of the fraction (%) of voltage drop across the test medium for small voltages, verses a and b. White points indicate actual data points, and the solid line shows the 50% value. Positions A-D show the numerical model output and the corresponding fit using the existing biogalvanic characterisation model for extreme locations within the parameter space.

6.4.7.2 NaCl

Table 6.1 contains the full range of Tafel parameters measured in this study for the anodic and cathodic polarisation of zinc and copper respectively under varied salt solution concentration. Significant increases in parameter values can be seen for potential gradient and exchange current density for Cu as [NaCl] is increased. For the Zn electrode, the exchange current density also increases with [NaCl], while the potential gradient was found to reduce. The parameter ranges presented were used to inform fitting of the numerical model. Biogalvanic repeat measurements for salt solutions are shown in Figure 6.9. A comparison of model fitting methods shows improved conformation to the measured data through application of the numeric model. The median fitting error along with the upper and lower range limits has also been presented for the two fitting methods across the range of external loads and [NaCl]. For all concentrations, the numerical model shows reduced fitting error indicating improved agreement with the measured data. The average absolute fitting error across the range of external loads tested for the median fits of 1.71, 17.1 and 154 mM [NaCl] was 0.0036, 0.0096 and 0.024 V respectively for the numerical model, while the existing characterisation method produced respective average fitting errors of 0.024, 0.035 and 0.033 V for the same concentrations.

The fitting parameters for the numerical model have been included in Table 6.2. A comparison of the conductivity fitting predicted across concentrations for the two methods is presented in Table 6.3 (graphically presented in Figure 6.10). Comparison of the model predictions with theory shows a dependence on the solution concentration (conductivity). For

the low concentration of 1.71 mM [NaCl], the prediction of the conductivity is close to the theoretical value for both systems. Fitting using the simplistic model does show improved accuracy as the system is bulk dominated and so electrode influence is minimised. For the middle concentration of 17.1 mM [NaCl] the fit conductivity using the existing method is much lower than theory, indicating an influence of the electrode resistance. The proposed method however, makes a more accurate prediction through separation of bulk and electrode parameters. Under high conductivity conditions of 154 mM [NaCl], the traditional fitting method becomes saturated, only giving prediction of electrode resistance. The proposed model also suffers under these conditions, as the electrode resistance is dominant making the fitting process insensitive to large variations in the value of the bulk conductivity.

Table 6.1: Full range of measured Tafel parameters for zinc (anodic) and copper (cathodic) electrodes within varied [NaCl] (mM) (n=5).

	0.01		0.1		0.9	
	α (mV)	i_0 (mA/m^2)	α (mV)	i_0 (mA/m^2)	α (mV)	i_0 (mA/m^2)
Cu	48	0.5 - 2	100	2.5 - 4	82	4 – 8
Zn	44	3 - 5	32	4 - 16	19	25 - 40

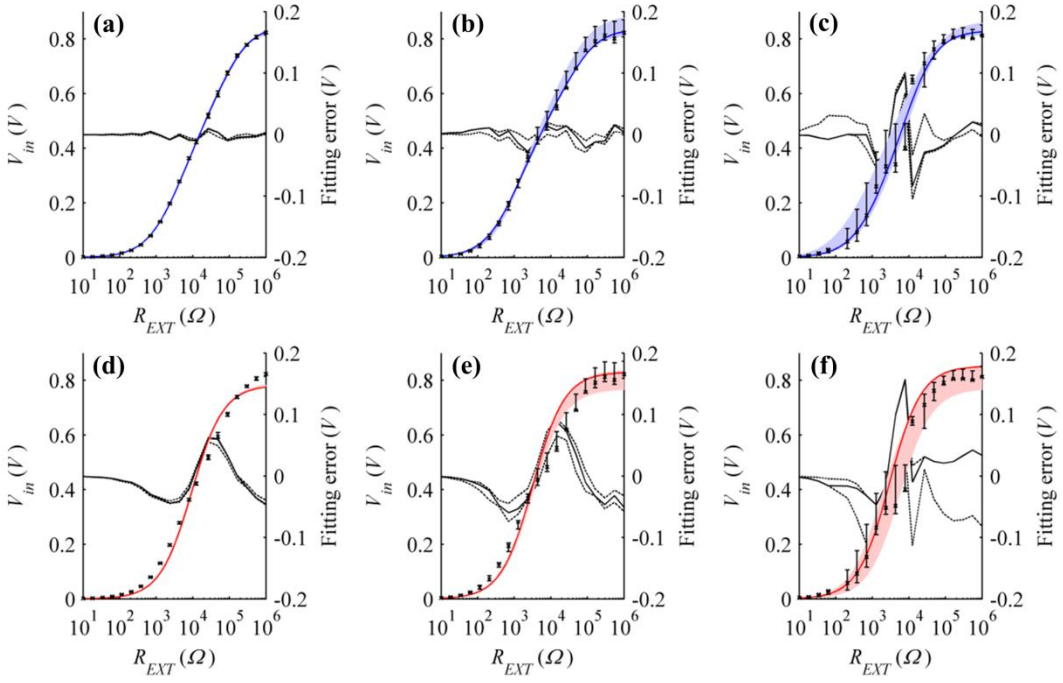

Figure 6.9: Median characterisation and range (shaded) of biogalvanic data measured in NaCl (n=5) using the numerical model for (a) 1.71 mM, (b) 17.1 mM, and (c) 154 mM, and using the existing biogalvanic fit for (d) 1.71 mM, (e) 17.1 mM, and (f) 154 mM; average fitting error (solid) and upper and lower fitting error ranges also shown (dashed).

Table 6.2: Numerical model fit parameters for repeat tests within varied [NaCl], showing variability as a function of concentration.

	σ (S/m)			α (mV)			i_0 (mA/m2)			OCV (V)		
[NaCl] (mM)	Mean	SE	% SE	Mean	SE	% SE	Mean	SE	% SE	Mean	SE	% SE
1.71	0.045	0.001	3.1	75	2	2.6	27	2	7.7	0.846	0.003	0.35
17.1	0.140	0.040	28.6	60	4	6.8	49	7	14.4	0.859	0.014	1.64
154	-	-	-	137	14	10.5	199	10	5.3	0.841	0.01	0.98

Table 6.3: Fit parameters for conductivity (S/m) of varied [NaCl] using the current and proposed biogalvanic characterisation techniques; theoretical conductivities also given.

	Existing model			Numerical model			Theoretical
[NaCl] (mM)	Mean	SE	% SE	Mean	SE	% SE	-
1.71	0.023	0.0008	3.5	0.045	0.0014	3.1	0.022
17.1	0.0668	0.0040	6.0	0.14	0.04	28	0.22
154	0.0703	0.0381	54.2	-	-	-	1.9

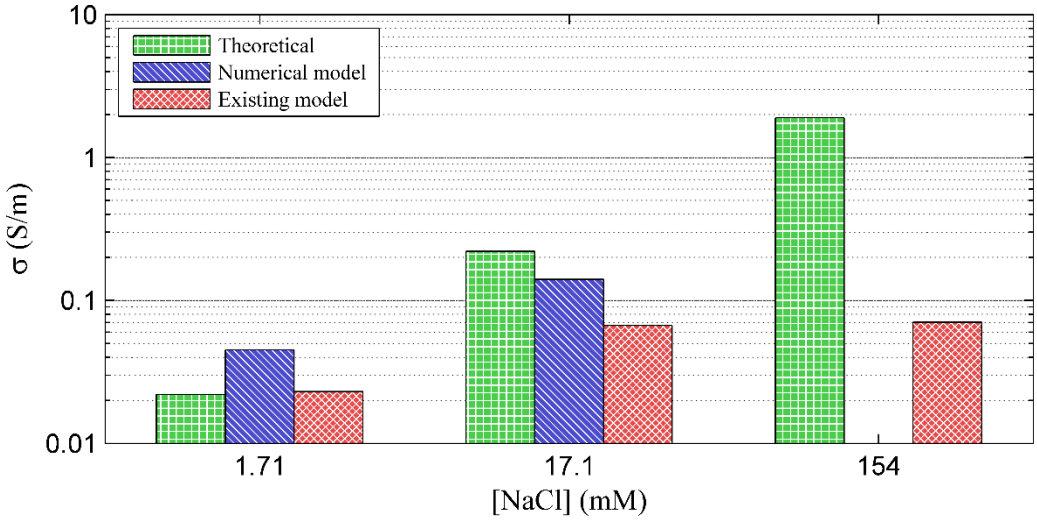

Figure 6.10: Comparison of theoretical conductivity for varied [NaCl] to the average determined conductivity using the numerical and existing characterisation models.

6.4.7.3 Human colon characterisation

Biogalvanic measurements on human colon show typical trends across the external resistor range. Figure 6.11(a) & (b) indicates the measured data and illustrates the fitting solutions achieved for each repeat using the numerical model. For comparison, a bulk dominant fit to the median repeat measured data for healthy and cancerous colon tissue using the existing model has been presented in Figure 6.11(c) and (d) respectively. This model shows poor fitting to the measured data points. The fitting parameters achieved using the numerical model are presented

in Table 6.4. Due to the dominance of the electrodes under these test conditions, a suitable conductivity value was not achieved. Statistical assessment (Student's t-test) of the two Tafel parameters (α and i_0) extracted independently showed no significant difference ($p > .05$) between healthy and cancerous tissue.

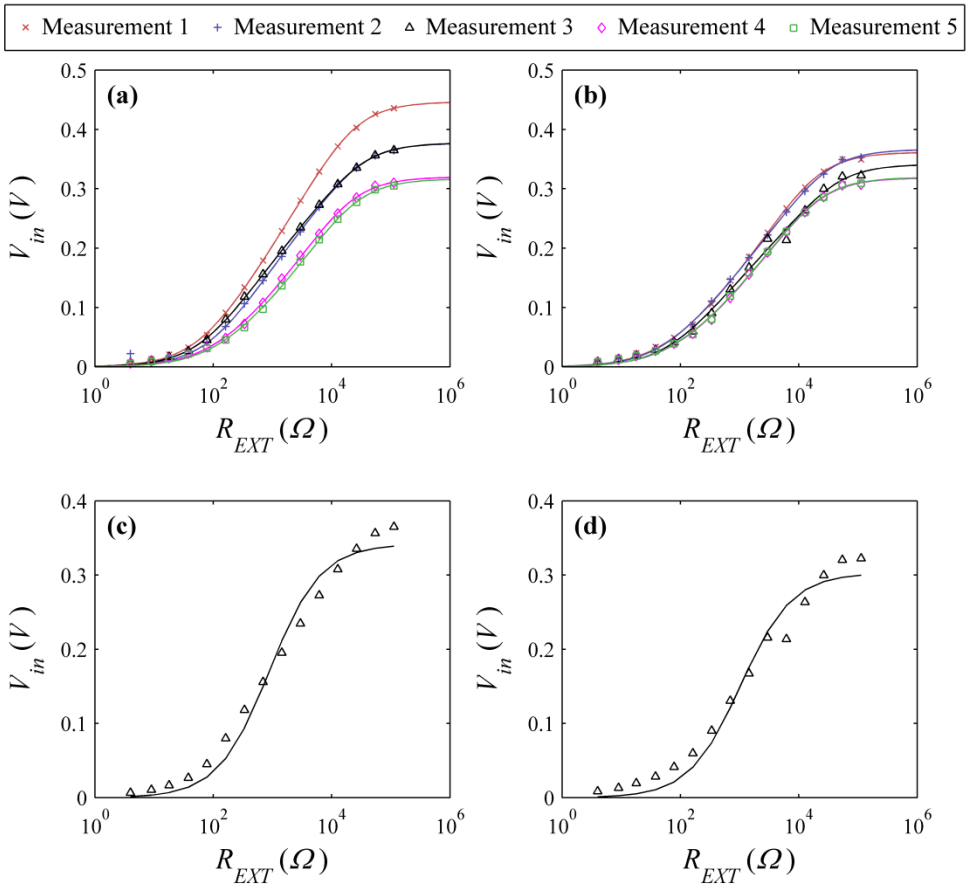

Figure 6.11: Repeat biogalvanic characterisation data from *ex vivo* human colon on (a) healthy region, and (b) cancerous region. Proposed model fits for each repeat are shown. Typical fits using the existing (bulk-dominant) model are also shown for the median healthy and cancerous biogalvanic measurements within (c) and (d) respectively.

Table 6.4: Numerical model fitting metrics for biogalvanic measurements conducted on healthy and cancerous colon tissue (n=5).

	σ (S/m)			α (mV)			i_0 (mA/m2)			OCV (V)		
Tissue type	Mean	SE	%	Mean	SE	%	Mean	SE	%	Mean	SE	%
Healthy	-	-	-	45.5	5.1	11.2	140	35.1	25.1	0.37	0.02	6.3
Cancerous	-	-	-	40.1	1.7	4.2	111	24.0	21.6	0.34	0.01	2.9

6.4.8 Parameter space comparison

The fitting results from the numerical model based characterisation of NaCl tests were used to define the parameter space positions for the varied concentrations. These estimated positions have been presented in Figure 6.12. The lowest concentration tested is shown to be at the limit of the bulk dominated regime, and higher concentrations extending well into electrode dominated systems. As the numerical fitting to colon tissue data presented no reasonable conductivity value, representative values from published BIS tests were used for parameter space position estimation. Parameter space calculations were made using conductivity values ranging from 0.15-0.6 S/m [182], which represent a wide range of soft tissue vales, and the geometry and Tafel parameters from the presented tissue tests. The range of positions for healthy and cancerous tissues have been indicated in Figure 6.12. The values clearly predict an electrode dominant regime even at the highest tissue conductivity. This is consistent with the measured data and associated fitting presented in Figure 6.11.

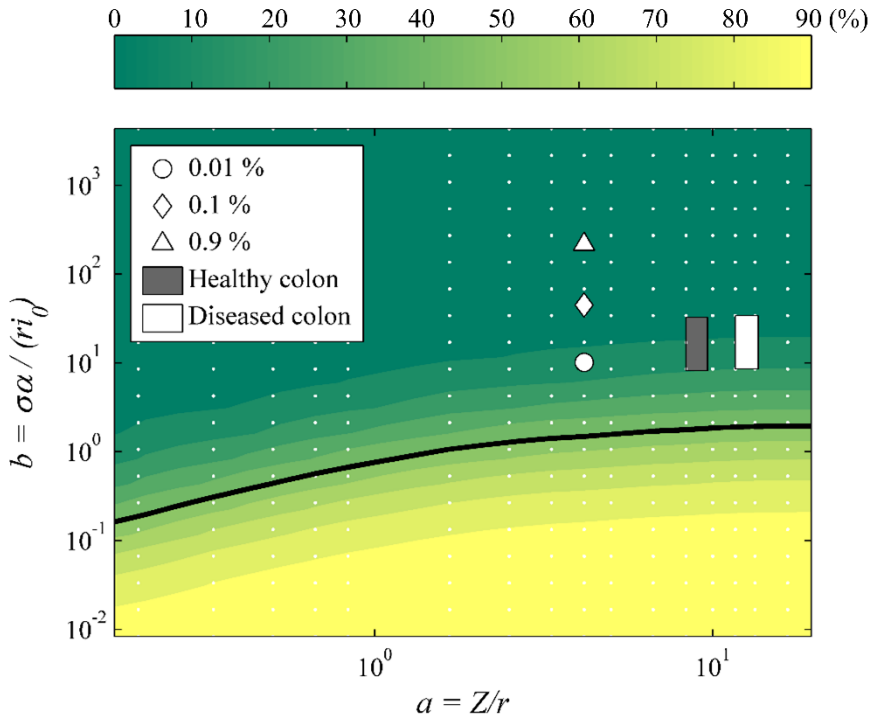

Figure 6.12: Model system parameter space including the defined positions for biogalvanic characterisation using the numerical model for varied [NaCl] and healthy and diseased colon tissues; conductivity values for colon tissues estimates from published soft tissue values [182].

6.4.9 Discussion

Fitting to biogalvanic data using the existing model offers no means of separating the electrode resistance inherent within the two electrode cell from the salt-bridge resistance of interest. The expanded numerical model reported has shown how knowledge and use of electrode properties

can allow for independent assessment of these aspects under certain operating regimes. However, the physical constraints of the practical tissue sensing system present real problems for either technique.

6.4.9.1 Numerical model

The numerical model described has allowed for a level of parameterisation of the system, making assessment of the expected system behaviour over a wide range of conditions possible. Figure 6.8 shows the linear (small-current) response for a range of geometries and electrochemical properties quantified by the two dimensionless parameters *a* and *b* (equations (6.8)& (6.9) respectively). Reliable estimation of tissue conductivity σ is only possible far from the electrode-dominated regime $b \gg 1$. Currents far in excess of $\pi r^2 i_0$ will also produce a medium-dominated response suitable for extraction of σ.

The spatially-extended finite element model for the medium resistance also allows the geometric dependence to be quantified. Two limiting cases can be readily understood. For $L \ll r$, *i.e.* closely separated electrodes, the net medium resistance obeys equation (6.10) (see Supplementary Information, Appendix B) as postulated in [115]. However, for far-separated electrodes $L \gg r$, each electrode can be represented as a point source or sink of electric current, and an alternative expression is derived as equation (6.11). The presented experiments correspond to $a = L/r \approx 4$, placing it intermediate between these two limits for which there is no analytical expression available, and numerical simulation is therefore required to determine the geometric dependence. There is no dependence on the medium geometry when the response is dominated by the electrode resistivity, as expected.

$$R_{med}^{L \ll r} = \frac{L}{\pi r^2 \sigma} \tag{6.10}$$

$$R_{med}^{L \gg r} = \frac{2}{\pi r \sigma} \tag{6.11}$$

The above suggests that application of the existing characterisation model, as presented in [115, 156], is inappropriate for the determination of resistance and also conductivity through application of the geometric relationship of equation (2.4). The efficacy of the existing method has therefore been discussed for the salt solution analogues and human colon tissue tested, and contrasted to the findings from the proposed numerical model.

6.4.9.2 NaCl testing

Through application of measured Tafel parameters over the range of test solutions it has been demonstrated that the numerical model may also be utilised to characterise measured data and, under certain regimes, extract conductivity parameters. Figure 6.10 makes a comparison of the two methods, showing that for a very low salt solution concentration either system may offer a suitable prediction of the system conductivity. The simplistic bulk dominated model in fact offers a more accurate prediction under these conditions. At moderate concentration, values of conductivity expected in soft tissues [108, 182, 183], the influence of the electrodes becomes dominant. The traditional characterisation method therefore greatly under predicts the conductivity, and is indeed saturated to this minimum resistance due to the system electrodes. This minimum resistance is carried through to the highest tested concentration, making the value misrepresentative of the solution conductivity. Utilising the numerical model allows improved prediction at the intermediate concentration, due the separation of electrode and bulk parameters. However, as the concentration is increased the solution to the model becomes insensitive to the conductivity, making its prediction inaccurate.

Figure 6.12 illustrates these systematic issues clearly, with NaCl concentrations under the geometric arrangement used being indicated within the a vs b parameter space. It is clear that increasing the concentration over two orders of magnitude shifts the system from partially electrode dominated into strongly electrode dominant. It is clear from both numerical and existing model characterisation of 154 mM [NaCl] that determination of meaningful conductivity under this position within the parameter space is not possible.

6.4.9.3 Tissue testing

Figure 6.11 (a) & (b) shows the data from a biogalvanic measurement on healthy and diseased human colon tissue with corresponding model fits using the numerical model. Figure 6.11(c) & (d) show the median datasets for each tissue condition and the associated fit using the existing model. It is clear that the numerical method allows for better conformation to the measured data. The existing model fit does not match the data points across the external resistor range, and gives a fit consistent with that of electrode dominance shown in Figure 6.8A & B.

Through combination of the average fitting parameters for α amd i_0 along with published conductivity values for soft tissues [182], a range of parameter space locations were estimated as shown in Figure 6.12. The positions indicated for healthy and cancerous tissues are both well into the electrode dominant regime. This suggests that application of the existing model to biogalvanic tissue data collected under the tested geometries may not be appropriate for estimation of a tissue specific resistance.

Consideration of the biogalvanic resistance as a cell resistance (electrodes and tissue) rather than a tissue resistance may still allow for determination of a health specific parameter. However, although the mean value for healthy colon (M = 1200, SD = 320 Ω) was higher than for cancerous colon (M = 1066, SD = 103 Ω), this difference, 133 CI [-213 480], was not significant $t(8) = 0.889$, $p = 0.416$. In addition, application of the existing model does not allow for analytic mitigation of the geometric influence on the system, and therefore conversion to conductivity or a geometrically normalised equivalent.

In contrast, the numerical model presented does allow for a geometrically independent conductivity to be determined. However, the electrode dominance within the tested tissue systems made the fitting process insensitive to this parameter. The electrode potential gradient and exchange current density also did not show specificity for tissue type.

6.4.10 System adaptation

An alternative approach to avoid altering the underlying assumption of the existing model is to modify the cell properties and move the system into the bulk dominant region. This can be achieved in three potential ways: (1) increasing the electrode surface area, (2) increasing the electrode separation, and (3) altering the electrode Tafel properties. The first two of these are more simplistic but have practical limitations when considering applications within surgery. As an example to move the b parameter toward a bulk dominated region (<2), electrodes of at least four times the radius would be required (24 mm). This geometry is practically unrealistic for the surgical setting, is assuming the lowest tissue conductivity and does not account for the associated negative influence on the a parameter. Electrode separation is not as easily evaluated for a practical case as the electrode carrying device, the tissue geometry and region of interest, and the mechanical application of the electrodes all influence the separation at point of measurement. The assessed tissue cases reported represent very large electrode separation, and it is therefore expected that measurements taken *in vivo* would in fact only be with reduced separation, thereby amplifying the electrode dominance of the system

The latter option of adjustment of Tafel parameters is not constrained by practical geometries, but by material properties. For a successfully passive system the galvanic cell should deliver a significant potential difference, therefore requiring specific half-cell reactions. For alternative materials that may offer more favourable Tafel parameters, the cell potential may be made too small for the measurement to be accurately taken. Ultimately, these parametric adjustments may reduce the influence of the electrodes on the measurement system, however the required shift may not be practically achievable within the desired application. Under the existing configuration, the findings presented suggest that the biogalvanic method is not a suitable candidate for assessment of tissue resistance.

6.5 Modelling outcomes

Two new approaches to biogalvanic system modelling have been presented and evaluated in this chapter. A common aim for both approaches was to improve the extraction of tissue specific resistance properties from measured biogalvanic test data. The outcomes from each modelling approach have been considered separately in this section.

In the first instance, the transient signatures of the voltage response were analysed. This response was assumed to be induced by the capacitive nature of the electrode-tissue interface (EDL). Transient features are common in measured biogalvanic data and the analytical model developed (equation (6.6)) offers a simplistic extension to the existing biogalvanic characterisation method. The positive outcomes from the presented work using this modelling technique are:

A time-dependent model: *A new analytic model has been developed based on a simple electronic analogue of the electrode-tissue interface and bulk tissue resistance. This model has been successfully integrated into a data fitting algorithm and applied to ex vivo porcine and human tissue data.*

Reduced load rate influence: *As part of the presented study the influence of external resistance loading was demonstrated. Through application of the time-dependent model it was found that the internal resistance variability may be reduced.*

Tissue health discrimination: *The transient model was successfully applied to measured biogalvanic characterisation from a single human colon specimen with a healthy and cancerous region. Using existing characterisation, no statistical difference was found between tissue type across five repeat. Application of the transient model produced a statistical difference between the tissue resistance metrics for the same dataset.*

Application of a numerical model of the biogalvanic system was investigated to study the influence of geometry and electrode properties on the determined resistance (conductivity). This work represents a more comprehensive system model and has been used to investigate the suitability of the biogalvanic method for tissue characterisation. The main positive outcomes from the presented work using this model are:

A numerical model: *A spatially extended finite element model was developed with inclusion of standard electrical and tissue properties. The model accounts for cell (electrode and tissue) geometry, allowing definition of the electrical field.*

System parameterisation: *Through combination of electrode and geometric properties, the relative influence of the electrodes on the biogalvanic system has been presented across a wide range of conditions. The parameter space produced has been compared to the existing model, showing its inefficacy when electrode influence is large.*

Model characterisation: *The numerical model has been successfully applied to measured data to allow extraction of electrode and tissue properties. Output metrics have been compared to those from the existing model in NaCl solution, and improved conductivity determination accuracy was found under certain conditions.*

Electrode dominance: *The characterisation results from NaCl solution and colon tissue allowed estimation of parameter space position for each test case. Findings suggest that, for the tissues tested, the system is heavily dominated by the electrodes. In addition, efforts to adjust the system properties may make the measurement system impractical for application within surgery.*

It is evident that the two modelling approaches focus on different aspects of the system. In each case necessary assumptions are made meaning that neither model fully captures the complexity of the system during measurement. Primarily these are the neglect of the influence of ionic diffusion for the transient model, and the assumption of steady-state currents in the numerical model. In addition, neither offers a direct means of accounting for the issues of diffusion limitation at the cathode as described in Chapter 5. However, although these models are not ideal, they have offered practical advancement of the biogalvanic technique, and given context to the influence of the electrodes in measured data.

6.6 Chapter Summary

The investigations presented in this chapter have demonstrated that there are a number of ways to adapt the modelling of the measured data from biogalvanic testing. Improved parametric control was realised through the integration of the Ivium CompactStat (Ivium Technologies), meeting Objective 6.1.

To meet Objective 6.2, a time-dependent analytic model of the biogalvanic system was developed and integrated into fitting software. This has been used to reduce the influence of switching rate on the characterised resistance. In addition, a statistical difference was shown between healthy and cancerous colon tissue, which was not found using the standard biogalvanic model.

A more comprehensive model of the system was generated as part of Objective 6.3. In conjunction with the School of Computing, a numerical model of the biogalvanic system during characterisation was developed. This was used to firstly understand the influence of the various system parameters on the expected measured data, and secondly to offer an alternative characterisation method. Combination of these two aspects allowed the level of electrode dominance expected in measured data to be estimated.

In relation to Objective 6.4, the findings to date have presented biogalvanic characterisation as an interesting technique, with some potential benefits for the proposed application as a surgical sensing tool. However, the benefits of simplicity and scalability have been outweighed by the complexities of the power generation system. In particular, the electrode-tissue interface and mass transport limitations at high currents produce significant artefacts in the output metrics. The methods presented in this chapter go some way toward alleviating these issues. However, they do not yet pose a solution with the accuracy and sensitivity required for the desired application. In conclusion, a more fundamental change to the technique is required to make this step toward a surgically appropriate sensor. Many of the findings presented may be relevant to the development of such a technique, and therefore should be considered within any future work.

Chapter 7
Multi-reference galvanostatic tissue resistance characterisation

---

The work of Chapters 5 and 6 has demonstrated that the biogalvanic characterisation technique is subject to significant errors. These arise from discrepancies between the electrochemical system and the electronic model assumptions upon which the technique is based.

Application of modelling modalities, as described in Chapter 6, may offer improvement or mitigation of the influencing system parameters. However, introduction of more comprehensive modelling methods is at the cost of increased system complexity and instability. One of the primary motivations for the use of a biogalvanic technique was that of simplicity, and with this removed the modality is arguably less appropriate than other techniques such as BIS.

The complexity of the galvanic cell and the lack of potential or current control make it an unfavourable element within a measurement system. The work of this chapter presents the initial formulation, system development, and testing of a new DC resistance characterisation technique. The proposed method has been developed through consideration of the problems associated with the biogalvanic system (detailed within Chapters 4-6) in conjunction with resistance compensation techniques from the fields of electrochemistry and corrosion science. Section 7.2 details the requirements for a successful sensor based on the findings from investigation into the biogalvanic technique. Relevant background information applicable to the developed technique and a description of the technique itself are contained within sections 7.3 and 7.4 respectively. Section 7.5 gives a technical description of the test system developed to allow suitable testing of the proposed modality. A general parametric investigation of the technique is detailed in Section 7.6, with tests specifically aimed at assessing the applicability of the technique to surgery being presented in Section 7.7. The concluding Section 7.8 summarises the work of Chapter 7.

7.1 Chapter aims

The aim of the presented technique is to consider and apply electrochemical phenomena to allow for a more accurate measurement of tissue resistance. To this end a discussion of some of the relevant resistance characterisation methods follow. The associated chapter objectives are:

Objective 7.1: *To detail relevant electrochemical theory pertinent to the elimination or measurement of cell resistance.*

Objective 7.2: *To propose and describe an improved resistance characterisation technique.*

Objective 7.3: *To develop and validate a control and measurement system capable of performing the required measurements and associated characterisation.*

Objective 7.4: *To investigate the efficacy of the characterisation method when applied to tissue and begin examination of the influencing parameters.*

Objective 7.5: *To investigate the efficacy of the characterisation method under conditions appropriate to the desired application of MIS.*

7.2 Sensor Requirements

The properties of an effective sensing modality depend heavily on the system in which it will operate. The focus of this research is on the measurement of tissue resistance, specifically within the realm of minimally invasive surgery. To this end, Table 7.1 reviews the most immediate factors to be considered and gives comments on their relation to the surgical environment.

The constraints outlined in Table 7.1 are in fact moveable, and for a truly accurate sensing modality with potential human benefit, concessions can be made to allow its application. Many of the modalities discussed in Chapter 2 may fall short in regard to some of these constraints but are still currently under development. However, the more easily a system can operate under current surgical constraints, the lower the barrier to entry for *in vivo* human testing required for real validation.

Table 7.1: Factors for consideration when developing a sensing technology for application in minimally invasive surgery.

Factor	Importance (High/Med/Low)	Comments
Fast measurement	High/Med	*To perform within the surgical environment without disruption to the procedure, the system should measure quickly. However, for specific measurements e.g. assessing the health of a tumour margin this time constraint could be relaxed.*
Scalable across materials and geometries	High	*A sensor would need to be able to function under contact with different tissue types (e.g. type, health, inter-person variation). For integration into a surgical tool the geometric constrains are likely to be restrictive.*
Low power	High	*The sensing modality should not cause undesired damage to the tissue region of interest.*
Stable (highly repeatable)	High	*The measurement metrics should be easy to obtain and give repeatable values for the same tissue type.*
Low impact to surgical procedures	Med	*The setup and operation of the sensing tools and auxiliary equipment should not create significant impact on the surgical preparation and operation.*
Simple output metrics	Med/Low	*Output metrics should be presented in a way to allow simple comparison of tissue health, so not to confuse the surgical decisions to be made with this information.*

Electrochemical and electrical assessment techniques offer only one methodology for sensing during surgery. The motivation for continuing research into this type of sensing is based on the positive findings from the biogalvanic investigation and the success shown with other electrochemical ([184, 185]), and EIS based ([132, 186, 187]) bio-sensing technologies. As a starting point, Section 7.3 outlines some background information pertinent to electrochemical based measurement systems and the sensor requirements of Table 7.1.

7.3 Background

Methods for determining electrolyte/analyte resistance in electrochemical systems are not exclusively as a means of resistance characterisation for analysis. In fact, often the motive for resistance measurement is in order to mitigate its influence upon an electrochemical aspect of interest. To this end, a large effort has been made to correct or reduce the uncompensated solution resistance as part of electrochemical experimentation [188].

Uncompensated solution resistance creates a fundamental issue in electrochemical systems, particularly those with low concentration (high resistivity) electrolytes [189]. For example, when simple polarisation techniques are employed, uncompensated resistance losses induce an error between the controlled potential set-point and the realised potential of the working electrode. In effect, the system is offset by the loss in potential between the working and reference electrodes. Therefore, inferences made regarding the behaviour of working electrode, particularly quantitative assessments, will be inaccurate. Additionally, for systems where variations of the internal resistance or electrode impedance occur, the measured artefacts will become significantly more complex [190]. For this reason numerous techniques have been considered and implemented in order to mitigate or measure and account for resistance losses between the working and reference electrode. In general, these fall into two categories: (1) adjustment of the physical arrangement of the test apparatus to minimise resistive influence, and (2) active measurement or calculation of the uncompensated resistance.

An example of the former is the use of a reference electrode connected through a tube of electrolyte. The end of tube is reduced to a fine capillary and positioned close to the polarised electrode, thus minimising the distance between the working and reference electrodes [191]. A common example of this is the Luggin-Haber capillary tube [83, 84, 192]. This arrangement is shown in Figure 7.1(a). This option is more prevention than cure and as such could offer the best results due to not being susceptible to the errors associated with resistance characterisation techniques. However, being able to position such a device is not always possible, particularly when assessments are to be made within closed or non-liquid systems (e.g. fuel cells/gels/biological tissues). Additionally, some errors still remain when using this method [189] and without careful placement, the system of interest can be influenced or the measurement corrupted [191, 192].

An alternative and more relevant corrective action is that of determination of the solution resistance through measurement or calculation followed by correction before or after the electrochemical test. The most basic application of this type is to calculate the effective uncompensated solution resistance using conductivity and geometric data and then removing the corresponding IR drop from the measured output. For simple geometries

this can be calculated by solving the Laplace equation, and for more complex geometries computational methods can be employed to solve finite element or boundary element models of the system configuration [189]. As such, for complicated geometric arrangements the determination of an accurate values of uncompensated resistance becomes particularly challenging, and combinations of empirical data and analytic and numeric modelling may be required [193].

A more practical approach is to directly measure the uncompensated resistance. Numerous methods have been proposed, with arguably the most common being the current interrupt technique [194, 195]. This method uses the transient potential response of a cell when it is interrupted (opened) from a controlled current via the auxiliary electrode lead [189]. Figure 7.1(b) shows a typical electronic arrangement for the current interrupter test and the typical output potential trace measured between the working and reference electrodes. The trace shows that the potential has a step response followed by a slower decay caused by the Ohmic solution resistance and capacitive electrode double layer respectively. Fitting and extrapolation of the transient allows the IR drop from the solution resistance to be evaluated. A number of issues associated with this type of measurement have been discussed [189, 196]. Nevertheless, this technique has been integrated as an automatic feature of numerous Potensiostats.

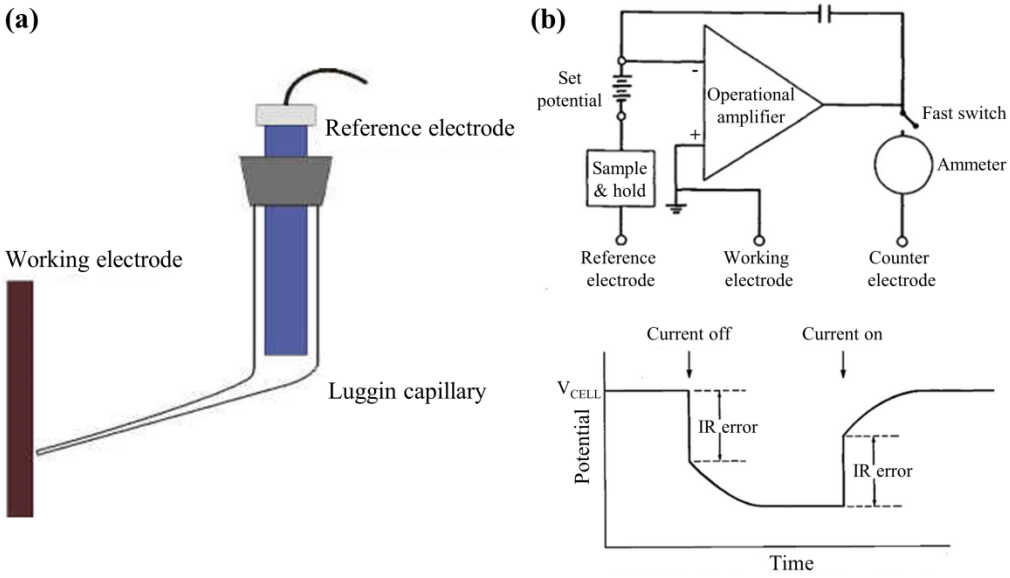

Figure 7.1: Uncompensated solution resistance correction methods: (a) experimental arrangement a Luggin-Haber type capillary tube reference electrode, and (b) electronic configuration (top) and typical voltage response (bottom) associated with the current interrupt technique; modified from [189].

Table 7.2: Available methods for the correction or measurement of uncompensated solution resistance.

Technique – *description*	Strengths	Weaknesses
Capillary tube reference electrode – *physical positioning of a tube electrolyte reference electrode close to the working electrode.*	Physical reduction of resistance. Requires no interpretation of data.	Not applicable when the aim is to determine internal resistance for a discrimination metric. Constrains of the solid tissue medium reduce the placement options for this type of equipment. Equipment can be fragile.
Calculation and subtraction from output – *model the geometry of the cell to estimate the IR drop corresponding to the solution resistance and subtract from the output trace.*	Simple methodology. Applied after data is recorded.	Determination of suitable system model can be challenging. No compensation prior to measurement. Complexity highly dependent on system geometry.
Current interrupt technique – *extrapolation of transient potential response of the system when constant current is interrupted.*	Fast technique. Simple model fitting.	Subject to noise and resolution errors, especially for low current densities. Polarising Can be influenced by the slow response of the reference electrode.
High frequency techniques – *use the properties of the system at high frequency to isolate the solution resistance.*	Established. Non-polarising method reduces errors from changes at current carrying electrodes.	Requires measurement over range of frequencies Model selection based on assumed knowledge of the system.

A high frequency method for determining the solution resistance again exploits the capacitive nature of the EDL. In this case the ratio of applied high frequency potential, and measured current gives the solution resistance [189]. This is based on the EDL behaving as a short circuit at high frequency, and so estimation of an appropriate high frequency value is an additional requirement. Characterisation of the system in question using EIS offers a practical means of determining a suitable high frequency value. In fact, electrical impedance measurements independently allow for characterisation of the solution resistance directly. Fitting of the response of a system to EIS to a suitable model allows determination of various components of the system, including the solution resistance. The issue is that measurements are required over a range of frequencies in order to have a reliable fit. Additionally, selection of an appropriate model is particularly challenging [108]. Table 7.2 summarises the main options used in mitigation of solution resistance in EC measurements, and includes some of the strengths and weaknesses of each technique.

The range of research into the topic of resistance compensation is vast, and numerous techniques have offered suitable solutions for electrochemical experimentation. However, the work presented in this chapter is concerned with determining the salt bridge (tissue) resistance in isolation from the electrode interfaces and is therefore subject to the constraints outlined in Table 7.1. The technology discussed in this section therefore informs the development of a practical sensing technique, rather than giving a complete solution. The strengths and weaknesses of these techniques have been considered in the development of the multiple reference DC technique described in section 7.4.

7.4 Technique Description

A simple method for measuring tissue resistance involves contacting the tissue of interest with two electrodes, controlling the current passing through the tissue cell, and measuring the corresponding potential difference across the cell. This is fundamentally the process employed by the biogalvanic characterisation method described and tested in Chapters 3-6. Resistance determination using this method is, however, flawed as a two electrode arrangement has an inherent inclusion of artefacts from the electrode-tissue interface (c.f. Section 5.6). These are associated with the induced polarisation of the electrodes when current flows between them. Losses in potential across each interface cause the measured cell voltage to not be representative of the tissue medium resistance. The addition of a single stable reference electrode allows the individual potential of the working electrode to be monitored with a higher degree of precision. However, this would not give an accurate reading of the working electrode potential as the response contains a resistive loss from the

tissue. Contrariwise, measurement of the tissue resistance still contains artefacts from the working electrode-tissue interface.

The addition of a second reference electrode to the system does not directly allow for a more accurate monitoring of the working electrode potential. However, it does allow for the measurement of the potential difference between the reference electrodes and therefore determination of the medium resistance between these points. Figure 7.2 illustrates the different cell configuration discussed and shows a simple representation of the potential profile and electrode positions across each cell case. The four electrode configuration is analogous to the four-wire (Kelvin) method for measurement of very low resistance material [197, 198].

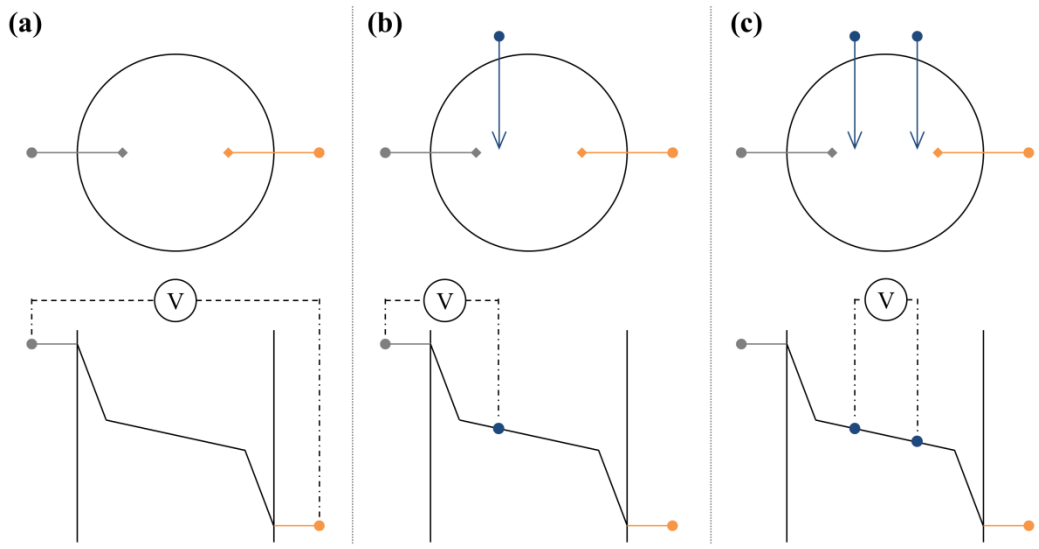

Figure 7.2: Schematic electrode representation (top) and potential response showing effective voltage measurement (bottom) in the cell for (a) two electrode cell, (b) three electrode cell, and (c) four electrode cell.

It is proposed that it is possible to obtain resistance specific information from a four electrode cell in a different and novel manner. The proposed method measures the potential response of the working electrode with respect to two (or more) separate reference electrodes, and subsequently uses the difference in responses to give a potential loss in the cell that is induced by the electrical resistance of the salt bridge medium. The technique is applicable to a standard electrochemical cell connected through a tissue salt bridge. This consists of a current carrying electrode pair (working (WE) and counter electrodes (CE)), and two stable reference (potential measurement) electrodes (RE). Application of significant current demand upon an EC cell necessitates a change in potential of the current-carrying electrodes. For an electrode under a kinetic regime of activation control, its overpotential η can be calculated using the Tafel equation (7.1), [83]. This relates the

change in electrode potential, relative to its equilibrium potential E, to the current density of the cell i via the Tafel parameters a and b.

$$\eta = a - b.\log i \tag{7.1}$$

Assuming a suitable counter electrode is present in the cell, the potential difference ΔE_{RE}^{WE} between the working and any reference electrode can be determined using equation (7.2). The terms η_a^{WE} and η_c^{RE} represent anodic polarisation of the working electrode (+ve) and cathodic polarisation of the reference electrode (-ve) respectively. A suitable reference electrode will have a stable equilibrium potential (E^{RE}) and be highly non-polarisable relative to the working electrode, leading to a negligible cathodic ovepotential ($\eta_c^{RE} \approx 0$). For the cell in question, $R_{WE\rightarrow RE}$ represents the resistance of the tissue salt-bridge between the working and reference electrodes. When multiplied by the current density, this indicates the potential drop across the tissue. Assuming identical, non-polarisable and stable reference electrodes, calculation of a potential difference ΔE, the comparison of the working electrode potential to two separate reference electrodes, yields equation (7.3). This crucially allows subtraction of the working electrode polarisation and leaves a current-potential relationship equal to a cell resistance, equation (7.4). This resistance ($\Delta R_{RE1\rightarrow RE2}$) is proposed as being representative of the tissue salt-bridge, potentially making it a useful comparative metric for assessment and discrimination during surgery. The resistance determined in equation (7.4) will be equal to the difference (in resistance) between the resistive pathways from the working electrode to each reference electrode respectively. As such its value will be highly dependent on geometry, making consideration of electrode configuration paramount.

$$\Delta E_{RE}^{WE} = (E^{WE} + \eta_a^{WE}) - (E^{RE} + \eta_c^{RE}) + iR_{WE\rightarrow RE} \tag{7.2}$$

$$\Delta E = \Delta E_{RE2}^{WE} - \Delta E_{RE1}^{WE} = i(R_{WE\rightarrow RE2} - R_{WE\rightarrow RE1}) \tag{7.3}$$

$$\Delta E/i = \Delta R_{RE1\rightarrow RE2} = \Delta R \tag{7.4}$$

The theoretical prediction of equation (7.3) is that measurement of the difference between the working electrode responses, measured from two separated reference electrodes, for a controlled current flow will give a linear correlation. The gradient of the E vs I plot will represent the difference in resistance for the two resistive pathways from WE

to the respective RE. Figure 7.3(a) shows two representative electrode arrangements that could be used to achieve the proposed measurements. A theoretical response of the working electrode, as measured from two independent reference electrodes, is shown in Figure 7.3(b). The corresponding theoretical potential difference (between measured responses of Figure 7.3(b)) against the polarisation current is shown in Figure 7.3(c). The gradient of this response has been indicated as the resistance of the tissue salt-bridge.

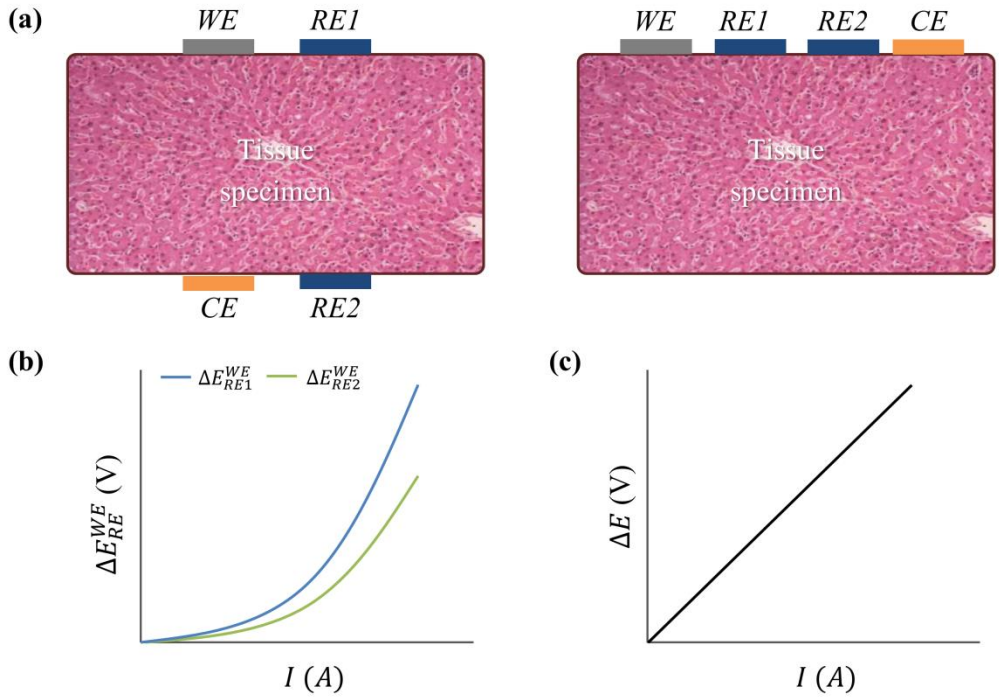

Figure 7.3: The proposed multiple reference resistance characterisation technique showing (a) possible electrode configuration for a four-electrode arrangement, (b) theoretical response of the working electrode (measured at two reference electrodes) to galvanic polarisation and (c) theoretical differential response of compared reference electrodes.

7.4.1 System considerations

The proposed system offers a means of determining a tissue specific resistance. There are a number of important benefits to the proposed system that make it suitable for the surgical sensing environment. In addition, there are also limitations and technical challenges that may need to be addressed prior to achieving a suitable sensing solution. The following list details some of these considerations:

7.4.1.1 Polarisation

To cause cell polarisation, the potential, current or load can be controlled. The proposed method is to use current control (galvanostatic polarisation), although the theory of technique extends to any means of cell polarisation as long as cell current is measured. This

suggests that the system may be operated in a passive capacity, as is the case for biogalvanic characterisation.

7.4.1.2 Electrode response

As the current levels are increased, the working and counter electrodes will polarise significantly. The response may be that of simple activation control as in equation (7.1), or it may be much more complex including mass transport limitation, time-dependent elements or passivation. The response is dependent on the materials and level of polarisation induced. However, the proposed technique is theoretically independent of this response. If equation (7.1) were replaced with the more general expression $\eta = f(j)$, then applied to equations (7.2) and (7.3) it is evident that no alteration of equation (7.4) is apparent. Therefore, as long as there is a working electrode response, a tissue resistance may still be determined. This also means that for a low resistance tissue where the difference in responses from the independent reference electrode may be small, a much greater polarisation can be induced to generate a measureable response.

7.4.1.3 Reference stability

A suitable reference electrode will have small changes in potential for a large increase in current (low resistance). However, for a solid tissue system under surgical constraints the choice of reference electrodes is somewhat limited. Under the traditional four-electrode arrangement (Figure 7.2(c)), the potential difference is measured between two reference electrodes, giving a low resistance input to the DAQ device. Although low resistance (impedance) is good for noise reduction, measurement accuracy and fast transients, it does give a higher current through the measured circuit. This may induce a larger polarisation (error) in the reference electrode. Additionally, when two reference electrodes are measured relative to one another the polarisation errors will oppose in direction, summing the resulting errors. This is not the case in the proposed technique, where any polarisation of the reference electrode is mirrored in the working electrode. Each reference electrode will polarise in the same direction, subtracting error. In addition, the working electrode may have a much larger resistance, therefore reducing current flow in the measurement circuit and the subsequent level of reference polarisation. Differences in the equilibrium potential of the two references will cause an offset in the characterisation response (shown in Figure 7.3(c)). However, this does not influence the resistance (gradient) unless there is relative change during the measurement.

7.4.1.4 Resistivity

Determination of a resistivity is useful as it allows comparison between tissues measured under different conditions. However, to convert resistance to resistivity it is necessary to know how the current flows between the electrodes. This is challenging for complex geometry and in particular the multiple reference system proposed. As the characterised resistance represents the difference in resistive pathways between the working electrode and each reference electrode, the issue is compounded. For simple geometric arrangements, numerical modelling may offer the best method for addressing this issue. In the short-term, consistent electrode geometry may be used and the resistance compared directly.

7.5 System Development

To achieve a suitable testing system capable of validating the proposed method, custom configuration of hardware and software components was required. The method can be viewed as two separate sections: (1) control of cell current between two electrodes (working and counter), and (2) measurement and processing of the voltage response of the working electrode at two separate reference points. Due to the wide range of unknowns at the time of method conception, a pragmatic approach to the system development was taken. To this end, the use of a reconfigurable potentiostat (CompatStat, Ivium Technologies) and simple programmable DAQ device (myDAQ, National Instruments, TX) was employed. Figure 7.4 shows the desired system configuration schematically, with justification for some of these system compenents being described within Section 7.5.1.

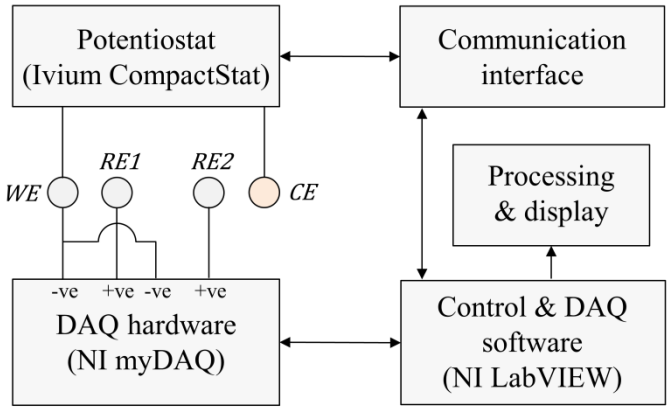

Figure 7.4: Schematic of the proposed multiple reference resistance characterisation equipment; arrows indicate communication direction, and electrodes WE, CE, RE1, and RE2 represent the working, counter, reference 1 and reference 2 electrode respectively.

7.5.1 System requirements and component selection

This section describes the key requirements for the testing system. These are then considered in the context of the components selected. Optimisation of these components was performed with significant attention to the early stage nature of the methodology and the time constraints of the project. Where appropriate, suggestions for the configuration of a more robust, longer-term system have been proposed.

7.5.1.1 Working/counter electrode pair

As the previous work of Chapter 5 gave a detailed electrochemical investigation into the potential/current characteristics of a Zn/Cu system, this has been taken as the starting cell for current control. A significant aspect of the system was found to be the current limitation of the copper cathode, where the rate of oxygen diffusion causes a large change in potential for a small increase in current. For the system under current control this may induce a large change in the measured potential at higher currents. However, based on the theory presented in Section 7.4 the working electrode polarisation response should not influence the characterised resistance.

7.5.1.2 Current range

Two main issues concern the current range selected and how it relates to the voltage/current response of the cell; (1) a high current can lead to saturation of the measured potential, and (2) a low current may not induce a large enough potential change to be accurately measured within the resolution and range of the DAQ device. These high and low values are arbitrary without consideration of a number of other dependent factors. These have been summarised as:

- the polarisation response of the working/counter pair
- the electrode areas
- measurement resolution of the DAQ device
- geometry of the four-electrode configuration
- the resistance of the tissue medium
- current output range/resolution of the current control device

It is clear that it may not be possible to directly control these factors within the measurement system. For example, the resistance of the tissue is the focus of the measurement and its value will alter the polarisation characteristics of the electrodes and the cell. The suitable current range was therefore chosen primarily based on the typical currents seen at the proposed electrode areas. Values of current ranging from 1-100 μA

were expected to give a wide polarisation, allowing resistance characterisation. The selection of a configurable potentiostat enabled this value to be adjusted if it was found to be inappropriate.

7.5.1.3 Reference electrodes

The reference electrode needs to be in direct contact with the tissue and allow for stable measurement of the working electrode potential. An ideal reference electrode would have a very low resistance, giving only a small change in potential for a large current. Typical commercial reference electrodes will contain a complete electrode/electrolyte system in isolation connected through a porous membrane [83]. Although this type offers a very stable reference point, the size of the electrode and requirements of a liquid junction make it an impractical solution for the proposed method.

With consideration of these requirements along with the available materials, cost and manufacturing ease, a zinc reference electrode was chosen. The zinc system has been extensively investigated as part of Chapter 5 and has been shown to be stable relative to the copper electrode against which it will be measured. The stable half-cell potential for the zinc oxidation reaction of equation (5.1) is -0.76 V under standard conditions. The settling time and stability of the zinc electrode are the primary concerns for the use of this reference. With the assumption of consistent settling rates, this error may be cancelled out due to the use of a second reference.

7.5.1.4 Data acquisition & control

As outlined in Figure 7.4, the system requires the control of current and the measurement of the potential of the working electrode from two separate reference electrodes. The standard potentiostat used (CompactStat, Ivium Technologies) allows for precise current control down to the low levels required (<1 μA), however it does not easily allow additional channels of potential measurements against the working electrode. Conversely, programmable data acquisition devices offer many voltage measurement channels at high precision; the NI myDAQ (National Instruments) offers a 2-channel ADC device with 16-bit resolution over +/- 10 V. This DAQ however does not allow for precise control of the low current levels required. As neither system offers a complete solution, both were coupled and custom software (LabVIEW) used to register systems to a common time base. Section 7.5.4 describes the development of the required software.

7.5.2 Electrode manufacture

The electrode materials selected where 1 mm diameter extruded copper (99.9 % pure) and zinc (99.9 % pure) wire (Goodfellow Cambridge Ltd, UK). This size was selected to allow for significant electrode separation without inducing a large overall size. To connect the electrodes to the control and DAQ devices, copper wire was soldered onto the back of each electrode. Stray conductive pathways and electrical shorting was mitigated by setting the electrodes into a non-conductive resin. Each soldered electrode was punctured through the base of a silicone mould at the desired separation. The solder connection for each was positioned so that it would be easily covered by the resin and not in contact with other electrodes. The exposed ends of the electrodes were inserted into re-useable adhesive (Blue-Tack®, Bostik, UK) to stop movement and leaking during resin setting. Non-conducting resin (Varidur™, Buehler, USA) was poured into the mould and allowed to set, leaving the end face of the electrodes and insulated wires exposed. The electrode faces were wet ground to 1200 grit and rinsed with distilled water prior to each test. Figure 7.5(a) shows the configuration of the manufactured electrode set, and Figure 7.5(b) shows the corresponding manufactured electrode.

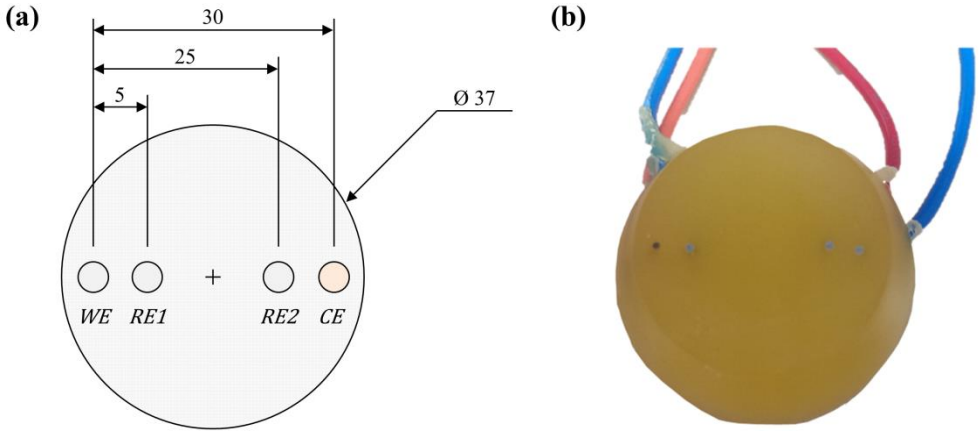

Figure 7.5: Four-electrode configuration showing (a) schematic of the desired electrode geometry and (b) an example manufactured electrode set; (units shown in mm).

7.5.3 Contacting equipment

The multiple reference electrode system requires consistent contact to the salt-bridge medium during measurement. For a tissue system, the loading conditions including stress and strain may become significant parameters and require investigation. However, for initial testing it was only essential to deliver a stable contact and allow for repeat measures to be taken under the same conditions. To this end a simple clamping system was developed to give adjustable planar contact with a tissue region of interest. The system, as shown in Figure 7.6, was designed with a large workspace to accommodate various sizes of

ex vivo tissue. A nylon nut was glued to the back of the electrode set directly onto the resin to allow for coupling to the clamp body, as shown in Figure 7.6(a). The electrode clamp was adjustable to allow minimal strain contact conditions to be met during testing.

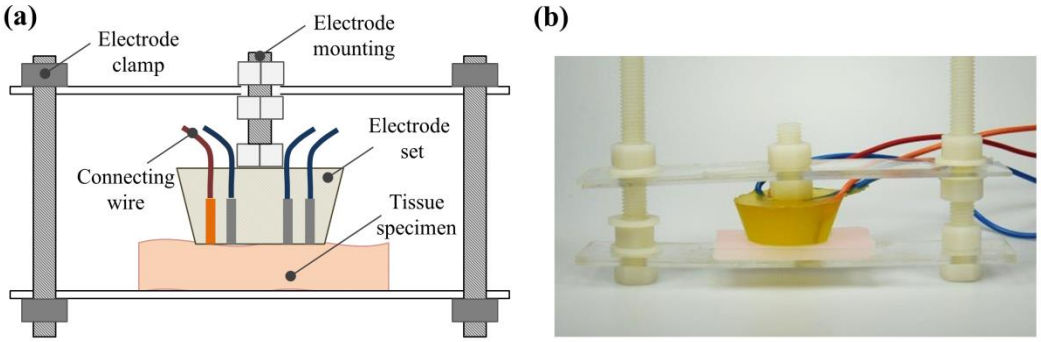

Figure 7.6: Electrode set clamp, showing (a) schematic of clamping system and (b) physical clamp acting on tissue phantom.

7.5.4 Software development

As the proposed testing method is not a standard technique used within EC analysis, the development of bespoke software was an essential part of the produced system. Software was written to control and measure the current and voltage through the cell, and additionally to extract, analyse and report the data from parametric tests. The following sections describe these software applications in more detail.

7.5.4.1 Testing system

For time coded measurement of potential differences and control of current it was necessary to develop custom software. The choice to combine the use of a potentiostat and DAQ device makes this task more involved as the two systems require configuration, control and synchronisation. The software requirements were defined as:

- Configuration of the DAQ device
- Communication with the potentiostat (setting/reading current)
- Configuration of testing parameters
- Processing and logging of data and determined metrics (resistance)

The configuration of DAQ hardware was enabled through the use of the standard DAQmx toolkit (LabVIEW, National Instruments). Communication with the potentiostat was made possible through the use of the IVIUM_remdriver dynamic link library (DLL) and associated LabVIEW files (Ivium Technologies). These files allow direct control of the IviumSoft software through LabVIEW. A flow chart detailing the architecture of the overall test software is shown in Figure 7.7; the sub-functions identified have representative schematics presented in Appendix C.

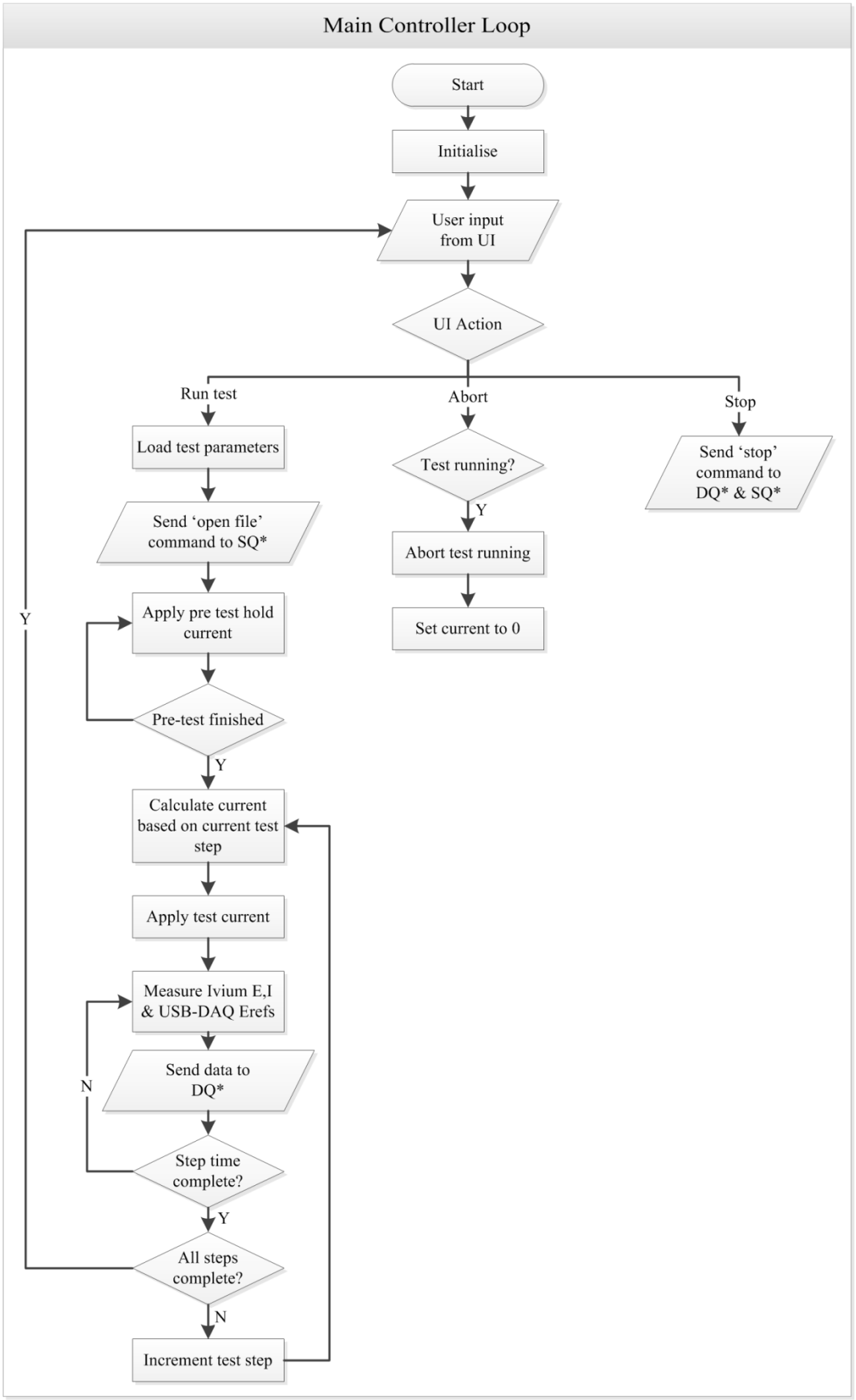

Figure 7.7: Software flowchart for the galvanostatic resistance characterisation technique; *indicates connection to sub-function diagrams presented in Appendix C.

The user interface developed for the testing software is shown in Figure 7.8. From this screen the operator can configure the test settings to indicate the type (potential or current) of cell control, the controlled current (or potential) step sizes, rate and range, as well as the pre-test holding current (or potential) and hold duration. When these parameters are selected the test may be started and will continue to completion automatically unless aborted by the user. Display of the measured cell and reference potentials is delivered to the user graphically along with a live update of the characterised resistance.

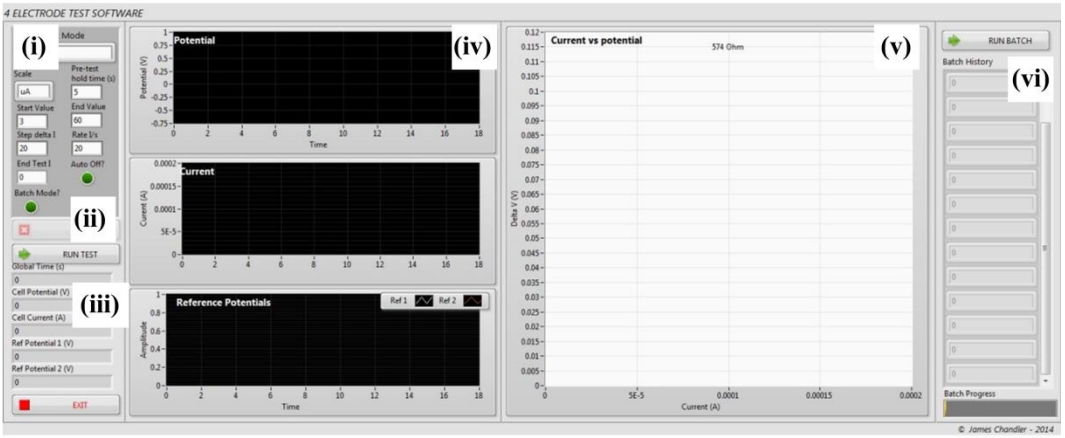

Figure 7.8: User interface for the four-electrode resistance characterisation technique software; various components are: (i) single test settings configuration, (ii) run/ stop test, (iii) raw current and voltage readings, (iv) cell potential, cell current and reference potentials time coded display, (v) resistance characterisation plot and (vi) batch test setup.

7.5.4.2 Analysis system

Using the software described in Section 7.5.4.1 for testing generates a raw measured data file and a test configuration file for each test. Running a batch of tests, including parametric changes or repeated measures, generates a large number of files. For this reason, separate analysis software was written to process and sort the measured data based upon testing parameters. Each file from within a selected folder is opened (along with its corresponding configuration file), pre-test hold data are removed, and potential and current data applied to a linear fitting function to generate a resistance. Resistance values are sorted by test condition and written to a summary file for further processing. The software was utilised for the results processing required in the following testing sections and in Chapter 8.

7.6 General Parametric Investigation

This section describes the necessary first stage testing required to assess the system performance and to establish baseline information regarding tissue resistance values,

current ranges, and repeatability. This work is also required to help define sources of error within the testing methodology and system. Investigation into the influence of current range and switching rate is also presented. Primarily the work was conducted using *ex vivo* porcine colon tissues.

7.6.1 System validation and technical comments

System validation was considered through performing and analysing a typical tissue measurement, including raw output variables and processed data. The aim of this testing was to show how a real characterisation compares to theoretical expectations presented in Section 7.4.

7.6.1.1 Example measurement

Characterisation tests were conducted on *ex vivo* porcine rectal tissue using the developed test system (cf. Section 7.5). Contact was maintained between the tissue mucosa and the four-electrode cell (cf. Section 7.5.2) using a tissue clamp (cf. Section 7.5.3), as shown in Figure 7.9. Based on the findings from initial testing, the test software was configured with the following parameters:

- Current range: 60 μA
- Pre-test hold current: 3 μA
- Current switching rate: 6 μA/s
- Current step size: 6 μA
- Pre-test settling time: 5 s

The corresponding recorded cell data was output from the testing software and processed for comparison to the expected cell behaviour.

Figure 7.9: Multiple reference resistance characterisation validation test configuration for *ex vivo* porcine rectal tissue.

The response of the control system was evaluated by monitoring the current response over the course of the above test (Figure 7.10(a)). The response indicates that the current is transitioned accurately in the demand steps specified. However, there is an accumulative error in switching time. This undesirable feature is associated with the communication interface between the control software and IviumSoft. Specifically, there is a time delay between commands being sent and received through the DLL. Although the timing accuracy is reduced, crucially the cell is maintained accurately at the desired current intervals. Correction to this error could be achieved through the use of a custom DLL, or a bespoke testing system. The cell voltage against time, measured between the working and counter electrode, is presented in Figure 7.10(b). Figure 7.10(c) shows the polarisation response for the anodic polarisation of the zinc working electrode. The characteristics of the response indicate an activation controlled response in line with equation (5.7).

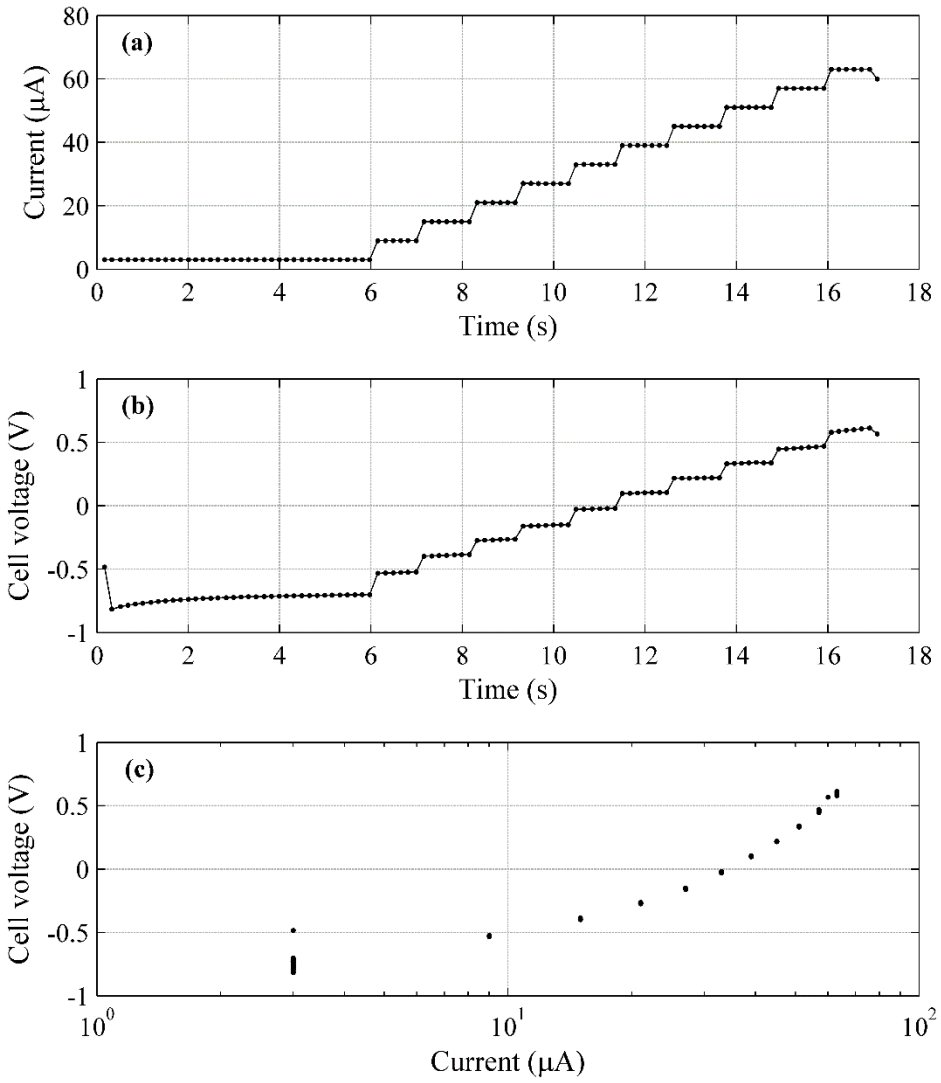

Figure 7.10: Example of measured cell data for step-wise galvanostatic polarisation, showing time response for (a) cell current (controlled factor) and (b) cell voltage, and (c) cell voltage against cell current.

As the current was stepped through the desired range, Figure 7.11(a) shows that the measured reference potentials increased significantly. The presented theory of Section 7.4 predicts that the potentials will have a current dependent offset induced by the tissue resistance and electrode geometry. This can be clearly seen within Figure 7.11(a), with the difference in potential increasing from 0-0.149 V over the test current range. Comparison of this voltage difference to the cell current shows highly linear correlation, as predicted within equation (7.4). Application of linear regression fitting to the data produces a tissue specific resistance ΔR.

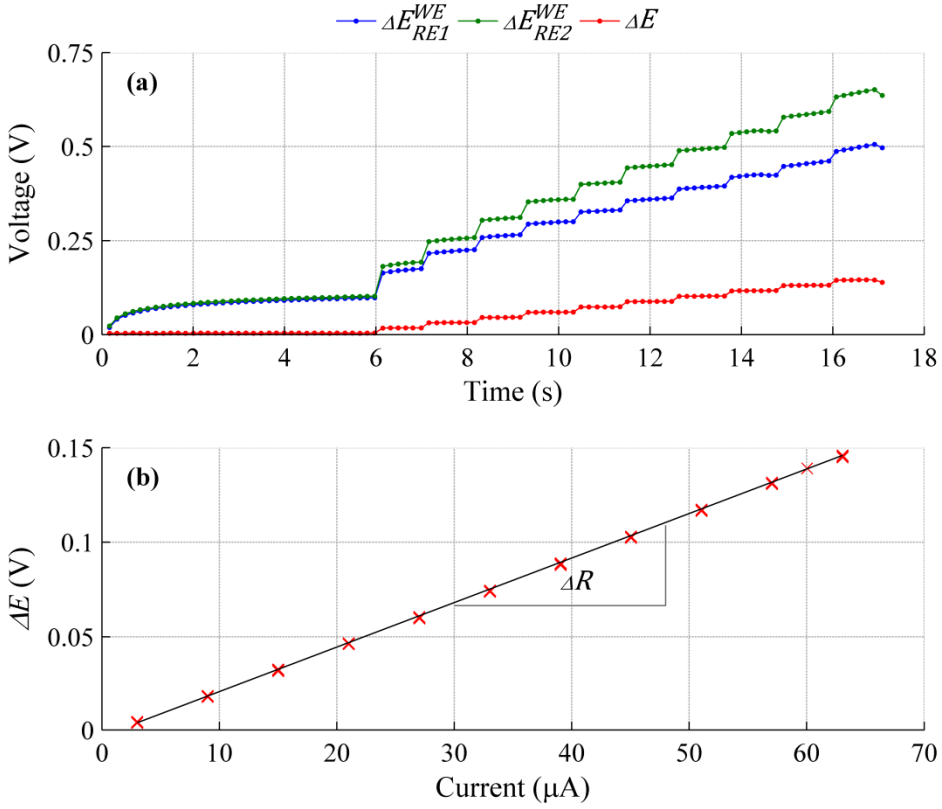

Figure 7.11: Example of measured cell data for multiple reference electrodes, showing (a) polarisation response for the two reference electrodes and their difference, and (b) corresponding voltage difference against current resistance characterisation, ΔR = 2450 Ω.

7.6.2 Time drift

During preliminary testing it became evident that a time variation in the characterised resistance was present. An investigation was therefore performed to assess the level of drift with time and assess this issue more rigorously. A single experiment is presented in this section although, this factor was also considered in other parametric testing along with *ex vivo* human tests described within Chapter 8.

A porcine rectum specimen was clamped with the electrodes under the configuration shown in Figure 7.6. Electrode contact was maintained throughout the experiment. To minimise the effect of electrode stabilisation of the tissue, the polished electrode set was subjected to 10 min of contact with a separate specimen prior to the testing. The test configuration for each repeat was:

- Current range: 60 μA
- Pre-test hold current: 3 μA
- Current switching rate: 6 μA/s
- Current step size: 6 μA
- Pre-test settling time: 5 s

The duration of each test was approximately 15 s, and repeats were performed successively for a 20 min period. Each repeat was subsequently analysed to produce a tissue resistance and a test time. Resistance variation found as a function of time is shown in Figure 7.12.

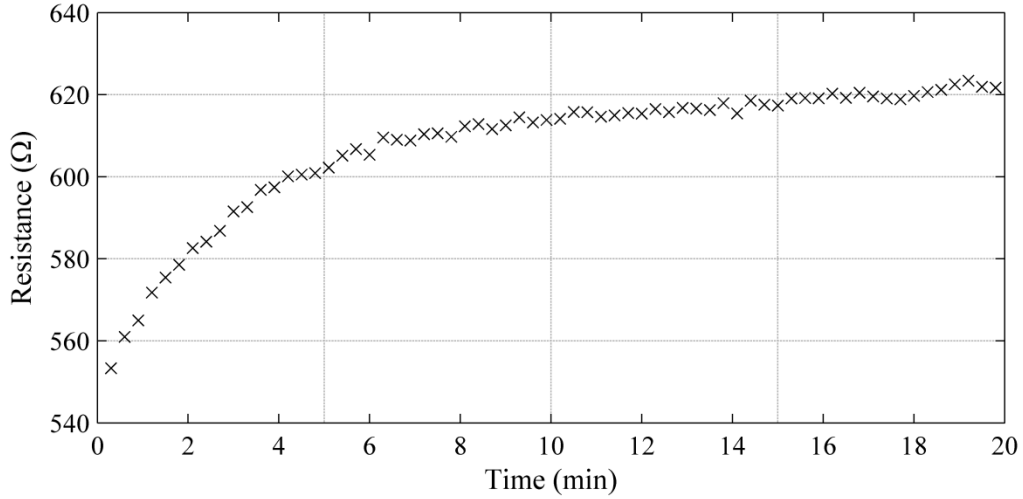

Figure 7.12: Influence of time on the characterised tissue resistance for a 20 min test on *ex vivo* porcine rectum.

Figure 7.12 clearly indicates an influence of time on the resistance. Over the 20 min testing period, an increase in resistance from 553 – 622 Ω (12.5%) was found. A decreasing rate of increase with time was also shown, indicating greater influence on the system at the early stages of testing. There are a number of potential explanations for the increase shown, these are:

Electrode drift: *Fresh electrodes (polished to 1200 grit) may have a potential far removed from that at equilibrium for the electrode-tissue interface. As such, upon initial contact there will be a settling period where the system moves to this new equilibrium. This applies to all of the system electrodes and while non-equilibrated, errors in the measurement may be present. An attempt to mitigate this issue was made through application of the electrodes to tissue prior to testing. Although transferring between tissues may create an additional shift in potentials that could again influence measurements.*

Tissue death: *From the point of animal slaughter, tissues will proceed to alter as the supply of oxygenated blood is not maintained. The specific processes of tissue death are complex but will include the self-digestion of cells (autolysis) and breakdown of proteins (purification) [199]. The level of influence of these processes on the resistance of the tissue tested is unclear. However, work by Haemmerich et al [200] showed an increase in extracellular resistivity (measured using BIS) over the first 2h followed by a steady decrease up to 12h. The findings of the presented test align with this work, indicating that post mortem tissue degradation may be one of the key influencing factors.*

Hydration: *As with tissue death, hydration will reduce from the point of animal slaughter. A reduction in the water content of the tissue will influence the concentration of ionic species and therefore resistance.*

Temperature: *Supplied animal tissue maintains a temperature above that of the laboratory during the transportation process. At the point of dissection, the temperature drops more rapidly toward room temperature. The conductivity of salt solutions is strongly influenced by temperature. Therefore, the tissue resistance will be increased as the temperature drops. As there is a trade-off between testing as soon as possible to maintain freshness and testing at a constant temperature, it is likely that this factor is influential.*

The list of influential factors discussed above is non-exhaustive, however, some or all of these are likely to be involved in the time-drift seen during experimentation. It is not possible to mitigate all factors and they are inherent issues with *ex vivo* tissue testing. However, utilisation of consistent protocols and a specific ordering of repeated measures were implemented for further investigations to minimise the impact of time-drift on the findings.

7.6.3 Measurement rate

The measurement rate is one factor directly responsible for the duration of a measurement. As stated in Table 7.1, it is desirable for a surgically appropriate sensor to be able to measure quickly. To this end, the stability of the output metric (resistance) should be evaluated over a wide range of measurement rates to assess the rate dependence of the technique.

An experiment was conducted to evaluate this factor. Two colon tissue sections were tested independently. Prior to each test, the colon mucosa was exposed and the electrodes clamped into contact. The test settings for each measurement were:

- Current range: 10 μA
- Pre-test hold current: 3 μA
- Current switching rate: varied from 0.1 - 40 μA/s (corresponding to measurement times ranging from 100 – 0.25 s respectively)
- Current step size: set equal to the current switching rate for 0.1 - 10 μA/s and 10 μA for faster rates
- Pre-test settling time: 10 s

The set of testing conditions used have been presented in Table 7.3. Each measurement time was employed six times for each tissue specimen. Tests were ordered in a oscillating pattern beginning with a reducing measurement rate. This was to minimise the influence of the time-drift on the investigation. The findings for the two tissue tests have been presented in Figure 7.13. Statistical assessment of each specimen using a single-factor analysis of variance (ANOVA) test (n=6). No statistical difference was found for the measurement rates tested on either tissue specimen, $p > .05$.

Table 7.3: Test settings used for investigation of measurement time.

Switching rate (μA/s)	Current step size (μA)	Measurement time (s)	No. of data points recorded
0.1	0.1	100	101
0.2	0.2	50	51
0.5	0.5	20	21
1	1	10	11
2	2	5	6
5	5	2	3
10	10	1	2
20	10	0.5	2
40	10	0.25	2

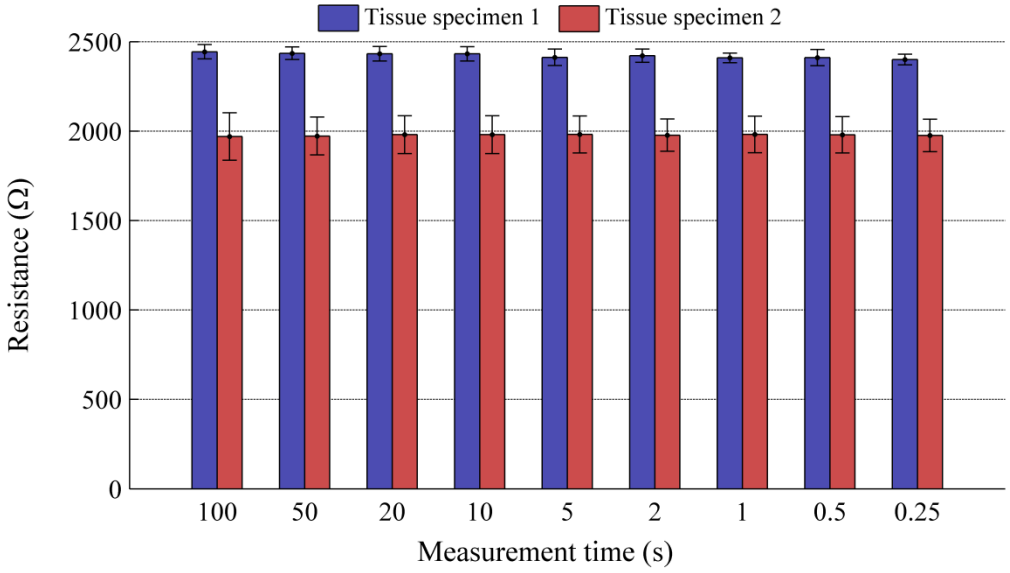

Figure 7.13: Characterised resistance values as a function of measurement time (n=6), for two colon mucosa specimens.

7.6.4 Current range

The current range of a measurement is the difference (increase) in the current from the test start (pre-test hold value) and the maximum test current. As the potential application of testing is within surgery on living tissues, it is desirable to control this factor to within safe levels. Mortimer et al., [201] suggest that current densities above 50 μA/mm^2 may induce tissue damage during skeletal muscle stimulation although this study is experimentally distinct from the proposed measurement technique of this chapter.

An investigation was therefore performed to evaluate the influence of the current range selected on the characterised tissue resistance. A single colon tissue specimen was

tested with pre-conditioned electrodes clamped into contact with the exposed mucosa. The test settings for each measurement were:

- Current range: Varied from 10-100 μA in 10 μA steps, with a low end tests at 5 μA
- Pre-test hold current: 3 μA
- Current switching rate: Two rate conditions tested (10 current steps over 10 s and 1 current step over 0.25 s)
- Current step size: set equal to the current switching rate for 0.1 - 10 μA/s and 10 μA for faster rates
- Pre-test settling time: 10 s

The set of testing conditions used have been presented in Table 7.4. Each current range and test time combination was tested over 10 repeats. The order of current range selection was randomised. Due to the long duration of the experiment analysis of the influence of the time-drift was also investigated. The mean ± SD resistance values of the current ranges tested have been presented in Figure 7.14.

Table 7.4: Test settings used for investigation of measurement current range.

Current range (μA) [max est. current density (μA/mm^2)]	Switching rate [10 s test] (μA/s)	Current step size [10 s test] (μA)	Switching rate [0.25 s test] (μA/s)	Current step size [10 s test] (μA)
5 [6.4]	0.5	0.5	20	5
10 [12.7]	1	1	40	10
20 [25.5]	2	2	80	20
30 [38.2]	3	3	120	30
40 [50.9]	4	4	160	40
50 [63.7]	5	5	200	50
60 [76.4]	6	6	240	60
70 [89.1]	7	7	280	70
80 [101]	8	8	320	80
90 [115]	9	9	360	90
100 [127]	10	10	400	100

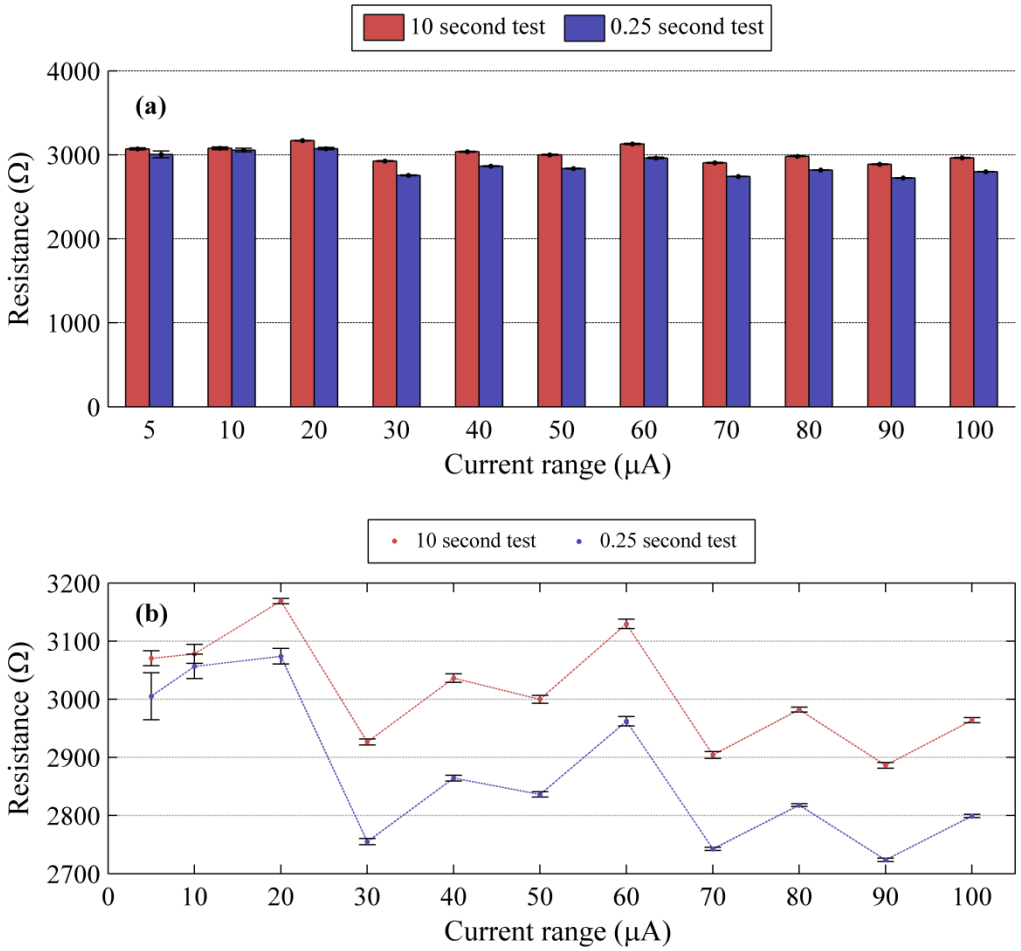

Figure 7.14: Mean resistance ± SD (n=10) as a function of current range used for two test times, showing (a) full scale data and (b) reduced ordinate axis scale; lines added for trend illustration.

Figure 7.14 indicates the variation introduced through changes in the current ranges tested. A range of approximately 500 Ohms was found across all test conditions. Two general trends are shown in Figure 7.14(b): (1) for higher current range, the repeatability of the test is improved (lower SD), and (2) for the faster test setting (0.25 s test), the characterised resistance is consistently lower. The same current dependence trend is shown for both measurement rates, although this difference is less pronounced for low current tests.

With further analysis of the time variation of the resistance values it became evident that the current range variation may be significantly influenced by alteration of the tissue condition. Figure 7.15 shows all repeats arranged in time order. It is clear that from measurement number 30 onward that there is a decreasing trend of tissue resistance. In addition, the two testing rates show a consistent offset of approximately 180 Ω. This indicates a dependence on measurement rate, which is contrast to the findings of Section 7.6.3.

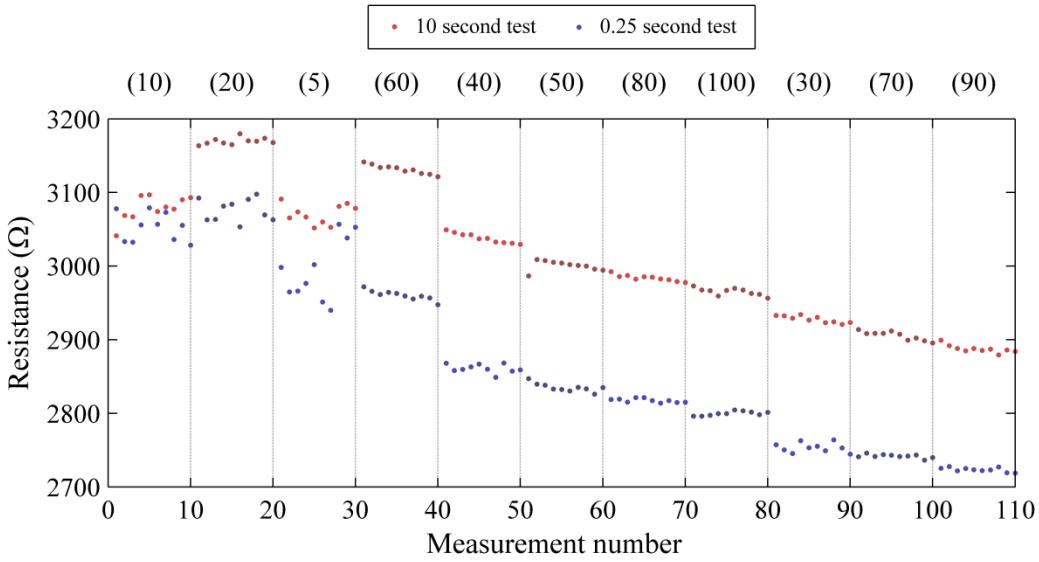

Figure 7.15: Measured resistance values in time order for current range testing for two testing times.

The range of resistance values across all test conditions was found to be less than 20%. Of this variation, a large part was attributed to tissue alterations (death and drying) as detailed previously. This suggests that there is flexibility in the selection of current range. The variability shown in Figure 7.14(b) suggests that the use of a higher current is desirable due to the larger potential shifts giving an improved signal-to-noise ratio for the measurement. The larger variability of low current tests may be explained by the lower voltage changes induced, leading to a higher influence of quantization error.

7.6.5 Electrode geometry

The arrangement of the electrodes, in particular the relative positioning of reference electrodes, was proposed as being of direct relevance to the characterised resistance. This is due to the resistance value being defined as the difference in resistance of the resistive pathways between the working electrode and the two reference electrodes respectively. Application to laparoscopic surgery imparts significant geometric constraints and is therefore an important variable for consideration. Geometric investigation was performed using two electrode configurations, as shown in Figure 7.16. These were selected as the maximum and minimum reference electrode separations practically attainable within a 30 mm footprint. Five repeat measurements were taken for each electrode configuration at the same range of measurement rates detailed in Table 7.3. Measurements were recorded at the same colon mucosa location for the two electrode configurations. The test settings for each measurement were:

- Current range: 10 μA
- Pre-test hold current: 3 μA
- Current switching rate: varied from 0.1 - 40 μA/s (corresponding to measurement times ranging from 100 – 0.25 s respectively)
- Current step size: set equal to the current switching rate for 0.1 - 10 μA/s and 10 μA for faster rates
- Pre-test settling time: 5 s

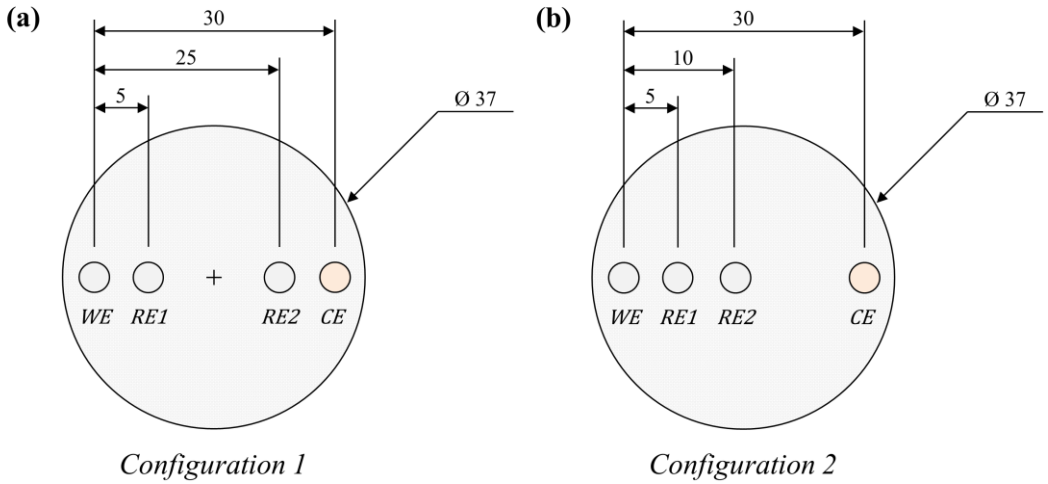

Figure 7.16: Schematic of the two electrode geometries used for assessment of reference electrode positioning; all dimensions in mm, not to scale.

A comparison of the characterised resistance values for the two electrode configurations is shown in Figure 7.17. The set of testing conditions used have been presented in Table 7.4. Each current range and test time combination was tested over 10 repeats. The order of current range selection was randomised. The mean ± SD resistance values of the current ranges tested have been presented in Figure 7.14. Statistical analysis of each testing time was performed (one-tailed Student's t-test, n=5). Statistically lower resistance ($p < .01$) was found for Configuration 2 for all test times.

The two configurations were tested to see the influence of the reference electrode positioning. In particular, the maximum and minimum reference electrode spacing within the 30 mm footprint of the current carrying electrodes. Figure 7.17 indicates a general trend as expected, with an increased reference electrode separation showing a higher resistance. Scaling the resistance to the separation does not give a linear correlation, indicating a more complex current pathway within the system. Modelling of the system under different arrangements may offer some further insight into this finding. For the purposes of initial testing, the maximum separation was taken as the most suitable geometry due to delivering the largest resistance.

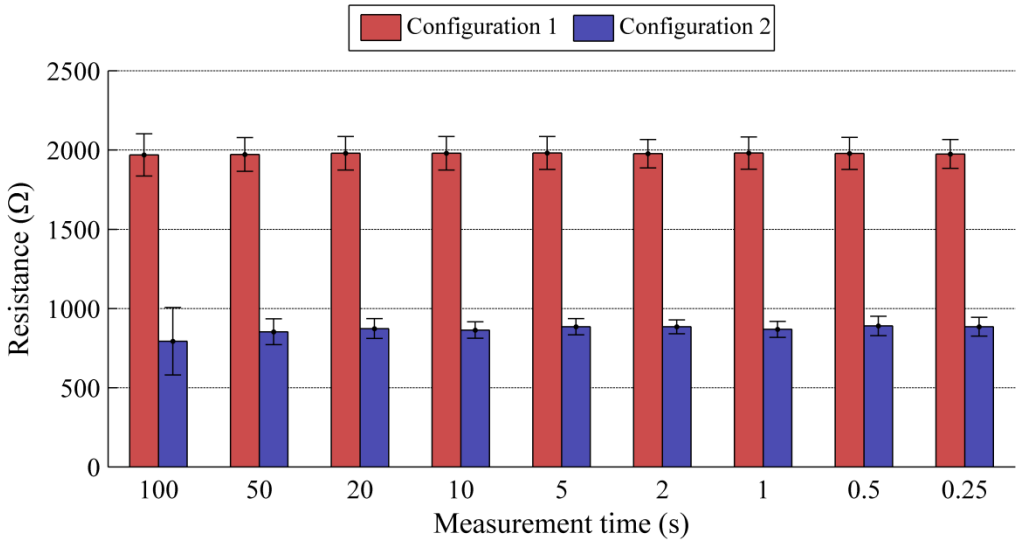

Figure 7.17: Average (mean ± SD) resistance characterised using two electrode configurations.

7.6.6 Tissue type variation

Acting as part of an instrumented laparoscopic grasper, measurements of tissue resistance have the potential to allow tissue identification aiding in the guidance and registration during MIS. The feasibility of using the method for tissue type differentiation was therefore investigated. Specifically, resistance variation between *ex vivo* porcine liver, colon and rectal tissue from a single animal was tested.

Tissues were contacted with the electrode cell under minimal strain as shown in Figure 7.6 and ten repeats of each specimen were taken. Measurement settings for all tests were:

- Current range: 10 μA
- Pre-test hold current: 3 μA
- Current switching rate: 6 μA/s
- Current step size: 6 μA
- Pre-test settling time: 5 s

The normalised ΔE against cell current values for all tests are shown in Figure 7.18(a). Linearity is shown with low variability induced across repeat measurements (shaded region). The gradients of each tissue type are shown to be distinct. Figure 7.18(b) summarises the mean ± SD (n=10) for each tissue type. A one-way ANOVA shows significant difference between the resistance of the different tissue types, $F(2, 28) = 1369$, $p < .01$. In order of increasing resistance, rectal, liver and colon tissues showed a range from 550-2300 Ω. A particularly distinct difference is shown between the colon and rectum

tissues, which may not be expected as they are anatomically connected. These tissues do however differ in muscle wall structure and thickness, with resistive differences previously reported [156]. In addition, it is possible that the relatively thin colon tissue may alter the current pathway under the electrode configuration tested, leading to an increased resistance. Detailed correlation of this resistance to the cellular structure of the tissues is beyond the scope of this chapter. However, the resistance values recorded are likely to be influenced by the fat content and salt concentration of the respective tissues. The significant difference shown between types in conjunction with the simplicity of the electrode materials and arrangement indicate suitability of the methodology to surgery.

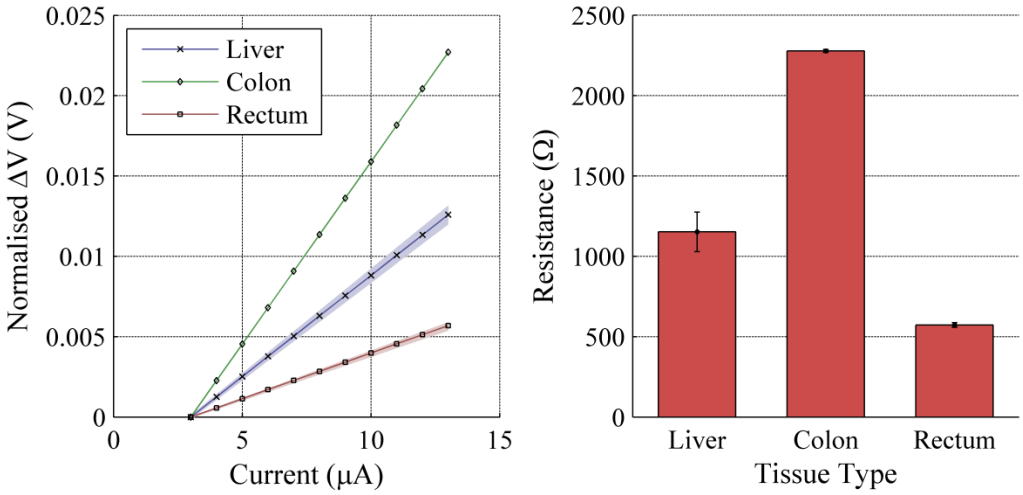

Figure 7.18: Results for *ex vivo* porcine liver, colon and rectum tissues showing (a) mean normalised measured voltage difference vs current (shaded region indicates range from repeats), and (b) mean calculated resistance ± SD (n = 10).

7.6.7 In situ investigation

Tissue measurements performed on *ex vivo* tissues allow for useful assessment of the measurement system performance. However, there is an assumption that the tissue is representative of the *in vivo* situation. To investigate the influence of tissue aging, application of the measurement technique to porcine colon tissue was performed *in situ*. Tests were conducted on a single male pig (~30 kg) under UK Home Office regulations for animal experimentation. The animal was given a terminal anaesthetic before a laparotomy being performed to expose a section of the mid colonic spiral. Electrode configuration 1 (Figure 7.16(a)) was clamped onto the tissue, as shown in Figure 7.19. Ten repeat tests were performed at three measurement rates and at three locations along the mid colonic spiral. The testing conditions for each measurement were:

- Current range: 120 μA
- Pre-test hold current: 3 μA
- Current switching rate: 12, 120 and 480 μA/s
- Current step size: 12, 120 and 120 μA in conjunction with the above switching rates respectively (corresponding measurement times of 10, 1 and 0.25 s respectively)
- Pre-test settling time: 5 s

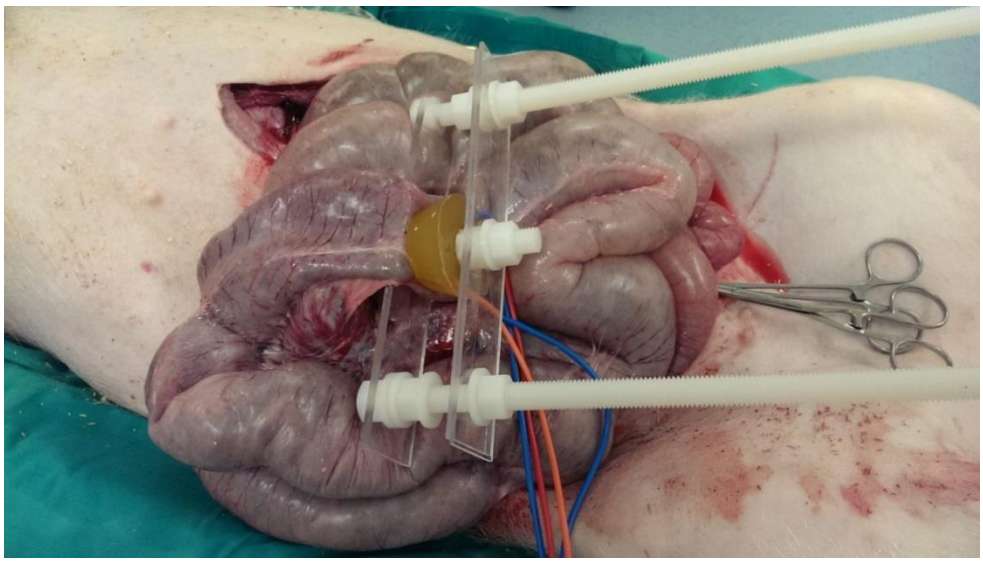

Figure 7.19: Image of *in situ* porcine testing of the mid colonic spiral, showing electrode configuration 1 clamped into test location 1.

The mean ± SD resistance values measured have been presented in Figure 7.20. It is evident that the values show a similar level of variability to *ex vivo* studies presented previously. Resistance values were all found to be below 800 Ω for *in situ* testing compared to values of above 2000 Ω typically found for *ex vivo* measurements. The lower resistance of the fresh tissue is in line with the findings of Haemmerich et al. [200] who suggest an increase in extracellular resistance over the first two hours post mortem. Sensitivity to measurement rate and tissue location was also examined, with the former showing no significant influence on the measured resistance. Tissue location 1 shows a significantly higher (two-tailed Stundent's t test, $p < .05$) resistance than measurements taken at locations 2 or 3. This indicates that there is variability within the same tissue type although a maximum difference of only 92 Ω (14.5%) was measured. A post mortem increase in resistance is also evident when individual repeats are analysed. Figure 7.21 shows the repeat measurements from each location as a function of repeat number. For all positions an increasing resistance trend is clear, again showing that variability measured is largely influenced by the tissue.

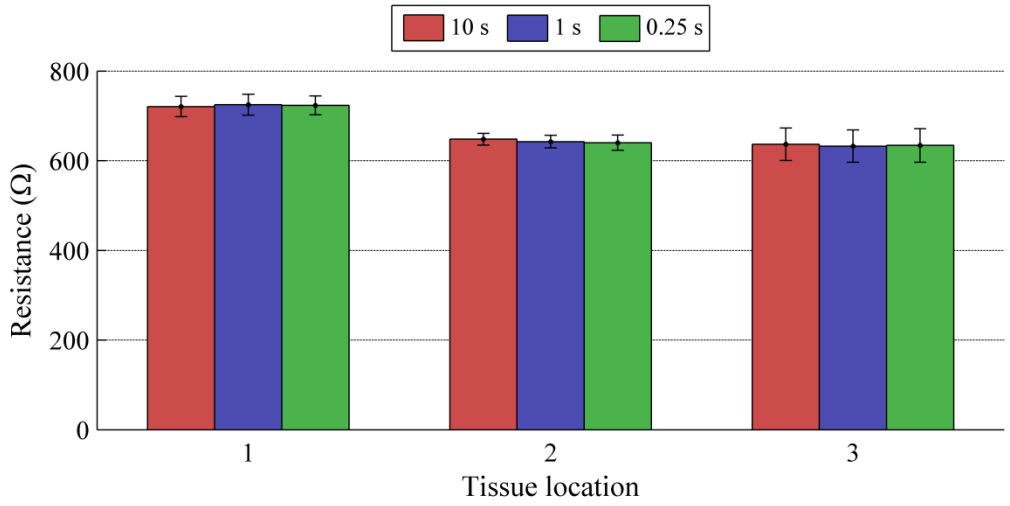

Figure 7.20: Average (mean ± SD) resistance values for three test locations measured at three measurement rates.

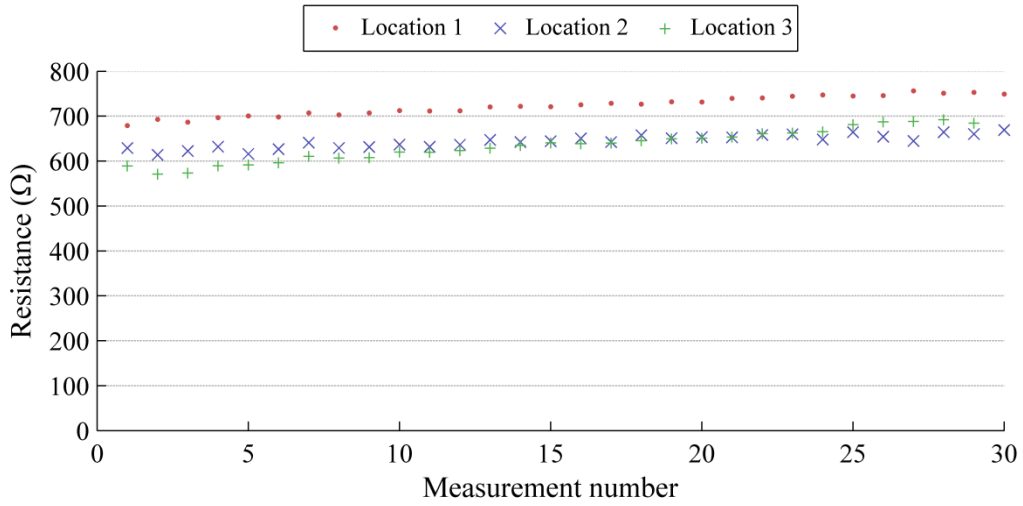

Figure 7.21: Resistance values for three *in situ* test locations as a function of measurement number; 10 s measurements shown only.

7.6.8 Summary

The parametric testing described in this section has been focused on addressing Objective 7.4. In general, the findings have repeatedly indicated that the measurement technique matches to the theoretical predictions of Section 7.4. Highly linear measurement responses have shown repeatedly for tests performed under similar conditions. A number of key findings from this section have been summarised as:

Measurement rate: *This parameter is essential for delivering a fast and therefore practical sensor. Tests presented in Section 7.6.3 illustrated the insensitivity of the technique to measurement rate. These*

findings have been consistently matched over other tests presented. Rates have been tested to deliver measurement times from 100-0.25s, with the lower limit being at the limit of the control system. Significant flexibility of this parameter is available for practical integration of the technique.

Current range: *As with measurement rate, the current range used is of practical importance for system integration of the technique. Findings from Section 7.5.1.2 suggest a complicated interrelationship between current range, measurement rate and tissue degradation (c.f. Figure 7.14 and Figure 7.15). However, the variation seen for current range remains low and is likely to be within the variation induced by time variation of the tissue. This should allow for safe current levels to be implemented for in vivo applications.*

Electrode geometry: *The measured resistance was proposed as being related to the relative positioning between the working and two reference electrodes. Results presented in Section 7.6.5 show the resistance to indeed be dependent on the reference electrode positioning. Reference electrode spacing was reduced from 20 – 5 mm which resulted in a 60% reduction in measured resistance. The relationship between spacing and resistance is complex and requires further investigation. However, for the two geometries tested, the technique independently produced consistent results.*

Tissue variation: *To assess the potentially influencing parameters, results were obtained from 6 different animals (5 ex vivo, 1 in situ). Ex vivo tests for colon resistance showed some variation between animals with a mean ± SD value of 2342 ± 444 Ω being obtained. Variability of this order was also found within the same animal (c.f. Figure 7.13). Significantly lower resistance values were found during a single testing session on colon tissue in situ. An average value of 668 ± 45 Ω was obtained in this case. At 71% lower, this indicates a significant alteration to tissue resistance as a function of time.*

Time drift: *Parametric testing has shown time to be the most influential ex vivo testing factor. The drift illustrated in Figure 7.12 is typical across measurements. A discussion of the potential causes for this has been presented in Section 7.6.2, with alterations to the tissue state being suggested as the main issue. It is apparent that following tissue death (cut of blood supply) the resistance rises for a time that coincides with ex vivo testing. This is therefore an important consideration for ex vivo testing, and should be a primary factor for investigation on tissues in vivo.*

7.7 Parametric investigation for surgery

With grasper based manipulations, surgeons will have a strong influence on the sensor configuration. As the surgeon conducts tasks, such as running the bowel, suturing, and retracting, the conditions at the tool-tissue interface are altered. From an electrochemical point of view, the interface is broken and re-established numerous times. The multi-reference system is based on some electrochemical assumptions (c.f. Section 7.4) and these may not be appropriate for a system under unstable conditions.

For a sensor to be integrated into surgical tools it is therefore necessary to consider the practical constraints on the sensing technology with a holistic view. For example, the measurements would ideally be fast and not create delays in the surgical procedure. Additionally, it is desirable to make a system with simple application and metrics to reduce the learning curve for the surgeon. Parametric testing presented in Section 7.6 was in many ways aimed at addressing some of these potential issues. However, to further the findings of this work, the performance of the multi-reference electrode system was investigated in the context of a surgical procedure.

7.7.1 The multi-reference electrode system in surgery

There are significant challenges in integration of a sensing modality into a useable surgical tool. However, prior to researching into overcoming these specific challenges, the sensing system can be evaluated with relation to the types of contacting conditions that would be experienced with suitable integration. As a simplistic view of the surgical environment, the sensor conditions can be broken down into three situations: (1) the sensor is not in contact with the tissue; (2) the sensor is in contact with the tissue but is not under test, i.e. no active modulation of current; and (3) the sensor is contacting the tissue and is under test, i.e.

current is being modulated. Figure 7.22 illustrates how these situations are represented within the surgical simulation system.

From analysis of the sensing system as these conditions are varied, the efficacy of the sensing technique can be established. For a system with slow settling time after being away from tissue contact, the surgical procedure would be significantly slowed when information from the sensor was desired. Conversely, if the sensor remains stable even with short settling times, then point-wise tissue characterisations could be performed during the routine manipulations of the tissue, minimising the impact on comportment.

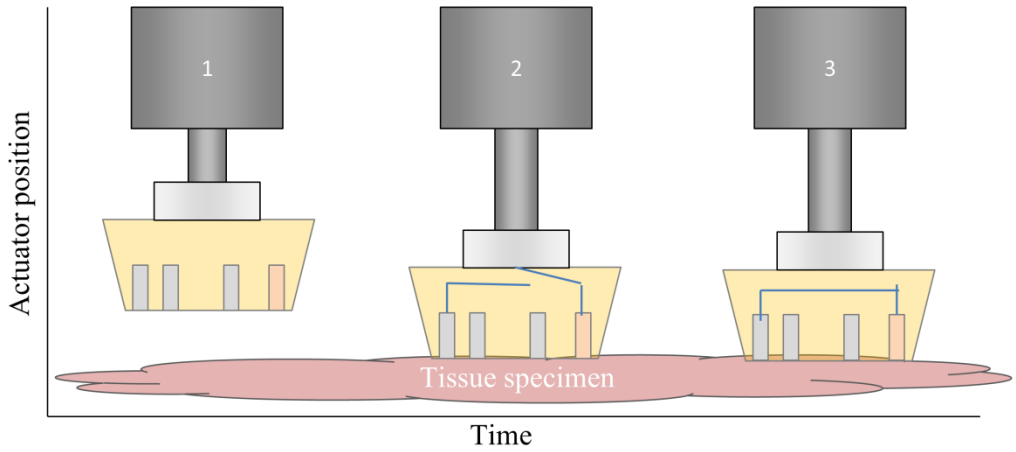

Figure 7.22: Potential contact conditions expected during a surgical procedure: (1) no contact with tissue, (2) contact with tissue with no active current control, and (3) contact with tissue with current modulation and resistance characterisation.

7.7.2 Surgical simulation system

To validate the sensing technique under surgical settings, a testing platform was developed. The aim of the testing platform was to allow for controlled variation over the following conditions:

- Tissue contact time
- Tissue contact load
- XYZ positional control of the electrode array
- Pre-test hold time (during tissue contact)
- Multi-reference galvanostatic testing conditions (current range, rate)
- Configurable repetition of test set
- Data logging, including test configuration and positional data

Table 7.5 describes the various elements of the developed system. These were integrated as shown in Figure 7.23.

Table 7.5: Details of the sub-system components involved in the surgical indentation platform.

System components	Description
Linear actuator (SMAC LCA25-010-55-1 & LCC11 controlled, SMAC Corporation, California USA)	Linear actuator with 10 mm range at 5 μm resolution. Configured through SMAC Control Center software & a bespoke LabVIEW interface (developed at the University of Leeds, UK).
XY stage	Stepper motor controlled XY stage offering linear resolution of ~0.1 mm over 150 x150 mm area. Interface circuity and software designed at University of Leeds, UK.
Multi-reference electrode characterisation system	Described in detail in Section 7.5. Integrates the Ivium CompactStat (Ivium Technologies), NI myDAQ (National Instruments), and custom software (adjusted to function as part of the indentation system.
Integration software	Developed to control the aforementioned subsystems, and allow data to be recorded for tests. Section 7.7.2.1 describes the developed software in detail.

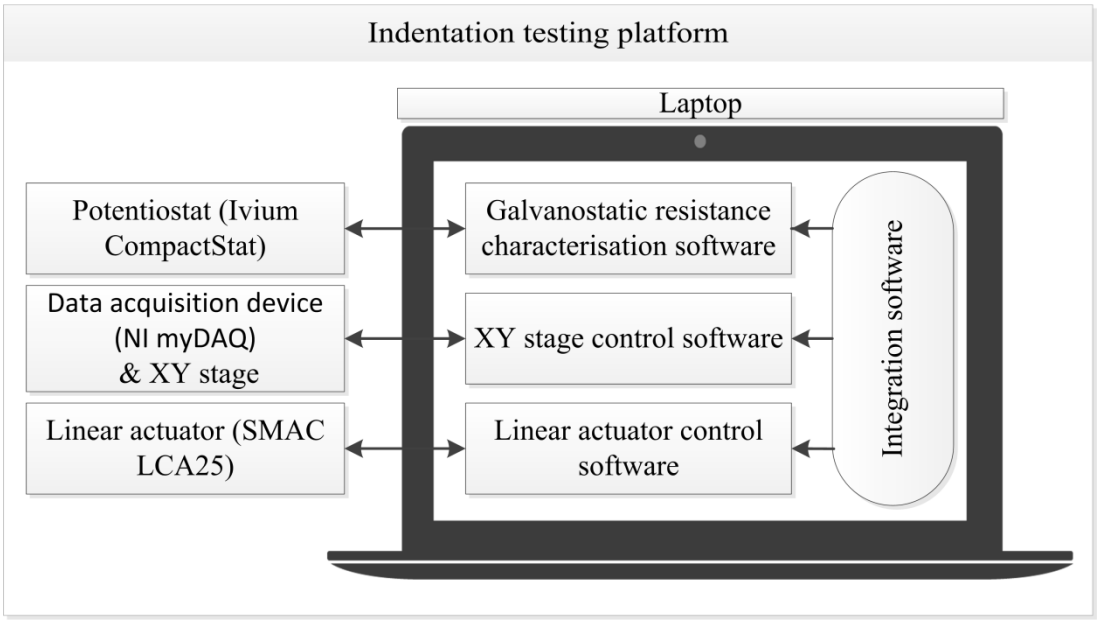

Figure 7.23: Schematic overview of the various sub-systems involved in the surgical indentation testing platform.

7.7.2.1 Software

To practically make multi-reference electrode measurements as a function of the electrode position/contact conditions, a software architecture utilising an adjusted version of the software described in Section 7.5.1.4 was employed as shown in Figure 7.24. The integration software was developed in conjunction with a summer internship project managed as part of the PhD programme.

7.7.2.2 System specification

The final system developed can be seen in Figure 7.25(a) with the electrode-tissue contact shown in Figure 7.25(b). The associated software front panel is shown in Figure 7.25(c).

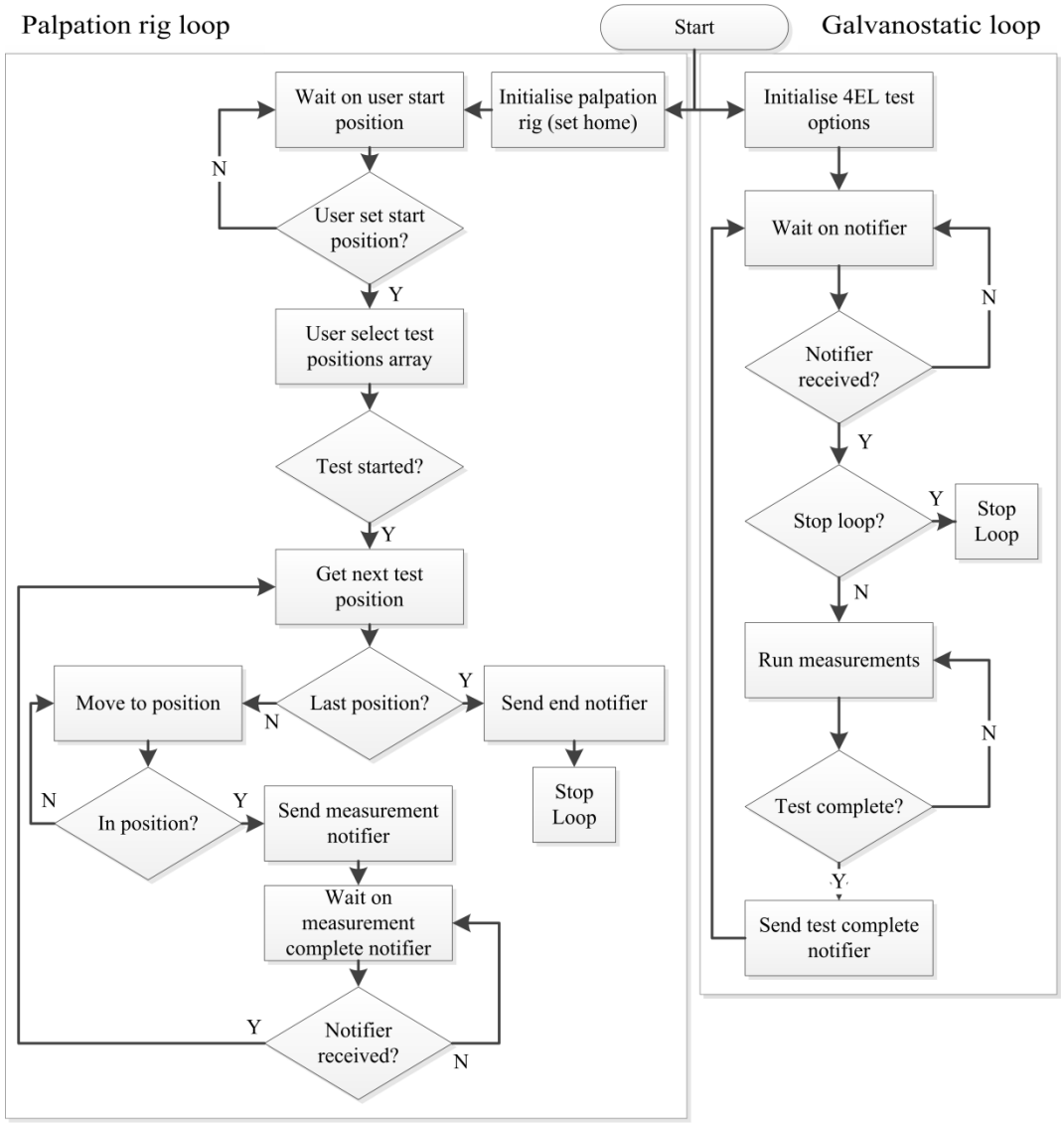

Figure 7.24: Simplified software flowchart for the integration of the multi-reference electrode galvanostatic resistance characterisation technique into the surgical indentation system.

The developed system was utilised for investigation as described in the following section. For each experiment the system allows:

- Calibration of the XY stage.
- Adjustment of the starting (0, 0) position.
- Selection of the desired test positions.
- Selection of the number of positional repeats.
- Configuration of the multi-reference electrode characterisation settings for each positional repeat.
- Selection of the number of repeats of each of the selected characterisation settings for each location.
- Adjustment of the down position of the actuator.
- Adjustment of the off-time (non-contact) between positions.

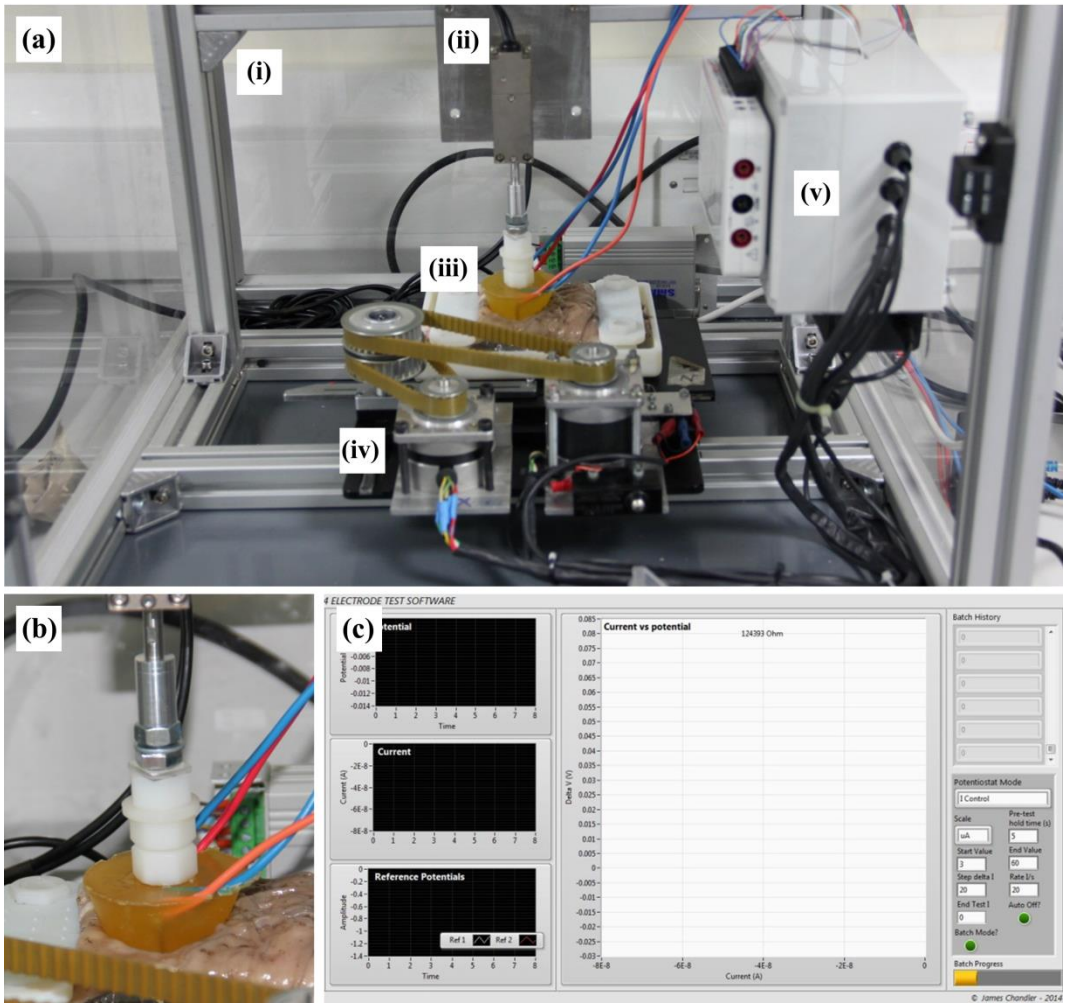

Figure 7.25: Indentation testing platform, showing (a) tissue indentation rig with (i) structural frame, (ii) SMAC actuator, (iii) indented electrode and tissue specimen holder, (iv) XY stage, (v) stepper controller electronics and DAQ device; (b) close-up of electrode-tissue contact; and (c) front panel of indentation testing software.

7.7.3 Experimentation

The design and use of the surgical simulation system served two primary aims: (1) to gain an understanding of the influence of the contact conditions on the four electrode measurement, and (2) to deliver information relating to the spatial variation of tissue resistance, and the spatial repeatability of the four electrode system. In addition, the system offers and effective platform for obtaining qualitative information relating to the technique.

7.7.3.1 Experiment 1: Influence of contact conditions

An initial experiment was conducted to assess the influence of the contact conditions on the repeatability of the multi-reference galvanostatic measurement technique. In accordance with the conditions illustrated in Figure 7.22, examination was made into the effect of making and breaking of the contact conditions.

7.7.3.1.1 Methodology

A single piece of *ex vivo* porcine rectum tissue was opened and mounted into the testing tray to present the mucosa surface to the testing probe. A four electrode probe (Configuration 1, Figure 7.5) was mounted onto the linear actuator and the system configured to apply a constant load to the tissue for each position tested. This was achieved through setting the maximum force output of the actuator to 5N and arranging the geometry to cause the actuator load limit to be tripped in attempt to reach the target depth.

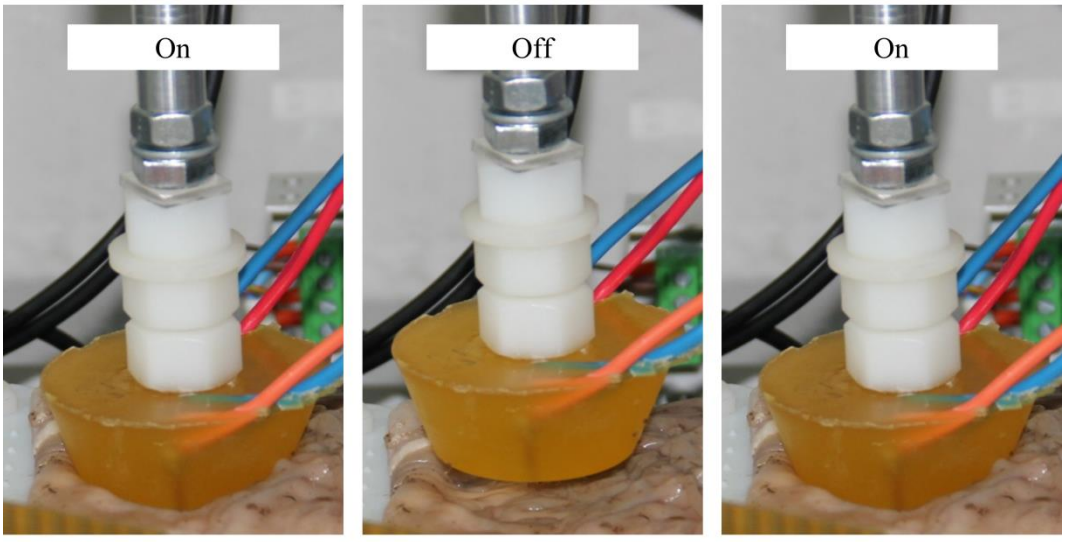

Figure 7.26: Electrode-tissue contact conditions realised during testing showing the contact (On), non-contact (Off) and re-contact (On) positions.

The contacting conditions illustrated in Figure 7.22 were assessed as part of the study. Two off-time situations (10 s and 60 s) were tested and four on-time values were configured (1, 10, 30 and 60 s) for each. The order of test configurations was randomised and the test location held constant throughout the experiment. A total of twenty repeats were performed for each test configuration. Figure 7.26 illustrates the non-contact and contact conditions achieved during the experiment. For each resistance characterisation, the following test settings were employed:

- Current range: 180 µA
- Pre-test hold current: 3 µA
- Current switching rate: 18 µA/s
- Current step size: 18 µA
- Pre-test settling time: varies to match the on time values of 1, 10, 30 and 60 s used.

7.7.3.1.2 Results & discussion

Average (mean ± SD) resistance values obtained for each combination of off-on time have been presented in Figure 7.27. It is evident that there are significant changes in the average resistance values with alteration of these conditions. Of particular interest is the level of variation seen for each of the test configurations. Figure 7.28 shows the standard deviation as a percentage of the mean resistance for the range of test conditions. This clearly shows that there is a much larger variation for the 1 s on time tests. This would be expected as this represents the minimum settling time for the system prior to measurement.

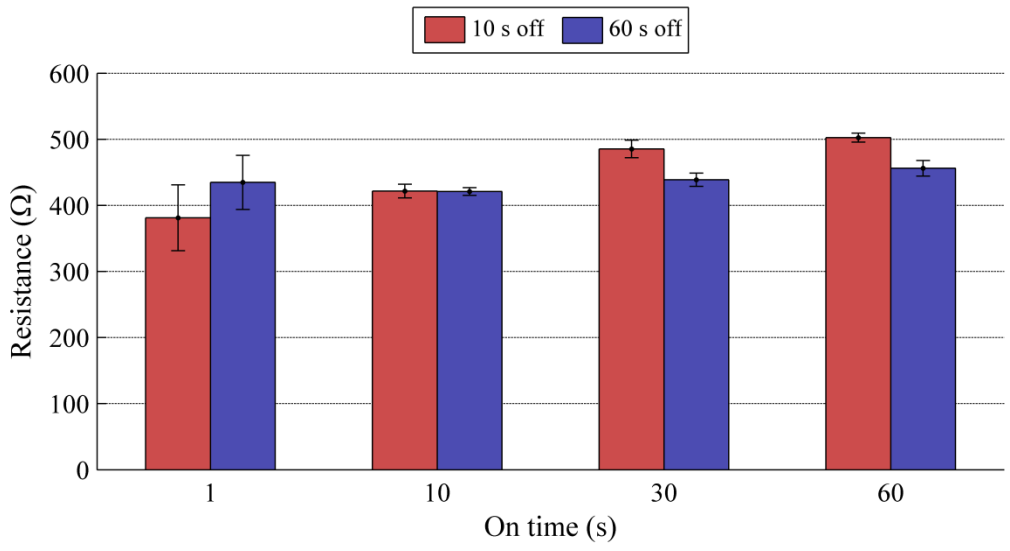

Figure 7.27: Average (mean ± SD) characterised resistance values for varied off-on time conditions during porcine rectal mucosa indentation (n=20).

No particular trend is apparent between the two off-times tested. However, the longer off-time delivers a more consistent average resistance across all on-times tested. An increased off-time would be expected to cause greater electrode drift and therefore increase the length of on-time required to achieve a stable measurement. It is therefore suggested that these findings are as a result of other factors. Specifically, the tissue time drift in conjunction with the testing order is proposed as the cause of this result. Figure 7.29 shows the measured resistance values as a function of measurement number. It is evident that the second half of testing (60 s off time) produced more stable measurements with a slow drop in resistance with time. This is consistent with the time influence seen in previous *ex vivo* testing.

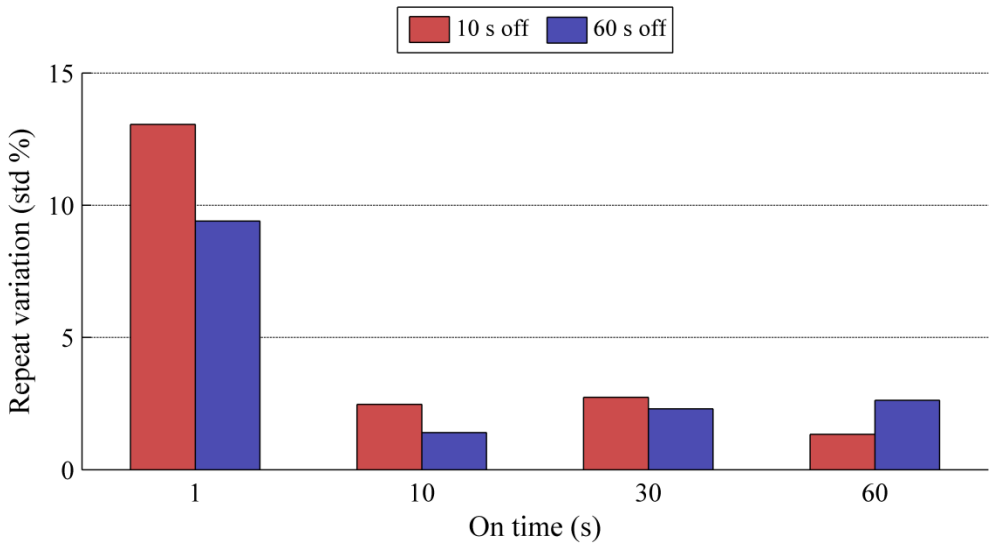

Figure 7.28: Variation within repeats calculated as percentage of standard deviation for varied off-on time conditions during porcine rectal mucosa indentation.

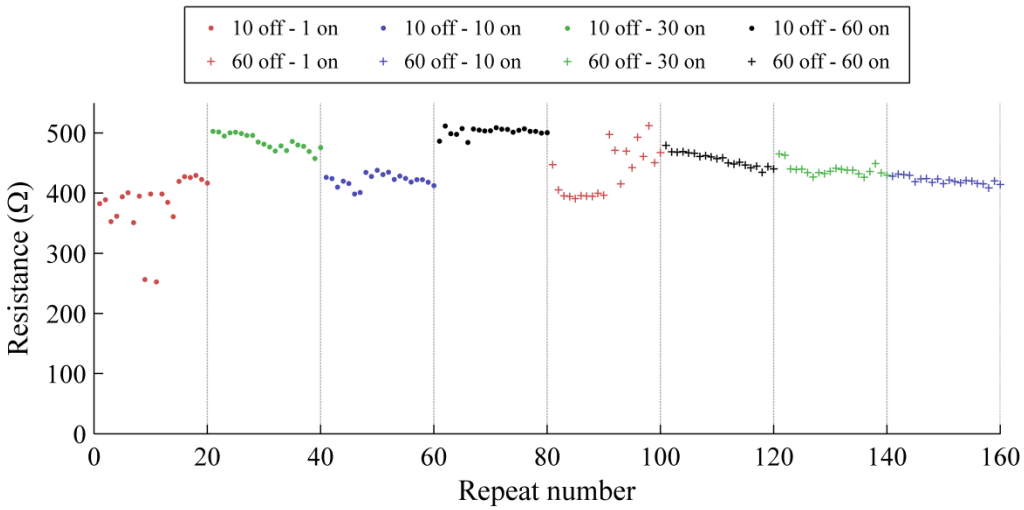

Figure 7.29: Resistance values determined as a function of measurement number for the off-on time conditions tested.

7.7.3.2 Experiment 2: Spatial variation of tissue resistance

As part of a surgical application, it may be necessary or desirable to map the resistance profile of a tissue region. A second experiment was therefore conducted to assess the variation in resistance over a tissue surface using the multi-reference galvanostatic measurement technique.

7.7.3.2.1 Methodology

The indentation rig was loaded with porcine rectum tissue with the mucosa exposed to the end effector. A four electrode probe in Configuration 1 (Figure 7.5) was attached to the rig and the system calibrated to a desired starting position. Figure 7.30 shows the tissue surface mounted in the testing tray with the positions of the testing sequence overlaid. A total of 28 test positions were used, forming a 7x4 grid with 10 mm separation between each point. The resistance was measured sequentially at each of the locations in the order indicated in Figure 7.30. This sequence was repeated to give 20 repeats for each location. The four electrode test was configured with a 2 second off-time and the following test configuration:

- Current range: 120 μA
- Pre-test hold current: 3 μA
- Current switching rate: 24 μA/s
- Current step size: 24 μA
- Pre-test settling time: 5 s

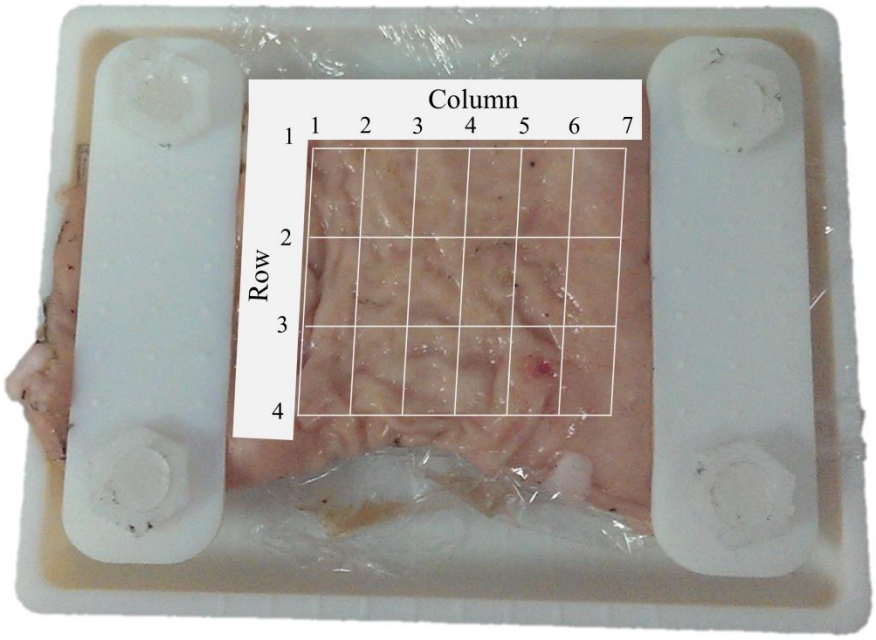

Figure 7.30: Test sample (opened rectum mucosa) mounted into the test tray with test position order over a 7x4 grid at even 10 mm spacing.

7.7.3.2.2 Results & discussion

To assess the influence of time on the measured resistance all measurements were plotted as a function of sample number, as shown in Figure 7.31. The data show a slight decrease in resistance with time, although the effect is smaller than found for other studies. This decline, although slight, will contribute to the variability seen for each position.

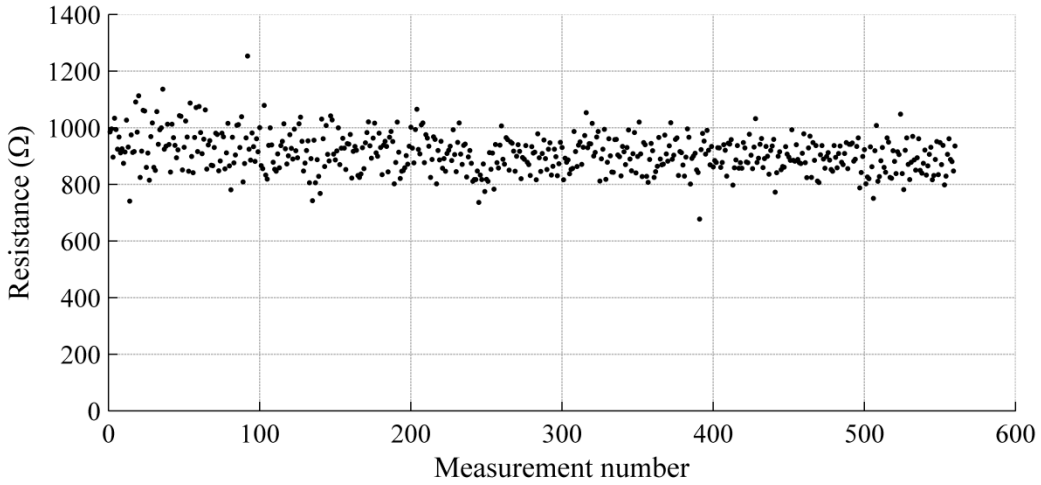

Figure 7.31: All measurement points as a function of measurement number for resistance mapping of rectal tissue specimen.

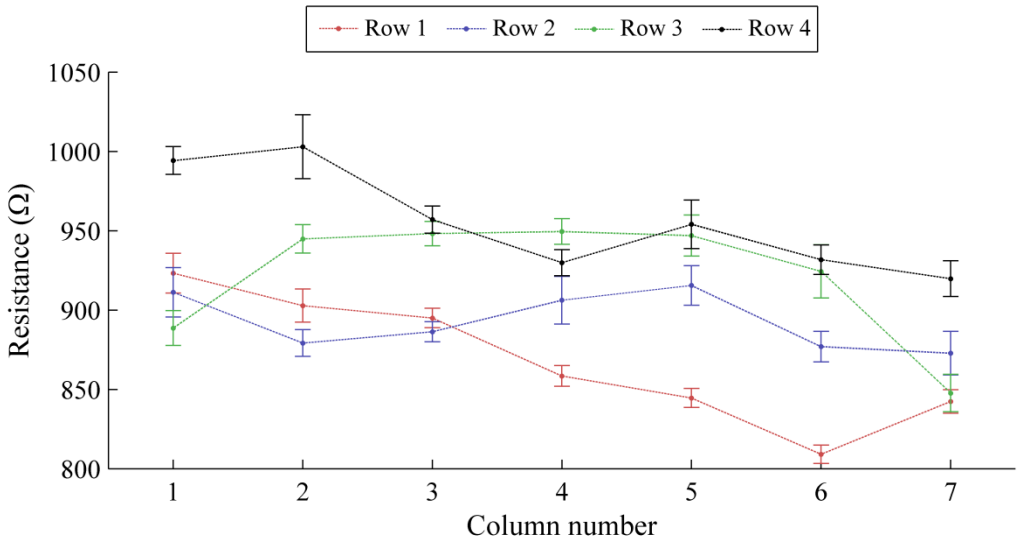

Figure 7.32: Average resistance ± SE for spatial positions across rectal tissue, demonstrated as test rows.

Resistance values were collated for each position and sorted into rows in accordance with Figure 7.30. The average (mean ± SE) values for each position are presented in Figure 7.32. Assessment of the tissue from left to right (as depicted in Figure

7.30) shows a decreasing resistance across all rows. This is also evident when moving from bottom to top of the tissue, and can be seen within the surface map presented in Figure 7.33. These findings showed qualitative correlation to the tissue thickness, although no quantitative evidence for this was recorded.

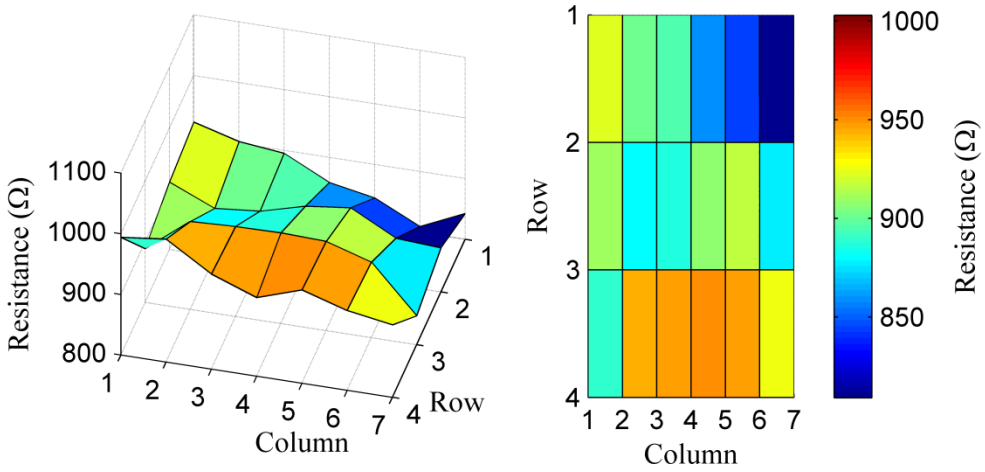

Figure 7.33: Surface distribution of average resistance values measured over the tissue surface; top-down view also shown.

In general, the grouping of the data for each position is quite tight, as illustrated with the small error bars in Figure 7.32. The small variation of each location indicates that the technique gives repeatable readings even with breaks in contact and tissue temporal variation. Based on the average resistance measurements, there is little variation with position (~ 20% across all tests). This would be expected for a small section of rectum mucosa. Tight grouping of measurements on healthy mucosa is imperative if subtle differences in resistance, caused by disease are to be discriminated.

7.8 Chapter Summary

The electrochemical theory reviewed as part of Objective 7.1 was used in the chapter to develop and describe the theory of a new DC resistance measurement technique. The multiple reference system is based on independent assessment and comparison of electrode polarisation from two independent reference electrodes. This method allows for subtraction of the electrode polarisation artefacts from the measured data and therefore isolation of a tissue resistance. Details of the technique are presented in Section 7.4 and relate to Objective 7.2. To meet the requirements of Objective 7.3, a testing system was developed allowing measurements to be made in line with the proposed theory. Details of the developed system are contained in Section 7.5.

Initial testing using this technique has shown higher linear data in line with theoretical expectation. Initial parametric investigation (Objective 7.4) assessed the system sensitivity to measurement rate, current range and geometry. Findings indicate that this parameters cause minimal influence of the characterised resistance, making the system flexible for application specific testing.

Variation with tissue type was found for tests on *ex vivo* tissues, and the influence of time drift was demonstrated. The exact cause of this phenomenon remains uncertain, although probable causes are tissue death, hydration levels and temperature fluctuations. Testing protocols were investigated with a focus on surgical relevance. The final chapter objective (7.5) was met through testing under simulation of the contact behaviour expected during surgical tool interaction. Contacting on and off time generally showed little influence on the measured resistance, although increased variation was found for the shortest on-time (1s). There may therefore be some practical considerations for surgical implementation of the technique, although the system is broadly applicable under the current configuration.

Chapter 8
Testing for tissue health (colorectal cancer)

The work of Chapters 7 presented a new DC resistance measurement technique. Initial parametric testing demonstrated the ability of the system to measure resistance with high repeatability and showed insensitivity to measurement rate and current range. The singular focus of this chapter is to apply this technique to healthy and diseased human tissues to determine if resistance (measured with the technique) is health specific for colorectal cancer.

Testing presented was conducted on fleshly excised human colon samples containing a cancerous element. A continuation of parametric investigations into measurement rate and current range has also included in this chapter. Results indicate a clear and consistent difference between tissue type (healthy vs diseased mucosa) and measured resistance. In each of the six test cases presented, the diseased element was found to be significantly ($p < .01$) lower than the corresponding healthy region. These findings were repeated across a range of measurement rates (10, 1 and 0.25 s) and current ranges (60 and 180 μA). Qualitative comparison of resistance results to histopathology slides indicates a potential correlation between resistance and tissue morphology. These findings are encouraging for the application of this sensing modality into laparoscopic tools for colorectal cancer surgery.

8.1 Testing aims

The primary aim of the presented testing is to apply the multi-reference galvanostatic polarisation tissue resistance measurement technique to human diseased tissue. It is an additional aim to investigate some of the potentially influencing parameters on human tissues and to make comparisons to previous porcine results. The associated chapter objectives are:

Objective 8.1: *To apply the galvanostatic polarisation resistance characterisation technique to heathy and diseased human colon tissues.*

Objective 8.2: *To assess and compare the resistance values between healthy and diseased tissues.*

Objective 8.3: *To explore the influence of time drift, measurement rate and current range on ex vivo human tissues.*

Objective 8.4: *To make comparisons between human testing and previous tests conducted on ex vivo porcine tissues.*

8.2 Resistance testing

Tissue resistance measurements using the multi-reference galvanostatic polarisation technique were performed on *ex vivo* human colon tissues immediately following surgical resection. The aims of the testing have been outlined in Section 8.1, with a primary interest being assessment of the resistive difference between healthy and disease colon mucosa. A total of six cases were assessed over a six month period. This section details the methodologies employed throughout the collation of this data.

8.2.1 Method

It is important to note that significant practical constraints were placed on the measurement procedure during these tests due to the surgical (hospital) environment and as testing is essentially an interruption to the normal flow of tissue processing. For this reason the methods presented may not appear ideal from a scientific perspective. Justification for the setups used has been given where appropriate.

Freshly excised human colon tissue was obtained in accordance with NHS and Leeds University Teaching Hospital Trust ethics procedures. Each tissue specimen was removed as part of a standard surgical procedure, with subsequent histopathology being performed after testing. Immediately following resection, the colon samples were moved from theatre into a rear room for testing with the measurement electrodes.

All testing was conducted with a single electrode configuration. Four 1 mm diameter electrodes (1 copper and 3 zinc) were set into non-conducting resin (Varidur™, Buehler, USA) with a geometric arrangement of Configuration 1 shown in Figure 7.16(a). The exposed electrode faces were wet ground to 1200 grit and rinsed with distilled water prior to testing each sample. Control of the current between the working and counter electrodes was performed using a commercial potentiostat (CompactStat, Ivium Technologies). This was configured to operate galvanostatically, thereby inducing electrode polarisation through control of the cell current. The potential differences between working and reference electrodes were recorded using a standard data acquisition device (NI myDAQ, National Instruments). Custom software (LabVIEW, National Instruments) was used to allow synchronisation, measurement and control of the system. The details of this measurement system have been given in Section 7.5. Current and voltage data from the system were recorded at 10 Hz.

The hospital environment was found to induce increased noise into measurements (compared to laboratory testing) due to the large number of active devices. As such, and based on initial testing in this environment, the current range of 3-13 µA was deemed too low for optimal assessment of tissue resistance. Therefore a higher current range was selected for standard measurements; described within Section 8.2.1.2.

8.2.1.1 Measurement locations

For the primary test locations, electrodes were clamped onto either healthy mucosa or the diseased element as shown in Figure 8.1. It was an experimental aim to clamp the electrodes under minimal strain, although maintaining contact with the heavy, slippery tissue often necessitated increased clamping load. This was assumed to not influence the measured resistance.

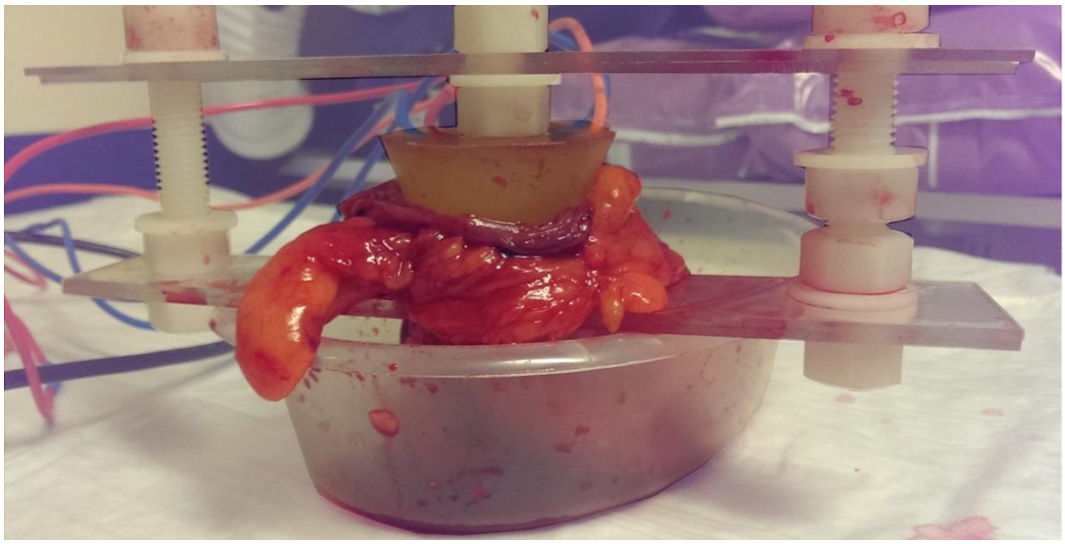

Figure 8.1: Electrode set clamped onto rectal mucosa during resistance measurement.

Due to the limitations on testing time these two locations were measured first across all investigated measurement conditions. However, when additional time was available, other tissue regions were also measured such as the serosa. Where possible, each tissue region was tested over 10 repeats. The voltage-current response for the electrodes was characterised using a linear regression fit (LabVIEW, National Instruments) to define the tissue resistance. A statistical comparison (independent samples t-test) of the tissue types (healthy vs diseased) was subsequently performed to establish if resistance is specific to the tissue type tested.

8.2.1.2 Measurement conditions

As part of the general parametric investigation into the sensing modality, a range of measurement settings were employed during health discrimination testing. The influence of these is discussed in detail in Section 8.3. These measurement settings were divided into: (1) standard settings for making tissue health comparison, (2) additional measurement rate settings and (3) additional current range settings. Due to the variable time constraints for testing, these were prioritised in the presented order. The standard measurement settings were:

- Current range: 60 μA
- Pre-test hold current: 3 μA
- Current switching rate: 6 μA/s
- Current step size: 6 μA
- Pre-test settling time: 5 s

The above settings result in a 10 s measurement time. When additional measurement rate settings were employed, the configuration was adjusted to deliver 1 s and 0.25 s tests with 5 and 2 data points respectively. For example, a 1 s test at 60 μA was achieved through a 60 μA/s switching rate at a 15 μA step size. When measurement rate testing was applied, an oscillating order was employed to minimise any influence of time drift. Adjustment to the current range was also evaluated through the addition of a 180 μA current range. Rate and step size settings were adjusted to achieve consistent measurement times under this current range. The cases presented were tested under all of these measurement conditions unless otherwise stated.

8.2.2 Case descriptions

As each test specimen was a different patient case, and therefore may have significant variation in disease type, stage and location among other factors, this section has been included to describe each individually. The following information was collated from the details of the

Histology/Cytology Report as well as testing notes. Table 8.1 details each case independently, and should be used as reference for the presented results.

Table 8.1: Human colon test case details including histopathology report references.

Case no.	Histology / Cytology Notes
1	- *Right hemicolectomy* - *Caecal cancer* - *Polypoid & exophytic tumour* - *Adenocarcinoma (T4)*
2	- *Synchronous mid rectal cancer and adrenal tumour* - *Anterior resection and left adrenalectomy* - *Adenocarcinoma (T1)*
3	- *Low anterior resection* - *Preoperative radiotherapy* - *Rectal cancer* - *Polypoid tumour* - *Adenocarcinoma (T1)*
4	- *Low anterior resection* - *Long course chemoradiotherapy* - *Mid rectal cancer* - *Adenocarcinoma (T3)*
5	- *Right colon* - *Located within appendix* - *Mucinous tumour* - *Adenocarcinoma (T3)*
6	- *Anterior resection* - *Long course chemoradiotherapy* - *Upper rectal cancer* - *Adenocarcinoma*

8.2.3 Results

This section summarises the results obtained for each test case (as described in Table 8.1). Descriptions have been separated into cases to allow separate assessment and analysis, although a summary of all of the results has been given in Section 8.2.3.7.

8.2.3.1 Case 1

A total of ten repeat measurements were obtained for healthy mucosa and diseased mucosa tissue regions under varied measurement rate only. Table 8.2 presents the average resistance measurements obtained for these measurements.

Table 8.2: Average (mean ± SD) resistance values (Ω) for case 1 tissue regions for all measurement conditions; test time (s) shown with current range (μA) in parentheses.

Tissue region	10 (60)	1 (60)	0.25 (60)
Healthy mucosa	389 ± 20	402 ± 24	375 ± 13
Diseased mucosa	317 ± 9	322 ± 15	312 ± 10

The average resistance values characterised for each tissue region have been presented within Figure 8.2. For the primary measurement case (Δt = 10 s, ΔI = 60 μA), the healthy mucosa was on average (M=389, SD = 20 Ω) found to be higher than the cancerous mucosa (M= 316, SD = 9 Ω). This difference, 72 Ω, CI[58, 87], was highly significant t(18) = 10.4, p < 0.01; this represented a large-sized effect, d = 3.6. A statistically significant difference was also found between healthy and cancerous mucosa for all other measurement configurations.

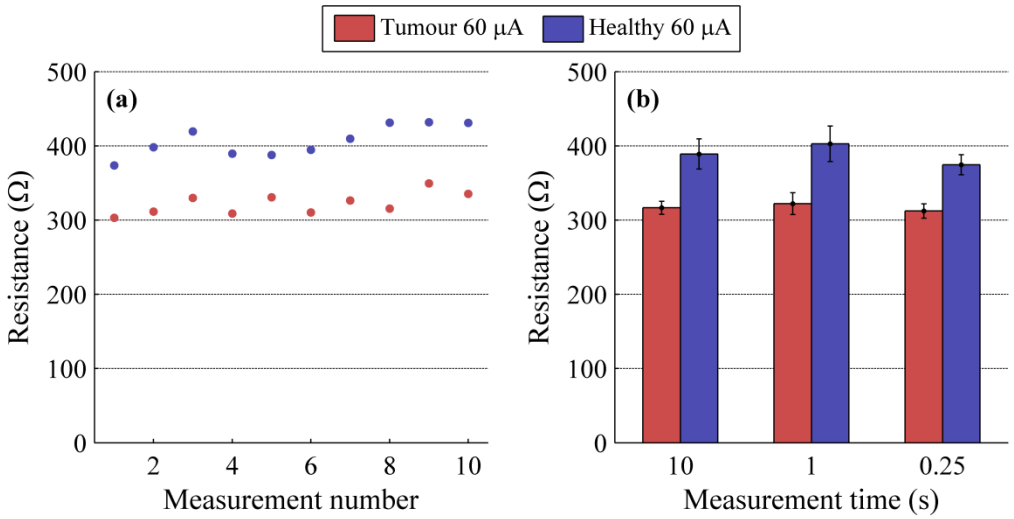

Figure 8.2: Case 1 data, showing (a) repeated measures for healthy and cancerous mucosa (tumour) (10 s measurement and 60 μA current range results shown), and (b) mean ± SD characterised resistance for tested tissue regions under varied measurement conditions.

Histology slides for the resected sample, showing a healthy reference region and a cross-section of adenocarcinoma, have been presented in Figure 8.3. The cancerous region (Figure 8.3 (b)) shows growth through multiple layers of the caecal tissue. The pathology report indicates an invasion level of T4 (c.f. Figure 2.2). Partial calcification was also noted within cancerous polyp.

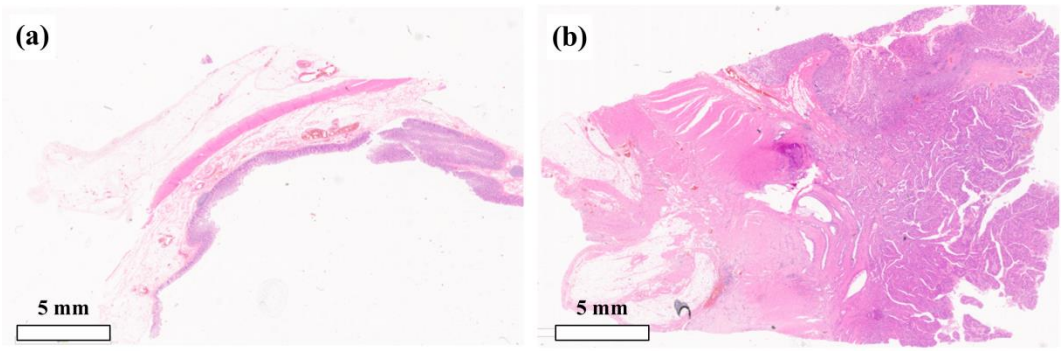

Figure 8.3: Case 1 micrograph sections of (a) normal tissue region (original magnification x0.5, hematoxylin-eosin [H-E] stain) and (b) polypoid tumour (original magnification x0.5, hematoxylin-eosin [H-E] stain); arrows indicate tumour region.

8.2.3.2 Case 2

A total of ten repeat measurements were obtained for healthy mucosa, diseased mucosa and serosa tissue regions under each measurement condition. The healthy and diseased tissue locations within the specimen have been presented in Figure 8.4. Table 8.3 presents the average resistance measurements obtained for these tests. Typical raw measured data and linear fitting are shown in Figure 8.5.

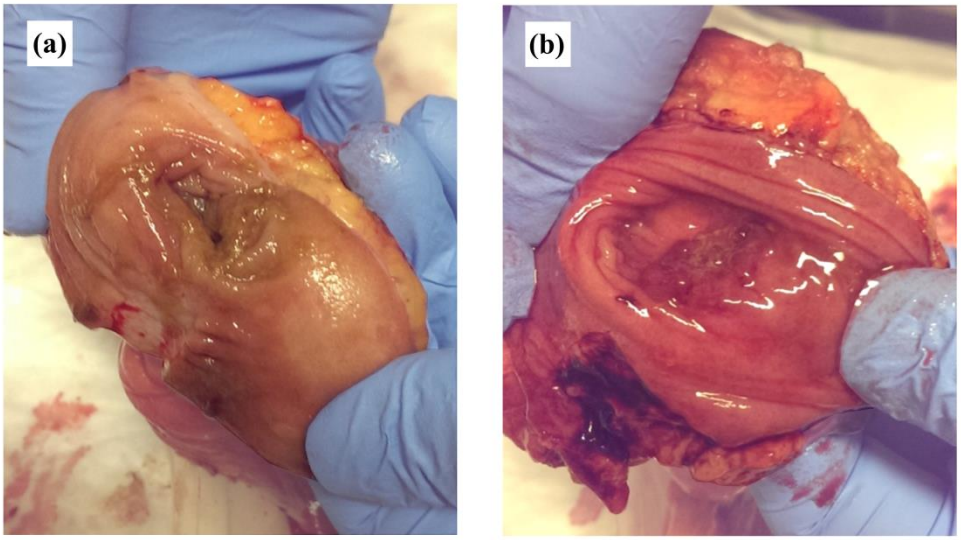

Figure 8.4: Image of case 2 tissue specimen, showing (a) healthy mucosa and (b) diseased region.

The average resistance values characterised for each tissue region have been presented in Figure 8.6. For the primary measurement case (Δt = 10 s, ΔI = 60 μA), the healthy mucosa was on average (M=374, SD = 6 Ω) found to be higher than the cancerous mucosa (M= 244, SD = 11 Ω). This difference, 130 Ω, CI[122, 139], was highly significant t(18) = 33.2, $p < 0.01$; this

represented a large-sized effect, d = 21.7. A statistically significant difference was also found between healthy and cancerous mucosa for all other measurement configurations.

Table 8.3: Average (mean ± SD) resistance values (Ω) for case 2 tissue regions for all measurement conditions; test time (s) shown with current range (μA) in parentheses.

Tissue region	10 (60)	10 (180)	1 (60)	1 (180)	0.25 (60)	0.25 (180)
Healthy mucosa	374 ± 6	358 ± 9	376 ± 6	360 ± 6	378 ± 6	360 ± 6
Diseased mucosa	244 ± 11	214 ± 10	233 ± 7	217 ± 6	231 ± 10	217 ± 7
Serosa (fatty)	821 ± 30	726 ± 25	837 ± 33	744 ± 28	823 ± 36	749 ± 30

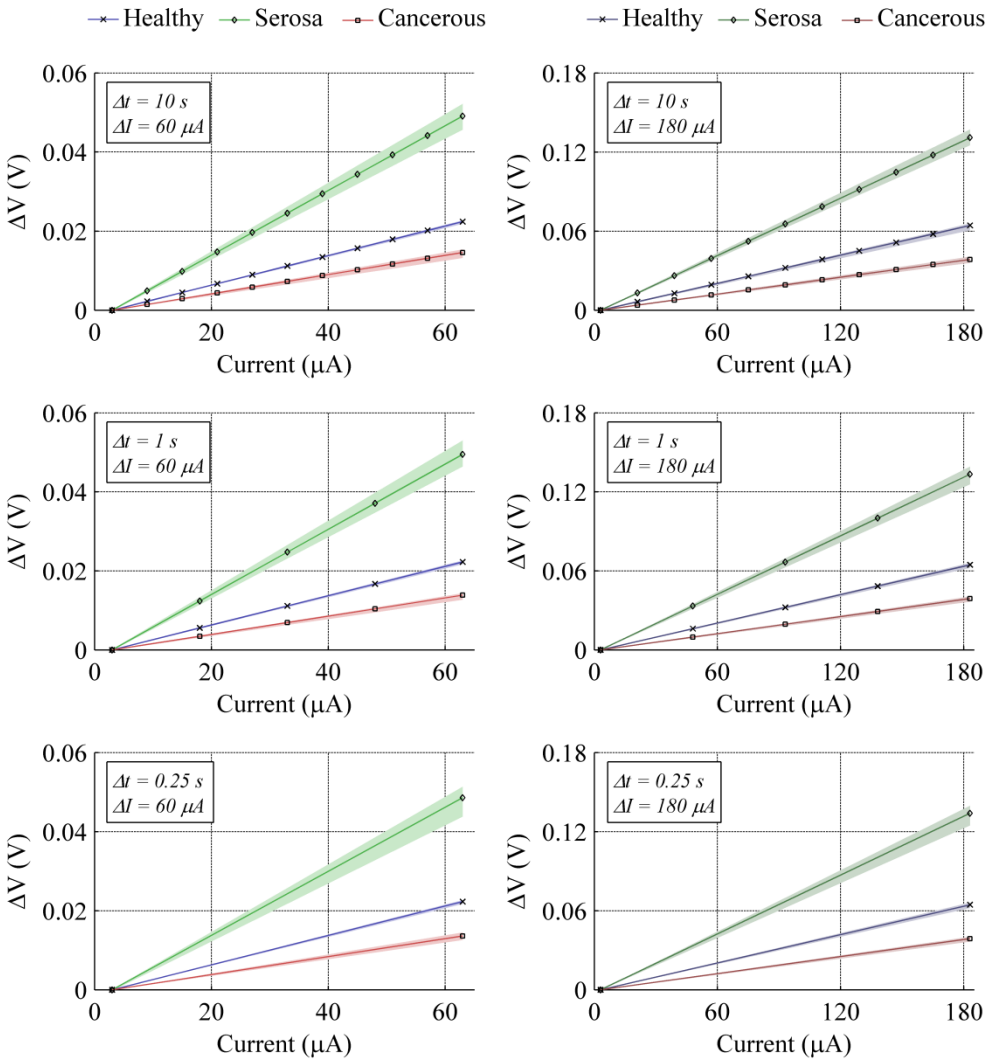

Figure 8.5: Mean measured data and characterisation fits for each tissue region for case 2 under varied test time (*Δt*) and current range (*ΔI*); shaded regions represent the full range of characterisations over all repeats (n = 10).

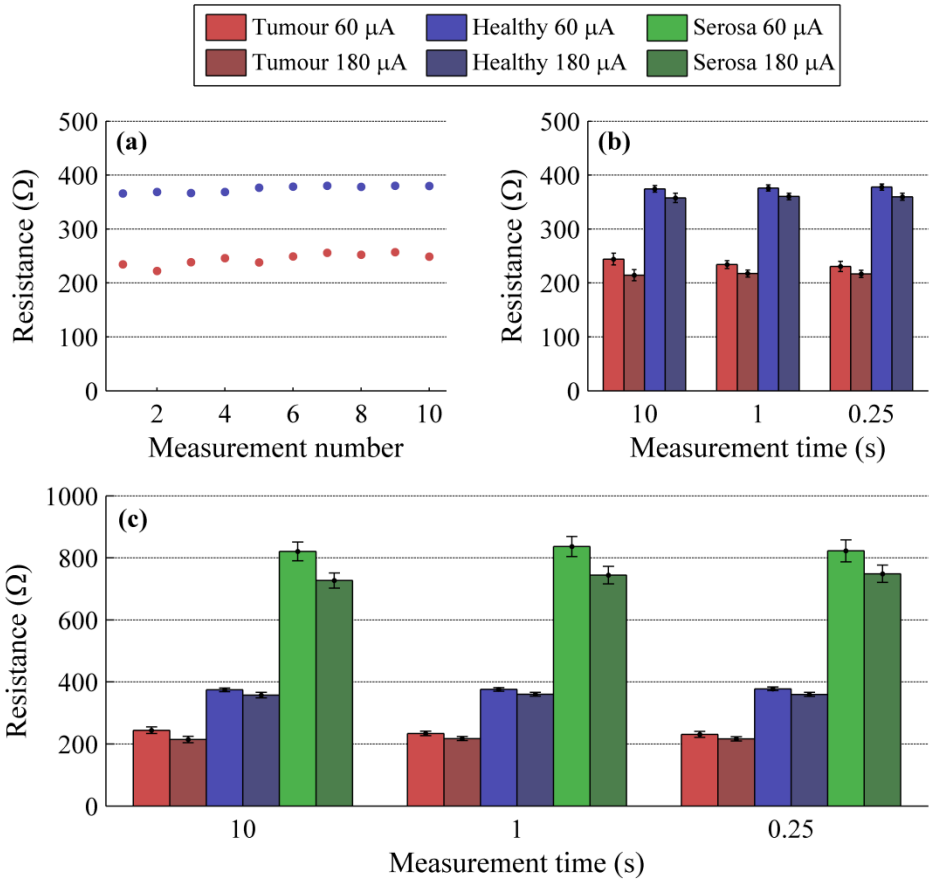

Figure 8.6: Case 2 data, showing (a) repeated measures for healthy and cancerous mucosa (tumour) (10 s measurement and 60 µA current range results shown), and mean ± SD characterised resistance for tested tissue regions under varied measurement conditions, showing (b) healthy and cancerous mucosa and (c) all tissue regions.

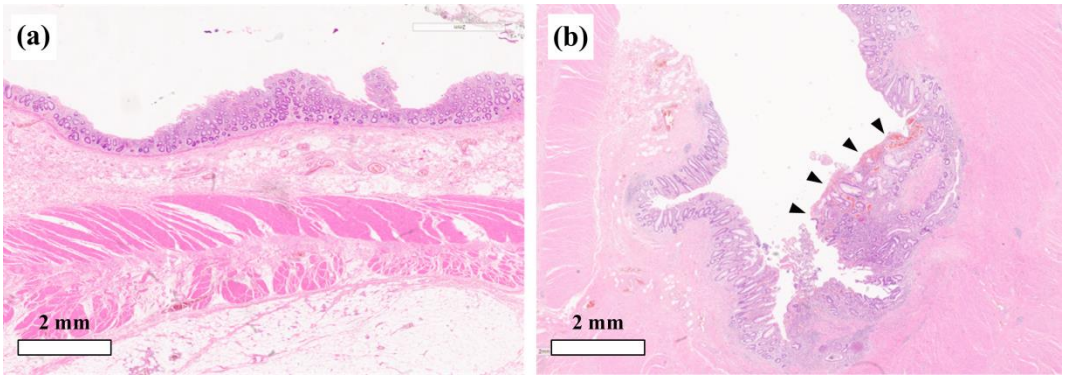

Figure 8.7: Case 2 micrograph sections of (a) normal tissue region (original magnification x1.2, hematoxylin-eosin [H-E] stain) and (b) adenocarcinoma (original magnification x1.2, hematoxylin-eosin [H-E] stain); arrows indicate tumour region.

Histology slides for the resected sample, showing a healthy reference region and a cross-section of adenocarcinoma, have been presented in Figure 8.7. The cancerous mucosa (Figure 8.7(b)) shows an average diameter of approximately 4 mm and was pathologically staged as T1

(c.f. Figure 2.2). It is evident visually that the mucosa has been significantly altered by the cancerous cells. Cancerous cells show less homogeneity and are particularly anisotropic. These properties appear to give a larger proportion of extracellular space, which may be the cause of a reduced resistance.

8.2.3.3 Case 3

A total of ten repeat measurements were obtained for healthy mucosa, diseased mucosa, close proximity to diseased mucosa and serosa tissue regions under each measurement condition. An image showing the diseased tissue location (polypoid tumour) has been presented in Figure 8.8. Table 8.4 contains the average resistance measurements obtained for these measurements.

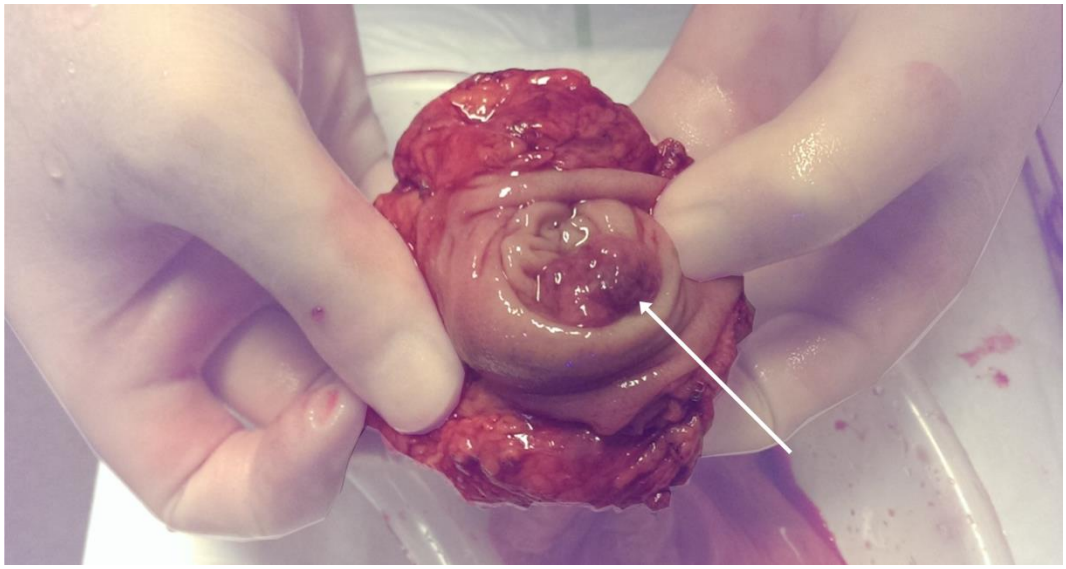

Figure 8.8: Image of rectal cancer case 3 tissue specimen, showing polypoid tumour within rectal mucosa (indicated with arrow).

Table 8.4: Average (mean ± SD) resistance values (Ω) for case 3 tissue regions for all measurement conditions; test time (s) shown with current range (μA) in parentheses.

Tissue region	10 (60)	10 (180)	1 (60)	1 (180)	0.25 (60)	0.25 (180)
Healthy mucosa	733 ± 13	754 ± 10	701 ± 17	753 ± 10	697 ± 17	751 ± 10
Diseased mucosa (on polyp)	290 ± 6	285 ±3	285 ± 2	285 ± 1	283 ± 2	280 ± 3
Diseased mucosa (near polyp)	347 ± 8	382 ± 6	347 ± 9	383 ± 7	346 ± 8	381 ± 7
Serosa (fatty)	1261 ±60	1454 ± 34	1285 ± 56	1456 ± 33	1283 ± 54	1456 ± 32

The average resistance values characterised for each tissue region have been presented in Figure 8.9. For the primary measurement case (Δt = 10 s, ΔI = 60 μA), the healthy mucosa was on average (M=733, SD = 13 Ω) found to be higher than the cancerous mucosa (M= 290, SD = 6 Ω). This difference, 443 Ω, CI[433, 452], was highly significant t(18) = 95.6, p < 0.01; this represented a large-sized effect, d = 33.4. A statistically significant difference was also found between healthy and cancerous mucosa for all other measurement configurations.

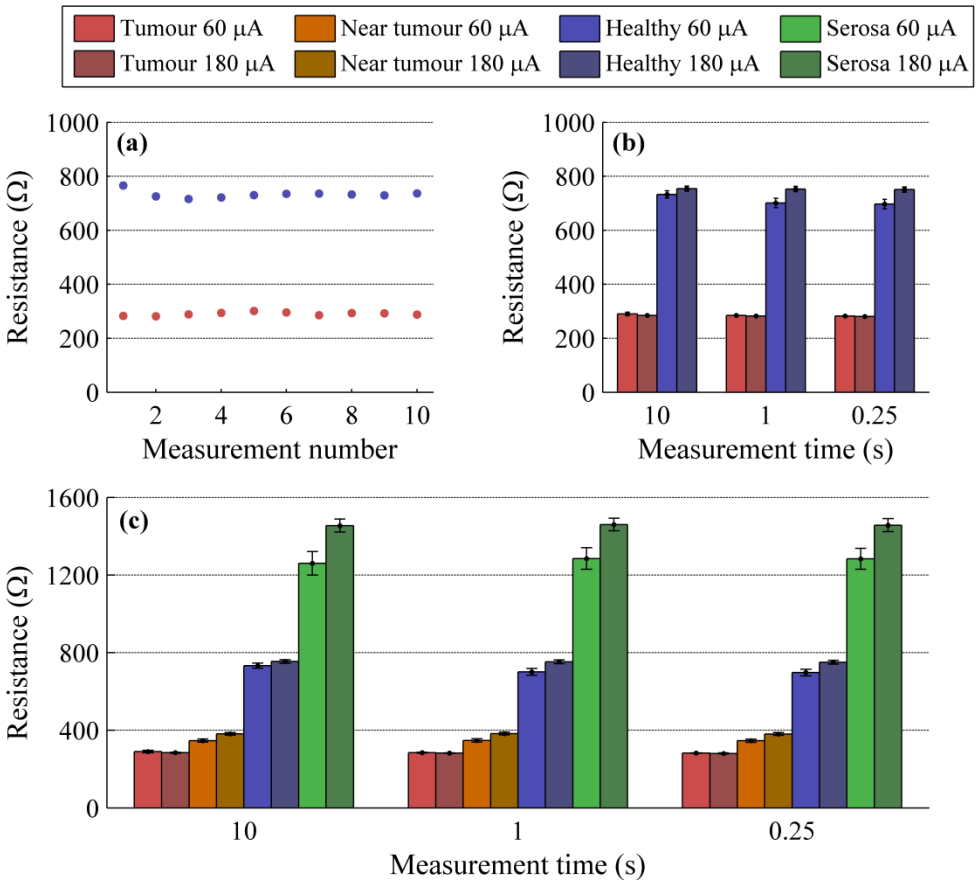

Figure 8.9: Case 3 data, showing (a) repeated measures for healthy and cancerous mucosa (tumour) (10 s measurement and 60 μA current range results shown), and mean ± SD characterised resistance for tested tissue regions under varied measurement conditions, showing (b) healthy and cancerous mucosa and (c) all tissue regions.

Histology slides for the resected sample, showing a healthy reference region and a cross-section of the polypoid tumour, have been presented in Figure 8.10. The cancerous mucosa (polypoid tumour) shows an average diameter of approximately 15 mm and was pathologically staged as T1 (c.f. Figure 2.2). Measurement positions for tumour testing and near tumour testing (Figure 8.9) represent electrodes completely covering and partially covering the tumour respectively. Qualitative correlation for these two locations indicates that the proportion of current flow through the tumour causes direct influence on the determined resistance. Therefore,

small misalignments of the electrodes may cause variability in resistance between samples. This indicates high sensitivity of the measurement technique which may allow for functionality such as spatial resistance mapping.

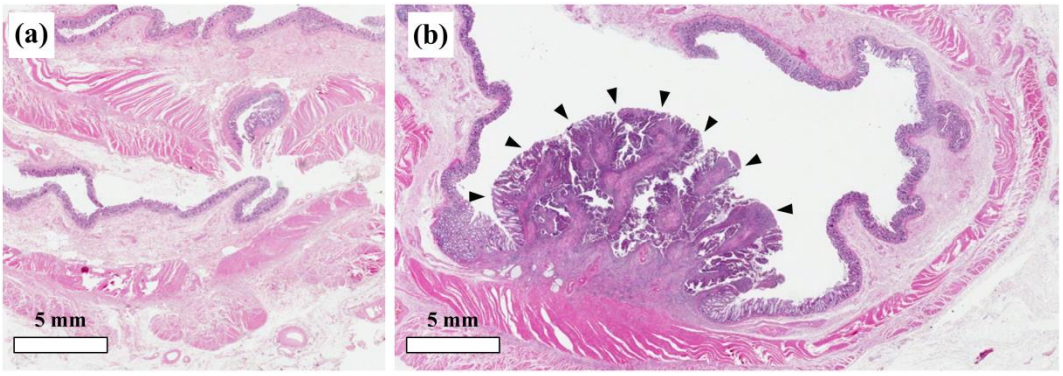

Figure 8.10: Case 3 micrograph sections of (a) normal tissue region (original magnification x0.4, hematoxylin-eosin [H-E] stain) and (b) cancerous polypoid tumour (original magnification x0.5, hematoxylin-eosin [H-E] stain); arrows indicate tumour region.

8.2.3.4 Case 4

A total of ten repeat measurements were obtained for healthy mucosa, diseased mucosa, and serosa tissue regions under each measurement condition. Table 8.5 contains the average resistance measurements obtained for these measurements. The average resistance values characterised for each tissue region have been presented in Figure 8.11. For the primary measurement case (Δt = 10 s, ΔI = 60 μA), the healthy mucosa was on average (M=535, SD = 17 Ω) found to be higher than the cancerous mucosa (M= 383, SD = 6 Ω). This difference, 152 Ω, CI[140, 164], was highly significant t(18) = 26.3, $p < 0.01$; this represented a large-sized effect, d = 8.2. A statistically significant difference was also found between healthy and cancerous mucosa for all other measurement configurations. At the time of writing, no histopathology slides were available for this test case. Pathology reports indicate a tumour of 7 mm and an invasion level of T3 (c.f. Figure 2.2).

Table 8.5: Average (mean ± SD) resistance values (Ω) for case 4 tissue regions for all measurement conditions; test time (s) shown with current range (μA) in parentheses.

Tissue region	10 (60)	10 (180)	1 (60)	1 (180)	0.25 (60)	0.25 (180)
Healthy mucosa	535 ± 17	564 ± 6	540 ± 7	563 ± 8	538 ± 10	562 ± 7
Diseased mucosa	383 ± 6	368 ± 7	380 ± 5	365 ± 6	380 ± 6	362 ± 7
Serosa (fatty)	1785 ± 23	1688 ± 55	1778 ± 23	1681 ± 55	1781 ± 22	1677 ± 56

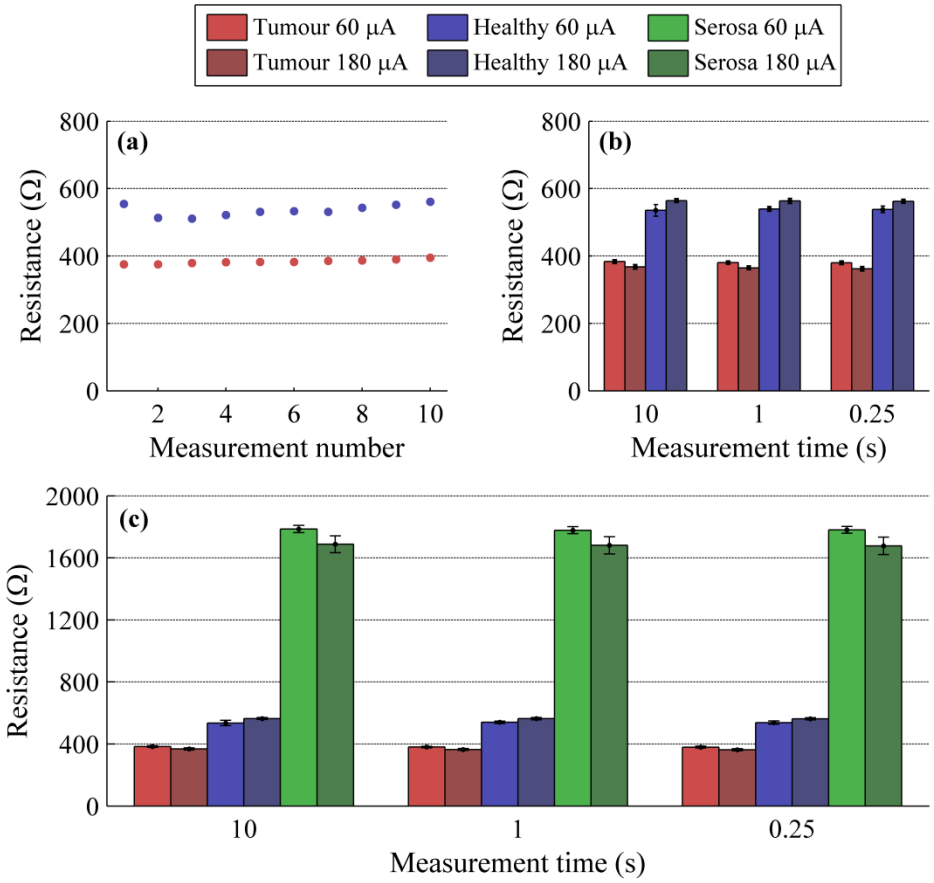

Figure 8.11: Case 4 data, showing (a) repeated measures for healthy and cancerous mucosa (tumour) (10 s measurement and 60 µA current range results shown), and mean ± SD characterised resistance for tested tissue regions under varied measurement conditions, showing (b) healthy and cancerous mucosa and (c) all tissue regions.

8.2.3.5 Case 5

A total of five repeat measurements were obtained for healthy mucosa and diseased mucosa tissue regions under each measurement condition. The testing range was limited for this case due to time constraints within the hospital. Table 8.6 contains the average resistance measurements obtained for these measurements. The average resistance values characterised for each tissue region have been presented in Figure 8.12. For the secondary measurement case (Δt = 1 s, ΔI = 60 µA), the healthy mucosa was on average (M=475, SD = 16 Ω) found to be higher than the cancerous mucosa (M= 162, SD = 13 Ω). This difference, 313 Ω, CI[292, 335], was highly significant $t(8) = 33.6$, $p < 0.01$; this represented a large-sized effect, $d = 19.0$. A statistically significant difference was also found between healthy and cancerous mucosa for all other measurement configurations.

Table 8.6: Average (mean ± SD) resistance values (Ω) for case 5 tissue regions for all measurement conditions; test time (s) shown with current range (μA) in parentheses.

Tissue region	10 (60)	10 (180)	1 (60)	1 (180)	0.25 (60)	0.25 (180)
Healthy mucosa	476 ± 63	505 ± 9	475 ± 16	492 ± 4	460 ± 8	491 ± 7
Diseased mucosa	150 ± 47	172 ± 15	161 ± 13	163 ± 14	156 ± 10	157 ± 8

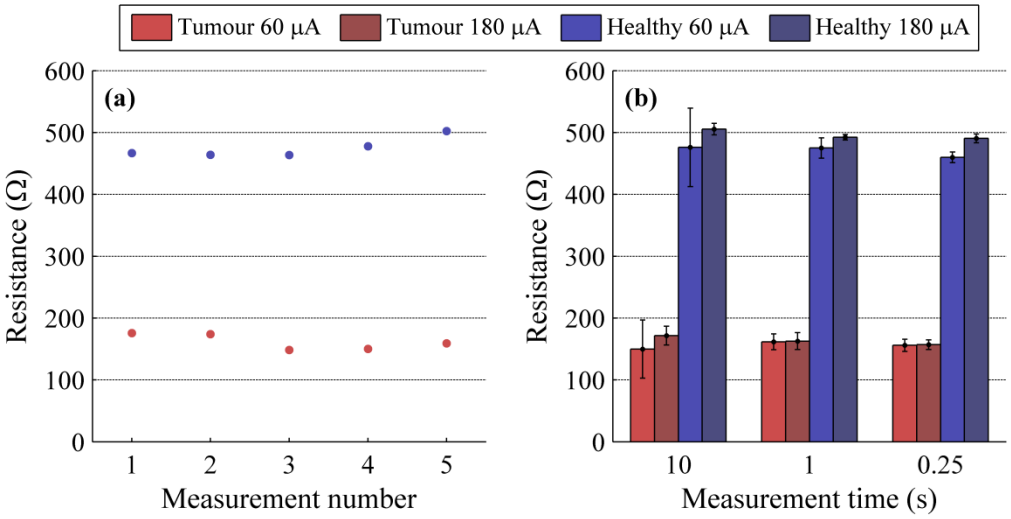

Figure 8.12: Case 5 data, showing (a) repeated measures for healthy and cancerous mucosa (tumour) (1 s measurement and 60 μA current range results shown), and (b) mean ± SD characterised resistance for tested tissue regions under varied measurement conditions.

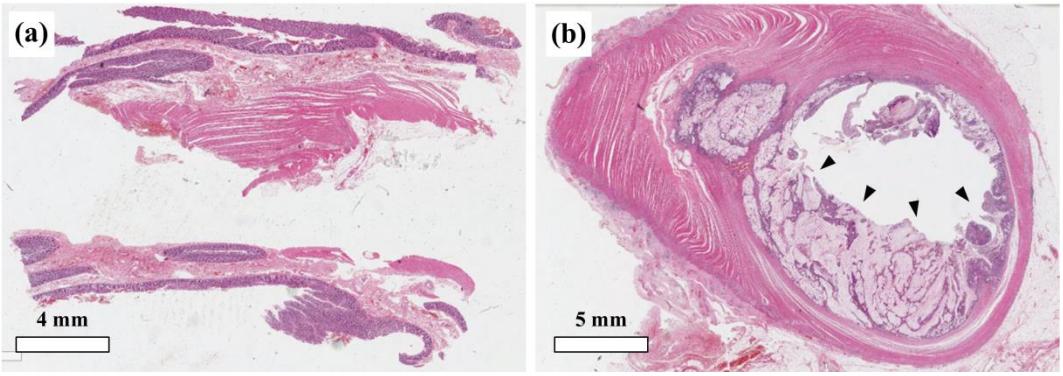

Figure 8.13: Case 5 micrograph sections of (a) normal tissue region (original magnification x0.5, hematoxylin-eosin [H-E] stain) and (b) mucinous adenocarcinoma (original magnification x0.4, hematoxylin-eosin [H-E] stain); arrows indicate tumour region.

Histology slides for the resected sample, showing a healthy reference region and a cross-section of the tumour, have been presented in Figure 8.13. The adenocarcinoma shows an average diameter of approximately 40 mm and was pathologically staged as T3 (c.f. Figure 2.2). The tumour was noted as being mucinous, as can be clearly seen from the histopathology slide. The high level of mucin (approximately 50 %) appears to correlate with the lowest resistance

measured across all cancer test cases. The viscous fluid containing mucin may act as a highly conductive salt bridge for the electrochemical cell. Therefore, the resistive pathway through the tissue will be reduced resulting in a lower characterised resistance.

8.2.3.6 Case 6

A total of ten repeat measurements were obtained for healthy mucosa, diseased mucosa, and serosa tissue regions under each measurement condition. An image showing the diseased tissue location has been presented in Figure 8.14. Table 8.7 contains the average resistance measurements obtained for these measurements. The average resistance values characterised for each tissue region have been presented in Figure 8.15. For the primary measurement case (Δt = 10 s, ΔI = 60 μA), the healthy mucosa was on average (M=473, SD = 17 Ω) found to be higher than the cancerous mucosa (M= 228, SD = 26 Ω). This difference, 246 Ω, CI[225, 266], was highly significant $t(18) = 24.6$, $p < 0.01$; this represented a large-sized effect, $d = 14.2$. A statistically significant difference was also found between healthy and cancerous mucosa for all other measurement configurations.

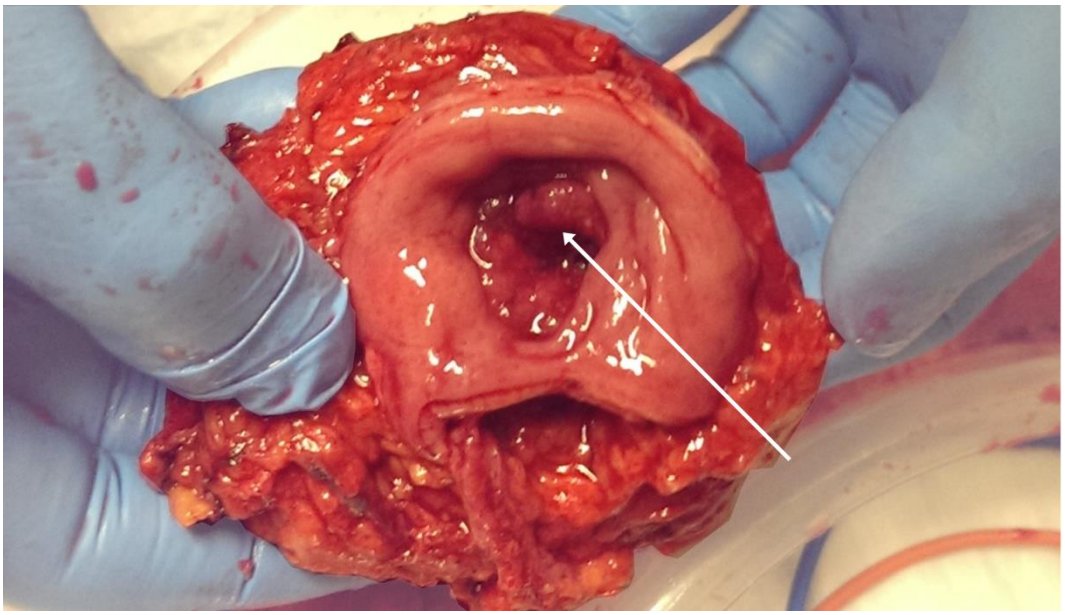

Figure 8.14: Image of rectal cancer case 6 tissue specimen, showing tumour within rectal mucosa (indicated with arrow).

Histology slides for the resected sample, showing a healthy reference region and a cross-section of the tumour, have been presented in Figure 8.16. The tumour invades the mucosa and submucosa, showing an average diameter of approximately 20 mm. The tumour was pathologically staged as T2 (c.f. Figure 2.2). As with Case 2, the inhomogeneity and anisotropy leave a reduced cell density leading to easier current flow through the cancerous tissue (reduced resistance).

Table 8.7: Average (mean ± SD) resistance values (Ω) for case 6 tissue regions for all measurement conditions; test time (s) shown with current range (μA) in parentheses.

Tissue region	10 (60)	10 (180)	1 (60)	1 (180)	0.25 (60)	0.25 (180)
Healthy mucosa	473 ± 17	494 ± 7	479 ± 18	489 ± 8	468 ± 12	491 ± 8
Diseased mucosa	228 ± 26	242 ± 5	212 ± 8	244 ± 6	214 ± 9	240 ± 6
Serosa (fatty)	2094 ± 127	2395 ± 61	2083 ± 117	2394 ± 63	2084 ± 114	2386 ± 62

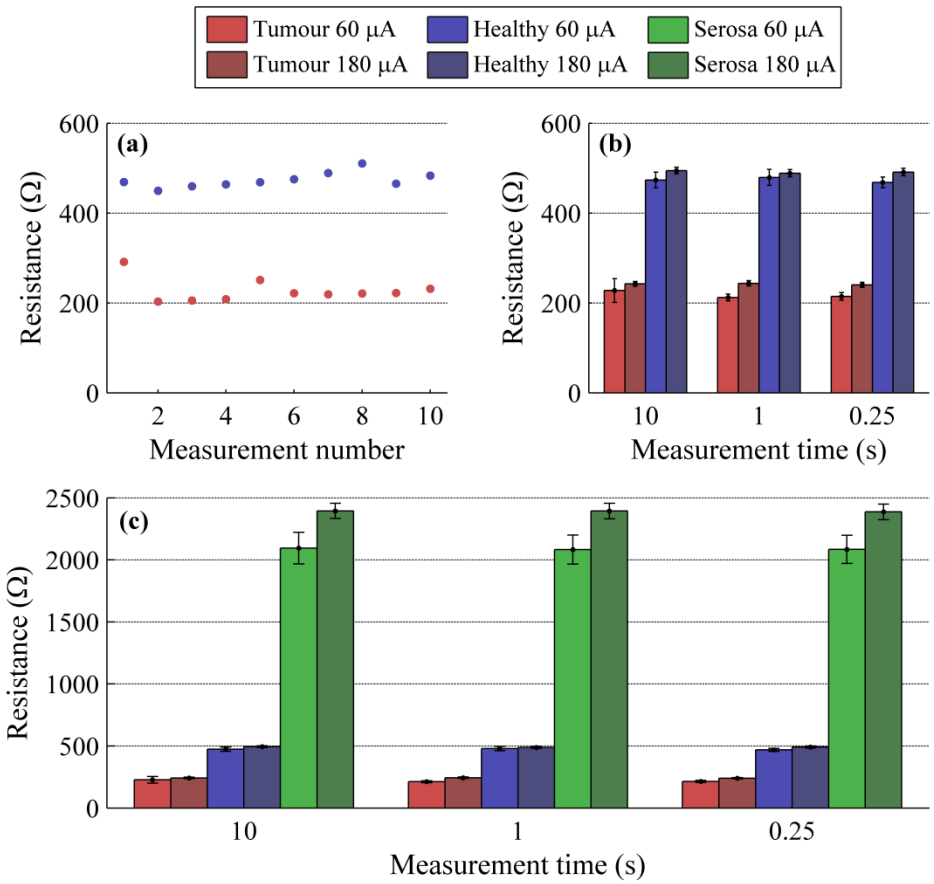

Figure 8.15: Case 6 data, showing (a) repeated measures for healthy and cancerous mucosa (tumour) (10 s measurement and 60 μA current range results shown), and mean ± SD characterised resistance for tested tissue regions under varied measurement conditions, showing (b) healthy and cancerous mucosa and (c) all tissue regions.

Figure 8.16: Micrograph section of cancerous tumour (original magnification x0.6, hematoxylin-eosin [H-E] stain); arrows indicate tumour region.

8.2.3.7 Combined data

Each case has been assessed independently, and from the histopathology reports it is evident that there is significant variation within the location, pre-treatment and staging of the tumours tested. However, comparison between all test cases has been presented in Figure 8.17.

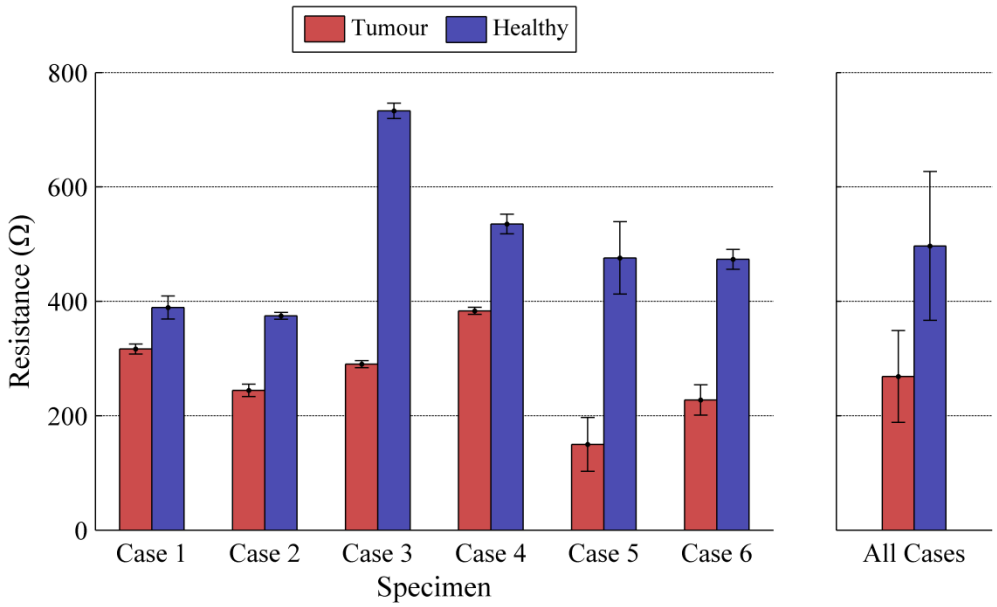

Figure 8.17: All cases average (mean ± SD, n=10) characterised resistance data for healthy and cancerous mucosa (10 s measurement and 60 μA current range results shown).

For all test cases the resistance of the cancerous tissue was found to be significantly lower than for the healthy reference. For all cases combined there remains a statistical difference between the healthy and cancerous tissue. However, the highest resistance measured for cancerous tissue was marginally higher than for the lowest resistance for healthy tissue. This may be due to relative time drift between cases (c.f. Section 8.3.1), inter-patient variability or electrode alignment.

8.3 Discussion (Parametric influence)

The testing presented in this chapter has allowed assessment of the multi-electrode resistance characterisation technique efficacy for differentiation of healthy and cancerous tissues of the colon. Additionally, a number of the parameters assessed in Chapter 7 have been revisited. The following sections discuss the relevant findings from these tests in relation to the time drift, measurement rate and current range. The correlation of measured resistance to tissue health and the relevance of the technique to surgery are also briefly addressed.

8.3.1 Time drift

The influence of time was evident and significant in the *ex vivo* porcine tissue testing described in Section 7.6.2. The testing cases of this chapter represent particularly fresh tissue, with measurements being taken directly after resection. Repeat measurements were conducted for each sample as part of the testing protocol, allowing for indirect examination of time drift for *ex vivo* human tissues to be tested. The influence of repeat number for the standard test conditions (10 s test at 60 μA current range) has been presented for each test case in Section 8.2.3. Acquisition of ten repeat measurements took approximately 4 minutes, meaning that time drift assessment can only be made over this relatively short period.

Figure 8.18 shows the time drift results for all test cases. It is evident that through all tests on healthy and cancerous tissues, all variation fell within ±15% and was primarily found to give an increasing resistance with time. An increasing resistance with time is consistent with porcine tissue results presented in Section 7.6.2. This would suggest the drying of tissue or the processes of dying may be acting to reduce current flow through the tissue. The variability found for repeated measures is likely to be due to this time drift phenomena. Measurements taken on tissues with a constant blood supply (*in vivo*) may deliver a further reduction in variability and therefore increase the specificity of the technique.

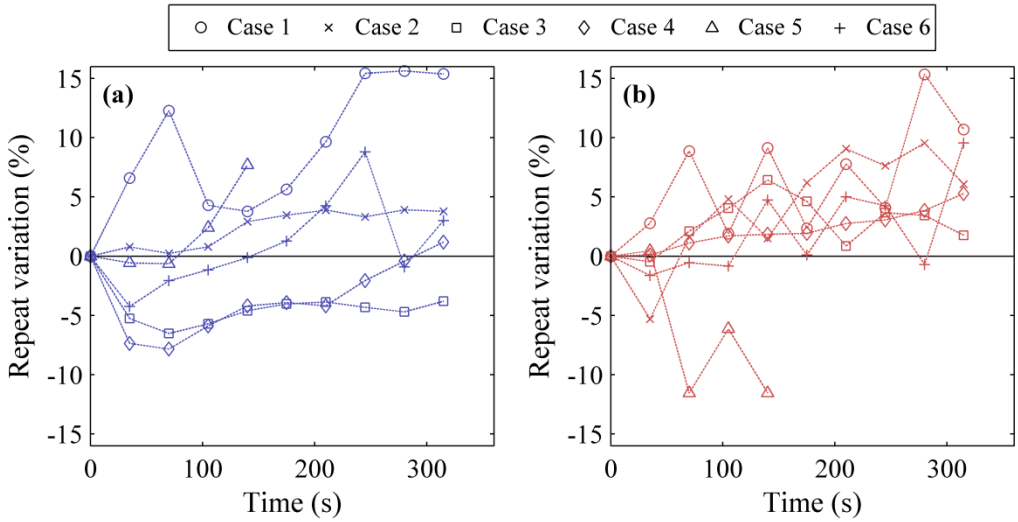

Figure 8.18: Variation in characterised resistance as a function of time for all cases, showing (a) healthy tissue tests, and (b) cancerous tissue tests.

8.3.2 Measurement rate

The influence of measurement rate was considered for *ex vivo* porcine tissues in Section 7.6.3. These findings showed that this parameter has little influence on the characterised resistance. For the human tissue samples tested, all relevant test cases also showed no significant variation across the three rates tested (rates delivering measurement times of 10, 1 and 0.25 s). The assumptions of the technique and its theoretical basis would predict that there is no influence with measurement rate, as the measurement is of an isolated, purely DC resistance. However, the measurement system (connection, wiring and data acquisition hardware) and the measurement environment would be expected to add sources of error into the system that may be time dependent. The findings from this chapter show that these errors are minimal relative to the measured tissue property and therefore the measurement rate can be selected within practical limitations to suit the application.

8.3.3 Current range

To measure the tissue resistance, significant polarisation of the cell electrodes is required. This allows for the relative difference in potential from two reference points to be compared. To achieve increased polarisation, the current is increased. Theoretically, the response difference (caused by the tissue resistance) should be evident across any polarisation range. However, in order to measure the difference, analogue to digital signal conversion is necessary and is therefore subject to quantisation error based on the resolution of the analogue to digital convertor (ADC). At low currents the polarisation overpotential for the working electrode will be small and the difference in this value between reference sources even smaller. It therefore

becomes necessary to increase the current range to achieve a suitable signal-to-error ratio for a meaningful resistance characterisation to be achieved.

For large currents, it is likely that the reference electrodes may become polarised and therefore break from ideal conditions. If this occurs to a different extent on the individual reference electrodes, this will be included in the resistance characterisation data and therefore the influence the determined resistance.

The results from this chapter are consistent with the findings of Chapter 7, where variation was noted with this parameter. Most of the test cases presented show a difference with current range. The direction of the change appears spurious; however, this can be correlated with testing order. Current range tests were performed in series, with all current rate repeats taken for a particular current and then all repeated for the second current range. Current range order was randomised and the order used correlates with the direction of change found. The second current range tested shows a higher value than the first for all cases. Therefore the differences are likely to be indicative of changes in tissue with time, rather than influence of current range. More specific current range testing would be required to validate this assertion, although changes do not influence the statistical separation for the two tissue types (healthy and cancerous).

8.3.4 Tissue health

The results presented in Section 8.2.3.7 show that the resistance for cancerous tissue is consistently lower than a healthy reference. The range of difference was from 72 Ω to 442 Ω, and a large variation between test cases was found. Consistent differences between health states is encouraging, and suggests that it may be possible to use the resistance technique to determine the presence of cancerous tissue during surgical procedures. However, this currently functions as a relative measurement meaning calibration with a healthy tissue region would be required. The influence of parameters such as time drift and electrode alignment increases the variation between cases and further testing would be required to understand to what extent. Testing on *in vivo* tissues with improved spatial tracking and co-registered histopathology would allow for improved assessment of these issues.

The histopathology reports and associated micrograph images indicate large tumour variability across cases (stages T1-T4 represented). Qualitative relation of measured resistances to the microscopic tissue structure (histopathology slides) was made for available test cases. Features such as reduced cell density, reduced homogeneity and increased mucin content may be influential in reducing the resistance of cancerous tissue. Based on the local resistance variation around the tumour found in Case 3, the determined resistance appears to be an average of the current pathway between the electrodes. Exploration of the electric field distribution as a

function of geometry and tissue properties may allow for improved correlation with micrograph imaging. However, this is outside the scope of this study.

8.3.5 System relevance to surgery

The tissue testing presented in this chapter represents the closest simulation of surgical tissue conditions without testing *in vivo*. In addition to ethical approval, there are a number of practical changes that are required to allow the device to be utilised *in vivo*, making this outside of the scope of this thesis. The work of this chapter therefore allows validation of the measurement technique rather than a specific surgical device. Findings from Section 7.7 and those discussed in Section 8.3 indicate that the technique meets many of the requirements outlined in Table 7.1. In particular, fast measurement has been demonstrated and shown to not influence the output metrics. Additionally, the system is low power and output metrics are simple to obtain and interpret. Further development and testing would be required to understand the ease of device integration and therefore the potential impact on surgical procedures.

Repeatability of results from on-off contact testing indicates that electrode elements may be integrated into a laparoscopic grasper and used as a point contact measurement tool during standard tissue manipulation. The suitability of this method of assessment would require investigation, as the data obtained may not be informative to the surgeon, and a different form-factor device may be more appropriate.

8.4 Chapter Summary

The concluding testing presented within this chapter detailed testing of the multiple reference electrode galvanostatic resistance measurement technique on healthy and cancerous human colon tissues. Application of the technique to human diseased tissues was the remit of Objective 8.1. Objective 8.2 required evaluation of the findings from testing for tissue health. Results for each case have been individually presented and a collation of all test cases presented in Section 8.2.3.7. The resistance of cancerous tissue has been found to be significantly lower than its healthy equivalent for all test cases. Parametric findings relating to Objective 8.3 indicate that time-drift appears to be the dominant influencing factor. In addition, the measurement rate and current range have been shown to have only a small impact on the characterised resistance. Regarding Objective 8.4, these findings are in accordance with the porcine testing conducted as part of Chapter 7. Human tissue values for mucosa resistance typically give a lower resistance than for a porcine equivalent. This is likely to be associated with the time drift of tissue, typically giving an increasing resistance with time. The results of this chapter are very encouraging, indicating the potential suitability of the multi-reference electrode technique as an intraoperative assessment tool.

Chapter 9
General discussion

The research presented in this thesis has demonstrated the development, application and analysis of new and unproven electrochemical based sensing technologies. More specifically, the proposed method of biogalvanic characterisation was investigated as a sensing candidate for tissue health assessment. Findings from extensive tissue and salt solution testing outlined a number of issues with the technique. Section 9.1.1 highlights the main outcomes from this testing and details the important results from the mitigation and modelling strategies explored in Chapter 6. The work of Chapters 7 and 8 has described and tested a novel multi-electrode tissue resistance measurement technique. Section 9.1.2 defines the main outcomes from testing with this in the context of a laparoscopic tool for tissue assessment during colorectal cancer surgery.

The discussion considers key features of the research regarding the generality of the technique, how it compares to alternative technology and how it may be applied under differing sensor configurations. The concluding comments of the chapter reassess the research objectives of the thesis and highlight some potential adaptations of the current research through the proposal of appropriate future work.

9.1 Overall discussion

Surgical intervention remains necessary for the treatment of colorectal cancer, and offers the most effective curative treatment. The advent of laparoscopic surgery has improved outcomes for the patient but in many ways made surgical tasks more challenging. With reduced visual and haptic feedback, laparoscopic resection of the colon is a complex procedure and requires years of training to perform competently. A move towards personalised surgery may offer the next step in improving outcomes for the patient. Real-time information regarding the health state of tissue around the tumour site coupled with assessment of associated lymph nodes may allow the surgeon to tailor resections and minimise unnecessary tissue removal.

For personalised resections to be possible, improved intraoperative sensing is required. Many technologies are currently under development that may be suitable for surgical integration. The research presented in this thesis has looked at one such technique; namely biogalvanic tissue characterisation. By evaluating this technique and identifying its limitations, a novel alternative for measuring the DC resistance of biological tissue has been developed. The following sections discuss the main findings from the thesis with regard to these two sensing approaches.

9.1.1 Biogalvanic tissue characterisation

Determination of an electrical resistance based metric using a biogalvanic cell was originally proposed by Golberg et al. [115]. The system was presented as simple and scalable, and the metrics were shown to be specific to tissue type and to be sensitive to tissue damage (electroporation). Initial research effort was made to develop a biogalvanic testing system to allow verification and exploration of this technique. The following points discuss the primary findings from development, testing and modelling of a biogalvanic characterisation system. The topics covered follow the order presented in Chapters 3-6.

9.1.1.1 Test system

An electrode manufacturing protocol was developed to deliver insulated and non-insulated cylindrical electrodes with connecting wires in a range of diameters. Electrodes were integrated into custom testing platforms (Testing platform & Surgical clip) to allow for fixed strain testing on *ex vivo* and *in vivo* tissues. Although this combination was suited to the initial stages of testing, the laborious electrode manufacturing protocol and discrete separation levels of the Surgical clip limited the scope of initial testing.

Improved measurement flexibility was achieved through the development and application of a controlled external load and voltage measurement system. The electronic circuit was

designed to allow alteration of fixed external loads and their connection state to be controlled through digital logic. The control software developed allows for switching rate and external load profiles to be configured rapidly. The 7-bit limit of the electronic circuit (allowing combinations of 7 external loads) was found to limit the range and resolution of the external load test set. Later testing was therefore conducted using a commercial potentiostat (CompactStat, Ivium Technologies) which gives a fully selectable external load range but requires separate testing protocol files to be implemented for each test to avoid current saturation.

Measured voltages were used as model inputs to allow for biogalvanic system metrics to be extracted (R_{INT} and OCV). Two new model approaches (Model A and Model B) were investigated for characterising measured data. These models both use data sets for a range of external loads to determine internal resistance and open circuit voltage values. This is in contrast to the original point-wise characterisation proposed by Golberg et al. [115], which uses discrete measurement points and an assumption of OCV to determine an internal resistance. Fitting to larger data sets was found to improve the accuracy and repeatability of the characterisation process (Figure 3.22), with Model B showing the best results. In addition, the sensitivity of the point-wise characterisation to small errors in the assumed OCV was demonstrated in Figure 3.21.

9.1.1.2 Tissue testing

Tissue experiments demonstrated efficacy of the testing system for *ex vivo* and *in vivo* arrangements. Characterisation models were able to successfully fit to measured data from these test cases, allowing extraction of internal resistance (R_{INT}) and open circuit voltage (OCV). The biogalvanic model assumptions presented by Golberg et al. [115, 116] (c.f. Section 3.7) were examined along with the validity of conversion of internal resistance to a normalised resistivity of $GAIR$. Accurate model fitting and production of consistent internal resistance values within the same tissue specimen suggested the appropriateness of the proposed biogalvanic model. The measured data was initially shown to conform well to the assumption of a fixed internal resistance. However, application of a $GAIR$ correction did not lead to tissue specific resistivity, and significant variation in the characterised OCV values was also demonstrated. Influence of tissue thickness and contact area was found. However, these parameters did not induce linear scaling of the internal resistance, as are the assumptions for conversion to $GAIR$.

A second assumption of the model presented by Golberg et al. [115] is that of a constant OCV equal to that predicated by the standard redox equation (5.3). It is particularly evident across the performed tests that there is significant variation in cell OCV, with deviation from the predicted OCV of 0.76 V. Values for tissue tests were all lower than this, ranging from 0.75 to

0.25 V across tissue types and test conditions. This indicates that the reaction conditions at the electrode-tissue interface differ significantly from those used in predicting the standard galvanic potential difference.

The influence of electrode interface resistance and capacitance was found to induce large transients within the measurement signals. Additional longer-term time dependence was noted as arising from tissue degradation (hydration and breakdown) and from electrode passivation. Separation and mitigation of these influencing factors is challenging and all are influential on the characterised biogalvanic parameters. The external load switch rate and direction dependence posed significant practical barriers to surgical integration.

9.1.1.3 Electrochemical aspects

An investigation into the electrochemical aspects of the biogalvanic system was presented in Chapter 5. The main findings of this study relate to the electrode redox reactions and associated electrode potentials and kinetics.

Average OCV values measured from the galvanic couple show statistical significance for varied NaCl concentration. Salt ion concentrations within physiological range alter the standard electrode potentials, generating a spread of OCV values spanning 0.1 V from 0.8-0.9V. Salt solution results are markedly different to OCV values measured *in vivo* on porcine tissues. The lower OCV found in tissues may be due to a lower open circuit potential at the copper electrode caused by a reduced dissolved oxygen concentration. The influence of oxygen can also be seen within the salt solution system (Figure 5.7), where the OCP at the copper electrode becomes more negative as the oxygen solubility is reduced by higher NaCl concentrations.

Polarisation of the individual galvanic cell electrodes indicated the dominance of the copper cathode on the system performance. To achieve closed cell current conditions, the copper cathode is polarised to a much greater degree than the zinc anode. The cathode response demonstrates the influence of mass transport limitation. This is associated with the maximum rate of oxygen diffusion to the cathode and forms a non-linear potential-current response which is not accounted for in the standard biogalvanic models. The extent to which this factor influences the characterisation depends on the resistance of the salt-bridge. However, even with a large salt-bridge resistance the influence of electrode polarisation will still be evident within the measured response and therefore the characterisation metrics. These electrochemical aspects of the system formed the motivation for investigation of improved system modelling strategies.

9.1.1.4 Modelling aspects

The work of Chapter 6 investigated the feasibility of using modelling to understand the biogalvanic system and improve tissue resistance specificity. Adaptation of the characterisation

model, utilising the recorded voltage-time data, is presented in Section 6.3. This approach was taken to understand and potentially exploit the transient voltage response found between external load switching. This phenomenon, induced by the electrode-tissue interface, causes the biogalvanic characterisation to be switching rate dependent, making it unsuitable for surgical applications. Through a simple model of the electrode interface (parallel resistor and capacitor) the influence of switching rate was reduced and therefore the surgical applicability of the system improved. Successful delineation of cancerous and health tissue was also shown using the technique for a single test case.

Through collaboration with the School of Computing (University of Leeds), a more comprehensive numerical model of the biogalvanic system was developed. Modelling of the individual electrode polarisation responses and the potential and current distributions within the biogalvanic cell has given insight into the system. This modelling approach allows for independent assessment of the tissue and electrode properties. However, this is only possible under conditions where the electrodes are not dominant within the system. Through parametric investigation, these favourable conditions were found to be achievable only for impractical geometries. Ultimately, the system model highlights the challenges associated with obtaining a specific and repeatable tissue resistance.

Modelling the biogalvanic cell in different ways has led to improved characterisation and given better insight into the behaviour of the system. However, there are of course limitations in the two models presented and these must be understood when making assertions based on their application. For the time-dependent model, the electronic analogy of the electrode-tissue interface is mathematically solved under the assumption of discrete current levels. The biogalvanic system under external load control in fact allows for potential (voltage) and current variation with time. The assumptions for the numerical model are that the system is at steady state, ignoring time-dependent factors. For both modelling approaches, the non-linear influence of the diffusion limited oxygen reduction reaction at high current is not accounted for.

The presented model assumptions are therefore not ideal and are partially responsible for the differences seen between the model fit and measured data. Modelling has proved to be beneficial in improving the understanding of the system, and in particular the significant influence of the electrodes on the characterisation. Without this insight, the improved characterisation methodology of Chapters 7 and 8 would not have been developed.

9.1.1.5 Summary

The findings of the various studies presented have clearly defined the complexity of the biogalvanic system. The simple model originally proposed has been found to be a vast oversimplification, where aspects of electrode kinetics and cell geometry are not adequately accounted for. Through improved modelling some detrimental aspects of the system may be

mitigated, however, the two electrode system fundamentally limits biogalvanic characterisation as a surgically appropriate sensing modality.

9.1.2 Multiple reference resistance characterisation

Through exploitation of the findings from chapters 4-6, a novel adapted DC resistance characterisation technique was developed. The aim of this research was to mitigate a number of the limiting issues found with the biogalvanic method. Three main alterations were made:

Cell electrodes: *The two electrode configuration of the biogalvanic system was identified as the primary source of measurement errors. Additionally, the large sized electrodes were found to be impractical for tumour testing on ex vivo samples. The multi-reference technique was designed to allow for separation of current carrying electrodes from potential measurement electrodes. This was to allow for a reduction of artefacts associated with polarisation of the measuring electrodes. Four cell electrodes of 1 mm diameter were employed to give a cell length of 30 mm. This arrangement was found to allow for adequate electrode positioning during tumour testing while maintain a measureable tissue resistance.*

Cell polarisation: *Polarisation using external resistive loads allows passive control of the cell current. However, the associated transient response makes accurate determination of the cell current, required for characterisation, challenging. For improved control of the cell performance, the multi-reference technique was galvanostatically polarised across discrete current levels.*

Characterisation: *The system model is based on comparison of two three-electrode electrochemical cells. The polarisation response of the working Zn electrode is assessed from two separate reference points. Subtraction of the signals allows isolation of the potential difference across the tissue for the specific current level. Application of a simple Ohmic based model has been shown to fit consistently to measured data across a wide range of conditions. The use of a simple model has led to extraction of unambiguous metrics and reduced the fitting sensitivity of the model to the measured data.*

The measurement and characterisation strategies employed within the multi-electrode technique have delivered highly linear voltage-current responses. The simple Ohmic model has given tissue specific resistances with only small variation with current stepping rate and range. These properties indicate the flexibility of the measurement configuration which has clear advantages in the context of surgical sensing. An additional study looking at the influence of electrode contact history on characterisation suggests that measurements may be accurately taken shortly after electrode contact.

9.1.2.1 Tissue health discrimination

The ultimate aim of the presented research was to develop and test a sensing technique capable of delineating healthy from cancerous colon tissue, with the potential for intraoperative integration. Chapter 8 presents results from six colorectal cancer cases which were tested using the multi-electrode technique. For all cases the measurement equipment and protocol allowed for rapid collection of resistance data across a selection of current stepping rates and ranges. Linear voltage-current responses were again realised for *ex vivo* human tissue allowing extraction of reliable resistance values for each tissue type across all cases.

All test cases showed a comparable resistance values for the same tissue type, and for all cases cancerous tissue was found to have a significantly ($p < 0.01$) lower resistance than its healthy equivalent. This statistical delineation was maintained for testing across current ranges of 60 and 180 μA and for measurement times from 10 s down to 0.25 s. Comparison to histological analysis suggested that resistive differences are based on the disordered cellular composition, inherent in cancer tissue. These findings reinforce those from porcine *ex vivo* testing, showing the suitability of the technique to surgical integration.

9.1.2.2 Generality of the technique

The specific test configuration used included two reference electrodes, a Zn-Cu EC cell, co-planar electrode geometry, and galvanostatic polarisation. This showed encouraging findings with high linearity, specificity to tissue health and low influence from sensing parameters. However, a real strength of the technique is that this initial sensor configuration is readily adjustable without compromising the underlying principles of the technique. Adaptations may allow the: use of different materials for EC cell and reference electrodes; addition of reference electrodes and with active EC cell pair switching; polarisation of the cell using potential or external resistive load control; and adjustment of the geometry for different device form factors.

9.1.2.3 Comparison to alternative technologies

It was highlighted in Chapter 2 that there are many technologies that may be suitable for tissue assessment intraoperatively. The proposed multi-electrode resistance technique of Chapter 7 has been found to be a suitable means of assessing tissue health. As a new and alternative method, it is pertinent to make comparisons to established measurement modalities. Of direct relevance are other resistance based techniques such as biogalvanic characterisation and BIS. Chapters 4-6 demonstrated the parametric sensitivity of the biogalvanic technique and showed relatively large resistance values due to influence of the cell electrodes. Many of these issues were considered and addressed in the development of the new DC resistance measurement method.

As a more established measurement technique, BIS appears to deliver more consistent resistance values for tissues. Success of BIS in the commercial cervical cancer screening device, ZedScan (Zilico, Sheffield, UK), has identified the efficacy of this approach [134, 186]. However, the numerous method permutations including electrode type and configuration as well as applied models to fit to measured data and statistical approaches for extraction of significant differences can add complexity and ambiguity to the BIS approach [108]. Further work is required to understand how the proposed technique is affected by these issues. However, the theoretical underpinning of the multi-reference DC approach leads to a single output metric that is unambiguous and representative across measurement conditions. Additionally, initial testing shows limited influence of measurement configurations including current range and switching rate.

Optical techniques have become increasing common in surgical procedures. For colorectal cancer, fluorescence or photoacoustic imaging are likely to become essential tools for helping to assess the tissue morphology. With the approval and testing of targeted contrast agents, delineation of cancer using optical properties may be possible [136]. These may be useful to deliver a broad picture of the diseased anatomy and help to identify regions of interest. Issues of penetration depth, imaging duration and lack of quantitative output metrics may limit the scope of this approach in surgery.

Arguably the most complete intraoperative solution to date is that of the iKnife [44]. Assessment of the vapour produced through electrosurgery offers a very accurate indication of tissue health. However, the analysis is performed following destructive intervention, bringing to question the possibility of preserving healthy tissue margins.

It is evident that for surgical procedures to have improved outcomes for the patient, information relating to tissue types and health is required intraoperatively. From the array of modalities available it is pragmatic to envisage a multiple sensing approach where the benefits of numerous techniques are collated to build a thorough picture of the tissue structure and health state. Initial testing with the proposed multi-electrode resistance technique has demonstrated the

potential for a new method of assessing tissue health intraoperatively that may form part of this combined approach.

9.2 Assessment of research objectives

Sections 1.1.1 detailed a number of research objectives. This section describes how each of these has been addressed in the presented research.

1. *To explore the state of the art of relevant sensing technologies that may be appropriate to laparoscopic colorectal surgery.*

A wide range of sensing technologies including mechanical, electrical, electrochemical and optical were investigated as part of the initial review presented in Chapter 2. This wealth of research is promising and helps to identify the need for intraoperative sensing and the timeliness of the work presented in this thesis.

2. *To define and justify a sensing technology suitable for use as a tissue health assessment tool within laparoscopic colorectal surgery.*

Many criteria were considered when selecting appropriate technology for detailed investigation. As discussed in Section 2.5, the biogalvanic tissue resistance characterisation method offered a simple technique with the potential for tool integration and scalability. This technology was investigated as part of Chapters 3-6.

3. *To develop a suitable testing platform for validation and parametric investigation of the selected sensing technology.*

The low technological overhead of the biogalvanic technique allowed for rapid development of a flexible testing platform [202]. The work of Chapter 3 describes the developed sub-systems along with the validation of the biogalvanic approach taken forward. Development of testing equipment for the multi-reference resistance sensing approach was also presented in Chapter 7.

4. *To investigate the suitability of the technique to surgery through testing with biological tissues.*

Tissue testing of the biogalvanic system was presented in Chapter 4. Some of the potentially influencing factors were tested and summarised in Table 4.6. The

variability seen for many of the parameters suggests a lack of suitability of the boigalvanic technique as an intraoperative sensor [156]. Testing of the multi-electrode resistance technique using porcine tissues (Chapter 7) showed more consistent results with low variability for different test configurations [203].

5. *To investigate the underlying properties of the technology through suitable experimentation and modelling.*

The electrochemical investigation into the biogalvanic system presented in Chapter 5 gave improved insight into the technique. Electrode resistance and current limiting kinetics were found to cause significant influence on the characterisation [176]. This experimental approach was combined with the modelling strategies explored as part of Chapter 6 to allow understanding of the system limitations. novel system models and characterisation strategies offered improved tissue specificity, [204] although electrode resistance was found to be dominant within the system. Ultimately, the work of these chapters set out the important considerations made when developing the alternative resistance measurement approach of Chapter 7.

6. *To evaluate the system in the context of colorectal cancer and assess its discrimination performance.*

Discrimination performance was assessed through direct contact testing on human colon tissue. Comparisons were made between healthy and cancerous tissue regions, as identified by the surgeon. Biogalvanic testing showed a poor ability to discriminate for health (c.f. Section 4.5.2) based on resistance. Adaptation of the characterisation technique, to reduce the influence of the cell electrodes, presented in Section 6.3 allowed some discrimination improvement. The majority of testing for colorectal cancer was performed with the multi-electrode resistance technique and described in Chapter 8. This technique was found to give consistent discrimination across all test cases.

9.3 Conclusions

The work presented in this thesis has contributed through the development and testing of electrochemical based tissue sensing techniques. Biogalvanic resistance characterisation was initially selected as a potentially suitable candidate for surgical integration. The simplicity and scalability supported this decision, although the published literature surrounding the technique was limited. Research effort was therefore focused on investigating the biogalvanic technique.

A developed testing platform was used to allow for parametric investigation. Extensive tissue tests demonstrated issues of dependence on strain, external load switching rate and external load switching direction. Investigation into the underlying properties of the system using salt solution tissue analogues showed issues with electrode polarisation resistance and current limitation through reaction kinetics. The biogalvanic method was found to be limited in terms of tissue specificity due to the influence of the cell electrodes. The tissue-electrode interface induces time-dependence into the characterisation and delivers an overestimation of tissue resistance. In addition the passive external load control across suitable test ranges induces current saturation through diffusion limited oxygen reduction at the copper cathode. Modelling the biogalvanic system gave improved insight into the limitations with findings indicating that tissue specificity at surgically appropriate geometries would not be possible.

A multi-reference electrode galvanostatic technique was developed to mitigate the limitations of the biogalvanic system. Though a combination of additional potential measuring electrodes and a current control strategy, improved measurement repeatability was achieved. Tissue specificity was enhanced through the employed measurement procedure, effectively removing the polarisation signature of the electrodes from the recorded data. In agreement with the theory behind the technique, insensitivity was found for polarisation rate and range, delivering potential flexibility for application specific device development. From resistance measurements on a range of healthy and cancerous colon tissues, statistical discrimination of diseased tissue was found and qualitatively correlated with histological findings.

9.4 Future work

The work of Chapters 7 and 8 has indicated the potential for the multi-reference resistance measurement technique. However there are many emerging research questions that may need to be addressed to allow integration of this technology into a useful surgical tool. Some of the primary considerations are discussed below.

9.4.1 Tumour margin delineation

Chapter 8 has demonstrated that distinction of health and cancerous tissue is possible with the technique. Figure 8.9 showed that there is measureable graduation with distance from the tumour centre. This initial finding is promising, however, verification and assessment of this capability is required to determine sensitivity of the technology for margin assessment.

9.4.2 *In vivo* testing

Testing of the multi-reference resistance measurement technique presented in this thesis has only been conducted on *ex vivo* tissues. The influence of time on measured tissue response has been demonstrated (c.f. Section 7.6.2) and therefore it is essential that the methodology be validated in an *in vivo* setting if it is to be proposed as an intraoperative tissue assessment tool.

9.4.3 Sensor modelling

The theory behind the technique predicts a resistance that is representative of the difference in resistive pathways between the working electrode and each reference electrode. The measured resistance is therefore highly dependent on the electric field distribution and current pathway. Numerical modelling of the electrode configuration under galvanostatic control would allow the influencing parameters such as electrode geometry and tissue resistivity to be explored. These findings would make evident the penetration depth and spatial range of the geometries previously tested and allow for optimisation of future sensors.

9.4.4 Device integration

The electrode sizes and materials used in the presented testing are appropriate for integration into surgical tools. However, some miniaturisation would be required and the electrode spacing has been shown to influence resistance magnitude (c.f. Section 7.6.5) and therefore impact on the achievable measurement resolution. More broad considerations are required to determine a suitable form-factor for delivering the electrodes to the tissue surface. Integration into a standard laparoscopic grasper is a clear option, however, the usefulness of the data obtained from this configuration may need to be assessed against possible alternatives.

9.4.5 Array electrodes

Single point measurement delivers a simple unambiguous metric representative of the resistance of the contact area under assessment. For the application of margin delineation, wider spatial mapping is necessary. Therefore, point measurements must be correlated with position or an electrode array must be used to quickly assess a larger area. Developing an electrode array which can conform to the tissue and deliver a precise position-resistance map is a challenging engineering problem requiring significant additional research.

References

[1] Ferlay, J., H.R. Shin, F. Bray, D. Forman, C. Mathers and D.M. Parkin, *GLOBOCAN 2008 v1.2, Cancer Incidence and Mortality Worldwide: IARC CancerBase No. 10*. 2010.

[2] CRUK, *Data Table: Cancer incidence and mortality rates in the UK*. [cited September 2015]; Available from: publications.cancerresearchuk.org.

[3] Tufano, R.P. and E. Kandil, *Considerations for personalized surgery in patients with papillary thyroid cancer*. Thyroid, 2010. 20(7): p. 771-6.

[4] Tiernan, J.P., I. Ansari, N.A. Hirst, P.A. Millner, T.A. Hughes and D.G. Jayne, *Intra-operative tumour detection and staging in colorectal cancer surgery*. Colorectal Disease, 2012. 14(9): p. e510-e20.

[5] Stummer, W., U. Pichlmeier, T. Meinel, O.D. Wiestler, F. Zanella and H.-J. Reulen, *Fluorescence-guided surgery with 5-aminolevulinic acid for resection of malignant glioma: a randomised controlled multicentre phase III trial*. The Lancet Oncology, 2006. 7(5): p. 392-401.

[6] van Dam, G.M., G. Themelis, L.M.A. Crane, N.J. Harlaar, R.G. Pleijhuis, W. Kelder, et al., *Intraoperative tumor-specific fluorescence imaging in ovarian cancer by folate receptor-α targeting: first in-human results*. Nat Med, 2011. 17(10): p. 1315-9.

[7] Săftoiu, A., P. Vilmann, T. Ciurea, G.L. Popescu, A. Iordache, H. Hassan, et al., *Dynamic analysis of EUS used for the differentiation of benign and malignant lymph nodes*. Gastrointestinal Endoscopy, 2007. 66(2): p. 291-300.

[8] Halter, R.J., A. Schned, J. Heaney, A. Hartov and K.D. Paulsen, *Electrical Properties of Prostatic Tissues: I. Single Frequency Admittivity Properties*. The Journal of Urology, 2009. 182(4): p. 1600-7.

[9] CRUK, *Types of Surgery for Bowel Cancer*. [cited September 2015]; Available from: cancerresearchuk.org/about-cancer/type/bowel-cancer/treatment/surgery/which-surgery-for-bowel-cancer.

[10] CRUK, *All cancers combined Key Stats*. 2015.

[11] National Cancer Institute, *Types of Treatment*. [cited August 2014]; Available from: cancer.gov/about-cancer/treatment/types/stem-cell-transplant.

[12] Smith, M.E. and D.G. Morton, *The Digestive System: Systems of the Body Series*: Elsevier Health Sciences UK. 2011.

[13] Krstic, R.V., *Human Microscopic Anatomy: An Atlas for Students of Medicine and Biology*: Springer Berlin Heidelberg. 2013.

[14] Fleming, M., S. Ravula, S.F. Tatishchev and H.L. Wang, *Colorectal carcinoma: Pathologic aspects*. Journal of Gastrointestinal Oncology, 2012. 3(3): p. 153-73.

[15] About Cancer, *Colon nodes*. [Image cited March 2015]; Available from: aboutcancer.com/colon_nodes_grays.gif.

[16] Cunningham, D., W. Atkin, H.-J. Lenz, H.T. Lynch, B. Minsky, B. Nordlinger, et al., *Colorectal cancer*. The Lancet, 2014. 375(9719): p. 1030-47.

[17] Sobin, L.H., M.K. Gospodarowicz and C. Wittekind, *TNM Classification of Malignant Tumours*: Wiley. 2011.

[18] CRUK, *Diagram showing T stages of bowel cancer CRUK 276*. [Image cited March 2015]; Available from: tinyurl.com/pf2r3v2.

[19] About Cancer, *Colon Stage*. [Image cited April 2015]; Available from: aboutcancer.com/colon_stage.htm.

[20] Beart, R.W., G.D. Steele, H.R. Menck, J.S. Chmiel, K.E. Ocwieja and D.P. Winchester, *Management and survival of patients with adenocarcinoma of the colon and rectum: a national survey of the Commission on Cancer*. Journal of the American College of Surgeons, 1995. 181(3): p. 225-36.

[21] Poston, G.J., D. Beauchamp and T. Ruers, *Textbook of Surgical Oncology*: Taylor & Francis. 2007.

[22] CRUK, *Cancer Reseach UK's Research Strategy*. 2008. p. 48.

[23] Emmanuelm, *Colon cancer 2*. [Image cited 22 April 2014]; Available from: upload.wikimedia.org/wikipedia/commons/c/cc/Colon_cancer_2.jpg.

[24] University of Utah, *Adenocarcinoma arising in villous adenoma*. [Image cited 22 April 2015]; Available from: pathologyoutlines.com/topic/colontumorvillousadenoma.html.

[25] Junqueira, L.C.U. and J. Carneiro, *Basic Histology: Text & Atlas*: McGraw-Hill. 2005.

[26] The, C.c.L.o.O.R.S.G., *Laparoscopic surgery versus open surgery for colon cancer: short-term outcomes of a randomised trial*. The Lancet Oncology, 2005. 6(7): p. 477-84.

[27] Harrell, A.G. and B.T. Heniford, *Minimally invasive abdominal surgery: lux et veritas past, present, and future*. The American Journal of Surgery, 2005. 190(2): p. 239-43.

[28] Medicare, D., *Laparoscopic sureries*. [Image cited 23 November 2014]; Available from: divjoninursinghome.com/laparoscopic_surgery.php.

[29] Jacobson, B. and A. Murray, *Medical Devices: Use and Safety*: Churchill Livingstone. 2007.

[30] MD, L., *Laparoscopic Trocars*. [cited 29/07/15 2015]; Available from: laparoscopic.md/instruments/trocar.

[31] Mishra, R.K. and R. Mishra, *Textbook of Practical Laparoscopic Surgery*: Jaypee Brothers, Medical Publishers Pvt. Limited. 2013.

[32] Jamieson, E.S., J.H. Chandler, P.R. Culmer, M. Manogue, M. Mon-Williams and R. Wilkie, *Can Virtual Reality Trainers Improve the Compliance Discrimination Abilities of Trainee Surgeons?* in Engineering in Medicine and Biology Society (EMBC), 2015 37th Annual International Conference of the IEEE, 2015: Milan, Italy

[33] Remzi, F.H., H.T. Kirat, J.H. Kaouk and D.P. Geisler, *Single-port laparoscopy in colorectal surgery*. Colorectal Disease, 2008. 10(8): p. 823-6.

[34] Wedmid, A., E. Llukani and D.I. Lee, *Future perspectives in robotic surgery*. BJU International, 2011. 108(6b): p. 1028-36.

[35] Faust, R.A., *Robotics in Surgery: History, Current and Future Applications*: Nova Science Publishers. 2007.

[36] Freschi, C., V. Ferrari, F. Melfi, M. Ferrari, F. Mosca and A. Cuschieri, *Technical review of the da Vinci surgical telemanipulator*. The International Journal of Medical Robotics and Computer Assisted Surgery, 2013. 9(4): p. 396-406.

[37] Tholey, G., J.P. Desai and A.E. Castellanos, *Force Feedback Plays a Significant Role in Minimally Invasive Surgery: Results and Analysis*. Annals of Surgery, 2005. 241(1): p. 102-9.

[38] Mayer, H., I. Nagy, A. Knoll, E. Braun, R. Bauernschmitt and R. Lange, *Haptic Feedback in a Telepresence System for Endoscopic Heart Surgery*. Presence, 2007. 16(5): p. 459-70.

[39] Rao, P.P., P.P. Rao and S. Bhagwat, *Single-incision laparoscopic surgery - current status and controversies*. Journal of Minimal Access Surgery, 2011. 7(1): p. 6-16.

[40] Autorino, R., R. Yakoubi, W.M. White, M. Gettman, M. De Sio, C. Quattrone, et al., *Natural orifice transluminal endoscopic surgery (NOTES): where are we going? A bibliometric assessment*. BJU International, 2013. 111(1): p. 11-6.

[41] Nordlinger, C., *The Internet of Things and the Operating Room of the Future*. 2015.

[42] Kopelman, Y., R.J. Lanzafame and D. Kopelman, *Trends in Evolving Technologies in the Operating Room of the Future*. JSLS : Journal of the Society of Laparoendoscopic Surgeons, 2013. 17(2): p. 171-3.

[43] Moustris, G.P., S.C. Hiridis, K.M. Deliparaschos and K.M. Konstantinidis, *Evolution of autonomous and semi-autonomous robotic surgical systems: a review of the literature*. The International Journal of Medical Robotics and Computer Assisted Surgery, 2011. 7(4): p. 375-92.

[44] Balog, J., L. Sasi-Szabó, J. Kinross, M.R. Lewis, L.J. Muirhead, K. Veselkov, et al., *Intraoperative Tissue Identification Using Rapid Evaporative Ionization Mass Spectrometry*. Science Translational Medicine, 2013. 5(194): p. 194ra93.

[45] Fung, Y.C., *Biomechanics: Mechanical Properties of Living Tissues*: Springer New York. 2013.

[46] Hayashi, K. *Mechanical Properties of Soft Tissues and Arterial Walls*. In: Holzapfel GA, Ogden RW, editors. Biomechanics of Soft Tissue in Cardiovascular Systems: Springer Vienna. 2014. p. 15-54.

[47] Hoyt, K., B. Castaneda, M. Zhang, P. Nigwekar, P.A. di Sant'agnese, J.V. Joseph, et al., *Tissue elasticity properties as biomarkers for prostate cancer*. Cancer Biomark, 2008. 4(4-5): p. 213-25.

[48] Krouskop, T.A., T.M. Wheeler, F. Kallel, B.S. Garra and T. Hall, *Elastic Moduli of Breast and Prostate Tissues under Compression*. Ultrasonic Imaging, 1998. 20(4): p. 260-74.

[49] Phipps, S., T.H.J. Yang, F.K. Habib, R.L. Reuben and S.A. McNeill, *Measurement of tissue mechanical characteristics to distinguish between benign and malignant prostatic disease*. Urology, 2005. 66(2): p. 447-50.

[50] Blanks, R.G., S.M. Moss, C.E. McGahan, M.J. Quinn and P.J. Babb, *Effect of NHS breast screening programme on mortality from breast cancer in England and Wales, 1990-8: comparison of observed with predicted mortality*2000.

[51] Barton, M.B., R. Harris and S.W. Fletcher, *Does this patient have breast cancer?: The screening clinical breast examination: should it be done? how?* JAMA, 1999. 282(13): p. 1270-80.

[52] Maxwell, J., White, J.R., David, P, O'Brien, III. *Prostate Examination*. In: Walker KH, Hall, W.D., Hurst, J.W, editor. Clinical Methods: The History, Physical, and Laboratory Examinations. 3rd ed. Boston: Butterworths. 1990.

[53] Lai, W.M., D. Rubin and E. Krempl, *Introduction to Continuum Mechanics*: Butterworth-Heinemann/Elsevier. 2009.

[54] Landau, L.D., L.P. Pitaevskii, A.M. Kosevich and E.M. Lifshitz, *Theory of Elasticity*: Elsevier Science. 2012.

[55] Flügge, W., *Viscoelasticity*: Springer Berlin Heidelberg. 2013.

[56] Mow, V.C. and W.M. Lai, *Recent Developments in Synovial Joint Biomechanics*. SIAM Review, 1980. 22(3): p. 275-317.

[57] Tholey, G., A. Pillarisetti, W. Green and J. Desai. *Design, Development, and Testing of an Automated Laparoscopic Grasper with 3-D Force Measurement Capability Medical Simulation*. In: Cotin S, Metaxas D, editors.: Springer Berlin / Heidelberg. 2004. p. 38-48.

[58] Zbyszewski, D., P. Polygerinos, L.D. Seneviratne and K. Althoefer, *A novel MRI compatible air-cushion tactile sensor for Minimally Invasive Surgery*. IEEE/RSJ International Conference on Intelligent Robots and Systems, 2009 (IROS) St. Louis, USA2009. p. 2647-52.

[59] Zbyszewski, D., B. Challacombe, J. Li, L. Seneviratne, K. Althoefer, P. Dasgupta, et al., *A comparative study between an improved novel air-cushion sensor and a wheeled probe for minimally invasive surgery*. Journal of endourology / Endourological Society, 2010. 24(7): p. 1155-9.

[60] Phipps, S., T.H.J. Yang, F.K. Habib, R.L. Reuben and S.A. McNeill, *Measurement of the mechanical characteristics of benign prostatic tissue: A Novel method for assessing benign prostatic disease*. Urology, 2005. 65(5): p. 1024-8.

[61] Yang, T.H., S. Leung Sk Fau - Phipps, R.L. Phipps S Fau - Reuben, S.A. Reuben Rl Fau - McNeill, F.K. McNeill Sa Fau - Habib, A. Habib Fk Fau - Schnieder, et al., *In-vitro dynamic micro-probing and the mechanical properties of human prostate tissues*. (0928-7329 (Print)): p.

[62] Hein, M., T.H. Yang, R.L. Reuben and E. R.W., *Dynamic measurement of intraocular pressure using a mechanical model of the human eye*. Medicine Meets Engineering, 2008. 133: p. 112-22.

[63] Hien, M.R. and R.L. Reuben. *Dynamic palpation device to evaluate IOP; simulation on a mechanical eyeball system*. In: Dössel O, Schlegel W, editors. World Congress on Medical Physics and Biomedical Engineering, September 7 - 12, 2009, Munich, Germany: Springer Berlin Heidelberg. 2009. p. 339-42.

[64] Scanlan, P., S.J. Hammer, D.W. Good, S. Phipps, G.D. Stewart, S.A. McNeill, et al., *Development of a novel actuator for the dynamic palpation of soft tissue for use in the assessment of prostate tissue quality*. Sensors and Actuators A: Physical, (0): p.

[65] Kersaudy-Kerhoas, M., F. Amalou, A. Che, J. Kelly, Y. Liu, M.P.Y. Desmulliez, et al., *Validation of a fully integrated platform and disposable microfluidic chips enabling parallel purification of genome segments for assembly*. Biotechnology and Bioengineering, 2014. 111(8): p. 1627-37.

[66] Gunn, C., *Digital and Radiographic Imaging: A Practical Approach*: Elsevier Health Sciences. 2008.

[67] Szabo, T.L., *Diagnostic Ultrasound Imaging: Inside Out*: Elsevier Academic Press. 2004.

[68] Taylor, L.S., B.C. Porter, D.J. Rubens and K.J. Parker, *Three-dimensional sonoelastography: principles and practices*. Physics in Medicine and Biology, 2000. 45(6): p. 1477-94.

[69] Parker, K.J., M.M. Doyley and D.J. Rubens, *Imaging the elastic properties of tissue: the 20 year perspective* Physics in Medicine and Biology, 2011. 56: p. R1-R29.

[70] Krouskop, T.A., D.R. Dougherty and F.S. Vinson, *A pulsed Doppler ultrasonic system for making noninvasive measurements of the mechanical properties of soft tissue*. Journal of rehabilitation research and development, 1987. 24(2): p. 1-8.

[71] Lerner, R.M., S.R. Huang and K.J. Parker, *"Sonoelasticity" images derived from ultrasound signals in mechanically vibrated tissues*. Ultrasound in Medicine & Biology, 1990. 16(3): p. 231-9.

[72] Parker, K.J., S.R. Huang, R.A. Musulin and R.M. Lerner, *Tissue response to mechanical vibrations for "sonoelasticity imaging"*. Ultrasound in Medicine & Biology, 1990. 16(3): p. 241-6.

[73] Ophir, J., I. Céspedes, H. Ponnekanti, Y. Yazdi and X. Li, *Elastography: A quantitative method for imaging the elasticity of biological tissues*. Ultrasonic Imaging, 1991. 13(2): p. 111-34.

[74] Garra, B.S., E.I. Cespedes, J. Ophir, S.R. Spratt, R.A. Zuurbier, C.M. Magnant, et al., *Elastography of breast lesions: initial clinical results*. Radiology, 1997. 202(1): p. 79-86.

[75] de Korte, C.L., E.I. Cespedes, A.F.W. van der Steen, G. Pasterkamp and N. Bom, *Intravascular ultrasound elastography: assessment and imaging of elastic properties of diseased arteries and vulnerable plaque*. European Journal of Ultrasound, 1998. 7(3): p. 219-24.

[76] Ophir, J., S.K. Alam, B. Garra, F. Kallel, E. Konofagou, T. Krouskop, et al., *Elastography: Ultrasonic estimation and imaging of the elastic properties of tissues*. Proceedings of the Institution of Mechanical Engineers, Part H: Journal of Engineering in Medicine, 1999. 213(3): p. 203-33.

[77] Lindop, J.E., *2D and 3D Elastic Imaging Using Freehand Ultrasound*. Pembroke College: Univerity of Cambridge; 2008.

[78] Tanter, M., J. Bercoff, A. Athanasiou, T. Deffieux, J.-L. Gennisson, G. Montaldo, et al., *Quantitative Assessment of Breast Lesion Viscoelasticity: Initial Clinical Results Using Supersonic Shear Imaging*. Ultrasound in Medicine & Biology, 2008. 34(9): p. 1373-86.

[79] Hoyt, K., K.J. Parker and D.J. Rubens, *Real-Time Shear Velocity Imaging Using Sonoelastographic Techniques*. Ultrasound in Medicine & Biology, 2007. 33(7): p. 1086-97.

[80] Bhatia, K.S.S., C.C.M. Cho, Y.-H. Yuen, D.D. Rasalkar, A.D. King and A.T. Ahuja, *Real-Time Qualitative Ultrasound Elastography of Cervical Lymph Nodes in Routine Clinical Practice: Interobserver Agreement and Correlation with Malignancy*. Ultrasound in Medicine & Biology, 2010. 36(12): p. 1990-7.

[81] Yoneda, M., K. Suzuki, S. Kato, K. Fujita, Y. Nozaki, K. Hosono, et al., *Nonalcoholic Fatty Liver Disease: US-based Acoustic Radiation Force Impulse Elastography 1*. Radiology, 2010. p.

[82] Miklavčič, D., N. Pavšelj and F.X. Hart. *Electric Properties of Tissues*. Wiley Encyclopedia of Biomedical Engineering: John Wiley & Sons, Inc. 2006.

[83] Gileadi, E., *Physical Electrochemistry*: Wiley. 2011.

[84] Bard, A.J. and L.R. Faulkner, *Electrochemical Methods: Fundamentals and Applications*. New York: Wiley. 1980.

[85] Schauble, M.K., H.D. Gullick and M.B. Habal, *Variations in tissue electropotentials and their possible significance*. Journal of Surgical Research, 1972. 12(5): p. 325-9.

[86] Schauble, M.K. and M.B. Habal, *Electropotentials of normal tissue*. Journal of Surgical Research, 1969. 9(9): p. 513-5.

[87] Gensler, W., *Tissue Electropotentials in Kalanchoë blossfeldiana During Wound Healing*. American Journal of Botany, 1978. 65(2): p. 152-7.

[88] Burr, H.S., G.M. Smith and L.C. Strong, *Bio-Electric Properties of Cancer-Resistant and Cancer-Susceptible Mice*. The American Journal of Cancer, 1938. 32(2): p. 240-8.

[89] Morris, D.M. *Detection of Surface Electropotentials of Human Breast Lesions*. In: Saha S, editor. Biomedical Engineering: I Recent Developments: Proceedings of the First Southern Biomedical Engineering Conference: Elsevier Science. 2013. p. 125-9.

[90] Miklavcic, D., G. Sersa, S. Novaković and S. Rebersek, *Tumor Bioelectric Potential and its Possible Exploitation for Tumor Growth Retardation*. Electromagnetic Biology and Medicine, 1990. 9(2): p. 133-49.

[91] Michaelis, L. and W. Davidoff, *Methodisches und Sachliches zur elektrometrischen Bestimmung der Blutalkalescenz. . Zschr., 46:131.* Biochem, 1912. 46: p. 131-50.

[92] Michaelis, L. and A. Kramsztyk, *Die Wasserstoffionenkonzentration der Gewebssafte*. Biochem, 1914. 62: p. 180-5.

[93] Buerk, D.G., *Biosensors: Theory and Applications*: Taylor & Francis. 1995.

[94] Turner, A., I. Karube and G.S. Wilson, *Biosensors: fundamentals and applications*. 1987. p.

[95] Shukla, P., *Biosensors*. 2014.

[96] DropSens, *Screen printed electrodes*. [Image cited Available from: dropsens.com/en/screen_printed_electrodes_pag.html#modified_carbon_spes.

[97] Chen, C., Q. Xie, D. Yang, H. Xiao, Y. Fu, Y. Tan, et al., *Recent advances in electrochemical glucose biosensors: a review*. RSC Advances, 2013. 3(14): p. 4473-91.

[98] Li, J., S. Li and C.F. Yang, *Electrochemical Biosensors for Cancer Biomarker Detection*. Electroanalysis, 2012. 24(12): p. 2213-29.

[99] Biomarkers Definitions Working, G., *Biomarkers and surrogate endpoints: Preferred definitions and conceptual framework*. Clinical Pharmacology & Therapeutics, 2001. 69(3): p. 89-95.

[100] Brenner, D.E. and D.P. Normolle, *Biomarkers for Cancer Risk, Early Detection, and Prognosis: The Validation Conundrum*. Cancer Epidemiology Biomarkers & Prevention, 2007. 16(10): p. 1918-20.

[101] Vaupel, P., F. Kallinowski and P. Okunieff, *Blood Flow, Oxygen and Nutrient Supply, and Metabolic Microenvironment of Human Tumors: A Review*. Cancer Research, 1989. 49(23): p. 6449-65.

[102] Kieninger, J., A. Dannenberg, K. Aravindalochanan, G. Jobst, E.O. Pettersen and G.A. Urban, *Amperometric Oxygen Sensor Array with Novel Chronoamperometric Protocols for Hypoxic Tumor Cell Cultures*. Solid-State Sensors, Actuators and Microsystems Conference, 2007 Transducers 2007 International2007. p. 1907-10.

[103] Kotanen, C.N., F.G. Moussy, S. Carrara and A. Guiseppi-Elie, *Implantable enzyme amperometric biosensors*. Biosensors and Bioelectronics, 2012. 35(1): p. 14-26.

[104] Grimnes, S. and O.G. Martinsen, *Bioimpedance and Bioelectricity Basics*: Academic Press. 2008.

[105] Chen, J.H. and S.A. Adelman, *Macroscopic model for solvated ion dynamics*. The Journal of Chemical Physics, 1980. 72(4): p. 2819-31.

[106] Nakahara, M. and K. Ibuki, *Is the Walden product useful?* The Journal of Physical Chemistry, 1986. 90(13): p. 3026-30.

[107] Zwanzig, R., *Dielectric Friction on a Moving Ion. II. Revised Theory*. The Journal of Chemical Physics, 1970. 52(7): p. 3625-8.

[108] Martinsen, O.G. and S. Grimnes, *Bioimpedance and Bioelectricity Basics*: Academic Press. 2000.

[109] Burger, H.C. and R.v. Dongen, *Specific Electric Resistance of Body Tissues*. Physics in Medicine and Biology, 1961. 5(4): p. 431.

[110] Kalvøy, H., G.K. Johnsen, O.G. Martinsen and S. Grimnes, *New method for separation of electrode polarization impedance from measured tissue impedance.* Open Biomed Eng J, 2011. 5: p. 6.

[111] Faes, T.J., H.A. van der Meij, J.C. de Munck and R.M. Heethaar, *The electric resistivity of human tissues (100 Hz-10 MHz): a meta-analysis of review studies*. Physiological measurement, 1999. 20(4): p. R1-10.

[112] Zanello, P. and R.S.o. Chemistry, *Inorganic Electrochemistry: Theory, Practice and Applications*: Royal Society of Chemistry. 2003.

[113] Galvani, L., R.M. Green and G. Aldini, *De Viribus Electricitatis in Motu Musculari Commentarius: A Translation of Luigi Galvani's de Viribus Electricitatisin Motu Musculari Commentarius*: Licht. 1953.

[114] Rao, J.R. and G. Richter, *Implantable bio-electrochemical power sources*. Naturwissenschaften, 1974. 61(5): p. 200-6.

[115] Golberg, A., H.D. Rabinowitch and B. Rubinsky, *Galvanic apparent internal impedance: An intrinsic tissue property*. Biochemical and Biophysical Research Communications, 2009. 389(1): p. 168-71.

[116] Golberg, A., S. Laufer, H.D. Rabinowitch and B. Rubinsky, *In vivo non-thermal irreversible electroporation impact on rat liver galvanic apparent internal resistance*. Physics in Medicine and Biology, 2011. 56(4): p. 951-63.

[117] Golberg, A., S. Laufer, H.D. Rabinowitch and B. Rubinsky, *In vivo non-thermal irreversible electroporation impact on rat liver galvanic apparent internal resistance*. Physics in Medicine and Biology, 2011. 56(4): p. 951-63.

[118] Spottorno, J., M. Multigner, G. Rivero, L. Álvarez, J.d.l. Venta and M. Santos, *Time dependence of electrical bioimpedance on porcine liver and kidney under a 50 Hz ac current*. Physics in Medicine and Biology, 2008. 53(6): p. 1701.

[119] Technologies, A., *Agilent Impedance Measurement Handbook*. A guide to measurement technology and techniques. 4th ed. literature.agilent.com2014.

[120] Schwan, H.P., *Electric Characteristics of Tissues*. Radiation and Environmental Biophysics, 1963. 1(3): p. 198-208.

[121] Gabriel, C., S. Gabriel and E. Corthout, *The dielectric properties of biological tissues: I. Literature survey*. Physics in Medicine and Biology, 1996. 41(11): p. 2231.

[122] Gabriel, S., R.W. Lau and C. Gabriel, *The dielectric properties of biological tissues: II. Measurements in the frequency range 10 Hz to 20 GHz*. Physics in Medicine and Biology, 1996b. 41(11): p. 2251.

[123] Laufer, S., A. Ivorra, V.E. Reuter, B. Rubinsky and S.B. Solomon, *Electrical impedance characterization of normal and cancerous human hepatic tissue*. Physiological measurement, 2010. 31: p. 995-1009.

[124] Chauveau, N., L. Hamzaoui, P. Rochaix, B. Rigaud, J.J. Voigt and J.P. Morucci, *Ex vivo discrimination between normal and pathological tissues in human breast surgical biopsies using bioimpedance spectroscopy*. Annals of the New York Academy of Sciences, 1999. 873: p. 42-50.

[125] Jossinet, J., *The impedivity of freshly excised human breast tissue*. Physiological measurement, 1998. 19(1): p. 61.

[126] Åberg, P., I. Nicander, U. Holmgren, P. Geladi and S. Ollmar, *Assessment of skin lesions and skin cancer using simple electrical impedance indices*. Skin Research and Technology, 2003. 9(3): p. 257-61.

[127] Aberg, P., P. Geladi, I. Nicander, J. Hansson, U. Holmgren and S. Ollmar, *Non-invasive and microinvasive electrical impedance spectra of skin cancer - a comparison between two techniques*. Skin Research and Technology, 2005. 11(4): p. 281-6.

[128] Dua, R., D.G. Beetner, W.V. Stoecker and D.C. Wunsch, II, *Detection of basal cell carcinoma using electrical impedance and neural networks*. Biomedical Engineering, IEEE Transactions on, 2004. 51(1): p. 66-71.

[129] B. Blad, P.W., M. Jonsson, K. Lindstrom, *An electrical impedance index to distinguish between normal and cancerous tissues*. Journal of Medical Engineering & Technology, 1999. 23(2): p. 57-62.

[130] Mongra, A.C., *Commercial Biosensors: An outlook*. Journal of Academic and Industrial Research, 2012. 1(6): p. 3.

[131] TearLab, *TearLab*. [cited January 2015]; Available from: tearlab.com.

[132] Zeev, M.S.-B., D.D. Miller and R. Latkany, *Diagnosis of dry eye disease and emerging technologies*. Clinical Ophthalmology (Auckland, NZ), 2014. 8: p. 581-90.

[133] Zilico, *What is ZedScan*. [cited August 2015]; Available from: zilico.co.uk/zedscan/zedscan.

[134] Brown, B.H., R.H. Smallwood, K.J. Boston, A.D. Blackett and J.A. Tidy, *Electrical impedance measuring method for differentiating tissue types*. In: Organization WIP, editor. G01N 33/487, 33/483, A61B 5/05 ed2001.

[135] Abdul, S., B.H. Brown, P. Milnes and J.A. Tidy, *The use of electrical impedance spectroscopy in the detection of cervical intraepithelial neoplasia*. International Journal of Gynecological Cancer, 2006. 16(5): p. 1823-32.

[136] Taruttis, A. and V. Ntziachristos, *Translational Optical Imaging*. American Journal of Roentgenology, 2012. 199(2): p. 263-71.

[137] Bu, L., B. Shen and Z. Cheng, *Fluorescent imaging of cancerous tissues for targeted surgery*. Advanced Drug Delivery Reviews, 2014. 76: p. 21-38.

[138] Sajja, H.K., M.P. East, H. Mao, Y.A. Wang, S. Nie and L. Yang, *Development of multifunctional nanoparticles for targeted drug delivery and noninvasive imaging of therapeutic effect*. Curr Drug Discov Technol, 2009. 6(1): p. 43-51.

[139] Alander, J.T., I. Kaartinen, A. Laakso, T. P, #228, til, et al., *A review of indocyanine green fluorescent imaging in surgery*. Journal of Biomedical Imaging, 2012. 2012: p. 7-.

[140] Recendt, *Principle of photoacoustic imaging*. [Image cited March 2015]; Available from: recendt.at/528_ENG_HTML.php.

[141] Schaafsma, B.E., J.S.D. Mieog, M. Hutteman, J.R. van der Vorst, P.J.K. Kuppen, C.W.G.M. Löwik, et al., *The clinical use of indocyanine green as a near-infrared fluorescent contrast agent for image-guided oncologic surgery*. Journal of Surgical Oncology, 2011. 104(3): p. 323-32.

[142] Kondo, Y., Y. Murayama, H. Konishi, R. Morimura, S. Komatsu, A. Shiozaki, et al., *Fluorescent detection of peritoneal metastasis in human colorectal cancer using 5-aminolevulinic acid*. International Journal of Oncology, 2014. p.

[143] Filonenko, E.V., A.D. Kaprin, A.A. Raszhivina, A.N. Urlova and A.M. Nechipai, *Fluorescence Diagnostics of Colon Malignant and Premalignant Lesions Using 5-Aminolevulinic Acid*. International Journal of Photoenergy, 2014. 2014: p. 4.

[144] Mehrmohammadi, M., S.J. Yoon, D. Yeager and S.Y. Emelianov, *Photoacoustic Imaging for Cancer Detection and Staging*. Current molecular imaging, 2013. 2(1): p. 89-105.

[145] Zackrisson, S., S.M.W.Y. van de Ven and S.S. Gambhir, *Light In and Sound Out: Emerging Translational Strategies for Photoacoustic Imaging*. Cancer Research, 2014. 74(4): p. 979-1004.

[146] Palmeri, M.L. and N.K. R.. *What challenges must be overcome before ultrasound elasticity imaging is ready for the clinic?* Imaging Med, 2011. 3(4): p. 11.

[147] Curiel, L., R. Souchon, O. Rouvière, A. Gelet and J.Y. Chapelon, *Elastography for the follow-up of high-intensity focused ultrasound prostate cancer treatment: Initial comparison with MRI*. Ultrasound in Medicine & Biology, 2005. 31(11): p. 1461-8.

[148] Clark, L.C., *Monitor and control of blood and tissue oxygen tensions*. Transactions of the American society for Articial Internal Organs 1956. 2: p. 8.

[149] Golberg, A., H.D. Rabinowitch and B. Rubinsky, *Zn/Cu- vegetative batteries, bioelectrical characterizations and primary cost analyses. J. Renewable and Sustainable Energy*. Journal of Renewable and Sustainable Energy, 2010. 2(3): p. 11.

[150] Li, G. and P. Miao. *Theoretical Background of Electrochemical Analysis*. Electrochemical Analysis of Proteins and Cells: Springer Berlin Heidelberg. 2013. p. 5-18.

[151] Instruments, N., *Specifications NI myDAQ*. 2014.

[152] Metrohm, *Basic overview of the working principle of a potentiostat/galvanostat (PGSTAT) - Electrochemical cell setup*. Autolab Application Note EC08. 2016.

[153] Technologies, I., *CompactStat: Hardware specifications*. [cited Available from: ivium.nl/CompactStat%20Hardware%20specifications.

[154] Schwarzenbach, J., *Essentials of Control*: Longman. 1996.

[155] Moré, J. *The Levenberg-Marquardt algorithm: Implementation and theory*. In: Watson GA, editor. Numerical Analysis. New York: Springer-Verlag. 1977. p. 105-16.

[156] Chandler, J.H., A. Hood, P.R. Culmer, D. Jayne and A. Neville, *Technological assessment of the biogalvanic method for tissue characterization*. Physiological Measurement, 2014. 35(2): p. 297.

[157] Lal, H. and H.R. Thirsk, *The anodic behaviour of copper in neutral and alkaline chloride solutions*. J Chem Soc, 1953. (0): p. 2638-44.

[158] Miklavčič, D., N. Pavšelj and F.X. Hart. *Electric Properties of Tissues*. In: Akay M, editor. Wiley Encyclopedia of Biomedical Engineering. New York: John Wiley & Sons, Inc. 2006. p. 3578-89.

[159] Bard, A.J. and L.R. Faulkner, *Electrochemical Methods: Fundamentals and Applications 2nd ed.* 2nd ed. New York: Wiley. 2001.

[160] Thomas, S., N. Birbilis, M.S. Venkatraman and I.S. Cole, *Corrosion of Zinc as a Function of pH*. Corrosion, 2012. 68(1): p. 015009-1--9.

[161] García-Antón, J., A. Igual-Muñoz, J.L. Guiñón, V. Pérez-Herranz and J. Pertusa-Grau, *Online Visualization of Corrosion Processes of Zinc and a Cu/Zn Galvanic Pair in Lithium Bromide Solutions*. Corrosion, 2003. 59(2): p. 172-80.

[162] Kear, G.A., C. Ponce de Leon Albarran and F.C. Walsh, *Reduction of dissolved oxygen at a copper rotating disc electrode*. Chemical Engineering Education, 2005. 39: p. 14-21.

[163] Igual-Muñoz, A., J. García-Antón, J.L. Guiñón and V. Pérez-Herranz, *Galvanic Study of Zinc and Copper in Lithium Bromide Solutions at Different Temperatures*. Corrosion, 2001. 57(6): p. 516-22.

[164] Grimnes, S. and O.G. Martinsen, *Bioimpedance and Bioelectricity Basics*. New York: Academic Press. 2000.

[165] Halter, R.J., A. Hartov, K.D. Paulsen, A. Schned and J. Heaney, *Genetic and least squares algorithms for estimating spectral EIS parameters of prostatic tissues*. Physiol Meas, 2008. 29(6): p. S111-S23.

[166] Gilányi, M., C. Ikrényi, J. Fekete, K. Ikrényi and A.G. Kovách, *Ion concentrations in subcutaneous interstitial fluid: measured versus expected values*. Am J Physiol, 1988. 255(3 Pt 2): p. 513-9.

[167] de Silva, C.W., *Mechatronics: An Integrated Approach*: Taylor & Francis. 2004.

[168] Carreau, A., B.E. Hafny-Rahbi, A. Matejuk, C. Grillon and C. Kieda, *Why is the partial oxygen pressure of human tissues a crucial parameter? Small molecules and hypoxia*. J Cell Mol Med, 2011. 15(6): p. 1239-53.

[169] Sherwood, J.E., F. Stagnitti, M.J. Kokkinn and W.D. Williams, *A standard table for predicting equilibrium dissolved oxygen concentrations in Salt Lakes dominated by sodium chloride*. Int J Salt Lake Res, 1992. 1(1): p. 1-6.

[170] Parthasarathy, A., S. Srinivasan, A.J. Appleby and C.R. Martin, *Temperature Dependence of the Electrode Kinetics of Oxygen Reduction at the Platinum/Nafion® Interface—A Microelectrode Investigation*. Journal of The Electrochemical Society, 1992. 139(9): p. 2530-7.

[171] Vukmirovic, M.B., N. Vasiljevic, N. Dimitrov and K. Sieradzki, *Diffusion-Limited Current Density of Oxygen Reduction on Copper*. Journal of The Electrochemical Society, 2003. 150(1): p. B10-B5.

[172] Tobias, C.W., M. Eisenberg and C.R. Wilke, *Fiftieth Anniversary: Diffusion and Convection in Electrolysis—A Theoretical Review*. Journal of The Electrochemical Society, 1952. 99(12): p. 359C-65C.

[173] Chandler, J.H., P.R. Culmer, D.G. Jayne and A. Neville, *Assessment of electrochemical properties of a biogalvanic system for tissue characterisation*. Bioelectrochemistry, 2015. 101: p. 138-45.

[174] Moisel, M., M.A.F.L. de Mele and W.D. Müller, *Biomaterial Interface Investigated by Electrochemical Impedance Spectroscopy*. Advanced Engineering Materials, 2008. 10(10): p. B33-B46.

[175] Walter, G.W., *Critical analysis of some electrochemical techniques including polarization resistance, for the study of zinc coating performance in near neutral chloride solutions*. Corrosion Science, 1975. 15(1): p. 47-56.

[176] Chandler, J.H., P.R. Culmer, D.G. Jayne and A. Neville, *Assessment of electrochemical properties of a biogalvanic system for tissue characterisation*. Bioelectrochemistry, 2015. 101(0): p. 138-45.

[177] Press, W.H., *Numerical Recipes 3rd Edition: The Art of Scientific Computing*: Cambridge University Press. 2007.

[178] Doig, P. and P.E.J. Flewitt, *A Finite Difference Numerical Analysis of Galvanic Corrosion for Semi-Infinite Linear Coplanar Electrodes*. Journal of The Electrochemical Society, 1979. 126(12): p. 2057-63.

[179] Munn, R.S. and O.F. Devereux, *Numerical Modeling and Solution of Galvanic Corrosion Systems: Part I. Governing Differential Equation and Electrodic Boundary Conditions*. Corrosion, 1991. 47(8): p. 612-8.

[180] Saad, Y. and M.H. Schultz, *GMRES: a generalized minimal residual algorithm for solving nonsymmetric linear systems*. SIAM J Sci Stat Comput, 1986. 7(3): p. 856-69.

[181] Hamann, C.H., A. Hamnett and W. Vielstich, *Electrochemistry*: Wiley. 2007.

[182] Faes, T.J.C., H.A.v.d. Meij, J.C.d. Munck and R.M. Heethaar, *The electric resistivity of human tissues (100 Hz-10 MHz): a meta-analysis of review studies*. Physiol Meas, 1999. 20(4): p. R1.

[183] Faes, T.J., H.A. van der Meij, J.C. de Munck and R.M. Heethaar, *The electric resistivity of human tissues (100 Hz-10 MHz): a meta-analysis of review studies*. Physiol Meas, 1999. 20(4): p. R1-10.

[184] Wang, J., *Electrochemical glucose biosensors*. Chemical reviews, 2008. 108(2): p. 814-25.

[185] Soper, S.A., K. Brown, A. Ellington, B. Frazier, G. Garcia-Manero, V. Gau, et al., *Point-of-care biosensor systems for cancer diagnostics/prognostics*. Biosensors and Bioelectronics, 2006. 21(10): p. 1932-42.

[186] Brown, B.H., J.A. Tidy, K. Boston, A.D. Blackett, R.H. Smallwood and F. Sharp, *Relation between tissue structure and imposed electrical current flow in cervical neoplasia*. The Lancet, 2000. 355(9207): p. 892-5.

[187] Tidy, J.A., B.H. Brown, T.J. Healey, S. Daayana, M. Martin, W. Prendiville, et al., *Accuracy of detection of high-grade cervical intraepithelial neoplasia using electrical impedance spectroscopy with colposcopy*. BJOG: An International Journal of Obstetrics & Gynaecology, 2013. 120(4): p. 400-11.

[188] Scribner, L.L. and S.R. Taylor, *The Measurement and Correction of Electrolyte Resistance in Electrochemical Tests*. Baltimore: ASTM. 1990.

[189] Hack, H.P., P.J. Moran and J.R. Scully. *Influence of Electrolyte Resistance on Electrochemical Measurements and Proceedures to Minimize or Compensate for Resistance Errors*. In: 1056 AS, Scribner LL, Taylor SR, editors. The Measurement and Correction of Electrolyte Resistance in Electrochemical Tests. Philadelphia: American Society for Testing and Materials. 1990. p. 5-26.

[190] Britz, D., *iR elimination in electrochemical cells*. Journal of Electroanalytical Chemistry and Interfacial Electrochemistry, 1978. 88(3): p. 309-52.

[191] Barnartt, S., *Primary Current Distribution Around Capillary Tips Used in the Measurement of Electrolytic Polarization*. Journal of The Electrochemical Society, 1952. 99(12): p. 549-53.

[192] Barnartt, S., *Magnitude of IR-Drop Corrections in Electrode Polarization Measurements Made with a Luggin-Haber Capillary*. Journal of The Electrochemical Society, 1961. 108(1): p. 102-4.

[193] Hong, S.H., C. Kraiya, M.W. Lehmann and D.H. Evans, *Evaluation of uncompensated solution resistance for electrodes with spherical-cap geometry*. Anal Chem, 2000. 72(3): p. 454-8.

[194] McIntyre, J.D.E. and W.F. Peck, *An Interrupter Technique for Measuring the Uncompensated Resistance of Electrode Reactions under Potentiostatic Control*. Journal of The Electrochemical Society, 1970. 117(6): p. 747-51.

[195] Williams, L.F.G. and R.J. Taylor, *iR correction: Part I. A computerised interrupt method*. Journal of Electroanalytical Chemistry and Interfacial Electrochemistry, 1980. 108(3): p. 293-303.

[196] Herrmann, C.C., G.G. Perrault and A.A. Pilla, *Dual reference electrode for electrochemical pulse studies*. Analytical Chemistry, 1968. 40(7): p. 1173-4.

[197] Pallás-Areny, R. and J.G. Webster. *Signal Conditioning for Resistive Sensors*. Sensors and Signal Conditioning, Second Edition: John Wiley & Sons, Limited. 2006. p. 133-206.

[198] Jha, C. and A. Sanchez. *Microprocessor Temperature Sensing and Thermal Management*. Thermal Sensors: Principles and Applications for Semiconductor Industries: Springer New York. 2015.

[199] Haglund, W.D. and M.H. Sorg. *Postmortem changes in soft tissues*. Forensic Taphonomy: The Postmortem Fate of Human Remains: Taylor & Francis. 1996. p. 151-64.

[200] Haemmerich, D., O.R. Ozkan, J.Z. Tsai, S.T. Staelin, S. Tungjitkusolmun, D.M. Mahvi, et al., *Changes in electrical resistivity of swine liver after occlusion and postmortem*. Medical and Biological Engineering and Computing, 2002. 40(1): p. 29-33.

[201] Mortimer, J.T., D. Kaufman and U. Roessmann, *Intramuscular electrical stimulation: Tissue damage*. Annals of Biomedical Engineering, 1980. 8(3): p. 235-44.

[202] Chandler, J.H., A. Hood, P.R. Culmer, D. Jayne and A. Neville, *A bio-galvanic approach to tissue characterisation: technological considerations*. in Hamlyn Symposium on Medical Robotics, 2013: London, UK

[203] Chandler, J.H., D.G. Jayne, A. Neville and P.R. Culmer, *A novel multiple electrode direct current technique for characterisation of tissue resistance during surgery*. in Engineering in Medicine and Biology Society (EMBC), 2015 37th Annual International Conference of the IEEE, 2015: Milan, Italy

[204] Chandler, J.H., P.R. Culmer, D.G. Jayne and A. Neville, *A time-dependent model for improved biogalvanic tissue characterisation*. Medical Engineering & Physics: p.

[205] Rutherford, D.E., *Vector Methods Applied to Differential Geometry, Mechanics, and Potential Theory*: Dover Publications. 2004.

Appendix A

External resistance values

Table A.1: Biogalvanic test external resistance values for equivalent binary index for Resistor set 1 and 2.

Index	Resistor Set 1 (kΩ)	Resistor Set 2 (kΩ)
1	5.1	0.0115
2	10.03	0.1006
3	15.13	0.1117
4	20	1.004
5	25.1	1.015
6	30	1.105
7	35.1	1.117
8	43	9.99
9	48.1	10
10	53	10.1
11	58.1	10.11
12	63	11
13	68.1	11.01
14	73	11.1
15	78	11.12
16	82.2	82.3
17	87.3	82.3
18	92.2	82.5
19	97.3	82.5
20	102.2	83.4
21	107.3	83.4
22	112.2	83.5
23	117.3	83.5
24	125.2	92.3
25	130.3	92.4
26	135.2	92.5
27	140.3	92.5
28	145.2	93.4
29	150.2	93.4
30	155.2	93.5
31	160.2	93.6
32	160.1	160.3
33	165.2	160.3
34	170.1	160.4
35	175.2	160.5
36	180	161.3
37	185.1	161.4
38	190	161.5
39	195.1	161.5
40	202	170.3
41	207	170.4
42	212	170.5
43	217	170.5
44	222	171.4
45	227	171.4
46	232	171.5
47	237	171.6

48	241	243
49	246	243
50	251	243
51	256	243
52	261	244
53	266	244
54	271	244
55	276	245
56	284	253
57	289	253
58	294	253
59	299	253
60	304	254
61	309	254
62	314	254
63	319	254
64	329	329
65	334	330
66	338	330
67	343	330
68	348	331
69	353	331
70	358	331
71	363	331
72	371	340
73	376	340
74	381	340
75	386	340
76	391	341
77	396	341
78	401	342
79	406	342
80	410	412
81	415	412
82	420	413
83	425	413
84	430	413
85	435	414
86	440	414
87	445	414
88	453	422
89	458	422
90	463	423
91	468	423
92	473	424
93	478	424
94	483	424
95	488	424
96	488	490
97	493	490
98	498	490
99	503	490
100	508	491
101	513	492
102	518	492
103	523	492
104	531	500
105	536	500
106	541	501
107	546	501
108	551	502

109	556	502
110	560	502
111	565	502
112	570	573
113	575	573
114	580	573
115	585	573
116	590	574
117	595	574
118	599	575
119	604	575
120	613	583
121	618	583
122	623	583
123	627	584
124	633	584
125	637	584
126	642	585
127	647	585

Appendix B
Numerical model supplementary information

This information was supplied by the School of Computing (University of Leeds). This forms supplementary information pertinent to the numerical model described in Chapter 6.

Voltage-current relations for the medium in the limits $L \ll r$ and $L \gg r$

The numerical solution of the geometry-dependent tissue resistance described in Section 6.4.2.1 can be tested against analytical solutions for when the electrodes are very close together (separation $L \ll r$, or $a \ll 1$, with r the radius of each electrode), and when they are far apart ($L \gg r$ or $a \gg 1$). For the former case, the field ϕ will not significantly vary in directions transverse to the electrode surfaces, and the bulk can therefore be treated as a quasi-1D problem for which the current density $i = \sigma V_{med}/L$ with V_{med} the voltage drop across the medium. Using the same normalisation as in Section 6.4, the voltage-current relation for the medium is readily found to be

$$\frac{V_{med}}{\alpha} = \frac{I}{\pi r^2 i_0}\frac{a}{b}. \tag{B1}$$

In the opposite limit $a \gg 1$, *i.e.* where the electrode dimensions are much smaller than their separation, each can be treated as a point charge, taken here to be $+q$ for the anode at $\boldsymbol{x} = (0,0,0)$, and $-q$ for the cathode at $\boldsymbol{x} = (0,0,L)$, with q determined below. However, to satisfy the boundary conditions $\boldsymbol{e_z} \cdot \boldsymbol{\nabla}\phi = 0$ at $z = 0$ and $z = L$ (where $\boldsymbol{e_z}$ is the unit vector in the z-direction), it is necessary to consider an infinite, linear array of image charges at $x = y = 0$ and $z = \cdots, -2L, -L, 0, L, 2L, \ldots$, alternating in sign. The field at any point is then found by summing that for each point charge [205], *i.e.*

$$\phi(\boldsymbol{x}) = \sum_{i=-\infty}^{\infty} \frac{(-1)^i q}{|\boldsymbol{x} - iL\boldsymbol{e_z}|}. \tag{B2}$$

V_{med} is evaluated as the voltage difference between hemispherical surfaces a small distance ε from each point charge, and I as the mean current across the same surfaces parallel to $\boldsymbol{e}_z$. Eliminating q and expanding in r/L then gives the voltage-current relation

$$\frac{V_{med}}{\alpha} = \frac{I}{\pi r^2 i_0}\frac{2}{b}\left\{1 - \frac{r}{L}2ln2 + O\left[\left(\frac{r}{L}\right)^2\right]\right\}. \quad \text{(B3)}$$

Equations (B1) and (B3) are then combined with the non-linear Tafel equations as per equation (6.7). Figure. B.1 overlays these solutions to the numerical results for the same four points as in Figure 6.8 in the main text, demonstrating excellent agreement.

The resistances $R_{med} = V_{med}/I$ for the medium-dominated regime in both limits can be found from (B1) and (B3) by simple rearrangement. For (B3) the leading-order correction in r/L was dropped from the expression given in Section 6.4.

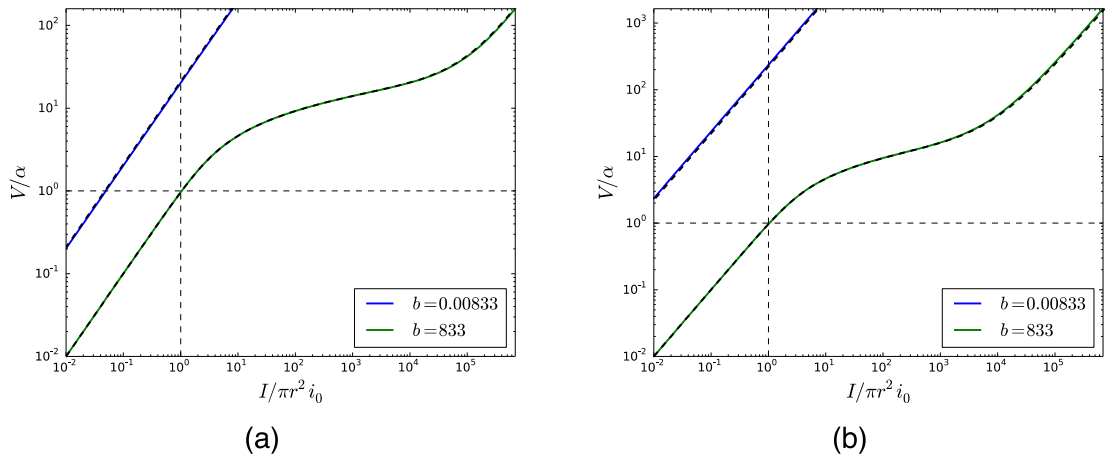

Figure B1.1: Comparison between the analytical and numerical solutions for (a) Equation (B1) and $\boldsymbol{a = 1/6}$, and (b) Equation (B3) and $\boldsymbol{a = 16.667}$. The Tafel equations gave been included following the same procedure described in Sec. 2.1 of the main text, and two values of $\boldsymbol{b}$ were selected as shown in the legends. The solid coloured lines correspond to the analytical predictions, and the dashed lines show the numerical solution for the same parameters.

Appendix C

Multi-electrode software flowcharts

Flow charts for the sub functions referenced in Figure 7.7 have been presented below. Figure C.1 shows the data processing and control loop architecture and Figure C.2 shows the data logging architecture.

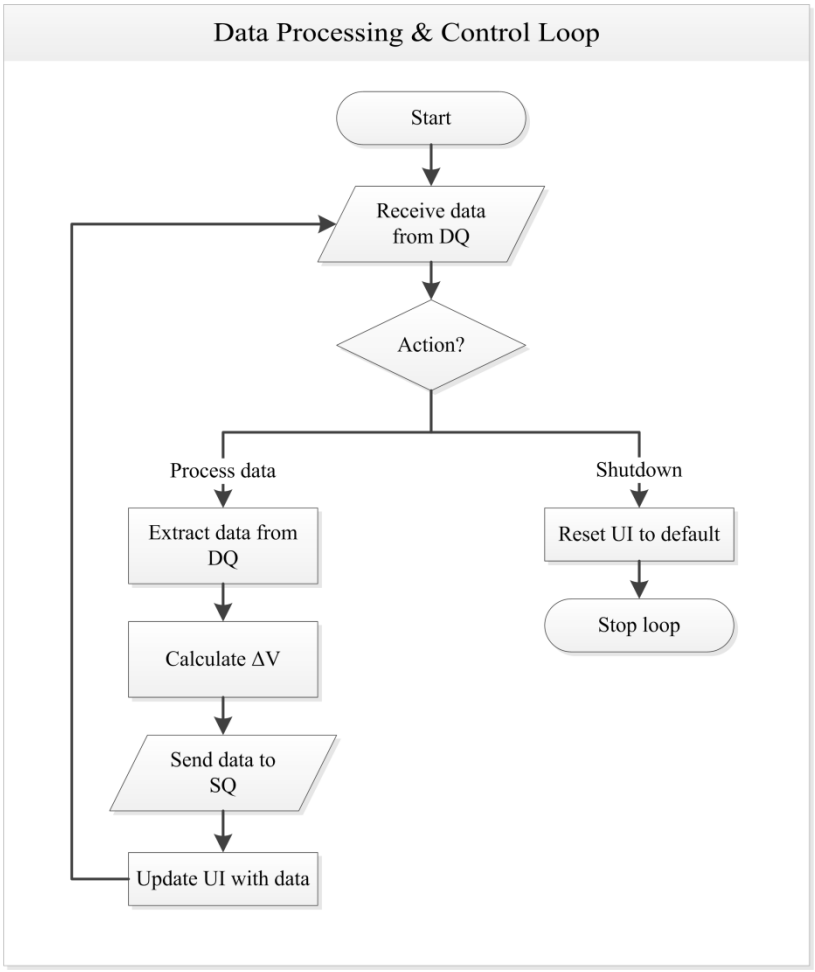

Figure C.1: Flow chart for the multi-electrode resistance software data processing & control sub function.

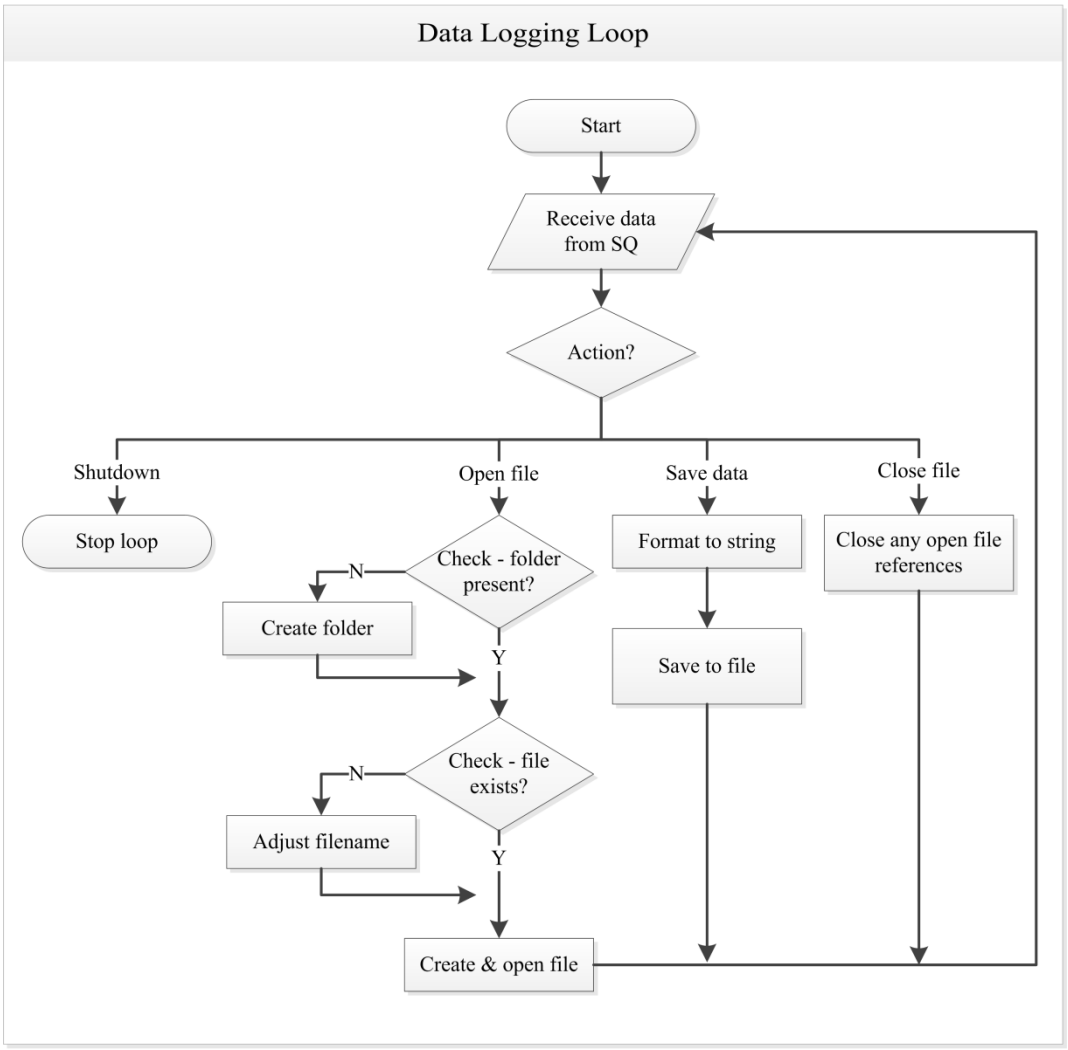

Figure C.2: Flow chart for the multi-electrode resistance software data logging sub function.